

Molecular mechanisms and sex differences in the circadian regulation of macrophages

Laura Bailey

Exeter College

University of Oxford

A thesis presented for the degree of

Doctor of Philosophy

Michaelmas 2025

Acknowledgements

Thank you to the Radcliffe Department of Medicine, the Oxford MRC-DTP, Novo Nordisk, and Exeter College for funding this work.

Chapter 5 draws in part on work I have previously published (Pu et al., 2025); thank you to my co-authors.

Thank you to my supervisors, David Ray, Matt Baxter, and Noelia Martinez-Sanchez, for their guidance and encouragement over the years. I am especially grateful to David, my primary supervisor, for welcoming me into his lab at OCDEM and for always believing in my potential, whether that meant encouraging my own ideas in the lab or backing opportunities beyond it. His mentorship throughout was instrumental in making this project a success. Thank you also to Matt, whose work this project led on from, for his wonderful combination of technical expertise and gallows humour. I couldn't have done this without him. And thank you to Noelia, who was always there for me. Your kindness, intelligence, and inventive problem-solving were a lifeline whenever I was stuck, and I cannot thank you enough.

My thanks also go to all past and present members of the Ray lab for their support; I really appreciate every one of you. Special thanks to Hania, Maria, and Lorna for making the lab such a warm and welcoming place when I first arrived.

Outside the lab, I am deeply grateful to the family and friends whose support made all of this possible. Thank you to my parents for everything they've done to help me get to this point, which would make for a very long list! Thank you to my friends and fellow PhD students at OCDEM, particularly Adam, Emily, and Siyu, for the good humour, good company, and excellent taste in office decorations. Thank you to Lara for being there every step of the way. I

can’t wait to see you cross the finishing line! And finally, thank you to Ivo for tirelessly listening to me talk about circadian macrophages, probably while making me tea and doing the washing up at the same time.

Abstract

Circadian clocks regulate diverse mammalian processes, including immune responses. Macrophages show circadian-regulated inflammatory responses, but the mechanisms underlying this regulation, and its dependence on intrinsic versus extrinsic timing cues, remain incompletely understood. In this work, I examined the mechanisms by which the macrophage clock regulates inflammatory responses *in vivo*, explored how these mechanisms vary with sex, and characterised a novel BMAL1-targeting pharmacological tool.

In peritoneal macrophages from myeloid-specific BMAL1-knockout mice, I found that almost all gene expression differences between timepoints were BMAL1-dependent. Clock-gating of LPS responses was driven by elevated basal expression at ZT12, suggesting that macrophages are primed with both pro- and anti-inflammatory regulators for rapid responses at the start of the active period. JAK-STAT activity was elevated at ZT12 in a BMAL1-dependent manner. Contrary to previous reports, REV-ERBα was not necessary for the anti-inflammatory functions of the circadian clock in response to LPS. Chromatin accessibility showed minimal timepoint differences.

Sex-specific circadian programs exist in a variety of tissues, with consequences for health outcomes. I identified significant sex differences in the macrophage transcriptomes and found that sex modifies the amplitude of clock-dependent gene expression in inflammatory macrophages, with male macrophages showing approximately threefold more clock-dependent genes and greater JAK-STAT differences between ZT0 and ZT12.

Much of our understanding of the circadian clock system comes from genetic models . To complement these models, I used a pharmacological tool, characterising the effects of a novel BMAL1-targeting compound, Core Circadian Modulator (CCM), on macrophages *in vitro*. I found that CCM inhibited

a broad program of pro-inflammatory gene expression under LPS stimulation, which involved the suppression of JAK-STAT activity. This provides orthogonal evidence (to genetic models) of the clock mechanisms regulating inflammatory responses.

Together, these findings support the role of the circadian clock as a "brake" on inflammation and provide transcriptional evidence that the macrophage clock is important for *in vivo* gating of inflammatory responses. JAK-STAT activity emerged as the key mediator across all three experimental approaches (genetic deletion, sex-stratified analysis, and pharmacological perturbation) identifying a targetable node in clock-controlled inflammation.

Keywords - Circadian - Macrophage - Transcription - Sex differences

Table of Contents

1 Introduction **1**

1.1 Motivation 1

1.2 The circadian clock 2

1.2.1 Evolution of circadian clocks 2

1.2.2 Key properties of a circadian clock 2

1.2.3 Transcription translation feedback loops (TTFLs) 3

1.2.4 A hierarchy of clocks 6

1.3 Chromatin accessibility and gene regulation 7

1.3.1 Epigenetics 7

1.3.2 Circadian control of gene expression 8

1.4 Macrophage biology and inflammation 10

1.4.1 Mechanisms of inflammation 12

1.5 Macrophage clocks 16

1.5.1 Circadian immunity 16

1.5.2 Circadian regulation in macrophages 18

1.5.3 Mechanisms of clock component-immune interaction 21

1.6 Sexual dimorphism in the immune system 23

1.6.1 Sexual dimorphism in macrophage biology 24

1.6.2 Sexual dimorphism in chronobiology 26

1.7 Pharmacological targeting of clock components 30

1.8 Thesis aims 32

1.8.1 Models used 33

2 Materials and Methods **35**

2.1 Animal models . . . 35

2.1.1 Genotyping . . . 36

2.2 Cell isolation and culture techniques . . . 38

2.2.1 Chapters 3 and 4: experimental set-up . . . 38

2.2.2 Isolation of peritoneal macrophages . . . 38

2.2.3 Production of bone-marrow derived-macrophages . . . 39

2.3 Next-generation sequencing assays . . . 40

2.3.1 RNA extraction . . . 40

2.3.2 ATAC-seq library preparation . . . 41

2.3.3 RNA-seq: primary data processing . . . 43

2.3.4 ATAC-seq: primary data processing . . . 43

2.3.4.1 Read processing and alignment . . . 43

2.3.4.2 Nucleosome-free region (NFR) enrichment and filtering . . . 45

2.3.4.3 Peak-calling and quantification . . . 46

2.3.5 RNA-seq differential expression analysis . . . 47

2.3.6 ATAC-seq differential accessibility analysis . . . 48

2.3.7 RNA-seq downstream functional analyses . . . 48

2.3.7.1 Gene ontology over representation analysis . . . 48

2.3.7.2 Gene set enrichment analysis (GSEA) . . . 49

2.3.7.3 DecoupleR: Transcription factor (TF) and pathway activity inference . . . 49

2.3.7.4 Selection of expressed TF motifs . . . 50

2.3.8 ATAC-seq downstream functional analyses . . . 51

2.3.8.1 Peak-gene proximity enrichment (PEGS) 51
2.3.8.2 Peak selection for motif analysis 51
2.3.8.3 Motif enrichment in PEGS-defined regions 51
2.3.8.4 Promoter motif enrichment 52

3 Intrinsic macrophage clock function 53

3.1 Introduction 53
3.1.1 *In vivo* clock-gating mechanisms are undefined. 53
3.1.2 The necessity of specific clock-components for gating inflammation is contested. 54
3.1.3 Chromatin mechanisms of clock-gating in macrophages remain untested. 56
3.1.4 Hypothesis and Aims 56
3.1.4.1 Hypotheses 57
3.1.4.2 Aims 57
3.2 Methods 58
3.2.1 Experimental design and contrasts 59
3.3 Results 61
3.3.1 Principal component analysis reveals dominant effects of LPS stimulation and biological sex on peritoneal macrophage transcriptomes. . . . 61
3.3.2 Almost all time-of-day differences are BMAL1-dependent in both saline and LPS-stimulated macrophages. 63
3.3.3 BMAL1 deletion abolishes time-of-day differences in LPS responsiveness for a set of inflammatory genes. 73
3.3.4 BMAL1-gated genes represent core inflammatory response pathways. . 80

3.3.5 Transcription factors implicated in the BMAL1-mediated repression at ZT12. 82
3.3.6 Inferred transcription factor activity implicates STAT/IRF pathways in ZT12 repression. 86
3.3.7 Pathway activity inference reveals increased JAK-STAT signalling at ZT12. 91
3.3.8 Motif analysis reveals E-box and hormone response elements in promoters of BMAL1-dependent inflammatory genes. 94
3.3.9 ATAC-seq reveals few differentially-accessible regions between timepoints. 95
3.3.10 Accessible chromatin regions are enriched within 50kb of BMAL1-dependent inflammatory genes. 97
3.3.11 REV-ERBα is not required for the circadian gating of BMAL1-dependent inflammatory genes. 99
3.3.12 Chromatin accessibility is largely unaffected by REV-ERBα deletion in basal peritoneal macrophages. 106
3.4 Discussion 109
3.4.1 The scope of BMAL1-dependent gating. 109
3.4.2 BMAL1-dependent repression of the ZT12 LPS response. 112
3.4.3 Transcription factors mediating BMAL1 effects. 113
3.4.4 Chromatin accessibility results indicate chromatin remodelling does not drive gating. 115
3.4.5 REV-ERBα does not mediate the repression of the LPS response at ZT12. 116
3.4.6 Limitations and future directions. 121

4 Sex differences in circadian programs in inflammatory macrophages 124

4.1 Introduction . . . 124

4.1.1 Hypothesis and Aims . . . 125

4.1.1.1 Aims . . . 126

4.2 Methods . . . 126

4.3 Results . . . 128

4.3.1 BMAL1-dependent gene expression shows pronounced sexual dimorphism. . . . 128

4.3.2 The majority of sex-specific clock-regulation is male-specific, enriched for inflammatory terms. . . . 131

4.3.3 Sex modulates amplitude of BMAL1-dependent programs. . . . 138

4.3.4 Transcription factor activity differs qualitatively between sexes. . . . 142

4.3.5 Males drive the JAK-STAT activation observed in mixed-sex analysis. . . 144

4.3.6 There is a small, but significant BMAL1-dependent sex-timepoint interaction. . . . 149

4.3.7 Sex-specific oscillation of key transcription factor expression. . . . 155

4.4 Discussion . . . 159

4.4.1 Sex predominantly modulates amplitude, not directionality. . . . 160

4.4.2 Inflammatory gating is amplified in males. . . . 161

4.4.3 Lipid metabolic gating is prioritised in females. . . . 162

4.4.4 Sex-timepoint interaction term consists of a small subset of genes with reversed directionality between sexes. . . . 164

4.4.5 Limitations and future directions. . . . 167

5 Pharmacological modulation of the macrophage circadian clock 171

5.1 Introduction . . . 171
5.1.1 Hypothesis and Aims . . . 173
5.1.1.1 Aims . . . 173
5.1.2 Contributions in this chapter . . . 174
5.2 Methods . . . 175
5.2.1 Luminometry . . . 175
5.2.2 Analysis of parameters . . . 176
5.2.3 ATP viability assay . . . 177
5.2.4 RNA-seq . . . 177
5.2.5 Downstream analyses for RNA-seq . . . 178
5.2.5.1 Epigenetic Landscape In Silico Deletion Analysis . . . 178
5.2.6 Morphology . . . 178
5.2.7 Motility . . . 180
5.2.8 Phagocytosis assay . . . 180
5.2.9 Statistical analysis for morphology, motility, and phagocytosis . . . 182
5.3 Results . . . 182
5.3.1 CCM alters circadian rhythm dynamics in peritoneal macrophages. . . . 182
5.3.2 CCM promotes anti-inflammatory gene expression profiles in BMDMs. 186
5.3.2.1 Effects of CCM in basal state macrophages. . . . 188
5.3.2.2 BMAL1-dependency of CCM effects in basal state macrophages. 193
5.3.2.3 Effects of CCM in LPS-stimulated macrophages. . . . 198
5.3.2.4 BMAL1-dependency of CCM effects in LPS-stimulated macrophages. 203
5.3.3 CCM attenuates LPS-effects on macrophage phenotypes. . . . 213
5.3.3.1 Morphology. . . . 213

5.3.3.2 Motility. 215
5.3.3.3 Phagocytosis. 216
5.4 Discussion 217
5.4.1 CCM alters circadian dynamics in macrophages. 217
5.4.2 CCM promotes anti-inflammatory transcriptional programs through BMAL1.218
5.4.3 CCM's effects concord with *in vivo* clock-gating mechanisms. 220
5.4.4 Mechanism of action. 220
5.4.5 Functional consequences. 221
5.4.6 Limitations and future directions 224

6 Discussion **226**

6.1 Summary of analysis 226
6.1.1 Strengths and limitations 232
6.1.2 Future directions 234
6.1.3 Translational outlook for chronobiology 235
6.2 Final conclusions 237

Appendix: Reprint - Pharmacological targeting of BMAL1 modulates circadian and immune pathways **238**

List of Figures

1.1 The core circadian clock network. 5

1.2 TLR4 siganalling pathways. 14

1.3 Circadian control of macrophages. 19

2.1 Workflow of CATCH-UP. 44

3.1 Schematic showing experimental groups and contrasts used to determine BMAL1-dependent time-gated inflammatory response genes. 60

3.2 Principal Component Analysis (PCA) for PC1 and PC2. 62

3.3 The effect of myeloid-specific BMAL1-KO on ZT12 vs ZT0 differential expression in peritoneal macrophages, in basal (saline-treated) conditions. 65

3.4 Top 15 enriched GO terms in the BMAL1-dependent ZT12 vs ZT0 differences, in basal state macrophages. 66

3.5 Top 15 enriched GO terms in genes exhibiting directional reversal between WT and BMAL1-KO macrophages at ZT12 in basal state. 67

3.6 The effect of myeloid-specific BMAL1-KO on ZT12 vs ZT0 differential expression in peritoneal macrophages, after 1 hour of LPS stimulation (1 mg/kg). 70

3.7 There are more saline-specific BMAL1-dependent differences than LPS. 71

3.8 Top 15 enriched GO terms in the BMAL1-dependent ZT12 vs ZT0 differences, in LPS-stimulated macrophages. 72

3.9 The effect of myeloid-specific BMAL1-KO on a timepoint-treatment interaction term in peritoneal macrophages. 75

3.10 The effect of timepoint on the magnitude and direction of change of the BMAL1-dependent gate set. 77

3.11 Heatmap for the BMAL1-dependent gate of the LPS-response shows greater time-of-day difference in saline samples in WT only. 79

3.12 Functional enrichment of the BMAL1-dependent gate set. 81

3.13 Functional enrichment of the BMAL1-dependent gate set. 82

3.14 The effect of genotype on expression of TF transcripts at ZT12, in basal-state and LPS-stimulated macrophages. 84

3.15 Expression of *Bmal1* across experimental conditions. 86

3.16 TF activity inference for the BMAL1-dependent timepoint-treatment interaction tested through the WT-gate. 88

3.17 The effect of timepoint and loss of BMAL1 on transcription factor activity in the LPS response. 90

3.18 BMAL1 deletion reverses the timepoint with greatest JAK-STAT and NFkB pathway activity in WT, and disrupts timepoint-dependence of non-inflammatory pathways. 92

3.19 BMAL1 deletion disrupts the coordinated regulation of NFkB and JAK-STAT pathway target genes at ZT0 and ZT12, respectively. 93

3.20 Effect of timepoint on global chromatin accessibility in peritoneal macrophages. 96

3.21 Heatmap showing enrichment of accessible chromatin regions near BMAL1-dependent clock-gated inflammatory gene set. 98

3.22 REV-ERBα deletion has minimal impact on both basal and LPS-stimulated transcriptomes at ZT8. 102

3.23 The response to LPS is highly conserved between WT and REV-ERBα-KO peritoneal macrophages. 105

3.24 Effect of REV-ERBα deletion on global chromatin accessibility in peritoneal macrophages. 107

3.25 Summary of results from Chapter 3. 120

4.1 The effect of myeloid-specific BMAL1-KO on ZT12 vs ZT0 differential expression in peritoneal macrophages, after 1 hour of LPS stimulation (1 mg/kg). 129

4.2 The effect of myeloid-specific BMAL1-KO on ZT12 vs ZT0 differential expression in peritoneal macrophages, after 1 hour of LPS stimulation (1 mg/kg). 130

4.3 There are more male-specific BMAL1-dependent differences than female. . . . 131

4.4 The set of 84 female-specific BMAL1-dependent ZT12 vs ZT0 differences, in LPS-stimulated macrophages. 132

4.5 The set of 487 male-specific BMAL1-dependent ZT12 vs ZT0 differences, in LPS-stimulated macrophages. 134

4.6 Enriched GO terms in the female-specific BMAL1-dependent ZT12 vs ZT0 differences, in LPS-stimulated macrophages. 136

4.7 Top 15 enriched GO terms in the male-specific BMAL1-dependent ZT12 vs ZT0 differences, in LPS-stimulated macrophages. 137

4.8 Male-specific BMAL1-dependent genes are similarly enriched in wild-type female macrophages. 139

4.9 Female-specific BMAL1-dependent genes are similarly enriched in wild-type male macrophages. 141

4.10 The effect of sex and loss of BMAL1 on differential transcription factor activity between ZT0 and ZT12 in LPS-stimulated macrophages. 143

4.11 BMAL1 deletion disrupts timepoint-dependence of inflammatory pathways in male LPS-stimulated macrophages. 145

4.12 BMAL1 deletion disrupts timepoint-dependence of inflammatory pathways in female LPS-stimulated macrophages. 146

4.13 BMAL1 deletion disrupts the coordinated regulation of JAK-STAT pathway target genes in males and females, respectively. 148

4.14 Myeloid-specific BMAL1 is necessary for sex-timepoint interactions in LPS-stimulated peritoneal macrophages. 150

4.15 The genes showing a BMAL1-dependent sex-timepoint interaction in LPS-stimulated macrophages. 151

4.16 Functional enrichment of the genes showing a BMAL1-dependent sex-timepoint interaction in LPS-stimulated macrophages. 152

4.17 The sex-timepoint interaction set show greater magnitude of change, and are largely upregulated at ZT12, in male macrophages. 154

4.18 The effect of timepoint on expression of transcription factor transcripts in WT macrophages, in males and females separately. 156

4.19 Boxplots for the expression of key TFs which vary across timepoints differently in males and females, respectively. 158

4.20 Summary of results from Chapter 4. 166

5.1 CCM is a novel synthetic ligand of the BMAL1 PASB domain. 172

5.2 Dose-dependent modulation of PER2 oscillations by CCM. 183

5.3 CCM significantly reduced amplitude of PER2 oscillations in a dose-dependent manner. 185

5.4 Design of experiment testing effects of CCM on BMDM gene expression. . . . 187

5.5 The genes perturbed by CCM in the basal state show modest effect sizes. 188

5.6 CCM upregulates transport and signalling pathways in WT macrophages. . . . 191

5.7 CCM downregulates cytoskeletal organisation, and inflammatory response pathways. 192

5.8 Residual *Bmal1* expression at the floxed exon confirms incomplete penetrance of the myeloid BMAL1-KO 194

5.9 Most CCM-effects are BMAL1-dependent in basal state macrophages. 194

5.10 BMAL1-dependent CCM effects in basal state macrophages relate to macrophage activation. 195

5.11 The effect of CCM on transcription factor activity in basal state macrophages. . 196

5.12 The effect of CCM on pathway activity in basal state macrophages. 197

5.13 The dominant effect of CCM is downregulation of gene expression in LPS-stimulated macrophages. 198

5.14 CCM upregulates endocytosis and vesicle-mediated transport pathways in LPS-stimulated macrophages. 201

5.15 CCM downregulates pro-inflammatory response pathways in LPS-stimulated macrophages. 202

5.16 A majority of CCM-effects are BMAL1-dependent in LPS-stimulated macrophages. 203

5.17 In LPS-stimulated macrophages, BMAL1-dependent effects of CCM are to upregulate endocytosis pathways while downregulating pro-inflammatory response terms. 205

5.18 CCM acts by inhibiting activation in response to LPS. 207

5.19 The effect of CCM on transcription factor activity in LPS-stimulated macrophages. 208

5.20 The effect of CCM on pathway activity in LPS-stimulated macrophages. 209

5.21 Predicted transcriptional regulators of BMAL1-dependent CCM-repressed genes are enriched for STAT/IRF proteins. 210

5.22 Expression of STAT1 and IRF1 is significantly downregulated by CCM in a BMAL1-dependent manner. 211

5.23 The effect of CCM on BMAL1-dependent inflammatory response genes identified in peritoneal macrophages. 212

5.24 CCM significantly reduces effect of LPS on cell area and height. 214

5.25 CCM significantly increases spontaneous motility, reducing the effect of LPS. . 215

5.26 CCM significantly reduces number of intracellular bacteria as a measure of phagocytic uptake. 216

5.27 Summary of results from Chapter 5. 223

List of Abbreviations

BH . . . . . Benjamini-Hochberg

bHLH . . . . . Basic helix-loop-helix

BMAL1 . . . . . Brain and muscle Arnt-like protein 1

BMDM . . . . . Bone marrow-derived macrophages

bZIP . . . . . Basic leucine zipper

CCG . . . . . Clock-controlled genes

CCL/CCR . . . . . C-C motif ligand/receptor

CLOCK . . . . . Circadian locomotor output cycles kaput

CRY . . . . . CRYPTOCHROME

CXCL/CXCR . C-X-C chemokine motif ligand/receptor

DBP . . . . . Albumin D-box-binding protein

DNA . . . . . Deoxyribonucleic acid

GO . . . . . Gene ontology

GBP . . . . . Guanylate-binding protein

GSEA . . . . . Gene set enrichment analysis

HDAC . . . . . Histone deacetylase

IFN . . . . . Interferon

IL . . . . . Interleukin

IRF . . . . . Interferon regulatory factor

ISG . . . . . Interferon-stimulated gene

LPS . . . . . Lipopolysaccharide

M1 . . . . . Pro-inflammatory macrophage

M2 . . . . . Anti-inflammatory macrophage

mRNA . . . . . Messenger RNA

MYD88 . . . . . Myeloid differentiation primary response 88

NCOR . . . . . Nuclear receptor corepressor

NFIL3 . . . . . Nuclear factor interleukin 3 regulated

NFkB . . . . . Nuclear factor kappa-light-chain-enhancer of activated B cells

NPAS2 . . . . . Neuronal PAS domain protein 2

NRF2 . . . . . Nuclear factor erythroid 2-related factor 2

PAR . . . . . Proline and acidic amino acid-rich (domain)

PAS . . . . . Per-Arnt-Sim (domain)

PER . . . . . PERIOD

ROR . . . . . Retinoic acid-related orphan receptor

RORE . . . . . ROR response element

SCN . . . . . Suprachiasmiatic nucleus

SREBP . . . . . Sterol regulatory element binding protein-

STAT . . . . . Signal transducer and activator of transcription

TF . . . . . Transcription factor

TLR . . . . . Toll-like receptor

TTFL . . . . . Transcription-translation feedback loop

ZT . . . . . Zeitgeber Time

1 | Introduction

1.1 Motivation

Many biological processes are compartmentalised not only through space but also in time. Circadian rhythms, oscillations with near-24 hour periodicity, are a fundamental feature of life in diverse organisms (Takahashi, 2017). Despite a diversity of components making up the clock in each taxa, the underlying architecture is strikingly consistent: transcription-translation feedback loops (TTFLs) generate self-sustained oscillations which can be entrained to environmental cycles (Partch et al., 2014).

In mammals, circadian rhythms coordinate physiology, ranging from metabolic function to immune responses, across many organ systems. This extensive circadian regulation has important implications for health. Modern environments increasingly disrupt circadian alignment: artificial lighting, shift work, and irregular schedules decouple internal timing from external cues. The consequences for those most affected can be severe, with shiftworkers facing increased risk of a spectrum of diseases (Fishbein et al., 2021). However, therapeutic opportunities are promising. By understanding how this regulatory network affects diverse physiological processes, we can learn how to manipulate a coordinated set of downstream systems through targeting key circadian regulatory factor nodes.

This thesis aims to improve our understanding of the regulatory networks linking the circadian clock system to inflammatory gene expression, using genetic knock-out systems and a novel tool compound, and exploring the impact of sex on these interactions.

This introduction will provide the necessary background to these topics and the rationale for the

studies described in the following chapters.

1.2 The circadian clock

1.2.1 Evolution of circadian clocks

Biological timing mechanisms vary from the simplest hourglass type (unidirectional, non-redundant sets of processes most relevant during development which ensure the correctly-ordered procession of biological processes within precise timescales), to self-sustaining oscillators maintained through the combination of positive and negative feedback loops. For example, self-sustaining oscillators regulate the cell cycle, ovarian cycle, and neural oscillations (Rensing et al., 2001). As life on Earth evolved in alternating light-dark cycles over the 24-hour period, many organisms have evolved timing mechanisms which synchronise activities to periodic external signals. Circadian rhythmicity is observed in most animals, plants, algae, and in many fungi, suggesting evolution in early eukaryotes (Bell-Pedersen et al., 2005). This rhythmic transcription of pathways with shared biological function serves to improve the efficiency of a cell: organising processes temporally as well as spatially, and allowing increased peak gene expression levels without an overall increase in energy expenditure (G.-Z. Wang et al., 2015). The appearance of functionally-similar but compositionally-varied circadian clocks across so many distinct taxa of life suggests an evolutionary advantages of compartmentalising energy-demanding biological processes temporally.

1.2.2 Key properties of a circadian clock

In each organism, external timing must be relayed to the intrinsic clock mechanism and used to synchronise rhythms to the environment. There are several key features defining the result-

ing circadian oscillation. These timing mechanisms are endogenous, and rhythms persist in the absence of external stimuli with an approximately 24-hour period. This means that the oscillation is anticipatory and not purely responsive to stimuli. However, the phase of the oscillation must be responsive to external signals, or 'zeitgebers', such as light-dark, feeding-fasting, and temperature cycles. Finally, the oscillation must have temperature compensation to ensure that periodicity is maintained over a range of biological temperatures (Shinohara et al., 2017; Takahashi, 2017).

While the molecular components of the clock vary between organisms, significant work over the past 50 years has led to the development of a model for the time-keeping mechanism in mammals based on a core transcription translation feedback loop.

1.2.3 Transcription translation feedback loops (TTFLs)

Almost all mammalian cells contain a self-sustaining oscillator regulating rhythmic gene expression to coordinate different biological functions to different times of the day, maintained by an interlocked set of TTFLs (Figure 1.1). The primary loop, establishing the period of the rhythm, is composed of the core heterodimer CLOCK:BMAL1 (circadian locomotor output cycles protein kaput (CLOCK), and brain and muscle ARNT-like 1 (BMAL1)), which are members of the bHLH-PAS (basic helix-loop-helix (bHLH), and Period-Arnt-Sim, (PAS)) transcription factor (TF) family. BMAL1 is the only non-redundant core clock component (Bunger et al., 2000), and will form a heterodimer with Neuronal PAS domain protein 2 (NPAS2) in place of CLOCK. This TF complex activates the expression of more than a thousand clock-controlled genes (CCGs) (some of which are dependent on cell type), including CLOCK:BMAL1's own repressors. In the primary loop, these are the PERIOD and CRYPTOCHROME proteins. There are three isoforms of PERIOD (PER1, PER2, PER3) and two isoforms of CRYPTOCHROME

(CRY1, CRY2), all of which interact in the cytoplasm and form complexes which may then translocate to the nucleus to repress CLOCK:BMAL1 activity (Aryal et al., 2017). When in the cytoplasm, the PER/CRY complexes recruit Casein kinase 1 (with three isoforms, CK1δ1, CK1δ2, and CK1ϵ), which phosphorylates PER1 and PER2, regulating their abundance and helping set the period of the oscillator (An et al., 2022). CK1 is important for key properties of the clock, such as temperature compensation, alongside mediating the repressive properties of PERIOD on CLOCK:BMAL1 complexes by enabling phosphorylation of CLOCK, which in turn enables the removal of CLOCK:BMAL1 from DNA (Cao et al., 2021; Shinohara et al., 2017).

The secondary TTFL which stabilises and influences the amplitude of the circadian oscillator is driven by CLOCK:BMAL1-activated expression of two nuclear hormone receptors, retinoic-acid related receptors (RORα, RORβ, and RORγ) and Reverse-ERBs (REV-ERBα and REV-ERBβ). These secondary arm TFs act antagonistically: RORs transcriptionally activate and REV-ERBs transcriptionally repress the CLOCK:BMAL1 complex. The ROR proteins show differential expression based on tissue, with RORβ mainly expressed in the retina and pineal gland, while RORα and RORγ have been implicated in a wider set of biological pathways with metabolic and immune functions (Cook et al., 2015). The REV-ERB proteins are reported to have redundant roles in circadian clock regulation, with similar expression patterns across cell types (Cho et al., 2012). In a REV-ERBα/β-deficient mouse embryonic stem cell model, only direct targets of REV-ERBα/β (*Bmal1, Npas2, Nfil3, Bhlh40*) were upregulated, consistent with the role of REV-ERBs as transcriptional repressors (Ikeda et al., 2019). As ligand-regulated TFs, RORs and REV-ERBs are thought to link circadian rhythms with metabolism alongside another nuclear hormone receptor PPARγ (Grimaldi et al., 2010; Kojetin & Burris, 2014). RORs bind cholesterol derivatives, while REV-ERBs bind haem (porphyrins). PERIOD-

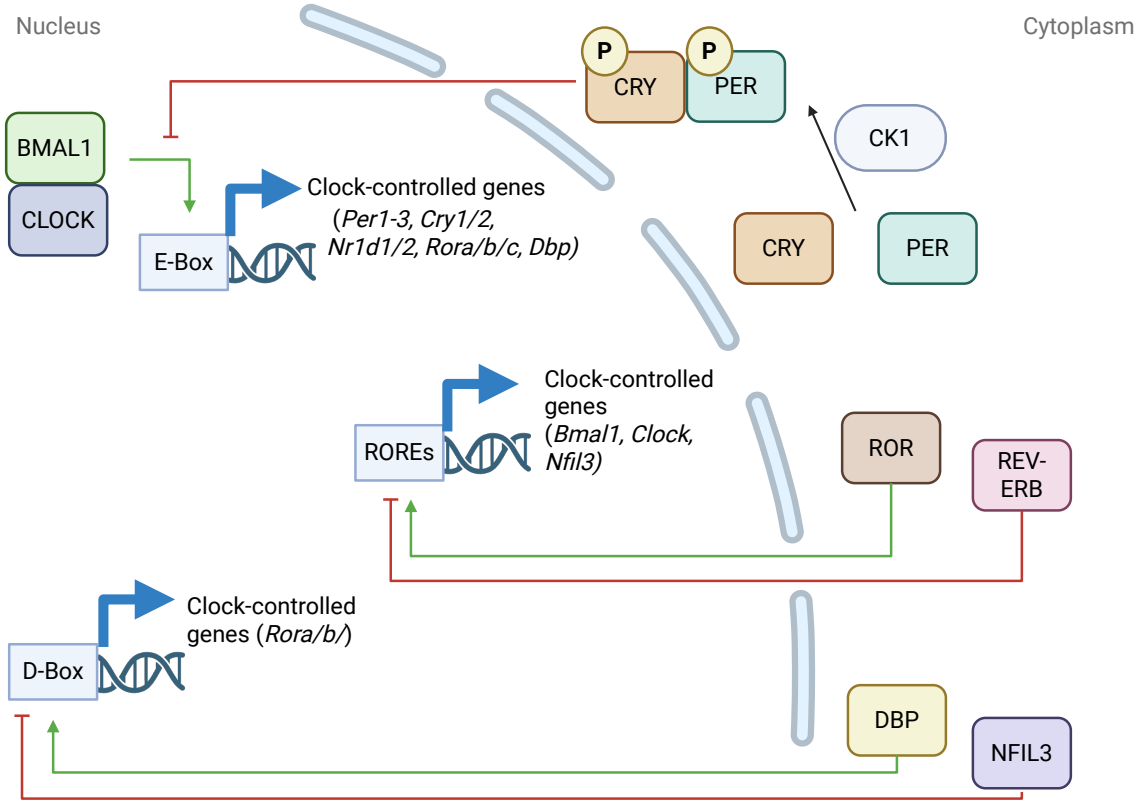

Figure 1.1: **The core circadian clock network.**
The clock machinery is composed of transcription factors (TFs) controlling rhythmic output genes (clock-controlled genes), mediating cell-autonomous approximate 24-hour rhythms in various biological processes dependent on cell-type. The primary transcription-translation feedback loop consists of the TFs CLOCK and BMAL1 forming a heterodimer to drive expression of target genes containing E-box sequences. Among these are PERIOD (PER) and CRYPTOCHROME (CRY) proteins, which become phosphorylated by CK1 and form complexes which translocate to the nucleus and inhibit CLOCK:BMAL1 action. CLOCK:BMAL1 also drive expression of REV-ERBs and RORs, which respectively activate and inhibit the expression of *Bmal1*. In another stablising loop, TF NFIL3 represses action of DBP to regulate the rhythm of ROR proteins. Modified from (Takahashi, 2017). Created in https://BioRender.com.

dependent regulation of nuclear hormone receptors are one way in which the primary and secondary TTFLs are interlocked (Schmutz et al., 2010).

An additional feedback loop exists, in which CLOCK:BMAL1 activates expression of PAR-bZIP transcription activator DBP, which promotes expression of RORα and RORβ. REV-ERBs and RORs control expression of *Nfil3* (via RORE regulatory elements), and the protein NFIL3 forms a negative feedback loop with RORα/β (via D-box elements).

How the delayed negative feedback loop achieves 24-hour periodicity is a subject of much research, with increasing evidence that levels of post-transcriptional, translational, and post-translational control act to modify periodicity of the oscillator (Crosby & Partch, 2020).

1.2.4 A hierarchy of clocks

In a basal state of health, the oscillators found in different tissues are kept in tight synchrony with one another, despite the variety of unique environmental signals received by each tissue. The major controller of this network of time-keeping is the "suprachiasmatic nucleus" (SCN), a network of approximately 20,000 cells located within the brain, known as the "master clock". It is uniquely protected from many of the circulatory changes affecting "peripheral clocks" (those locally governing the activities of other organs). It receives "zeitgebers" (inputs from the external world), the most important of which are light signals received by photosensitive retinal cells. The SCN itself signals via both stimulating the production of clock-resetting hormones (glucocorticoids) and autonomic nervous communication to peripheral tissues (and their clocks). SCN ablation via lesions or genetic deletion alters the phases and amplitudes of many peripheral organs' clocks, such as those of the liver, epidermis, heart, and adrenal gland (Husse et al., 2014; Koronowski et al., 2019; Welz et al., 2019). Clocks across the body communicate to produce rhythmic outputs (Koronowski & Sassone-Corsi, 2021): when they receive varying

and conflicting timing signals, risks are elevated for metabolic syndromes, and cardiovascular and neurodegenerative diseases (Rijo-Ferreira & Takahashi, 2019).

The periodic build-up and degradation of these TFs results in the periodic expression of sets of target genes: both the core clock components composing the oscillator, and thousands of tissue-dependent clock-controlled genes to generate oscillations and temporal organisation of biological functions (Takahashi, 2017). CLOCK:BMAL1 interacts with E-box (Enhancer) elements (with consensus sequence CACGTG) and co-regulators (including PER/CRY complexes) to drive these oscillations. This sequence is highly common across the genome, and CLOCK:BMAL1 is expressed in nearly every cell type, though the rhythmic transcriptome is highly tissue-dependent (Mure et al., 2018). An essential layer of control over when and where TFs like CLOCK:BMAL1 can access genomic target sites like E-boxes is the regulation and remodelling of the dynamic chromatin environment. It is hypothesised that lineage-determining TFs can render E-boxes accessible or inaccessible to CLOCK:BMAL1 in a cell-specific manner (Beytebiere et al., 2019b).

1.3 Chromatin accessibility and gene regulation

1.3.1 Epigenetics

All cells within an organism contain the same genetic code, but the way in which this information is used varies from cell to cell without alteration to the primary DNA sequence. Modifications to nucleic acids and amino acid residues enable differential regulation of gene expression in cells with identical genomes, allowing plasticity in responses to signalling molecules. These processes, under the umbrella term of “epigenetics”, are necessary for normal cellular and organismal function (Portela & Esteller, 2010).

Gene expression is regulated through multiple layers of control. Cis-regulatory elements, promoters and enhancers, are present in the direct vicinity of each gene, although enhancers may be located at distances up to 1 Mb away from the transcriptional start site (TSS). At promoters, binding of TFs regulates recruitment of the mediator complex and so RNA polymerase II. Enhancer elements contain motifs regulating the binding of TFs (Spitz & Furlong, 2012). As they are often located far from the regulated gene in the genome, chromatin looping is instrumental in bringing target gene promoters into proximity to these regulatory elements (Galouzis & Furlong, 2022). E-boxes (and therefore CLOCK:BMAL1 binding sites) are found in both promoters and enhancers, indicating that the clock plays a role in both promoter-driven and enhancer-driven regulation of gene expression (Trott & Menet, 2018).

DNA associates with histone proteins to form dynamically-structured chromatin. This serves to package the DNA within the nucleus, and acts as a layer of control over gene expression. Modifications can be made to these histones, including acetylation and methylation at specific amino acid residues, to regulate the accessibility of the DNA and so the ability for TFs to bind regulatory elements. Areas of increased accessibility are termed “euchromatin”, while “heterochromatin” is more densely packaged and transcriptionally inactive (Bannister & Kouzarides, 2011).

1.3.2 Circadian control of gene expression

Circadian clock components BMAL1 and CLOCK modulate gene expression through rhythmic binding to E-box regulatory elements for target genes. Rhythmic binding of CLOCK:BMAL1 to E-box elements is necessary and sufficient for rhythmic transcription to occur (Ripperger & Schibler, 2006). In mouse liver, the majority of rhythmic transcription occurs due to rhythmic PolII loading to promoters (instead of a rhythmic transition from pause to elongation) (Le

Martelot et al., 2012). At enhancers, there is evidence that at some genomic sites, CLOCK:BMAL1 may exhibit pioneer function and facilitate the binding of other TFs to coordinate the rhythmic transcriptome (Menet et al., 2014).

Steady-state mRNA levels reflect multiple layers of regulation beyond transcription. Using a combination of nascent-seq and mRNA-seq, in mouse liver, approximately 20% of cycling mRNAs have been found to have a corresponding cycling nascent transcript, indicating substantial post-transcriptional contributions to rhythmic gene expression (Menet et al., 2012). These include: rhythmic poly-adenylation (Kojima et al., 2012), alternative splicing (Preußner et al., 2014), and miRNA-mediated regulation (Du et al., 2014). Ribosome profiling has revealed circadian oscillations in protein synthesis that are independent of mRNA cycling (Janich et al., 2015).

Circadian gene expression has been associated with rhythmic chromatin remodelling. CLOCK has intrinsic histone acetyltransferase activity (Doi et al., 2006). CLOCK:BMAL1 and PER/CRY complexes have been shown to interact with epigenetic modifiers KDM5A, EZH2, MLL1, WDR5, CBP-p300, and some histone deacetylases (including SIRT1). The circadian binding of these modifiers to promoters and enhancers generates rhythmic chromatin modifications and remodelling. REV-ERBα, a member of the core repressive arm of the clock, recruits the NCoR-HDAC3 co-repressor complex to oppose the formation of loops between enhancers and target gene promoters (Y. H. Kim et al., 2018). In liver, BMAL1 global deletion resulted in the loss of circadian oscillations in promoter-enhancer loops (Mermet et al., 2021). PARP1 and CTCF regulate the circadian recruitment of loci to the nuclear periphery, where loci gain repressive chromatin marks (Zhao et al., 2015). More recently, in mouse liver, it was shown that periodic gene expression is not under direct control of a rhythmic association of chromatin with nuclear lamina (Brunet et al., 2019), so the mechanism may be specific to the cell type or context.

The CLOCK:BMAL1 heterodimer directly interacts with nucleosomes to gain access to DNA (Michael et al., 2023). CLOCK:BMAL1 binds thousands of sites in the genome, but for many of these, CLOCK:BMAL1 binding is not sufficient to drive rhythmic transcription: for example, targets are expressed either constitutively or in antiphase to CLOCK:BMAL1 expression (Trott & Menet, 2018). It is a current goal of the field to identify these uncharacterised regulatory mechanisms initiating rhythmic transcription. One such mechanism is the nucleosome-mediated cooperativity of CLOCK:BMAL1 with tissue-specific TFs, giving rise to tissue-specific rhythms through enhancer-enhancer interactions (Beytebiere et al., 2019a). Whether similar cooperativity mechanisms exist in macrophages is unclear, although in a study investigating the effects of ageing on circadian rhythms in macrophages, rhythmic chromatin accessibility has been observed in bone-marrow derived macrophages (BMDMs) (Blacher et al., 2022).

Recent single-nucleus multi-omics approaches have started to resolve circadian gene expression at the resolution of cell-type and cell-state. Integration of snRNA-seq and snATAC-seq in a mouse liver time-course enabled linking of cis-regulatory elements to target genes in a cell-type-specific manner (C. Y. Tong et al., 2025). These approaches may be particularly valuable for heterogeneous tissues where bulk sequencing averages across cell populations with distinct rhythmic programmes.

1.4 Macrophage biology and inflammation

Macrophages are a key cell type in the initiation, maintenance, and resolution of inflammation. They are long-lived, mononuclear cells and are found in most tissues within the human body. Tissue-resident macrophages have one of two origins: they may be embryonic yolk-sac derived, or monocyte-derived (and so produced from bone-marrow myeloid precursors). Populations of

macrophages within an organ are often heterogenous, with variability in gene expression and protein production often related to differences in the source of origin, alongside any stimuli the macrophage has been exposed to (Lazarov et al., 2023). Bone-marrow derived macrophages (BMDMs) are a widely-used *in vitro* model for macrophage biology. BMDMs are produced by culturing bone marrow myeloid progenitors *ex vivo* with macrophage colony-stimulating factor (M-CSF) over approximately seven days to drive differentiation, yielding a relatively homogenous population for downstream analysis. BMDMs respond to activation with core macrophage functions such as phagocytosis and cytokine production, but lack tissue-specific programmes shaped by local environmental cues, and so findings from BMDM models must be validated in tissue-resident populations.

Macrophages may be considered sentinel cells responding to environmental signals, often in a tissue-specific manner. Within tissues, macrophages work in tangent with surrounding cells to optimise tissue functions. For example, as robust mucosal immunity is essential on any surfaces exposed to the external environment, alveolar macrophages patrol alveoli in the lungs for inhaled pathogens while maintaining surfactant homeostasis (Hussell & Bell, 2014). Whereas in the central nervous system, microglial cells mediate synaptic pruning, a process essential for the synapse formation and the regulation of neuronal activity (Ueno et al., 2013). In the liver, Kupffer cells are crucial for recycling iron from haemoglobin via ferroportin (Scott & Guilliams, 2018). Within serous cavity spaces, pleural membrane macrophages and peritoneal macrophages consist of both long-lived resident cells protecting the cavity against infection, as well as small pro-inflammatory monocyte-derived cells. Like many resident macrophages, peritoneal macrophages self-maintain, with significant replacement by monocytes occurring only in the context of inflammatory responses (Rosas et al., 2014).

Regardless of origin or tissue-residence, macrophages share a conserved core set of functions.

They are antigen-presenting phagocytic cells and are crucial in creating an inflammatory microenvironment through the secretion of cytokines which recruit more lymphocytes to the site of infection. Macrophage output depends on the signals received: macrophages carry a broad range of pattern recognition receptors (PRRs) mediating the initial recognition of host- and pathogen-associated molecular patterns (PAMPs) and initiating inflammatory responses (S. Chen et al., 2023). The most well-studied group of PRRs are the Toll-like receptors, of which downstream signalling has been best characterised for TLR4.

1.4.1 Mechanisms of inflammation

The transcriptional mechanisms of macrophage inflammatory activation have been particularly well-characterised through TLR4-dependent activation by endotoxin (lipopolysaccharide (LPS)), a major component of Gram-negative bacterial outer membranes. Downstream signalling has been mapped in detail by (Luo et al., 2025).

LPS-TLR4 intracellular signalling acts primarily through two discrete, spatially-separated pathways, after LPS has been captured by LPS-binding protein (LBP), and bound by CD14 (a cell surface co-receptor for LPS) and TLR4 on the cell surface (Figure 1.2). The myeloid differentiation primary response protein 88 (MyD88)-dependent pathway involves recognition of LPS at the plasma-membrane by MyD88, and primarily leads to nuclear translocation of NFkB (RelA/p65 and p50 subunits) and AP-1, with the sequential involvement of TIRAP, IRAK, TRAF6, and TAK1 signalling molecules.

In the MyD88-independent pathway, TLR4 endocytosis is mediated by CD14, followed by endosomal TRAM-TRIF activation leading to IRF3/7 phosphorylation and activation and type-I interferon production, with involvement of TRAF3, TANK, IKBKG, TBK1, and TKBKE (Figure 1.2). CD14 regulates TLR4 endocytosis and so enables the switch to TRIF signalling (Ka-

gan et al., 2008). However, endocytosis of TLR4 is not required for endosomal TLR4 signalling (Schultz et al., 2025). What determines MyD88-dependency and the requirement for specific signalling molecules remains an active area of investigation. The preference appears mediated by which sets of adaptors the cytoplasmic Toll-IL-1-receptor (TIR) domain of TLR4 recruits. TIR domain post-translational modifications regulate pathway activation, with enhanced TIR domain acetylation in the TLR4 complex increasing NFkB activation and pro-inflammatory cytokine production (X. Li et al., 2024). Ligand-induced endocytosis has also been put forward as a crucial negative regulator of the MyD88-dependent pathway (Schultz et al., 2025). Type I interferon production and the subsequent JAK–STAT activation occurring downstream of IFNAR engagement is predominantly a feature of the MyD88-independent pathway (Darnell et al., 1994).

LPS-inducible genes are divided into "early" or "late", based on induction kinetics and chromatin status, and/or dependency on MyD88-dependence and signalling molecules. Early genes (in the primary response) are characterised by low nucleosome occupancy at promoters and high prevalence of permissive chromatin marks or stalled RNA polymerase II. Early response to LPS consists of transcripts encoding TFs or associated with transcriptional regulation (including cytokines *Cxcl1, Il1b* and inhibitors *Dusp1/5/8/10/14* (Raza et al., 2014).

Late genes (part of the secondary response) are the result of secondary feedback loops, including autocrine/paracrine IFN-β signalling. IFN-β acts on type I IFN receptor (IFNAR), leading to STAT1 phosphorylation. Downstream transcription of interferon-stimulated genes (ISGs) is mediated by two complexes: ISGF3 (STAT1/STAT2/IRF9), which binds interferon-stimulated response elements (ISREs), and STAT1 homodimers, which bind gamma-activated sequences (GAS elements) (Darnell et al., 1994). There are secondary response genes produced through the TRIF pathway independent of IFNAR-signalling (A.-J. Tong et al., 2016), including T-cell

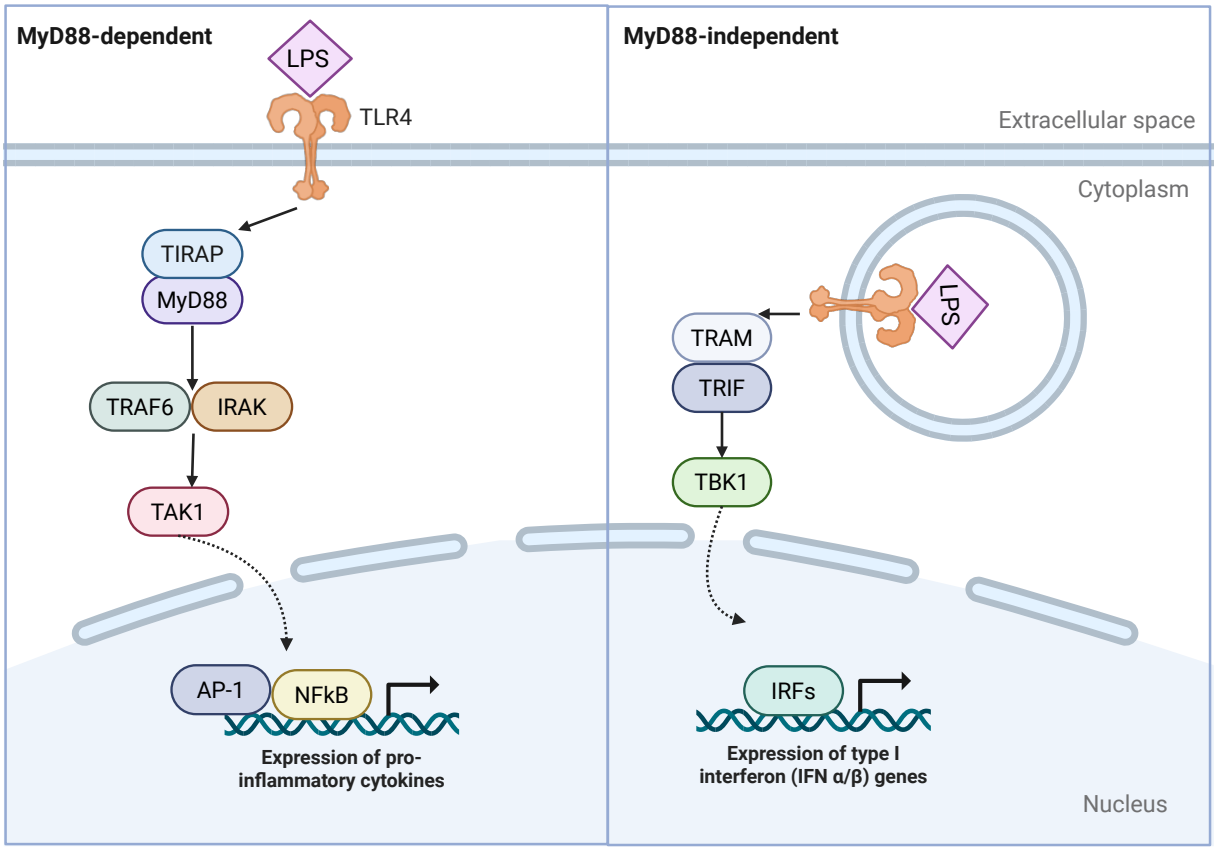

Figure 1.2: **TLR4 siganalling pathways.**
On TLR4 activation by LPS, an intracellular signal is transmitted via one of two pathways. Left: In MyD88-dependent signalling, the recruitment of MyD88 and TIRAP to the TIR domain of TLR4 promotes signalling via IRAKs, facilitated by TRAF6, and TAK1, which activates MAPKs and the IkB kinase complex (IKK) leading to activation of NFkB and AP-1, promoting production of pro-inflammatory cytokines. Right: MyD88-independent signalling takes place following the internalisation of the LPS-TLR4 complex, and is activated through recruitment of TRIF and TRAM to the TIR domain of TLR4. This pathway activates TBK1 and facilitates IRF activation and type-I interferon production. Figure modified from (Luo et al., 2025). Created in https://BioRender.com.

polarising cytokines *Il12b, Il6, Lif, Il27*. Tong et al. stimulated BMDMs with lipid A (a component of LPS) and identified weakly induced and potently induced genes (>10-fold induction). Interestingly, for most weakly induced genes, basal transcript levels were higher than those of strongly induced genes. Robust transcriptional response to IFNAR signalling began between 60-120 minutes post-stimulation. The transition to late gene expression involves chromatin post-translational modification upon cell activation, supported by shifts in cellular metabolism providing substrates. LPS stimulation results in a shift to glucose uptake and increased glycolysis and tricarboxylic acid (TCA) cycle flux, generating acetyl-Coenzyme A and leading to increased histone acetylation (Lauterbach et al., 2019).

Macrophages can be primed by prior IFN exposure, influencing the magnitude of the LPS response. Before encountering pathogen-associated molecular patterns (PAMPs), macrophages prime inflammatory responses through autocrine IFN-STAT amplification: constitutive low-level production of type I interferons maintains tonic IFNAR signalling (Gough et al., 2012). Tonic IFN signalling is functionally important *in vivo* despite the low concentrations produced (Gough et al., 2012). Unstimulated BMDMs express guanylate binding proteins (GBPs) in an IFNAR-dependent manner, implying tonic interferon signalling without infection. Constitutive IFN signalling is sufficient to enable GBP activity against intracellular bacteria, enabling release of bacterial components from vacuoles to the cytosol to activate downstream inflammatory pathways (Liu et al., 2018).

Additionally, priming of macrophages by IFNγ, produced by innate lymphoid and natural killer cells, results in macrophages that are hyper-responsive to inflammatory stimuli such as cytokines, type I interferons, and TLR ligands. Priming also promotes production of anti-inflammatory factors (IL10/4/13), cytokines promoting tissue-healing and inflammation resolution. Some evidence suggests mouse peritoneal macrophages express low-level constitutive

IFNγ (Gessani & Belardelli, 1998).

At the 1-hour timepoint post-LPS stimulation, the primary transcriptional response is dominated by MyD88-dependent NFkB activation, as found in an analysis of the transcriptional networks underpinning the activation of murine macrophages by LPS (Raza et al., 2014). The TRIF-dependent IRF3 activation has begun, but IFN-STAT amplification (of secondary response genes) is not yet established. Analysis of this 1-hour timepoint enables investigation of the primary inflammatory transcriptional response, rather than the subsequent secondary response the primary response helps to shape.

The magnitude and character of TLR4 responses are regulated by cellular state at the time of activation: for example, prior inflammatory exposure establishing tolerance, and metabolic status. TLR4 responses are understood to be circadian-regulated, which is consistent with the role of the circadian clock in regulating cellular state.

1.5 Macrophage clocks

1.5.1 Circadian immunity

The mammalian immune system is complex, energy-intensive, adaptable, and operates on multiple timescales in response to threat. Many of the cell types and organs involved in mounting both an innate and adaptive immune response have been found to follow some form of circadian regulation, reviewed by (C. Wang et al., 2022).

In the 1960s, the timing of a dose of LPS in the 24-hour period was first shown to affect the host response to infection, as measured by the number of mice surviving (Halberg et al., 1960). LPS given at ZT10, late in the resting period of these nocturnal animals, resulted in highest

mortality. Adaptive immune observations soon followed such as the observation that antibody-forming cells in spleen varied with timing of immunisation (Fernandes et al., 1976).

This temporal organisation may optimise immune responses to coincide with periods of greatest pathogen exposure during the active phase. In the adaptive system, lymphocyte trafficking, antigen presentation, and T-cell activation all show time-of-day dependence. The presentation of antigens to T-cells is highest in the morning (start of the active period), when an organism is most likely to encounter pathogens (Druzd et al., 2017).

In humans, time-of-day variation is characteristic for certain chronic inflammatory disease conditions. In cases of rheumatoid arthritis, rhythmic effector cells have been identified in arthritic joints (Hand et al., 2016). In asthma, symptoms such as airway inflammation and bronchoconstriction often worsen overnight and in the early morning (Burioka et al., 2010). Lung function also varies through 24-hour-time, with enhanced fluctuations in asthma patients' forced expiratory volume (Durrington et al., 2014). Scheer et al. found that the clock independently modulates asthma severity, disentangling this from behavioural processes like sleep using constant routines or "forced desynchrony" protocols (Scheer et al., 2021).

Acute inflammatory disease similarly has been shown to have time-of-day variation in outcome. In humans, the severity of myocardial injury provoked by surgery is dependent on time-of-day (Montaigne et al., 2018). Outcomes to infection have also been shown to depend on time-of-day. Mice infected with influenza at ZT11 show greater mortality and pathology than those infected at ZT23 (Sengupta et al., 2019). More recently, the same group has shown that IL10 signalling drives this time-of-day difference, with monocytes and macrophages contributing to the gating effect in the whole lung tissue analysed (Forrest et al., 2025).

Mechanisms underpinning the circadian regulation of immunity centre around central-nervous

system derived immunomodulatory signals (nervous or humoral), cell-trafficking and cell-intrinsic clock function (C. Wang et al., 2022). A conserved trait across multiple mammalian species is the rhythm in the number of circulating leukocytes found in the blood. Egress from bone marrow, the origin of haematopoetic stem cells, occurs at the onset of the rest phase, while cells immigrate into peripheral tissues at the start of the active phase, resulting in lower blood leukocyte counts in the active relative to the rest phase (He et al., 2018). This rhythmic recruitment to peripheral tissues is dependent on the global expression of *Arntl*, and on the sympathetic nervous system: time-of-day changes are ablated following surgical sympathetic denervation of tissues or removal of β-adrenoreceptors (Scheiermann et al., 2012).

1.5.2 Circadian regulation in macrophages

There are multiple distinct layers of regulation for macrophage inflammatory responses, both spatial (where the macrophage is in the organism (Lazarov et al., 2023)), and temporal (where it is in its lifecycle (Blacher et al., 2022), in the cell cycle (Daniel et al., 2023), and in the 24-hour light/dark cycle).

The first layer of control the clock imposes on macrophage-driven inflammatory responses is over rhythmic trafficking, with leukocyte numbers peaking in blood during the rest phase (ZT5), and in tissues during the active phase (ZT13) (Scheiermann et al., 2012) (Figure 1.3). The number of monocytes recoverable from blood show troughs at the start of the active period (ZT13). In a thioglycollate-elicitation model, Ly6Chi monocytes showed peak recruitment to the peritoneal cavity at ZT8 (K. D. Nguyen et al., 2013). The adhesion cascade is also dependent on BMAL1 intrinsic to monocytes. However, it is the circadian clock in endothelial cells which seems to be master regulator of rhythmic migration of leukocytes (He et al., 2018).

The clock regulates phagocytosis, imposing time-of-day variation on bactericidal ability. Diur-

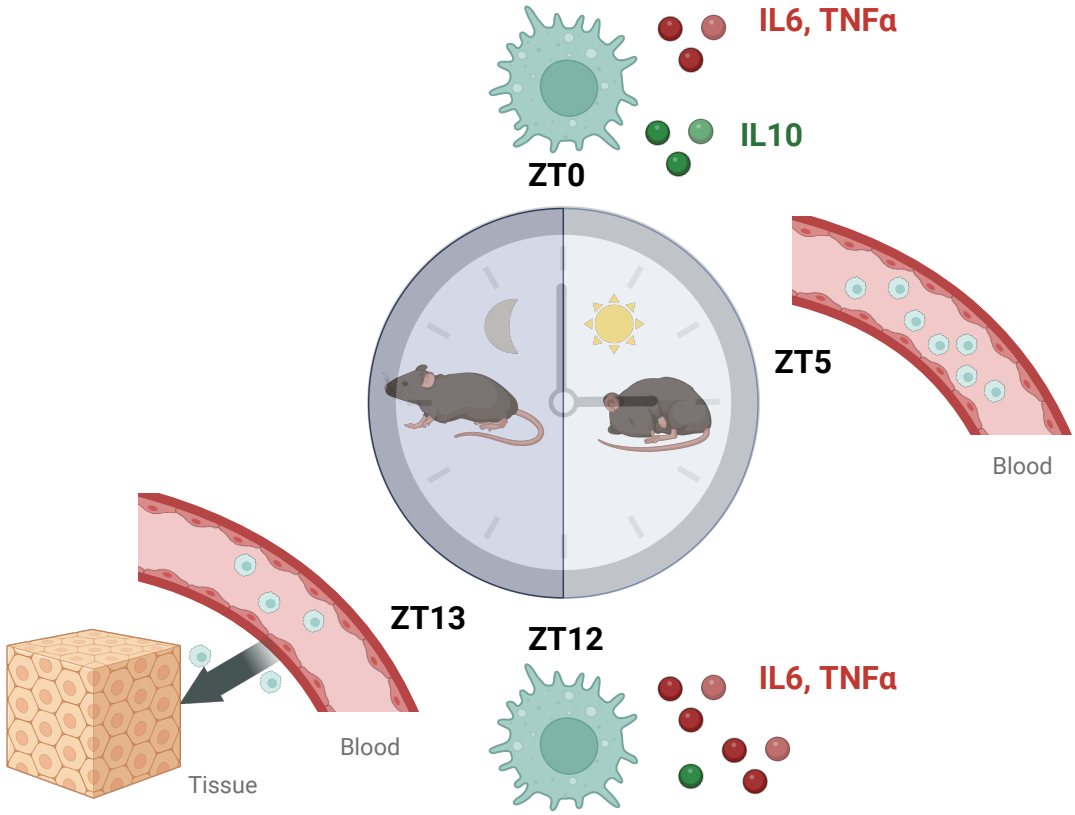

Figure 1.3: **Circadian control of macrophages.**
Within a given tissue, across the 24-hour light/dark cycle there is variation in myeloid cell number and function driven by the molecular clock. Leukocytes are rhythmically trafficked, with peak numbers in blood in the rest phase (ZT5) and in tissues in the active phase (ZT13) (Scheiermann et al., 2012). The peak of pro-inflammatory cytokine production is at ZT12 relative to ZT0, whereas the production of anti-inflammatory cytokine IL10 is higher at ZT0 than at ZT12 (Curtis et al., 2015). The NLRP3 inflammasome shows greatest activation at ZT12 (O'Siorain et al., 2024). Created in https://BioRender.com.

nal regulation of phagocytosis was observed first in *ex vivo* peritoneal macrophages (Hayashi et al., 2007), with circadian observations made in *ex vivo* synchronised peritoneal macrophages (Oliva-Ramírez et al., 2014). More recent reports are conflicting, with Geiger et al. finding that the pattern is lost *in vivo* (Geiger et al., 2019), while Kitchen et al. finding that BMAL1-deletion increased bactericidal ability of macrophages *in vivo*, and that BMAL1 regulates motility and phagocytosis through Rho-A dependent cytoskeletal effects (Kitchen et al., 2020).

There are extensive reports that the macrophage clock gates the production of cytokines, at the level of both transcript and protein. Keller et al. first demonstrated the relevance of the cell-intrinsic clock to macrophage function, with >8% of the macrophage transcriptome oscillating, including inflammatory signalling molecules *Ikba* and *Adam17*. This was followed by demonstration that the macrophage clock gates the production of pro-inflammatory cytokines (IL6 and IL12) and chemokines (CCL5, CXCL1, and CCL2) at transcript and protein level, and that REV-ERBα negatively regulates this process (Gibbs et al., 2012). Later work has found a limited macrophage-intrinsic REV-ERBα effect (Pariollaud et al., 2018), discussed further in the introduction to Chapter 3. LPS responses show time-of-day variation in peritoneal exudate cells treated *ex vivo*, with higher induction of TNFα, IL6, and CXCL1 at ZT12 versus ZT0 (Curtis et al., 2015) (Figure 1.3). BMAL1 deficiency is associated with a heightened inflammatory phenotype (reduced IL10 and increased proinflammatory cytokine/chemokine output). The circadian gating effect for TNFα is lost upon deletion of miR-155, supporting a role for miR-155 in linking the core clock component BMAL1 to inflammatory regulation (Curtis et al., 2015). While these studies establish that the core clock gates macrophage inflammatory responses, the precise mechanisms by which this regulation occurs remain incompletely understood.

1.5.3 Mechanisms of clock component-immune interaction

TLR4 itself does not show circadian variation in macrophages (Silver et al., 2012). Instead, clock components regulate inflammatory responses through transcriptional and metabolic mechanisms operating downstream of receptor activation.

BMAL1 directly regulates the antioxidant response by binding E-box elements in the *Nrf2* promoter (Early et al., 2018). Loss of BMAL1 disrupts this axis, resulting in elevated reactive oxygen species (ROS), HIF-1α accumulation, and increased pro-IL1β production (Early et al., 2018; Timmons et al., 2021). More recently, overexpression of BMAL1 was shown to activate NRF2 signalling, resulting in reduced intracellular ROS release and the inhibition of inflammatory responses (Zeng et al., 2025). BMAL1 also suppresses enhancer RNA transcription at inflammatory loci; its deletion increases *Hif1a* and *Il1b* expression through this mechanism (Oishi et al., 2017). Mitochondrial function is similarly tuned by BMAL1, with heightened mitochondrial membrane potential enhancing NLRP3 inflammasome activation at CT12 relative to CT0 (corresponding to ZT12 and ZT0 respectively) (O'Siorain et al., 2024).

Emerging evidence shows the importance of BMAL1 in regulating macrophage cholesterol homeostasis, with important implications for inflammatory responses. Myeloid-specific BMAL1-deficient mice showed higher cholesterol accumulation in macrophages due to deficiencies in cholesterol efflux capabilities (Pan et al., 2025). The authors show that BMAL1 regulates *Abca1* (cholesterol efflux protein), with reduction of *Bmal1* reducing *Abca1* expression, and overexpression of BMAL1 increasing *Abca1* expression, in part through control of repressor ZFP202.

Genetic deletion of BMAL1, the only non-redundant core clock component, affects activity and expression levels of other clock components, which interact with inflammatory pathways through distinct mechanisms. CLOCK acts as a pro-inflammatory factor, increasing

NFkB activity in mouse endothelial fibroblasts (MEFs), boosting expression of *Il6, Il1b, Tnfa, Cxcl1, Ifnb,* and *Ccl2*. BMAL1 sequesters CLOCK from NFkB subunit RelA (Bellet et al., 2013). Consistent with this, BMAL1-deletion increases RelA phosphorylation, increasing pro-inflammatory cytokine expression (Curtis et al., 2015). PER1/2 suppress basal and LPS-induced *Tnfa* and *Il1b* expression, potentially via PPARγ-mediated repression of *Ccr2* (T. Wang et al., 2016; H. Xu et al., 2014). CRY negatively regulates the cAMP-PKA-NFkB pathway, with CRY-deficient macrophages showing constitutive upregulation of *Il6, Tnfa,* and *iNos* (Narasimamurthy et al., 2012). RORα deletion in human THP-1 cells similarly increases basal pro-inflammatory cytokine expression for TNF, pro-IL1β and IL6 (Moharrami et al., 2018).

Overall, macrophages mount a greater inflammatory response at the end of the rest phase (ZT8-12), corresponding to peak host susceptibility to endotoxic shock (Curtis et al., 2015). However, this time-of-day mortality effect appears to be conferred by systemic cues (such as light-dark cycles) (Lang et al., 2021). The myeloid clock modulates time-of-day mortality, but myeloid-specific deletion of BMAL1 does not completely ablate this time-of-day effect, highlighting the complexity of using sepsis mortality as a read-out of macrophage clock function, due to the involvement of multiple cell types and organ systems.

Beyond NFkB-dominant cytokine production, the clock regulates interferon production and response. Deletion of CRY1/2 results in upregulation of viral recognition proteins and type I interferon (IFN) effectors in basal homeostatic conditions in lung fibroblasts (Major-Styles et al., 2025). Similarly, BMAL1 deletion or inhibition enhances ISG expression upon TLR stimulation in mouse skin and human lung cells (Greenberg et al., 2020; Zhuang et al., 2021). This suggests clock disruption results in constitutively primed cells, with enhanced responsiveness to inflammatory stimuli.

Inflammatory signalling is bi-directional with clock outputs. The macrophage clock responds

to inflammatory signalling, including IFN-signalling, by dampening amplitude (S. Chen et al., 2020; Curtis et al., 2015).

While individual clock-immune interactions have been characterised, the genome-wide landscape of clock-dependent inflammatory gating remains incompletely defined, particularly in tissue-resident macrophages and across sexes. Moreover, the clock has been shown to exert effects on disparate aspects of the inflammatory response system, but there is limited understanding of the gene regulatory mechanism(s) which underly these observations.

1.6 Sexual dimorphism in the immune system

For many years any differences in immune function between sexes has been poorly understood due to a male bias in pre-clinical and clinical research. Biological sex at birth (as opposed to self-identified gender) has been found to affect the function of multiple organ systems outside of the reproductive system, and to predispose individuals to different diseases, recently reviewed by Sharma et al. (Sharma et al., 2025). This bias in the evidence base reduces the scope for successful translation to clinical applications. Males are typically at higher risk (in terms of both incidence and severity) for acute viral and microbial infections, and certain cancers associated with infection (Klein & Flanagan, 2016). However, females are more likely to develop chronic effects of infection (inflammatory conditions), and autoimmune diseases more widely (Silva & Iwasaki, 2024). Exceptions include autoimmune diseases starting in childhood before sex hormones peak, such as type 1 diabetes.

Outside of environmental factors such as differences in nutrition or chemical exposures, there are two non-mutually-exclusive major genetically-determined mechanisms influencing the immune system: sex hormone effects, and cell-intrinsic effects linked to X-chromosome dosage.

Steroid hormones shape inflammatory responses. Ratios of immune cell types differ between sexes, with females showing higher T and B cell counts due to lower testosterone, and males exhibiting greater natural killer cell counts (Silva & Iwasaki, 2024). Androgen inhibits the production of antibodies post-vaccine through regulation of effector CD8+ T cell proliferation (Vom Steeg et al., 2019), potentially also the mechanism by which males show poorer response to certain cancer treatments (Guan et al., 2022). In general, testosterone exerts immunosuppressive effects while estrogen exerts immunostimulatory effects, although for each sex hormone the regulation of immune function is context-dependent and not simply pro or anti inflammatory (Sharma et al., 2025). Estrogen contributes to sex differences in asthma, which is consistent with the observation of higher asthma prevalence in females in the age ranges post-puberty and pre-menopause (Keselman et al., 2017)).

Typically, every female has two X chromosomes, with one mostly inactivated through condensation into heterochromatin early in embryonic development in a process mediated by the long noncoding RNA *Xist* and other RNA-binding proteins. The X-chromosome contains a high number of immune-related genes, and so the incomplete X-inactivation of approximately 20-30% of genes in the inactive chromosome results in different dosage of these gene products in individuals with one copy versus individuals with two copies. Immune genes on the X chromosome include PRRs (*Tlr7, Tlr8)* and transducers of activation like *Irak1, Foxp3, Cd40l* (Forsyth et al., 2024).

1.6.1 Sexual dimorphism in macrophage biology

Sexual dimorphism in macrophage biology has been observed within many kinds of animals from mammals to reptiles (Klein & Flanagan, 2016). For example, when untreated and interferon-stimulated immune cells from male and female mice are profiled, macrophages consistently

show transcriptional sexual dimorphism, which is amplified after interferon stimulation (Gal-Oz et al., 2019).

The functional consequences of macrophage sexual dimorphism are context-dependent, varying with stimulus, tissue, and species. Female macrophages generally show higher phagocytic activity (Klein & Flanagan, 2016). Sex-dependence of cytokine responses depends on the pathway examined: in mice, the first study to document sex differences in TLR4 activation found that male peritoneal macrophages express higher TLR4 levels, and female macrophages produced higher levels of anti-inflammatory prostanoids (lipid mediators) (Marriott et al., 2006). In human peripheral blood mononuclear cells (PBMCs, lymphocytes and monocytes), more TNF is produced by males than females following LPS stimulation (Asai et al., 2001), and male PBMCs also produce more IL10 upon TLR9 activation (Torcia et al., 2012).

The effects of hormones on macrophage activity are complex. Macrophages express progesterone receptors (PR, broadly anti-inflammatory action), estrogen receptors (ERα/β, bipotential effects on human macrophages with low doses immunostimulatory for IL1/ IL6/ TNF and high doses reducing production of the same pro-inflammatory cytokines), and androgen receptors (AR, considered anti-inflammatory) (Klein & Flanagan, 2016). The levels of hormone receptor expression has functional consequences in macrophages: greater expression of AR has recently been found to drive higher expression of cytokines IL6 and iNOS (X. Wang et al., 2025).

In addition to hormonal regulation, cell-intrinsic differences persist *ex vivo*. Male-female differences in BMDMs remain present when cells are cultured *ex vivo*, with no steroid hormone stimuli (Bhasin et al., 2008). Consistent with a model where female cell-autonomous immunity is more robust (at the cost of autoimmune pathology), female monocytes produce a more robust IL6 response than male, which is attributed to regulation by autonomic mechanisms (vagal tone) and not sex hormones (O'Connor et al., 2007).

Peritoneal macrophages have been identified as one of the most sexually dimorphic immune cells at the level of gene expression and chromatin accessibility (Gal-Oz et al., 2019). In accordance with these transcriptomic findings, Bain et al. have extensively characterised the murine basal state peritoneal cavity for males and females and found that the rate of replenishment and proliferation is higher in male macrophages (Bain et al., 2020). This effect was dependent on the absence of the female reproductive tract and was re-created in gonadectomised female mice.

1.6.2 Sexual dimorphism in chronobiology

In recent years, progress has been made establishing where biological sex regulates differences in circadian parameters in humans and other organisms, recently reviewed by Paschos et al. (Paschos et al., 2025). In humans, there are sex differences in circadian behaviour: females show phase-advanced timing relative to males (as shown by core body temperature minimum and the evening rise in melatonin), and melatonin rhythm with shorter period and larger amplitude.

Recent molecular evidence of sex differences comes from an analysis of gene expression rhythms in 46 tissues from 914 donors (Talamanca et al., 2023). The authors found that most tissues examined showed greater numbers of rhythmic transcripts in females. However, tissues with high immune cell content showed the opposite pattern: spleen showed greater rhythmicity in males than females.

Consistent with this, recent studies have identified significantly more rhythmically-expressed genes in female heart tissue relative to male, driven by cardiomyocyte-intrinsic clocks (this difference was reduced upon cardiomyocyte-specific BMAL1-deletion) (X. Zhang et al., 2025), and greater number of oscillating genes in female liver than male (Astafev et al., 2024). This sex difference may reflect increased robustness of female behavioural and metabolic rhythms:

a synchronisation in behaviour and feeding between sexes (through 30% caloric restriction) reduced these differences in rhythmicity of genes between sexes (Astafev et al., 2024).

Evidence for sex-clock interactions in pathology suggests sex is a risk factor for negative effects of circadian disruption, although this is context-dependent. The directionality of sex on outcome depends on the tissue or disease, as well as the desynchrony protocol and additional interventions used. Whether the greater rhythm amplitude typically observed in females confers resilience to circadian disruption or instead amplifies pathological consequences remains debated (Lok et al., 2024; Paschos et al., 2025). If females show more robust rhythms, we might expect female immune cells to show greater clock-dependence. However, tissue-specificity in circadian sex differences suggest the relationship may depend on tissue-context.

In humans, the evidence that females are more affected by circadian disruption includes the higher injury rates during night work observed in females than males, despite similar rates in day workers (Spitschan et al., 2022). After forced desynchrony protocols (uncoupling endogenous circadian rhythms from the sleep-wake cycle), females showed higher rates of negative consequences: greater impairment in cognitive performance during circadian misalignment, alongside altered metabolic hormone profiles changing food choices (Walton et al., 2022). Most recently, Maidstone et al. showed that shift work increases asthma exacerbation risk in females but not males (Maidstone et al., 2025).

However, a greater increase in onset of metabolic disorders (diabetes, metabolic syndrome) has been observed in male shift workers compared to female (Anderson et al., 2023). Among irregular shift workers, males showed impaired cardiac performance (Zhou et al., 2023).

In mice, evidence is similarly dependent on context. In an atherosclerosis model, Apolipoprotein E-deficient mice with chronic jet-lag exacerbated atherosclerosis in female and not male

mice. This was attributed to increased atherogenic VLDL/LDL particles, as no changes in feeding-fasting cycles were observed. In general, females showed greater pathology resulting from perturbation of the clock (Chalfant et al., 2023).

In contrast, male mice were more greatly affected by a chronic jet-lag protocol combined with high-fat diet, resulting in males losing rhythmicity in peripheral tissues and developing glucose intolerance, while females were resilient to changes. This appears linked to a shift in rhythms in gut microbiota abundance (changed in males, and not females), mediated in part through estrogen (evidenced by ovariectomy impairing female re-entrainment to misalignment protocol) (Anderson et al., 2023). Males were more affected by genetic perturbation of clock components in models investigating circadian blood pressure (Paschos et al., 2025).

Despite these observations, we lack information on mechanisms linking sex and the clock: work to investigate these mechanisms may explain the context-dependence of sex effects on circadian disruption. Sex differences in circadian physiology may stem from the different systemic rhythmic signals in females and males due to differing metabolic or hormonal profiles, and/or sex-specific cell-intrinsic rhythm mechanisms.

In humans, sex-dependent clock-gene polymorphisms have been identified: SNPs of RORA has been found with decreased melanoma susceptibility in women only, with different SNPs in RORA with lower risk found in men, implicating sex differences in core clock function (Benna et al., 2021). Sex hormones affect the anatomy of the SCN, and SCN structures express estrogen and androgen receptors in different patterns. Hormones show circadian rhythms: estradiol and progesterone show circadian rhythmicity in the follicular phase only, and follicle-stimulating hormone shows rhythmicity throughout the menstrual cycle. Similarly, testosterone secretion in males shows diurnal fluctuations, with peak levels around waking (Lok et al., 2024).

In rodents, there is greater evidence of sex differences in cell-intrinsic clock function. Cell-intrinsic sex differences have been identified in cardiac tissue (X. Zhang et al., 2025). Sex differences have been found in the regulation of circadian blood pressure, mediated by kidney collecting duct BMAL1-deletion affects males and not females (D. Zhang et al., 2020). Johnston et al. found that global BMAL1-KO affects sodium excretion rhythms in males, and not females, suggesting a greater influence of systemic signals on female rhythms (Johnston et al., 2020). Studies have also identified sex-specificity of circadian transcriptomic programs in liver, with female rhythms enriched for cell-signalling and protein transport, and male rhythms enriched for drug/steroid metabolism (Weger et al., 2019).

Increasing our understanding of sex-clock interaction mechanisms will directly benefit chronotherapy and personalised medicine approaches. Sex affects chemotherapy tolerability, with female patients more susceptible to side effects of widely-used drugs. The optimal timing for anti-cancer drugs oxaliplatin and 5-FU leucovorin (as determined by timepoint of least toxicity) was delayed by 6 hours in female patients relative to males (Lévi et al., 2007). Moreover, a recent study investigating chronotherapy for lymphoma has found that female patients are more likely to benefit from time-specific therapy relative to male, associated with a higher amplitude in circulating leukocyte and neutrophil numbers (D. W. Kim et al., 2023).

Given sexual dimorphism in chronobiology, and in the prevalence of inflammatory diseases, an interaction between sex and circadian immune regulation presents a plausible hypothesis. Peritoneal macrophages show significant sex-dimorphism (Gal-Oz et al., 2019), making the peritoneal compartment an ideal system to test this question.

1.7 Pharmacological targeting of clock components

A key goal for the chronobiology field is the pharmacological manipulation of the circadian clock for the development of refined experimental tools and potential therapeutics. Small molecules that stabilise, activate, or inhibit core clock components could alter clock amplitude and phase alignment, while the TF activity of clock components themselves represents a therapeutic target for their downstream programmes. Circadian rhythm dynamics often reflect health status: deviations from population-normal function of circadian rhythms are pathological hallmarks in many diseases, including cancers, metabolic disorders, and psychiatric conditions, and there is a notable decrease in amplitude of rhythms associated with ageing (Rasmussen et al., 2022). Additionally, efficacy of drugs has been shown to vary based on the time given, with more than half top-selling drug targets being proteins from rhythmic genes (R. Zhang et al., 2014). The potential for clock-targeting molecules to improve outcomes in metabolic disease and cancer has been reviewed extensively (Laothamatas et al., 2023; Tavsanli et al., 2024).

Beyond translation into circadian therapeutics, developing clock-targeting small molecules as tool compounds would address the problems of using genetic knock-out models to advance understanding of circadian programs. As a network of interlocking feedback loops, the manipulation of one component often has compensatory effects on the activity of others. Small molecule tools can be used with temporal precision and are not permanent. This avoids the confounding developmental effects of genetic deletion and allows researchers to probe the functions of BMAL1 in each cellular type or state, rather than BMAL1's functions during the development of the same system.

CRY stabilisers identified include KL001, which directly binds CRY1/2 to block ubiquitin-dependent degradation and lengthen period (Hirota et al., 2012), shown to improve glucose

tolerance *in vivo*. A CRY inhibitor has been found to exert anti-proliferative effects in human breast cancer cells, proof of principle for targeting the clock for disease (Chun et al., 2015). Much of the early-stage discovery work has focused on ligands for nuclear receptors (REV-ERBs, RORs), TFs with endogenous ligands. However, many of the compounds developed do not achieve criteria necessary as high-quality tools: for example, the widely used REV-ERBα ligand SR9009 has been documented to have REV-ERB independent effects (Dierickx et al., 2019). Additionally, for many of these compounds use *in vivo* has been limited by poor pharmacokinetic profiles (Rasmussen et al., 2022).

BMAL1 is the only non-redundant core clock component: unlike PER1/2, CRY1/2, or REV-ERBα/β, which show functional compensation, BMAL1 deletion alone abolishes circadian rhythmicity (Bunger et al., 2000). Pharmacological BMAL1 modulation would therefore enable testing of BMAL1-centric hypotheses without the compensatory effects that confound interpretation of other clock gene perturbations. BMAL1 and CLOCK belong to the bHLH-PAS family of TFs, many of which have been implicated in human disease, leading to the targeting of these proteins for drug screens. HIF2α has been shown to bind small molecules in the PAS-B pocket, which inhibits transcriptional activity of HIF2α:ARNT, proving the PAS-B pocket can be targeted successfully (Scheuermann et al., 2013). Structural studies reveal that BMAL1 possesses a larger PAS-B binding pocket than CLOCK, though smaller than HIF2α, suggesting tractability for small molecule targeting (Rasmussen et al., 2022). Until the recent development of BMAL1-targeting Core Circadian Modulator (CCM), no small molecule tool for BMAL1 modulation has been available (Pu et al., 2025).

1.8 Thesis aims

This thesis addresses three interconnected questions regarding the circadian regulation of macrophage inflammatory responses.

Aim 1: Identify BMAL1-dependent mechanisms of circadian inflammatory gating *in vivo*. Previous work has established that macrophages show time-of-day variation in inflammatory responses, but the molecular mechanisms and requirement for intrinsic macrophage clock function *in vivo* remain unclear (section 1.5.2). Experiments have largely been performed *ex vivo*, and we lack evidence in tissue-resident macrophage populations as to whether the time-dependent transcriptome is dominated by a) systemic cues (glucocorticoids, sympathetic signalling/hormonal signals, metabolites), b) signals from clock-regulated non-myeloid cells, or c) intrinsic, macrophage clock–regulated effects. Moreover, previous work has identified specific clock component REV-ERBα to be essential in mediating the anti-inflammatory effects of the macrophage clock *ex vivo*, but its necessity for clock-dependent gating of the LPS response has not been definitively tested *in vivo*. Using myeloid-specific BMAL1 deletion, I aimed to:

- Define the scope of BMAL1-dependent transcriptional gating at ZT0 versus ZT12.
- Test whether REV-ERBα is necessary for circadian gating.
- Determine the relative contributions of chromatin accessibility and TF availability to mediating gating.

Aim 2: Test whether sex modifies BMAL1-dependent circadian gating *in vivo*. Sex-clock integration in immunity is unexplored. Peritoneal macrophages show pronounced sexual dimorphism (section 1.6.1), but whether sex and clock systems interact has not been tested. I aimed

to:

- Quantify sex-specific BMAL1-dependent gene sets.
- Test for statistical interaction between sex and time-of-day.
- Identify TFs showing sex-specific circadian regulation.

Aim 3: Evaluate pharmacological BMAL1 modulation of macrophages *in vitro* using a novel compound. Pharmacological manipulation of the clock in macrophages affects inflammatory responses. No tool has previously been available for acute BMAL1 manipulation (section 1.7). Using the novel compound CCM, I aimed to:

- Characterise CCM effects on circadian oscillation parameters.
- Identify BMAL1-dependent transcriptional responses to CCM.
- Assess CCM effects on macrophage morphology, motility, and phagocytosis.

1.8.1 Models used

Studies on macrophage circadian biology have predominantly used BMDMs and global clock gene knockouts, which carry limitations such as i) the differentiation of macrophages in non-physiological context, and ii) confounding effects on multi-organ systems. In this thesis, I used myeloid-specific BMAL1-deletion in peritoneal macrophages to isolate cell-intrinsic clock function in tissue-resident context, and I used BMDMs to characterise the effects of the novel BMAL1-targeting compound CCM.

For Aims 1-2, the LPS stimulation used (1 hour, 1 mg/kg intra-peritoneal injection) captures the early transcriptional response prior to secondary feedback loops. The timepoints used (ZT0 and ZT12) represent antiphasic timepoints for BMAL1 expression and correspond to well-studied

troughs and peaks for inflammatory gene expression.

2 | Materials and Methods

2.1 Animal models

PER2::Luc mice, in which a luciferase reporter is knocked into the endogenous *Per2* locus, were originally obtained from Joseph Takahashi's laboratory (University of Texas Southwestern Medical Center) and maintained as homozygotes (Yoo et al., 2004). LysM-Bmal1$^{flox/flox}$ mice were obtained from Andrew Loudon's laboratory (University of Manchester). In this model, exon 8 of *Bmal1* is flanked by LoxP sites (Lamia et al., 2008). Cre recombinase is expressed under the control of the Lyz2 promoter (encoding lysozyme-M), enabling myeloid lineage specific deletion of BMAL1 (Clausen et al., 1999). Mice were bred to maintain Cre heterozygously, such that offspring heterozygous for Cre exhibited myeloid-specific BMAL1 deletion and were compared to Cre-negative littermate controls with intact BMAL1. LysM-Rev-Erb$\alpha^{flox/flox}$ mice were generated at the University of Manchester using a similar strategy, where LoxP sites were inserted into intron 2 and intron 6 of *Rev-Erb*α (Hunter et al., 2020). Cre recombinase expression was similarly targeted to the myeloid lineage via the Lyz2 promoter. Mice were bred to maintain Cre heterozygously, such that offspring heterozygous for Cre exhibited myeloid-specific REV-ERBα deletion and were compared to Cre-negative littermate controls with intact REV-ERBα.

For all experiments, the Cre-positive mice were age- and sex-matched with Cre-negative littermate controls. Mice were 10-16 weeks old at the time of experiments and included both males and females unless otherwise stated.

All animals were maintained in the University of Oxford Biomedical Services under specific pathogen-free conditions. All protocols were approved by the University of Oxford Animal

Welfare and Ethical Review Body and carried out according to the Animals (Scientific Procedures) Act 1986 (under PPL PP7065079). Food and water were provided ad libitum, and routine housing was under 12 hour light/dark cycles, under controlled room temperature (21–23°C) and 50% humidity.

2.1.1 Genotyping

Ear clips were taken from all experimental animals at approximately 2 weeks old. DNA was extracted using REDExtract-N-Amp Tissue PCR (Sigma-Aldrich 254-457-8) according to manufacturer's protocols.

PCR was performed using the extracted gDNA as a template. Each reaction contained Extract-N-Amp PCR Reaction Mix, nuclease-free water, and sequence-specific primers (IDT, custom oligonucleotides). Amplification was carried out on a thermocycler. All primer sequences, reaction component volumes, and thermal cycling parameters for each specific mouse line are detailed below:

PER2::Luc primer sequences

Forward	5′-CTGTGTTTACTGCGAGAGT-3′
WT Reverse	5′-GGGTCCATGTGATTAGAAAC-3′
Mutant Reverse	5′-TAAAACCGGGAGGTAGATGAGA-3′

Step	Temperature (°C)	Time
1	94	2 minutes
2	94	30 seconds
3	58	30 seconds
4	72	1 minute
5	72	5 minutes (final extension)
6	4	Hold

Table 2.1: **PCR cycling program for PER2::Luc genotyping.**

Notes: Repeat steps 2–4 for 30 cycles. Expected band sizes: WT ≈ 230 bp; Mutant ≈ 650 bp.

LysM-*Bmal1*$^{\text{flox/flox}}$ primer sequences

LysM WT Forward	5′-CTTGGGCTGCCAGAATTTCTC-3′
LysM WT Reverse	5′-TTACAGTCGGCCAGGCTGAC-3′
LysM Cre Reverse	5′-CCCAGAAATGCCAGATTACG-3′

Step	Temperature (°C)	Time
1	94	2 minutes
2	94	30 seconds
3	63	30 seconds
4	72	1 minute
5	72	5 minutes (final extension)
6	4	Hold

Table 2.2: **PCR cycling program for LysM–*Bmal1* genotyping.**

Notes: Repeat steps 2–4 for 30 cycles. A LysM-Cre band (WT Fwd + Cre Rev) is ≈ 700 bp and is scored as present (+) or absent (-).

PCR amplicons were analysed by gel electrophoresis on 2% agarose (Appleton) gels prepared in Tris-Borate-EDTA (TBE) buffer and containing SYBR Safe (Thermo Fisher) nucleic acid stain. Electrophoresis was conducted at a constant 110V for approximately 40 minutes. Gels were visualised using the EpiBlue channel on an Azure 600 imaging system. For LysM-Rev-Erba$^{flox/flox}$ mice, Transnetyx (Cordova, TN) determined genotypes using specific probes designed for each gene.

2.2 Cell isolation and culture techniques

2.2.1 Chapters 3 and 4: experimental set-up

Mice were entrained to 12:12 light:dark cycles in light tight cabinets (LTCs). At the desired timepoint (ZT0 or ZT12), LPS (1 mg/kg, isolated from *E.coli* 0127:B8, Sigma-Aldrich L4516-1 mg) in saline vehicle (sodium chloride 9 mg/ml, Kent Pharmaceuticals), or vehicle alone, was administered by intraperitoneal injection. 1 hour later (ZT1 or ZT13) mice were sacrificed via cervical dislocation.

2.2.2 Isolation of peritoneal macrophages

Mice were sacrificed via cervical dislocation. Using scissors and forceps, the outer skin of the peritoneum was cut, pulled back to expose the peritoneum, and 10 ml ice-cold PBS (Gibco, 14190-094) was injected into the peritoneal cavity using a 25G needle (Terumo Agani). After injection, the peritoneum was gently massaged to dislodge any attached cells into the PBS solution. An 18G needle, attached to a 10 ml syringe, was inserted bevel up in the peritoneum and the fluid was collected while gently moving the tip of the needle to avoid clogging on tissue. The collected cell suspension was kept on ice, and if visibly contaminated with blood the sample was discarded. Peritoneal exudate was then purified using magnetically activated cell sorting (MACS) according to manufacturer's instructions (Miltenyi Biotec, 130-110-434). Macrophages were negatively selected: non-target cells were labelled with a cocktail of biotin-conjugated monoclonal antibodies. Use of a secondary labelling reagent, anti-biotin monoclonal antibodies conjugated to microbeads, enabled the retention of the magnetically labelled non-target cells in MACS columns in the magnetic field of a MACS separator. Unlabelled macrophages passed through the column, without modification/labelling.

To perform MACS, the collected peritoneal cell suspension was centrifuged (300 x G, 10 minutes, 4°C). Supernatant was aspirated and discarded, and the pellet resuspended in 36 μl of MACS buffer with 4 μl of FcR blocking reagent.

MACS buffer: PBS, 0.5% bovine serum albumin (Sigma-Aldrich), 2 mM EDTA (Invitrogen, AM9260G)

10 μl of biotin-antibody cocktail reagent was added, and the suspension was incubated for 10 minutes (4°C). Cells were washed with the addition of 1 ml MACS buffer and spun at 300 x G for 10 minutes. Supernatant was aspirated and discarded, and pellet resuspended in 80μl MACS buffer. 20 μl of anti-biotin beads were added and incubated at 4°C for 15 minutes. Cells were washed with the addition of 1 ml MACS buffer and spun at 300 x G for 10 minutes. Supernatant was aspirated and discarded, and pellet resuspended in 500 μl MACS buffer. MACS columns were placed in the field of the MACS separator magnet and prepared with rinsing of 500 μl MACS buffer. The cell suspension was then passed through the column, and the flow-through fraction enriched for macrophages was collected. The column was washed with 3 x 500 μl MACS buffer, continuously collecting the flow-through fraction. Cell suspension was spun at 300 x G for 10 minutes (4°C), before resuspension of the cell pellet in the appropriate reagent for downstream experiments.

Enrichment was assessed by flow cytometry on singlet events after exclusion of debris by FSC-H/SSC-H and doublets by FSC-Width. F4/80-FITC and MHCII-PE were quantified. In two QC preparations, 91.4% and 92.5% of singlets were F4/80$^+$, and 8.8% and 7.6% were MHCII$^+$.

2.2.3 Production of bone-marrow derived-macrophages

BMDM medium: DMEM, 10% heat-inactivated FBS (Gibco, 16000044), 20 ng/ml recombinant M-CSF (Invitrogen, PMC2044), 1% Pen/Strep (Gibco, 15140-122), 1% L-Glutamine (Gibco,

25030-024)

Isolation of BMDMs was performed as follows. Tibias and femurs were dissected; bone marrow was flushed using 10 ml DMEM for each bone. The suspension was spun at 500 x G for 5 minutes (room temperature), and the pellet resuspended in 2 ml RBC lysis buffer (Life Technologies, 00-4333-57). After 3 minutes on ice, the solution was quenched with 10 ml BMDM media and resuspended. The suspension was filtered using 100 μM cell strainers (Greiner, 542000) and spun at 500 x G for 5 minutes (room temperature). The pellet was resuspended in 10 ml BMDM media. The resulting suspension was plated out to two non-tissue culture treated petri dishes (Fisher Scientific, 11349273) and incubated. On day 4 after isolation, 5 ml of fresh BMDM media was added to each plate. On day 7, BMDM were replated. 8 ml ice-cold PBS was added to each plate, and each plate left on ice for 2 minutes. Then, a 5 ml pipette was used to lift the cells and transfer to a 50 ml tube. A sample was taken for cell-counting, and the remaining cells were spun at 500 x G for 5 minutes. The pellet was resuspended in BMDM media at 1x10^6 cells/ml and plated out at the required density.

2.3 Next-generation sequencing assays

2.3.1 RNA extraction

Cells were lysed in TRIzol reagent (Invitrogen, 15596026) following manufacture's instructions, and RNA was extracted using chloroform followed by RNA Clean & Concentrator (Zymo Research, R1013).

For each sample, 0.5 ml TRIzol was used per 1x$10^5 - 10^7$ cells. The lysate was centrifuged at 12000 x G for 10 minutes at 4°C. The clear supernatant was transferred to a new 1.5 ml low DNA-binding tube (Sarstedt, 72.706.700) and incubated at room temperature for 5 minutes.

Chloroform was added (200 μl per 1 ml of TRIzol), vortexed for 15 seconds, incubated at room temperature for 3 minutes, then spun at 12000 x G for 15 minutes at 4°C. The colourless aqueous phase was transferred to a new 1.5 ml tube. One volume of 100% ethanol (150 μl) was mixed with the aqueous phase, vortexed, and added to a Zymo-Spin IC Column. The sample was spun at 16000 x G for 30 seconds before 400 μl RNA Wash Buffer was added to the column and spun at 16000 x G for 30 seconds. Each sample was treated with 40 μl DNase I reaction mix (DNase I (reconstituted; 1 U/μl) 15 μl, DNA Digestion Buffer 35 μl) and incubated at room temperature for 15 minutes. 400 μl RNA Prep Buffer was added to the column and spun at 10000 x G for 30 seconds. 700 μl RNA Wash Buffer was added to the column and spun at 10000 x G for 30 seconds. 400 μl RNA Wash Buffer was added to the column and spun at 10000 x G for 1 minute to ensure complete removal of the wash buffer. The column was transferred into a new tube, and 15 μl DNase/RNase-free water was added to the column matrix directly and spun at 10000 x G for 30 seconds to elute RNA.

RNA was quantified using Qubit RNA assay (ThermoFisher, Q32852), and quality assessed by Tapestation 4150, High Sensitivity RNA ScreenTape (Agilent Technologies, 5067-5579).

2.3.2 ATAC-seq library preparation

ATAC-seq libraries were prepared according to the kit manufacturer's instructions with modifications as described below (Active Motif, 53150). Peritoneal macrophages or BMDMs were counted (Cellometer Auto T4, Nexcelom) and 75,000 cells were aliquoted, spun at 500 x G for 5 minutes (4°C). Supernatant was aspirated, and cells resuspended in 100 μl ice-cold PBS. Cells were spun at 500 x G for 5 minutes (4°C), supernatant aspirated, and cells resuspended in 100 μl ice-cold ATAC lysis buffer and transferred to PCR tubes on ice. Samples were immediately centrifuged at 500 x G for 10 minutes at 4°C to pellet nuclei. During centrifugation,

Tagmentation Master Mix was prepared for each sample, containing 25 μL 2X Tagmentation Buffer, 2 μL 10X PBS, 0.5 μL 1.0% Digitonin, 0.5 μL 10% Tween-20, 12 μL H_2O, and 10 μL Assembled Transposomes. After centrifugation, supernatant was carefully removed without disturbing the nuclear pellet. 50μl of Tagmentation Master Mix was added to each sample and nuclei were gently resuspended by pipetting. To assess optimal tagmentation conditions, two technical replicates were performed with tagmentation times of 30 minutes and 35 minutes at 37°C with shaking at 800 rpm in a thermomixer. Immediately following tagmentation, samples were transferred to 1.5 mL microcentrifuge tubes and 250 μL DNA Purification Binding Buffer plus 5 μL 3 M sodium acetate were added. Solution pH was verified by visual inspection of the pH indicator dye (bright yellow colour, indicating pH <7.5) before proceeding. Tagmented DNA was purified using the provided spin columns according to manufacturer's instructions, including two washes with 750 μL Wash Buffer (containing 80% ethanol) and elution in 35 μL DNA Purification Elution Buffer. Purified tagmented DNA (33.5 μL) was amplified by PCR using unique i7 and i5 indexed primers (2.5 μL each at 25 μM), 1 μL 10 mM dNTPs, 10 μL 5X Q5 Reaction Buffer, and 0.5 μL Q5 Polymerase (2 U/μL). The PCR program consisted of an initial extension at 72°C for 5 minutes, denaturation at 98°C for 30 seconds, followed by 10 cycles of 98°C for 10 seconds, 63°C for 30 seconds, and 72°C for 1 minute, with a final hold at 10°C. Libraries were purified using SPRI beads at a 1.2X ratio (60 μL beads per 50 μL PCR reaction), with two washes using 180 μL freshly-prepared 80% ethanol, and elution in 20 μL DNA Purification Elution Buffer. Final libraries were quantified using Qubit dsDNA assays (ThermoFisher, Q32851), and quality assessed by Tapestation 4150, High Sensitivity DNA ScreenTape (Agilent Technologies, 5067-5584) prior to sequencing by Novogene.

2.3.3 RNA-seq: primary data processing

RNA-seq was performed by Novogene. Messenger RNA was purified from total RNA using poly(T) oligo-attached magnetic beads. After fragmentation, the first-strand cDNA was synthesised using random hexamer primers, followed by second-strand cDNA synthesis. The library was checked with Qubit and real-time PCR for quantification and Bioanalyzer for size distribution detection. Libraries were sequenced on an Illumina NovaSeq 6000 platform using 150 bp paired-end sequencing with a target depth of 20 million reads per sample.

Raw data (raw reads) of fastq format were first processed using fastp software. In this step, clean data (clean reads) were obtained by removing reads containing adapter, reads containing poly(N) and low-quality reads from raw data. At the same time, Q20, Q30 and GC content for the clean data was calculated. Index of the reference genome was built using HISAT2 version 2.0.5, and paired-end clean 2 reads were aligned to the reference genome using HISAT2 version 2.0.5. featureCounts version 1.5.0-p3 was used to count the read numbers mapped to each gene.

2.3.4 ATAC-seq: primary data processing

The prepared ATAC libraries were submitted for sequencing to Novogene. Libraries were sequenced on an Illumina NovaSeq 6000 platform using 150 bp paired-end sequencing with a target depth of 40-50 million reads per sample.

2.3.4.1 Read processing and alignment

To ensure reproducibility, pre-processing of the ATAC data was performed using CATCH-UP, a Snakemake-based pipeline incorporating best practice bioinformatics tools (Figure 2.1) (Riva et al., 2023). Software versions are listed in Table below (Table 2.3).

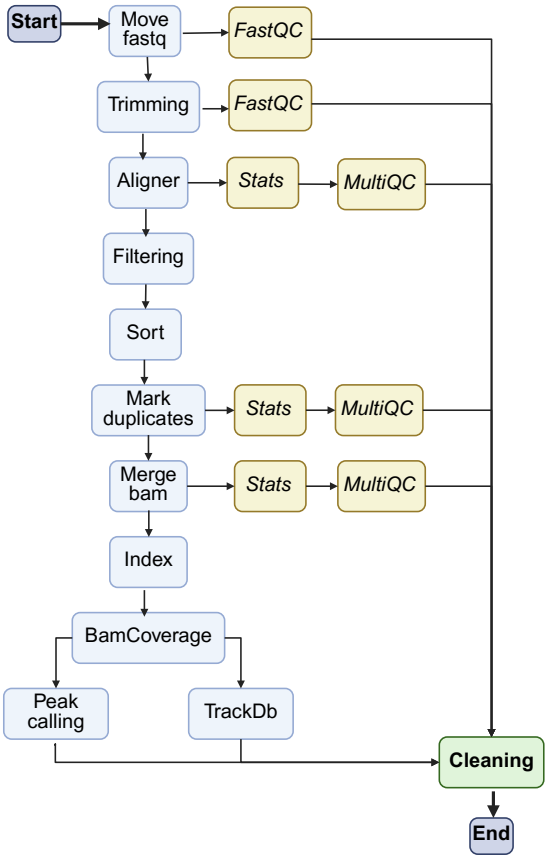

Figure 2.1: **Workflow of CATCH-UP.**
From an input list of fastq files, CATCH-UP was used to process all samples through upstream steps (in blue), producing a result, log, and quality control output for each step. Modified from (Riva et al., 2023). Created in https://BioRender.com

Tool name	Version	Reference
Trimmomatic	0.39	(Bolger et al., 2014)
Bowtie2	2.5.1	(Langmead & Salzberg, 2012)
bwa-mem2	2.2.1	(Vasimuddin et al., 2019)
samtools	1.16.1	(Danecek et al., 2021)
MarkDuplicates	2.27.5	(Picard Toolkit http://broadinstitute.github.io/picard)
bamCoverage	3.5.1	(Ramírez et al., 2016)
LanceOtron	1.0.8	(Hentges et al., 2022)
FastQC	0.12.1	("FastQC", 2015)
MultiQC	1.14	(Ewels et al., 2016)

Table 2.3: **Software and versions used in the CATCH-UP preprocessing pipeline.**

In brief, initial quality control of raw paired-end reads was performed using FastQC to assess base quality scores, GC content, and adapter contamination. Inspection revealed adapter readthrough, prompting the removal of the terminal 110 bp from the 3' end of each paired-end read using Cutadapt (cutadapt –cut -110). Adapter trimming and quality filtering was then performed using Trimmomatic with the following parameters: ILLUMINACLIP:adapters/NexteraPE.fa:2:40:15: to remove Nextera transposase adapter sequences (allowing up to 2 mismatches, a palindrome clip threshold of 40, and a simple clip threshold of 15); SLIDINGWINDOW:4:20: to trim the 3' end when average quality within a 4 bp window dropped below 20.

Trimmed, quality-filtered paired-end reads were then aligned to the Mus musculus reference genome (mm10/GRCm38) using Bowtie2, with default sensitivity settings (–sensitive) for paired-end reads. Following alignment, the resulting BAM files underwent several filtering and processing steps within the catch-up pipeline. Reads were filtered using SAMtools with the parameters -bShuF 4 -f 3 -q 30 to retain only properly paired reads (-f 3) with a high mapping quality score (MAPQ > 30), while discarding any unmapped reads (-F 4). The filtered BAM files were sorted by genomic coordinate using samtools sort with 4GB of memory (-m 4G). PCR duplicates, which can arise during library preparation, were identified and marked using Picard MarkDuplicates. Duplicates were flagged but not removed at this stage (–REMOVE_DUPLICATES False). For samples with any technical replicates (from different tagmentation times (30 vs 35 minutes), and/or different sequencing lanes), reads were merged into a single BAM file per biological sample using samtools merge.

2.3.4.2 Nucleosome-free region (NFR) enrichment and filtering

Following the CATCH-UP pipeline, the BAM files were processed further to produce clean, nucleosome-free region (NFR)-enriched BAM files for each individual biological replicate. The

previously marked PCR duplicates were removed using samtools view with the flag -F 1024). All reads aligning to the mitochondrial chromosome (chrM) were excluded. Problematic genomic regions were filtered using the ENCODE mm10 v2 blacklist (mm10-blacklist.v2.bed) via bedtools intersect (-v flag) to remove reads from regions known to produce artifactual signals. To enrich for open chromatin signal, reads were filtered based on their fragment length. Only fragments corresponding to NFRs (insert size < 150 bp) were retained, by using an awk command on the 9th column of the SAM format, which stores the template length. For visualisation and peak-calling, NFR-enriched BAM files from individual replicates were then merged into experimental groups (e.g., ZT0_male, ZT12_female) using samtools merge. signal coverage tracks were generated for both the individual replicates and the merged groups, using deepTools bamCoverage (vX) at 1 bp resolution (–binSize 1) with RPKM normalisation (–normalizeUsing RPKM).

2.3.4.3 Peak-calling and quantification

LanceoTron, a deep learning based peak caller that outperforms traditionally used peak-callers in sensitivity, specificity, and reproducibility for ATAC-seq data, was used to call peaks with default parameters (Hentges et al., 2022). Peak calling was performed on the BigWig files generated from the merged experimental groups (e.g., ZT0_male_merged_40bp.nfr.bw). To create a unified set of peaks for differential accessibility analysis across all conditions, the the peak BED files from all experimental groups were concatenated and merged using BEDtools merge to generate a non-redundant consensus peak set representing all accessible regions identified across conditions. Read counts within consensus peaks were quantified for each individual biological replicate. This was done using featureCounts (Subread package) in paired-end mode (-p). The consensus BED file was converted to a Simplified Annotation Format (SAF), and parameters –largestOverlap and -O were used assign multi-mapping reads to the peak with largest

overlap and to allow assignment to overlapping features, respectively. This generated a counts matrix, with consensus peaks as rows and individual samples as columns, suitable for downstream differential accessibility analysis using edgeR.

2.3.5 RNA-seq differential expression analysis

Raw counts were imported into R (version 4.4.1) and differential expression analysis was performed using the DESeq2 (version 1.20.0, (Love et al., 2014). Genes with total counts <100 across samples within the smallest experimental group were filtered prior to analysis. A zero-intercept design model was employed, enabling direct estimation of group means and straightforward extraction of custom contrasts. For Chapter 3 (circadian gating of LPS response), the model was specified as design = 0 + group8 + sex, where group8 represented each unique combination of genotype, timepoint, and treatment (e.g., WT_LPS_ZT0), and sex was included as a covariate to account for baseline sex differences in peritoneal macrophages. For Chapter 4 (sex differences in circadian regulation), the model was design = 0 + group8, where group8 defined each unique combination of genotype, timepoint, and sex for all LPS-stimulated samples (e.g., WT_ZT0_Male). For Chapter 5 (pharmacological manipulation of BMAL1), the model was design = 0 + group, where group defined each unique treatment condition (e.g., CCM_LPS). Due to imbalanced sample sizes (n=3 WT, n=5 KO) and heterogeneous variance between genotypes, each genotype was analysed separately. Log2 fold changes were shrunk using the lfcShrink function with the ashr method, an empirical Bayes approach that moderates effect size estimates for low-count genes while preserving interpretability (Stephens, 2016). Independent filtering was enabled to increase statistical power by removing low-count genes unlikely to show significance. P-values were adjusted for multiple testing using the Benjamini-Hochberg false discovery rate (FDR) method, and genes with adjusted $p < 0.05$ were considered

differentially expressed.

2.3.6 ATAC-seq differential accessibility analysis

The consensus peak count matrix was imported into R and differentially accessibility analysis was performed using edgeR (Y. Chen et al., 2025) which demonstrates robust performance with low replicate numbers and maintains appropriate type I and type II error control in ATAC-seq datasets (Gontarz et al., 2020). Peaks were filtered using the filterByExpr function with group-aware filtering (design = design, min.count = 10) to retain only peaks with sufficient coverage for statistical testing. Library sizes were normalised using the trimmed mean of M-values (TMM) method. The model was specified as design = 0 + group, where group defined each unique combination of sex and timepoint for wild-type LPS-stimulated macrophage ATAC-seq experiments, or sex and genotype for LysM-Rev-Erb$\alpha^{flox/flox}$ peritoneal exudate cell and bone marrow-derived macrophage ATAC-seq experiments. Differential accessibility was assessed using quasi-likelihood F-tests (glmQLFit, glmQLFTest), which provide robust error rate control. P-values were adjusted using the Benjamini-Hochberg FDR correction, and peaks with adjusted $p < 0.05$ were considered differentially accessible.

2.3.7 RNA-seq downstream functional analyses

2.3.7.1 Gene ontology over representation analysis

clusterProfiler (S. Xu et al., 2024) was used to perform over-representation analysis on Gene Ontology terms (established by the Gene Ontology Project) associated with genesets of interest. Appropriate background gene lists were selected for each comparison, and hypergeometric testing provided statistical enrichment analysis. The background gene universe was defined as all genes with valid statistical tests in the contrast of interest (e.g for WT CCM vs Vehicle, all

genes with non-NA p values, that were not filtered out by DEseq2 independent filtering). The BH method was used for FDR control, with p value cutoff at 0.05, and qvaluecutoff was set to 0.05. Enriched terms were de-duplicated with simplify() cutoff = 0.5, by = p.adjust, select_fun = min (keep the most significant term per cluster). Simplified results were visualised using the dotplot function from clusterProfiler.

Versions: clusterProfiler (4.12.6)

2.3.7.2 Gene set enrichment analysis (GSEA)

Custom gene sets were compiled from curated lists. For each contrast of interest, genes were ranked by DESeq2 Wald statistic (decreasing), with the ranked vector providing the universe. Enrichment was tested using fgseaMultilevel (fgsea; minSize = 5, maxSize = 50000), reporting normalised enrichment scores (NES), nominal p values, BH adjusted p values, and leading-edge genes. Positive NES indicates enrichment at the up-regulated end of the ranked list. Figures display enrichment curves for the top results.

Versions: fgsea (1.30.0)

2.3.7.3 DecoupleR: Transcription factor (TF) and pathway activity inference

Variance-stabilised counts were obtained from DESeq2 (vst, blind = TRUE) and mapped from ENSEMBL IDs to mouse gene symbols (org.Mm.eg.db). Where multiple ENSEMBL IDs mapped to the same symbol, I retained the row with the highest variance across samples, yielding a unique-symbol expression matrix. TF activities were inferred with decoupleR (Badia-i-Mompel et al., 2022) using the CollecTRI and DoRothEA (levels A-C) mouse regulon resources (Garcia-Alonso et al., 2019; Müller-Dott et al., 2023) . Activities were computed with using signed interaction weights. To obtain contrast-level activities, I constructed ranked, signed

gene-level signatures from DESeq2 Wald statistics for each contrast and scored them with the Univariate Linear Model (ULM) (run_ulm, minimum regulon size = 5), against each TF resource. Many techniques have been developed to identify pathways significantly affected by a perturbation of interest within bulk-sequencing data (comprehensively evaluated by (T.-M. Nguyen et al., 2019)). Pathway activities were estimated with PROGENy (mouse; top k target genes per pathway) using the Multivariate Linear Model (MLM) (run_mlm, minimum set size = 5). Contrast-level scores were derived from the Wald-statistic signatures for each contrast. For all analyses, p-values returned by decoupleR were adjusted using the BH procedure, and terms with FDR < 0.05 were considered significant. Figures show top activities by absolute score. Agreement between CollecTRI and DoRothEA TF activities was assessed by scatter of matched TF scores with the identity line.

Versions: org.Mm.eg.db (3.19.1), decoupleR (2.10.0)

2.3.7.4 Selection of expressed TF motifs

TFs were defined as "expressed" if DESeq2 size-factor-normalised counts were $\geq$ 100 in at least 50% of samples. Gene identifiers were converted to official mouse gene symbols using org.Mm.eg.db. The JASPAR 2024 vertebrate (redundant) MEME motif collection was parsed (Rauluseviciute et al., 2024); TF names were normalised (removing family separators and aliases), and motifs whose TF symbol matched the expressed set were retained. Differential expression of TFs for the contrast of interest was assessed with DESeq2 using ashr LFC shrinkage; TF tables were restricted to TFs present in JASPAR.

2.3.8 ATAC-seq downstream functional analyses

2.3.8.1 Peak-gene proximity enrichment (PEGS)

PEGS (version 0.6.6) was run with the built-in mm10 reference TSS intervals (derived from UCSC refGene) to quantify enrichment of custom gene sets near DARs (Briggs et al., 2021). For each distance δ (1 kb, 5 kb, 10 kb, 50 kb, 100 kb, 200 kb, 500 kb, 1 Mb, 5 Mb), peaks were symmetrically expanded +/- δ d from interval centres, genes whose TSS overlapped expanded peaks were collected, and enrichment of each input gene set was tested via a hypergeometric test. PEGS reports p-values and counts per (peak set x gene set x distance) and produces a heatmap of -log 10 p.

2.3.8.2 Peak selection for motif analysis

PEGS was used to identify the genomic distance from transcription start sites (TSS) at which a consensus peakset was most enriched around the target gene set. Using TxDb.Mmusculus.UCSC.mm10.knownGene, TSSs were defined and windows centred on TSSs were built that matched the PEGS-selected distance bin (inner, outer). The GenomicRanges package was used to store and manipulate genomic intervals (Lawrence et al., 2013). GRanges were built around both the given geneset, and a control geneset (non-clock controlled genes). For each condition of interest, peaks were intersected with the shell to obtain foreground peaks and a matched background (same chromosome and width distribution) was drawn from peaks intersecting the non-clock shell.

2.3.8.3 Motif enrichment in PEGS-defined regions

HOMER was run (findMotifsGenome.pl, mm10) on peaks located within the PEGS-selected TSS windows around the gene set of interest (Heinz et al., 2010). Foreground peaks used

the exact peak lengths (-size given). Background peaks were length-matched from peaks located within non-clock shells derived from the same experiment. *De novo* and known motif enrichment were computed using motif lengths 8, 10, and 12, with repeat masking enabled. Enrichment p-values and FDR-adjusted q-values from HOMER are reported for known motifs.

2.3.8.4 Promoter motif enrichment

For gene-centric analysis, HOMER (findMotifs.pl) was run on promoter regions (regions -300bp, +50bp from TSS) of the BMAL1-dependent geneset of interest, with a background list of BMAL1-independent genes responsive to the same treatment. Input identifiers were mouse gene symbols. Enrichment p-values and FDR-adjusted q-values from HOMER are reported for known motifs.

3 | Intrinsic macrophage clock function

3.1 Introduction

The circadian clock regulates macrophage inflammatory responses chapter 1. Genetic deletion of BMAL1 modulates the LPS-responsive control of cytokine production, phagocytosis, and inflammasome activation (Gibbs et al., 2012; Kitchen et al., 2020; Shim et al., 2024). Macrophages lacking BMAL1 exhibit amplified pro-inflammatory responses compared to wild-type controls. However, there are mechanistic gaps remaining in our understanding of how BMAL1 and the other core-clock components function to control inflammatory responses in macrophages.

3.1.1 *In vivo* clock-gating mechanisms are undefined.

Most studies advancing our understanding of macrophage clock function have used *in vitro* cultures of bone marrow cells to study BMDMs, or cell lines. *In vivo* studies have measured physiological outcomes in the whole-organism, such as sepsis, mortality, or serum cytokines, but not the transcriptome-wide effects of LPS on the responding tissue-resident macrophages themselves. We have an incomplete understanding of the mechanisms involved in the peritoneal macrophage clock-gated LPS-response *in vivo*. Specifically, it remains unknown which clock proteins contribute to the time-of-day gating of inflammation. Clock proteins consist of transcriptional activators and repressors, and the extent to which these transcription factors (TFs) directly activate or repress inflammatory response genes is uncertain. Additionally, the role of clock controlled genes (for example, TLRs) in tuning the inflammatory response is incompletely defined. These questions require *in vivo* study, where macrophages integrate physiological sig-

nals absent *in vitro*.

3.1.2 The necessity of specific clock-components for gating inflammation is contested.

How core clock components impose time-of-day gating on early LPS-driven transcription remains incompletely defined. A strong body of evidence suggests that REV-ERBα exerts anti-inflammatory effects on gene expression in multiple cell types, including macrophages.

Initial work characterising the tissue-specific roles of core-clock components established the importance of REV-ERBα in mediating anti-inflammatory effects. REV-ERBα was first demonstrated to block pro-inflammatory signals through the demonstration that REV-ERBα represses the Toll-Like Receptor 4 (TLR4) gene (Fontaine et al., 2008), as a target of the liver X receptor. Later, REV-ERBα was found to be critical for the clock-gating of cytokine production as part of the LPS-induced endotoxic response (Gibbs et al., 2012). Specifically, peritoneal exudate cells (PECs) from mice with global deletion of REV-ERBα show loss of time-of-day gating of serum IL6 after *in vivo* LPS stimulation, and *Rev-erb*α shRNA knockdown in THP-1 cells increased *Il6*. In this study, synthetic REV-ERB ligands were found to modulate *Cxcl11*, *Ccl2*, *Cxcl6*, and *Il19*: each gene was downregulated with co-application of the ligand (REV-ERB agonist) GSK4112 and LPS, consistent with the documented roles of REV-ERBs as transcriptional repressors (Ikeda et al., 2019). Mapping of macrophage REV-ERBα and REV-ERBβ cistromes (using biotin-tagged REV-ERBs expressed in RAW264.7 macrophages) suggests REV-ERBα mediates effects on transcription in macrophages through the repression of distal enhancers selected by lineage-determining TFs (Lam et al., 2013).

More recent evidence suggests that the importance of myeloid REV-ERBα for circadian control of inflammation has been overstated. In a model of pulmonary fibrosis, REV-ERBα mutation

in myeloid cells had no effect on the bleomycin-induced fibrotic phenotype, while REV-ERBα mutation in fibroblasts exaggerated the fibrotic response (Cunningham et al., 2020). In a separate model of acute pulmonary inflammation, GSK4112 attenuated LPS-induced inflammatory responses in the lung, but LysM-REV-ERBα mutation did not alter the aerosolised LPS response, and the immunomodulatory effects were instead attributed to the role of REV-ERBα in bronchiolar epithelial cells (Pariollaud et al., 2018).

Studying the importance and mechanisms of action of REV-ERBα has been difficult in part due to the models available. In animal models, global deletion of REV-ERBα has widespread impact on behaviour and physiology (Hunter et al., 2020). In both studies examining the role of REV-ERBα in pulmonary inflammation (Cunningham et al., 2020; Pariollaud et al., 2018), REV-ERBα was mutated through targeted deletion of the DNA-binding domain, and so the protein retained function as a co-factor for other TFs outside of binding to classical response elements. This mutation allows REV-ERBα to continue to regulate metabolic gene expression, and studying this model in liver revealed only 25% of REV-ERBα target genes were DNA-binding domain-dependent (Y. Zhang et al., 2015). In addition, widely-used REV-ERBα ligands have been shown to have off-target effects (Dierickx et al., 2019).

In this study I defined the full extent of REV-ERBα's role in gating the LPS-induced endotoxic response in peritoneal macrophages. To characterise *in vivo* macrophage-intrinsic REV-ERBα function in inflammatory responses, I used a conditional knockout (LysM-Cre x *Rev-erb*$\alpha^{flox/flox}$) with loxP sites inserted at intron 2 and intron 6, which results in loss of REV-ERBα. This approach avoids both the systemic effects of global deletion, and the residual DNA-binding domain-independent activity (the remaining 75% of genes in liver (Y. Zhang et al., 2015)).

It must be noted that redundancy in REV-ERB function has been demonstrated in fibroblasts,

where only the simultaneous loss of both REV-ERBα and REV-ERBβ leaves fibroblasts arrhythmic in culture (Bugge et al., 2012).

3.1.3 Chromatin mechanisms of clock-gating in macrophages remain untested.

Circadian clock TFs interact with chromatin-modifying enzymes to regulate target gene expression. CLOCK:BMAL1 recruits histone acetyltransferases, depositing activating H3K27ac marks at enhancers, increasing genome accessibility for RNA polymerase II and leading to increased transcription. REV-ERBα interacts with the NCoR/HDAC3 repressive complex, removing activating histone modifications and inhibiting gene expression. In the liver, these interactions generate genome-wide rhythms in chromatin accessibility (Koike et al., 2012).

If the clock modulates inflammatory responses through direct TF activity at inflammatory gene loci, we would predict time-of-day differences in chromatin accessibility at the promoters and enhancers of inflammatory genes. However, if the circadian gating of inflammatory responses operates through mechanisms upstream of inflammatory loci, such as clock-dependent regulation of signalling pathway activity, chromatin accessibility at inflammatory loci may remain stable. These possibilities have not been tested in macrophages.

Many questions remain which are pertinent to understanding circadian-controlled inflammatory pathologies. This chapter aims to elucidate the pathways and mechanisms underlying clock-controlled inflammatory responses in order to better understand human disease pathologies.

3.1.4 Hypothesis and Aims

I hypothesised that peritoneal macrophages show a time-of-day gated early inflammatory response *in vivo*, and this gating requires both BMAL1 and REV-ERBα, and is mediated through chromatin remodelling.

3.1.4.1 Hypotheses

My specific testable hypotheses were:

1. BMAL1 deletion eliminates ZT0 vs ZT12 differences in transcriptional response to LPS stimulation, demonstrating that the intrinsic macrophage clock is required for normal macrophage function *in vivo*.
2. REV-ERBα deletion derepresses the expression of inflammatory genes which are negatively-regulated by the clock.
3. Chromatin accessibility at the promoters and enhancers of LPS-responsive genes differs significantly in LPS-stimulated macrophages at ZT0 vs ZT12 .
4. Changes in TF availability or activity mediate the gating effects.

3.1.4.2 Aims

1. Identify which time-of-day-gated macrophage inflammatory genes are BMAL1-dependent *in vivo*.

- Compare the transcriptomes of WT and BMAL1-KO peritoneal macrophages at ZT0 and ZT12 to define the scope of the intrinsic macrophage clock's control over inflammatory responses, in physiological context.
- Analyse BMAL1-dependent genes to identify which inflammatory pathways are clock-controlled.

2. Determine whether REV-ERBα is required for the clock-driven negative regulation of inflammation in macrophages *in vivo*.

- Compare the transcriptomes of WT and REV-ERBα-KO peritoneal macrophages at a sin-

gle timepoint (with high expression of REV-ERBα) to define the scope of REV-ERBα's control over inflammatory responses, in physiological context.

- Analyse REV-ERBα-dependent genes to identify which inflammatory pathways are clock-controlled.

3. Determine whether chromatin accessibility changes mediate circadian gating of inflammatory gene expression *in vivo*.

- Use ATAC-seq to profile chromatin accessibility in WT macrophages at ZT0 and ZT12 following 1 hour LPS stimulation *in vivo*, to test whether accessibility changes correspond to gated transcription.
- Perform ATAC-seq in REV-ERBα-KO and WT littermate controls to define necessity of REV-ERBα for circadian chromatin accessibility changes.

4. Determine which changes to TF availability and activity mediate circadian gating of inflammatory gene expression *in vivo*.

- Analyse differential TF expression, TF activity, and pathway activity, between timepoints and genotypes.
- Perform motif enrichment in the chromatin landscape surrounding clock-gated genes to help identify TFs involved in circadian gating of the macrophage LPS-response.

3.2 Methods

In this study, I performed transcriptomic and chromatin accessibility profiling in peritoneal macrophages responding to LPS *in vivo*, at ZT0 and ZT12. Using the same *in vivo* system, I

used myeloid-specific deletions of either *Bmal1* or *Rev-erbα* to discern the contribution of each. To build on previous *in vivo* macrophage-clock studies, here I used unbiased transcriptome-wide readouts paired with chromatin-accessibility data.

LPS-stimulation lasted for 1 hour, to capture the early transcriptional response dominated by immediate-early genes, and avoiding secondary feedback loops (autocrine IFN leading to STAT activation at 2-4 hours) which would obscure direct clock effects.

ATAC-seq was chosen for this study due to the lower requirement for cell input numbers, while capturing all accessible regions and not being limited to one TF. By performing the time-of-day ATAC-seq in LPS-stimulated macrophages, the chromatin landscape at inflammatory loci profiled captured any early 1 hour LPS-induced accessibility changes.

3.2.1 Experimental design and contrasts

Two timepoints were chosen to contrast peritoneal macrophage transcriptomes from LPS or saline treated mice, at ZT0 (onset of light period) and ZT12 (onset of dark period) (Figure 3.1). These timepoints were chosen to closely match previous studies identifying time-gated cytokine and/or phagocytic ability in macrophages, while remaining close to peak and trough expression of BMAL1: in PECs isolated from LysM-*Bmal1*$^{flox/flox}$ mice, *Bmal1*$^{flox/flox}$ expression levels peak at ZT4, and nadir 12 hours later, when *Rev-erbα* peaks antiphasically with *Bmal1* (Gibbs et al., 2012).

PECs were harvested from wild-type (*Bmal1-flox/flox*, referred to as WT) and myeloid-specific BMAL1-knockout (*LysM-Cre;Bmal1-flox/flox*, referred to as BMAL1-KO) mice of both sexes, one hour following intraperitoneal injection of either LPS or saline. Macrophages were MACS-purified and RNA-seq and/or ATAC-seq was performed (Chapter 2).

(a) Experimental groups

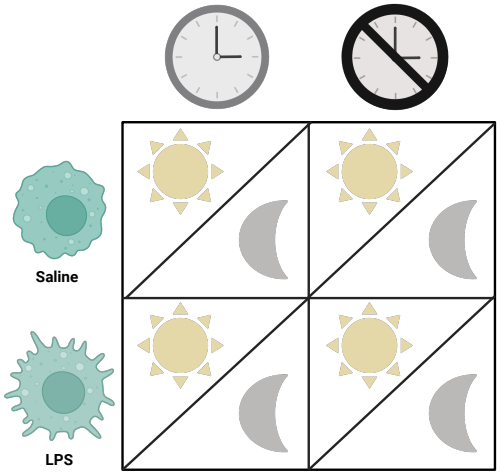

(b) Gate definitions

$$\text{WT gate: } (\text{LPS} - \text{Saline})_{\text{ZT12}} - (\text{LPS} - \text{Saline})_{\text{ZT0}}$$

$$\textit{BMAL1KO} \text{ gate: } (\text{LPS} - \text{Saline})_{\text{ZT12}} - (\text{LPS} - \text{Saline})_{\text{ZT0}}$$

$$\text{WT-only: } \text{gate}_{\text{WT(padj)}} < 0.05 \;\&\; \text{gate}_{\text{KO(padj)}} > 0.05$$

Figure 3.1: **Schematic showing experimental groups and contrasts used to determine BMAL1-dependent time-gated inflammatory response genes.**
(a) Experimental groups: LysM-Bmal1$^{flox/flox}$ (referred to as BMAL1-KO) and Bmal1$^{flox/flox}$ (referred to as WT) mice were entrained to 12:12 light:dark cycles in light-tight cabinets for 2 weeks. Peritoneal exudate cells were retrieved from mice 1 hour after intraperitoneal injection with saline or LPS (1 mg/kg) at ZT0 or ZT12. Peritoneal macrophages were then purified using magnetic-activated cell sorting (MACS). (b) Gate definitions: the contrasts used in DESeq2 to define the interaction terms in WT and BMAL1KO, and to define WT-only gated responses.

Group	Male	Female	Total
WT Saline ZT0	2	1	3
KO Saline ZT0	2	2	4
WT Saline ZT12	1	2	3
KO Saline ZT12	3	1	4
WT LPS ZT0	3	3	6
KO LPS ZT0	3	3	6
WT LPS ZT12	3	2	5
KO LPS ZT12	2	3	5

Table 3.1: **Summary of experimental group sample sizes.** Animals per group split by sex.

To identify genes where the LPS response is gated by time-of-day, I tested for statistical interaction between treatment (LPS vs saline) and zeitgeber time (ZT12 vs ZT0) using DESeq2. A significant interaction (padj < 0.05) indicates that the magnitude or direction of the LPS-induced fold-change differs between ZT12 and ZT0. For example, a gene may show strong LPS induction at ZT0 but weak induction at ZT12, indicating that the clock "gates" the magnitude of the inflammatory response. I classified an interaction as BMAL1-dependent if it was statistically significant in wild-type mice (padj < 0.05) but not in BMAL1-KO mice (padj ≥ 0.05), indicating that BMAL1 is necessary for time-of-day modulation of the LPS response at that locus (Figure 3.1(b)).

I also analysed time-of-day differences independently within each treatment condition (Saline-only and LPS-only) by comparing ZT12 vs ZT0. Genes were classified as BMAL1-dependent if they showed significant time-of-day differences in wild-type mice (padj < 0.05) but not in BMAL1-KO mice (padj ≥ 0.05).

3.3 Results

3.3.1 Principal component analysis reveals dominant effects of LPS stimulation and biological sex on peritoneal macrophage transcriptomes.

To establish which experimental variables most strongly influence peritoneal macrophage gene expression, and to determine whether time-of-day effects are detectable above other sources of variation, I performed principal component analysis (PCA) on variance-stabilised (VST) counts from all samples (n = 36 mice across 2 genotypes, 2 treatments, 2 timepoints, and 2 sexes, (Table 3.1)).

The primary source of variation in the dataset was from LPS treatment (PC1 = 88%), in accordance with the global re-shaping of transcriptional pathways in the presence of inflammatory stimuli. Second to this was sex (PC2 = 4%) (Figure 3.2), consistent with prior reports of significant peritoneal macrophage sexual dimorphism (Bain et al., 2020). Sex was therefore included in the DESeq2 model design as a covariate. Samples were seen to cluster by genotype along PC3 (= 2%), and by timepoint along PC5 (= 1%).

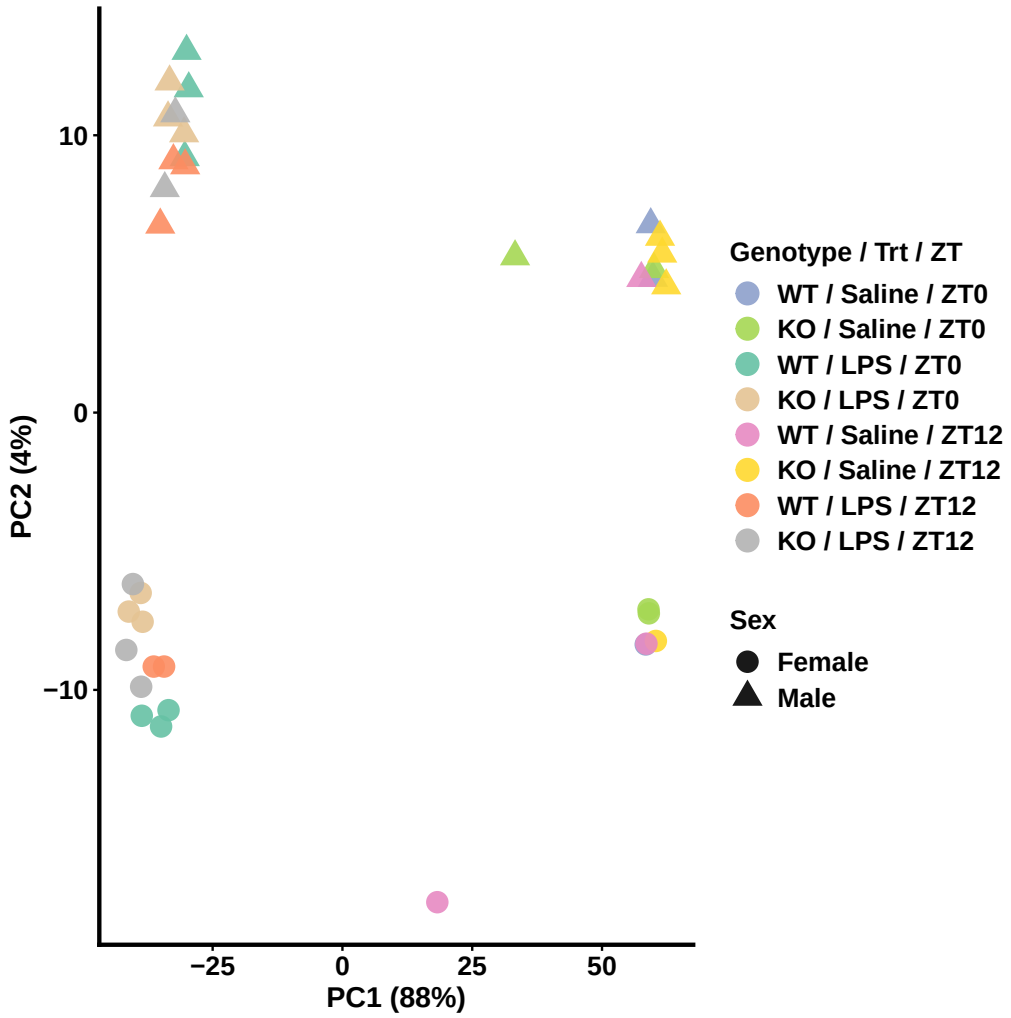

Figure 3.2: **Principal Component Analysis (PCA) for PC1 and PC2.**
DESeq2 plotPCA function was used with the top 500 variable genes on counts normalised with the variance stabilising transformation. WT = Bmal1$^{flox/flox}$, KO = LysM-Bmal1$^{flox/flox}$

3.3.2 Almost all time-of-day differences are BMAL1-dependent in both saline and LPS-stimulated macrophages.

Macrophages isolated from the peritoneal cavity have been exposed to a variety of physiological signals which may govern timepoint-dependent differences in transcriptional activity. To identify which of these differences are driven by the intrinsic macrophage clock, I first identified BMAL1-dependent changes to gene expression between ZT0 and ZT12 in both basal saline and LPS-stimulated conditions. Genes showing time-of-day differences in WT but not in BMAL1-KO mice represent BMAL1-dependent differences.

In basal state conditions for peritoneal macrophages, many genes are differentially expressed between timepoints (Figure 3.3). These genes show few significant differences in BMAL1-KO, demonstrating dependence on the presence of the macrophage-intrinsic clock for their gated expression. Of the 9,875 transcripts passing the expression-level filter, 982 (9.9%) were differentially expressed between ZT12 and ZT0 in WT macrophages (padj < 0.05). In contrast, BMAL1-KO macrophages showed markedly reduced time-of-day differences, with 240 genes differentially expressed between timepoints (2.4% of total) (Figure 3.3). Of the 982 wild-type time-of-day genes, 875 genes (89%) were BMAL1-dependent, demonstrating that the majority of basal state ZT12 vs ZT0 differences require the intrinsic macrophage clock. Of the BMAL1-dependent genes, 619 genes (71%) were higher at ZT12, with 256 genes (29%) higher at ZT0.

BMAL1-dependent genes included core clock components (*Bmal1* itself, *Nr1d1, Per1/2/3, Cry1/2*) and clock-controlled genes involved in the regulation of inflammatory pathways. Notably, *Nfkbia/Nfkbib, Jun/Fos, Tlr2, Irf5, Cd80, IL1a* and *Il10* showed time-of-day regulation in the basal state, suggesting that the clock primes inflammatory pathways even in the absence of immune challenge.

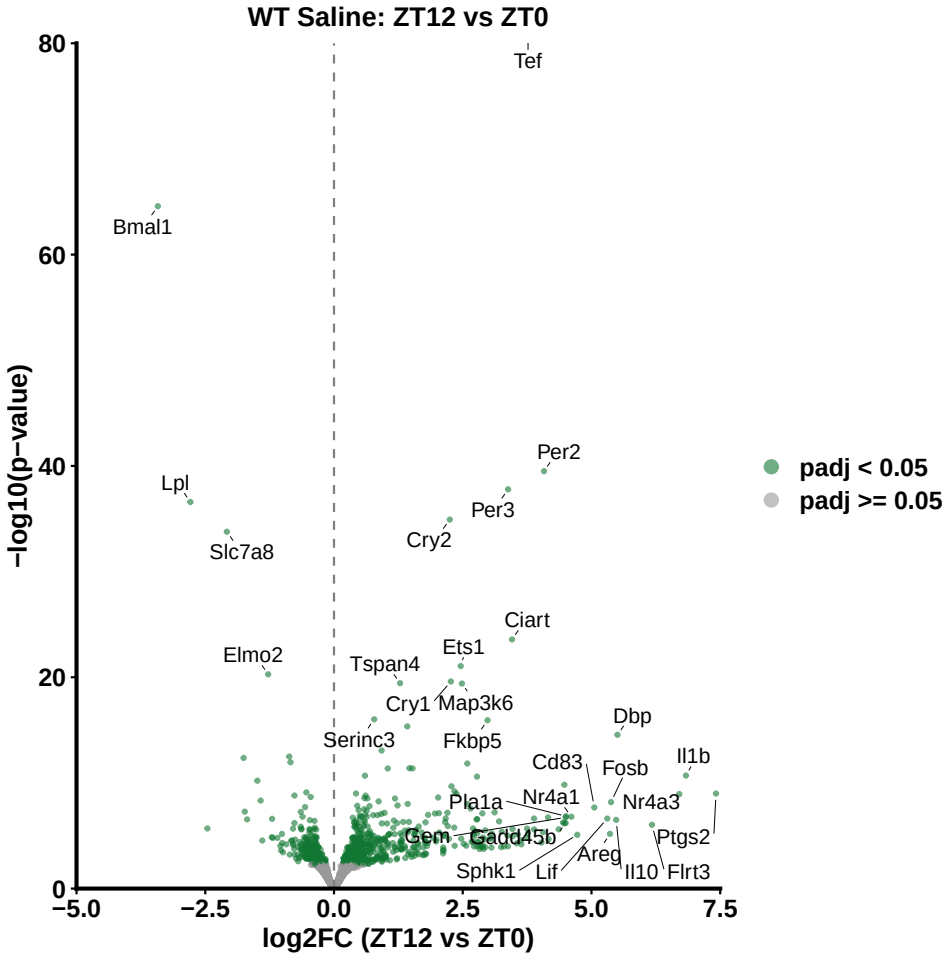

(a) Wild-type (WT)

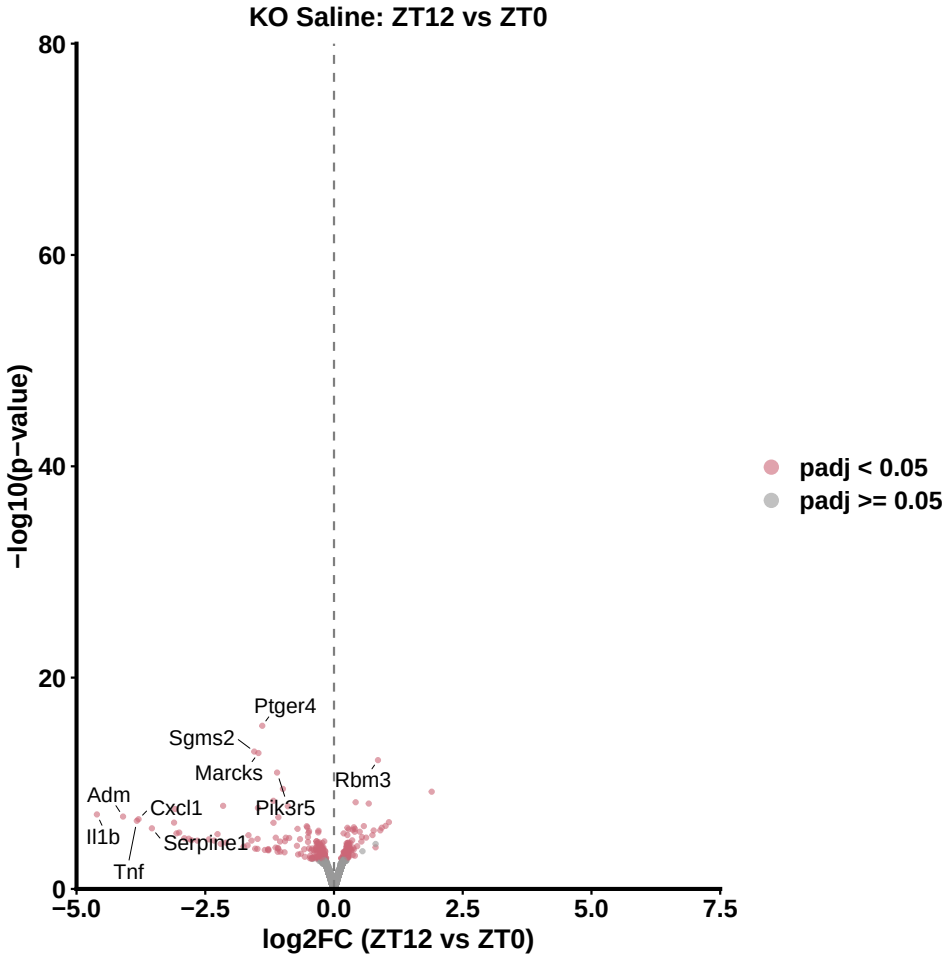

(b) BMAL1-KO (KO)

Figure 3.3: **The effect of myeloid-specific BMAL1-KO on ZT12 vs ZT0 differential expression in peritoneal macrophages, in basal (saline-treated) conditions.**
DEGs were identified using DESeq2 with sex as a covariate, at BH-adjusted < 0.05. WT $n = 3$, BMAL1-KO $n = 3$–4. The top-ranked DEGs (by Wald statistic) are labelled. Panel (a) shows WT DEGs (green), and panel (b) shows BMAL1-KO DEGs (pink).

To determine the biological processes regulated by BMAL1 in basal macrophages, I performed pathway enrichment analysis on BMAL1-dependent genes using the enrichGO function from clusterProfiler against a background of all basal-state expressed genes.

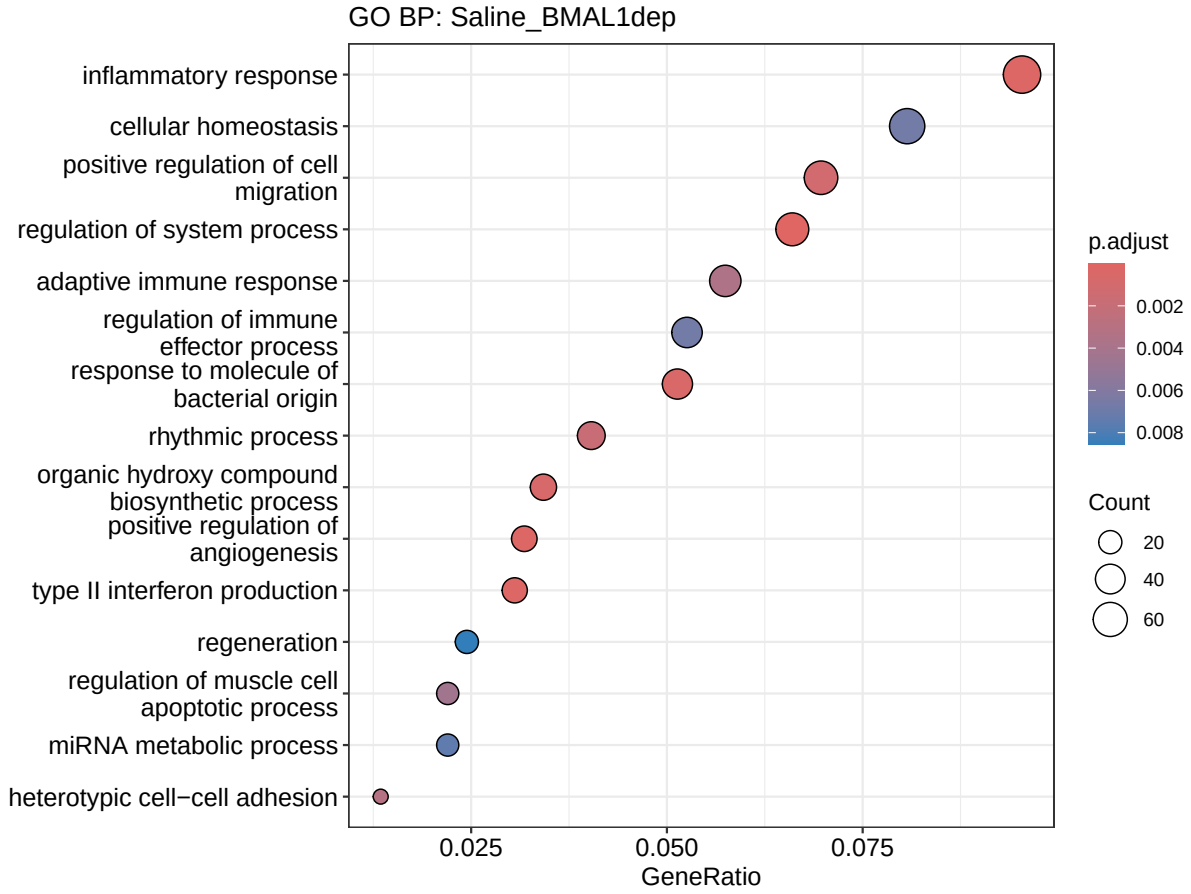

Figure 3.4: **Top 15 enriched GO terms in the BMAL1-dependent ZT12 vs ZT0 differences, in basal state macrophages.**
BMAL1-dependent timepoint-differences were defined by the inclusion of significant ZT12 vs ZT0 DEGs in WT, excluding any significant ZT12 vs ZT0 DEGs in BMAL1-KO macrophages. BMAL1-dependent timepoint differences were defined as genes which passed WT padj < 0.05 and BMAL1-KO padj ≥ 0.05

BMAL1-dependent ZT12 vs ZT0 DEGs were enriched for several inflammatory-related GO terms including the inflammatory response, response to molecule of bacterial origin, and type II interferon production (Figure 3.4). Performing GO enrichment analysis on the ZT0-elevated and ZT12-elevated subsets separately revealed that genes with higher expression at ZT12 were enriched for the pathways involved in the inflammatory response to LPS, while genes higher at ZT0 showed no significant enrichment for pathways but contained genes involved in lipid

metabolism *Cers6, Lpcat1/3, Lpl* and nuclear-encoded mitochondrial ribosomal proteins *Mrpl13/14/17/27/42*.

A subset of genes (n=31) exhibited striking directional reversal in BMAL1-KO macrophages: these genes were upregulated at ZT12 in WT but downregulated at ZT12 in BMAL1-KO. These genes included inflammatory inhibitors *Nfkbiz, Acod1*, pro-inflammatory cytokines *Il1b, Il6, Tnf, Ptgs2,* and pro-inflammatory chemokines *Ccl-2/7, Cxcl-1/2/3/10*.

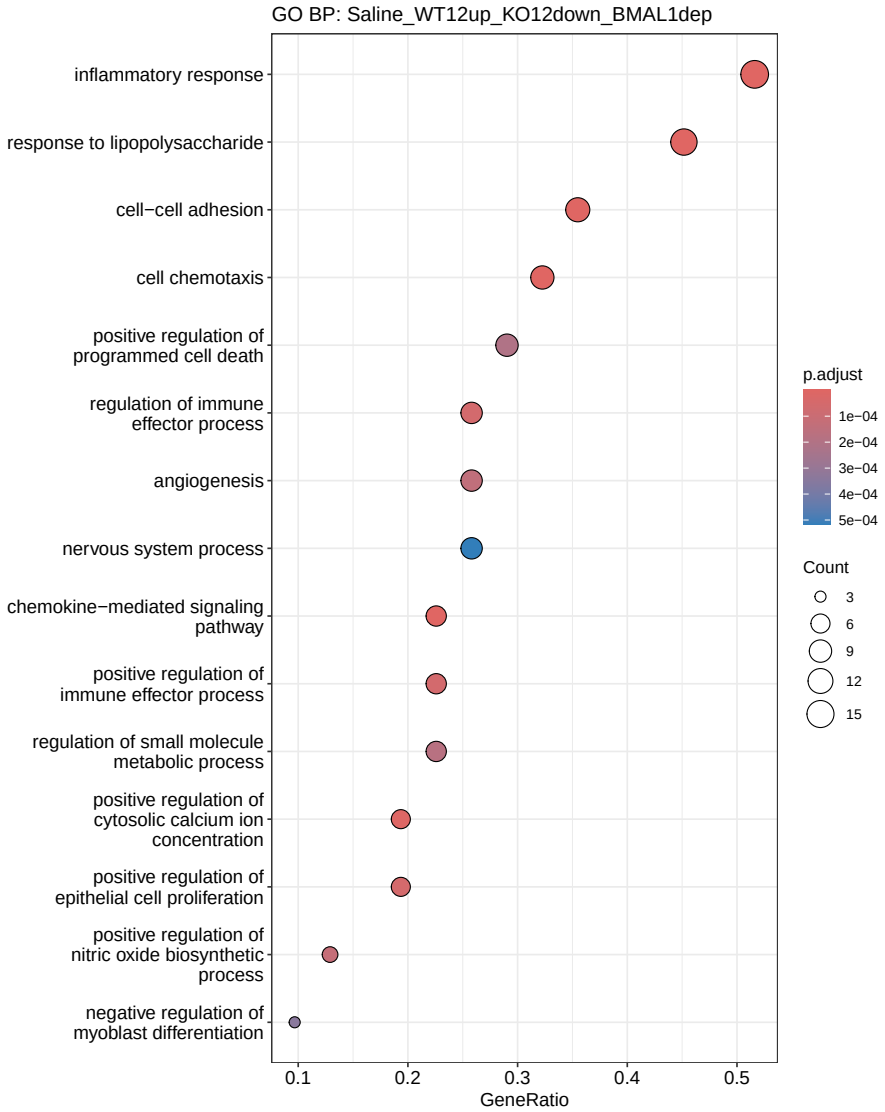

Figure 3.5: **Top 15 enriched GO terms in genes exhibiting directional reversal between WT and BMAL1-KO macrophages at ZT12 in basal state.**
Directional reversal genes (n=31) were defined as those upregulated at ZT12 vs ZT0 in WT but downregulated at ZT12 vs ZT0 in BMAL1-KO macrophages. This subset includes key pro-inflammatory mediators, chemokines, and inflammatory regulators.

Despite the small set size, there was significant enrichment for multiple GO terms, which related to inflammatory response, indicating that BMAL1 controls basal expression of LPS-responsive genes, potentially priming inflammatory responses (Figure 3.5).

Having established that BMAL1 is necessary for the majority of ZT12 vs ZT0 differences in basal state macrophages, I next asked whether these patterns are maintained, altered, or amplified, in the condition of LPS-stimulation.

To determine how LPS stimulation affects circadian transcriptional control, I compared ZT12 vs ZT0 gene expression in LPS-treated macrophages (1 hour post-stimulation) from WT and BMAL1-KO mice. This reveals whether the clock continues to impose time-of-day differences during acute inflammation, and what specific aspects of early inflammatory responses are gated by time-of-day.

In wild-type LPS-stimulated macrophages, 574 genes showed time-of-day differential expression (padj < 0.05). In BMAL1-KO macrophages, only 196 genes showed time-of-day differences (Figure 3.6). 58 genes were shared between these conditions, indicating that 516/712 (72%) of LPS-state timepoint-differences are BMAL1-dependent. Of these BMAL1-dependent genes, just over half were higher at ZT12 (272 genes) and 244 genes were higher at ZT0. This represents a decrease compared to saline conditions (where 619 and 256 genes were found respectively per timepoint), suggesting that the LPS-induced remodelling of the transcriptome suppresses basal state circadian transcriptional control at these timepoints. Taken together, these results support Hypothesis 1: BMAL1 deletion eliminates the majority of ZT0 vs ZT12 transcriptional differences, in both basal and LPS-stimulated macrophages.

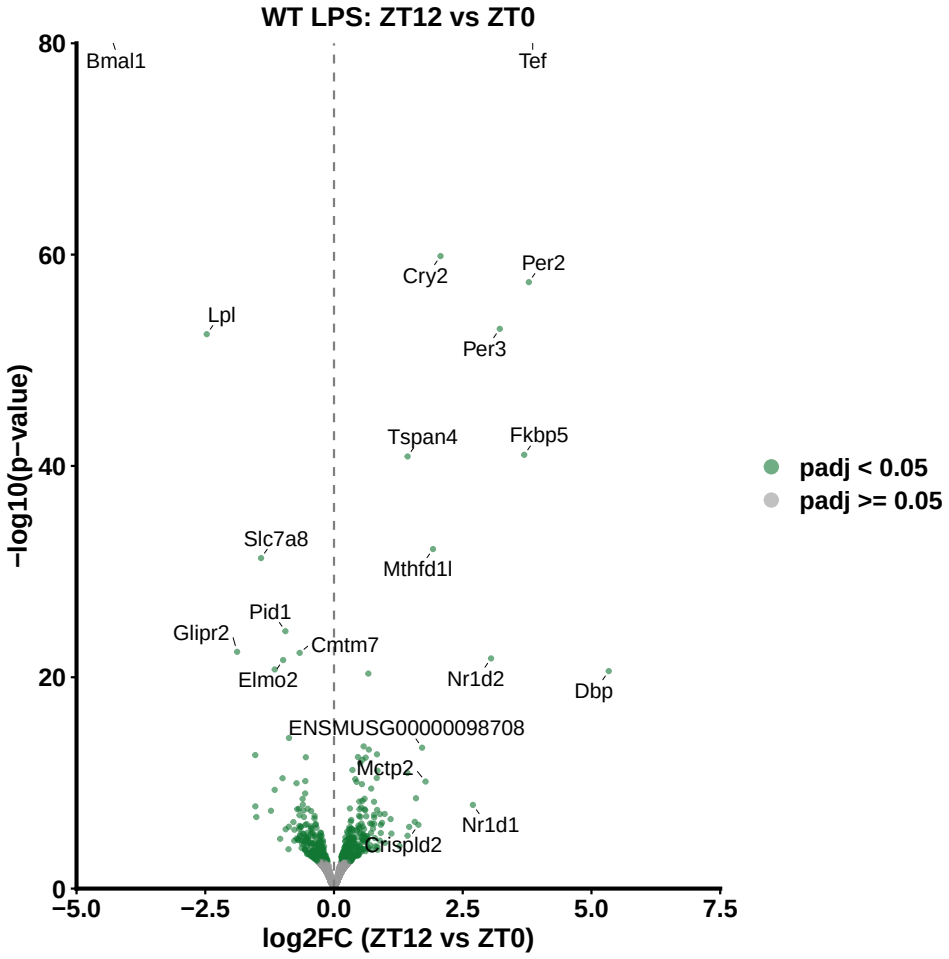

(a) Wild-type (WT)

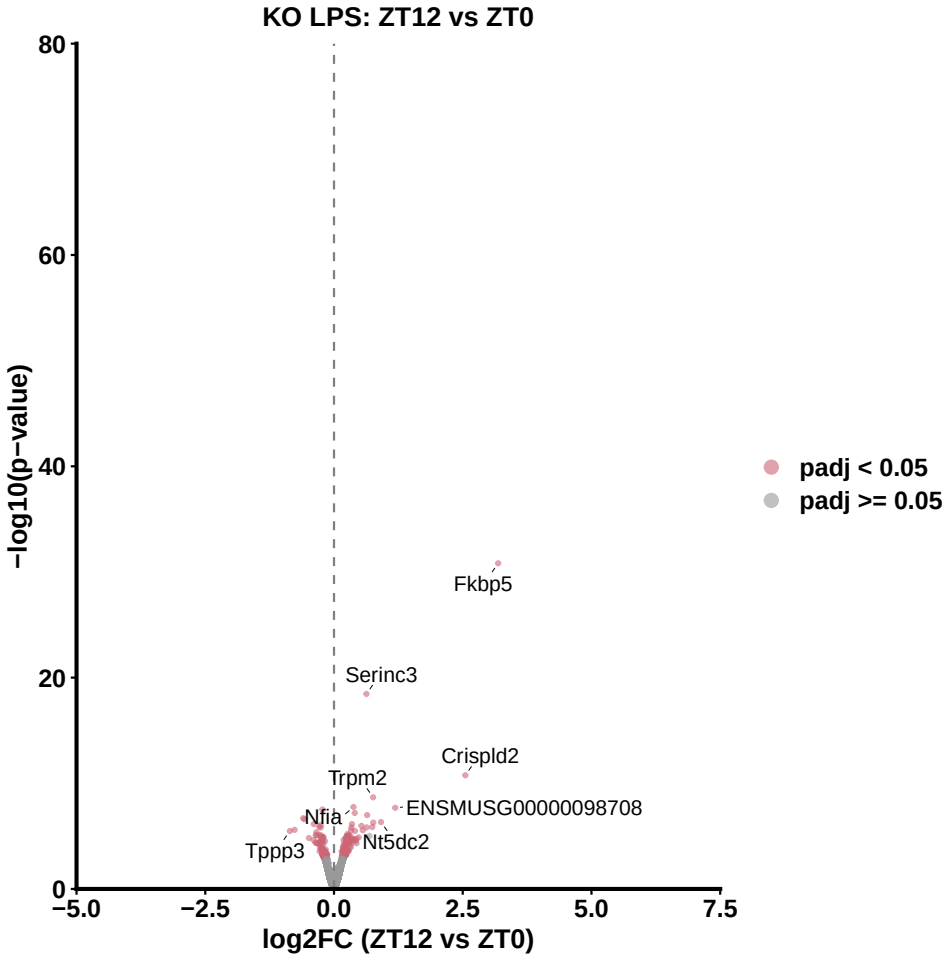

(b) BMAL1-KO knockout (KO)

Figure 3.6: **The effect of myeloid-specific BMAL1-KO on ZT12 vs ZT0 differential expression in peritoneal macrophages, after 1 hour of LPS stimulation (1 mg/kg).**
DEGs were identified using DESeq2 with sex as covariate, at BH-adjusted < 0.05. WT, BMAL1-KO $n = 5$–6. The top-ranked DEGs (by Wald statistic) are labelled. Panel (a) shows WT DEGs (green), and panel (b) shows BMAL1-KO DEGs (pink).

Importantly, the identity of time-of-day genes differed substantially between saline and LPS conditions. Only 141 genes (11%) were shared between basal and LPS BMAL1-dependent gene sets, while 734 and 375 genes were uniquely time-gated in the basal and LPS conditions, respectively (Figure 3.7). LPS stimulation recruits a distinct set of BMAL1-dependent genes, rather than simply maintaining basal circadian rhythms.

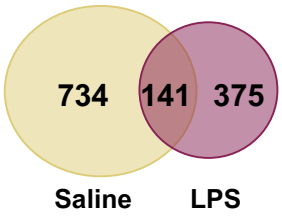

Figure 3.7: **There are more saline-specific BMAL1-dependent differences than LPS.** WT and myeloid-specific BMAL1-KO mice were stimulated with LPS for 1 hour at ZT0 or ZT12, before isolation of peritoneal macrophages. ZT12 vs ZT0 differential expression was analysed using DESeq2. BMAL1-dependent timepoint differences were defined as genes which passed WT padj < 0.05 and BMAL1-KO padj ≥ 0.05. Saline-specific genes in yellow, LPS-specific genes in magenta. WT, BMAL1-KO $n = 5$–6.

In LPS-stimulated macrophages, BMAL1-dependent genes included inflammatory modulators *Nfix, Il12b, CD40,* and lipid metabolism gene *Lpl*. Core clock genes *(Bmal1, Clock, Nr1d1/2, Per2, Cry1/2, Dbp,* and *Tef*) remained rhythmic in LPS-stimulated macrophages, indicating that the clock mechanism is not abolished by acute inflammation, although inflammatory stimuli are known to dampen oscillation amplitude (S. Chen et al., 2020).

Surprisingly, GO enrichment analysis revealed that BMAL1-dependent ZT12 vs ZT0 DEGs in LPS-stimulated macrophages were only enriched for canonical inflammatory pathways relating to interferon signalling (GO term “response to protozoan”), and were otherwise enriched for lipid metabolism and cellular homeostasis (Figure 3.8).

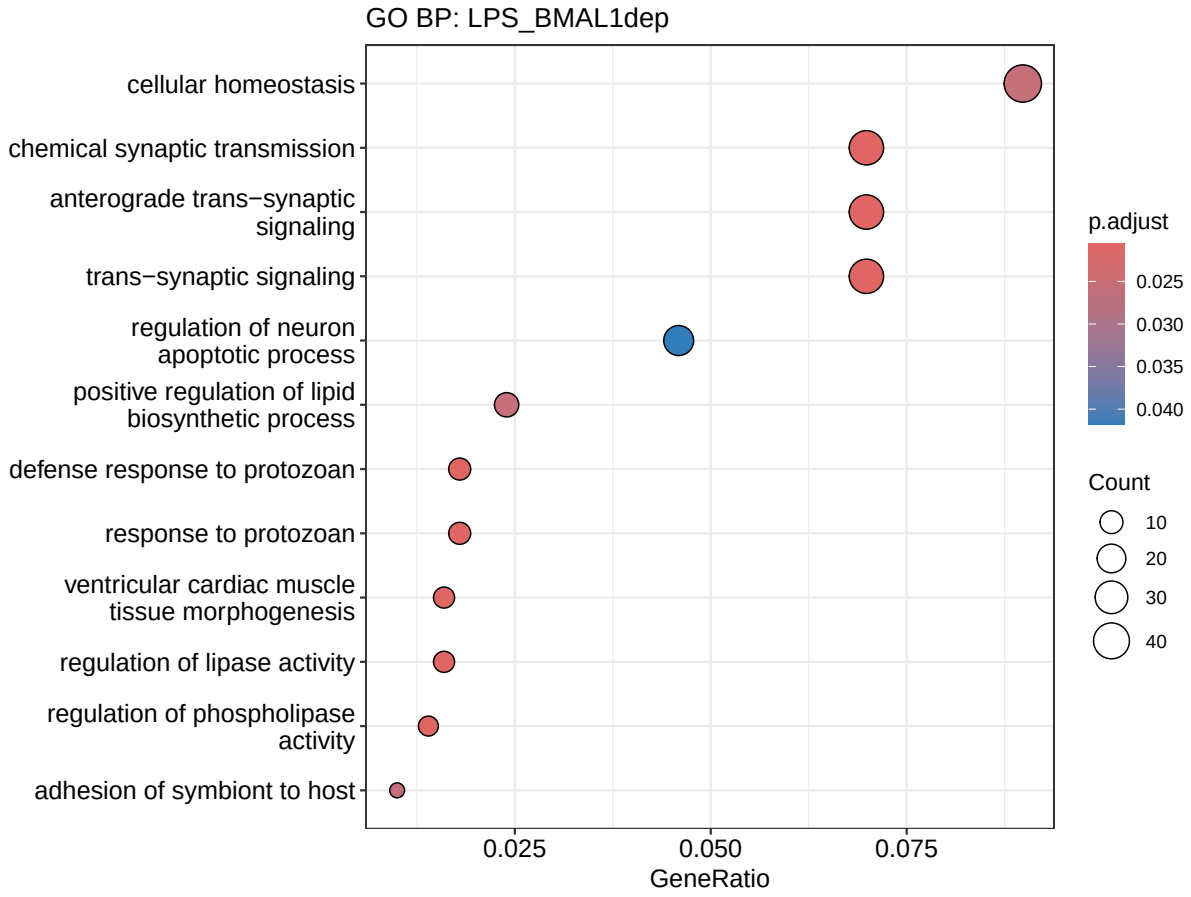

Figure 3.8: **Top 15 enriched GO terms in the BMAL1-dependent ZT12 vs ZT0 differences, in LPS-stimulated macrophages.**
BMAL1-dependent timepoint differences were defined by the inclusion of significant ZT12 vs ZT0 DEGs in WT, excluding any significant ZT12 vs ZT0 DEGs in BMAL1-KO macrophages. BMAL1-dependent timepoint differences were defined as genes which passed WT padj < 0.05 and BMAL1-KO padj ≥ 0.05.

LPS-state genes upregulated at ZT12 were enriched for regulation of lipase activity, and defense response to protozoan (interferon response, driven by presence of guanylate-binding proteins *(Gbp2/3/6/7/9* and *Iigp1, Cd40,* and *Il12b*). Genes upregulated at ZT0 showed significant enrichment of one GO term only: ERBB signalling pathway, which is involved in diverse cellular functions such as cell growth, division, migration, adhesion, and apoptosis.

The recruitment of inflammatory genes to BMAL1-dependent control in the basal state suggests that the clock primes immune responses through constitutive rhythms in unstimulated macrophages. To identify the directionality of clock regulation on inflammatory genes *in vivo*, I next examined the LPS response itself at each timepoint, through comaprison of the basal vs LPS-stimulated states.

3.3.3 BMAL1 deletion abolishes time-of-day differences in LPS responsiveness for a set of inflammatory genes.

To examine clock-regulation of the LPS response at each timepoint, I asked i) whether the clock promotes or represses LPS-induced expression at specific times of day, and ii) how this LPS responsiveness relates to basal timepoint differences in inflammatory genes. To do this, I tested for timepoint-dependence in the LPS response using an interaction term in DESeq2, and defined BMAL1-dependence using the gating contrasts given in Figure 3.1.

A subset of LPS-responsive genes (LPS contrasted with saline baseline (Section 3.2.1)) are "gated" (are statistically significant in the timepoint-dependence of their LPS response). The majority of these are gated in a BMAL1-dependent manner (Figure 3.9). 225 genes were identified as significant (padj < 0.05) in the WT-gate, while 13 genes were identified as significant in the KO-gate. Genes in WT-gate include direct CLOCK:BMAL1 targets (*Per1, Cry1, Noct, Ciart),* alongside targets regulating inflammatory pathways. These included positive regulators

of inflammation (*Il6, Ptgs2*), chemokines *Ccl2/7, Cxcl1/2*, matrix metalloproteinase *Mmp9*, and the negative regulators of inflammation *Tnfaip3, Dusp1, Nfe2l2 (NRF2)* and *Il10*. Also included were *Fosb, Fosl1, Fosl2, Jund* (AP-1 TF family members that have binding motifs enriched at BMAL1 binding sites). Genes in KO-gate include *Tnf* and *Relb*, and sphingomyelin synthase *Sgms1*. Two genes showed significant gating in both WT and KO: *Il-1b* and *Sgms2*, another sphingomyelin synthase. *Sgms2* shows identical pattern of regulation by LPS in both genotypes, while *Il-1b* is the only gene that maintained significant time-of-day gating in BMAL1-KO, but with reversed directionality (greater upregulation at ZT0 in WT with log2FC 12 vs 4 at ZT12, greater upregulation at ZT12 in BMAL1-KO with log2FC 13 vs 7 at ZT0; interaction significant in both genotypes). The timepoint with greatest upregulation in both is the same timepoint at which basal *Il-1b* expression is lowest (Figure 3.3).

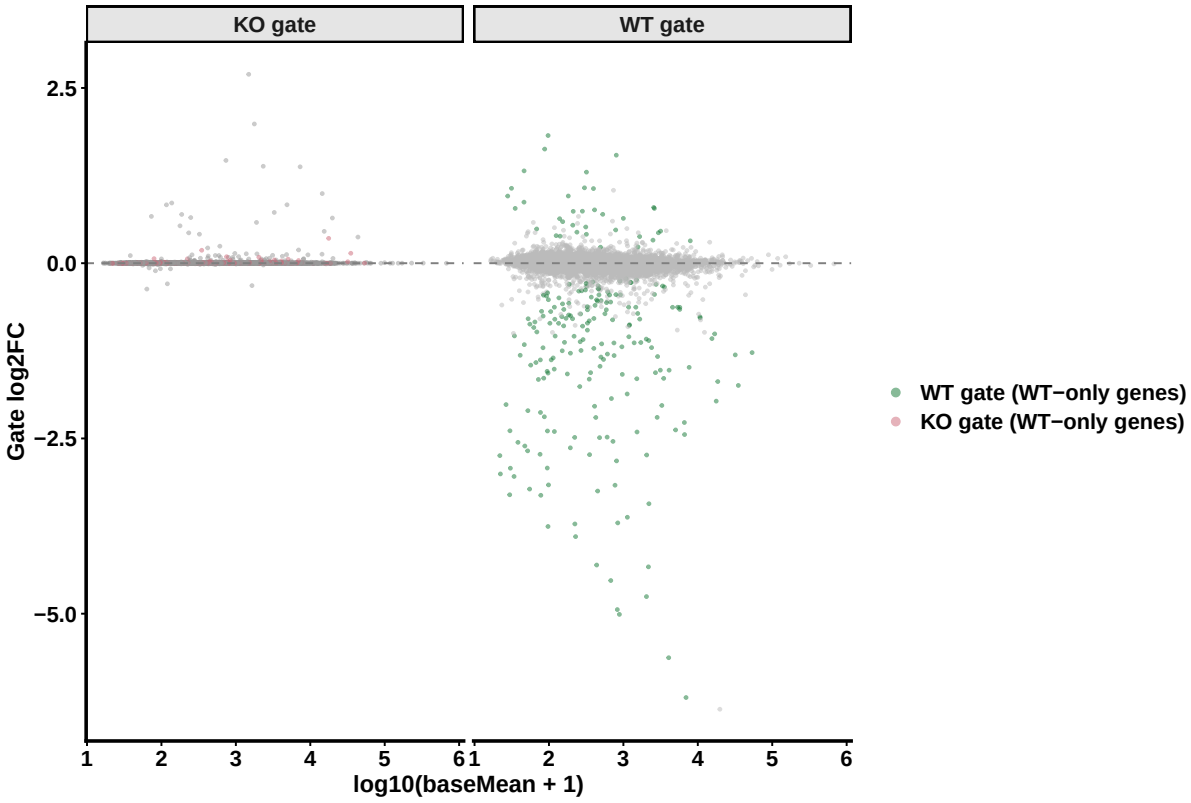

Figure 3.9: **The effect of myeloid-specific BMAL1-KO on a timepoint-treatment interaction term in peritoneal macrophages.**
This term defines which genes show dependence on timepoint (ZT0 or ZT12) for their expression 1 hour after treatment with saline, or LPS (1 mg/kg). DEGs were identified using DESeq2, with sex as covariate, where BH-adjusted p-values < 0.05. Positive sign of Gate log2FC (y-axis) is equivalent to a more positive LPS vs Saline log2FC at ZT0. Saline WT n=3, BMAL1-KO n=3-4. LPS WT, BMAL1-KO n=5-6. WT DEGs in green, BMAL1-KO DEGs in pink.

Asking whether the BMAL1-dependent gate set in WT macrophages is predominantly upregulated or downregulated in response to LPS at each timepoint, I found that for the majority of this gene set, the direction of change (whether LPS induces or represses expression) is consistent across timepoints, and it is the magnitude of change which is gated (Figure 3.10(a)). Most of the subset has a more negative Gate log2FC at ZT12 (189 of the total 225 genes). Of these, there are 121 genes which are activated by LPS, with smaller magnitude of activation at ZT12, including inflammatory regulators *Il6, Ccl2/7, Mmp9, Tnfaip3, Dusp1, Nfe2l2, Il10, Fosb, Fosl1/2, Jund*. A subset of 58 genes shows upregulation at ZT0 and repression at ZT12, including *Nr4a1, Ets1,* and *Esr1*. 17 genes show repression at ZT0 and activation at ZT12, including *Casp7* and *Gata6*. 11 genes are upregulated in response to LPS at both timepoints, with greater expression at ZT12, including *Gbp6* and *Il27*.

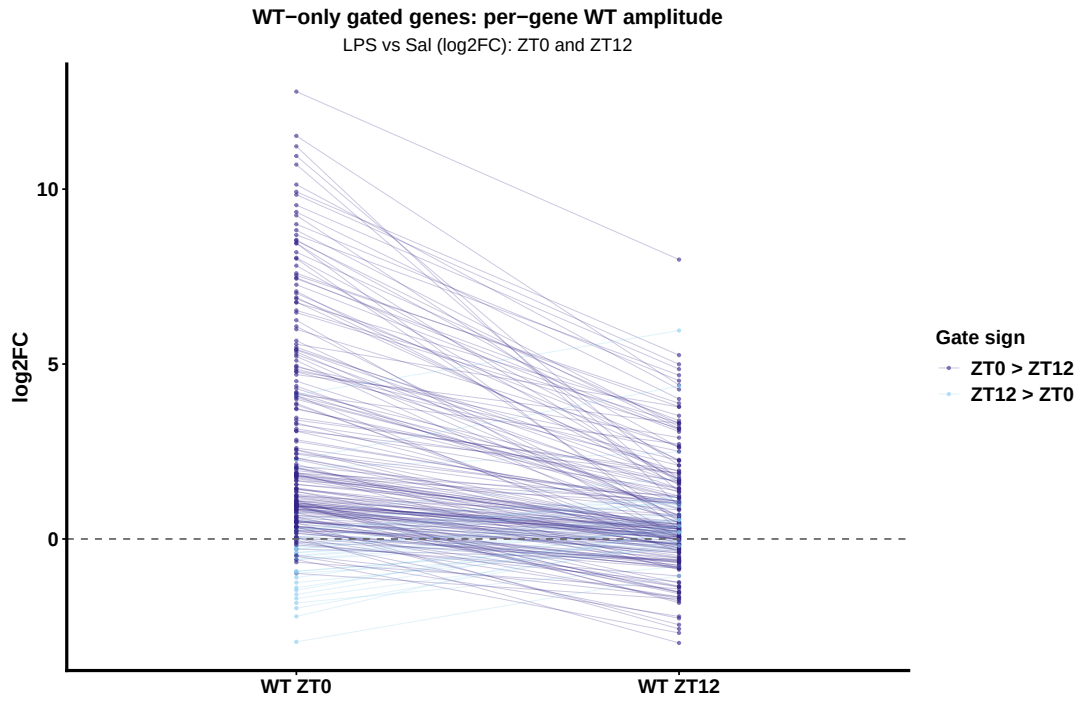

(a)

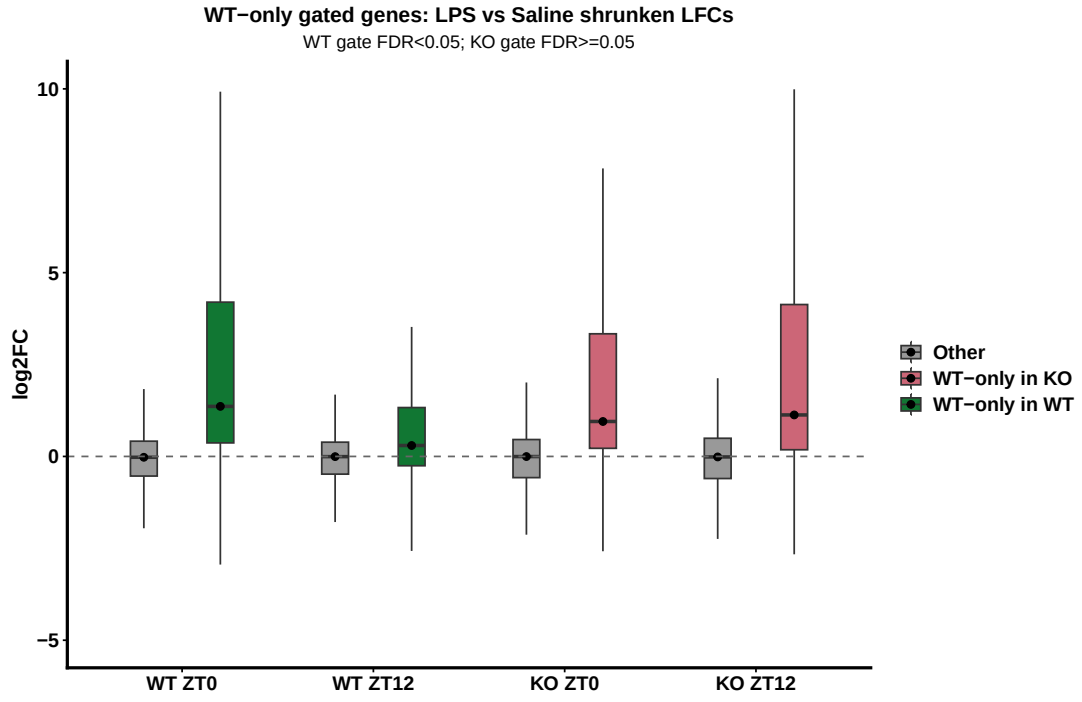

(b)

Figure 3.10: **The effect of timepoint on the magnitude and direction of change of the BMAL1-dependent gate set.**
Peritoneal macrophages from WT or BMAL1-KO mice were treated with saline, or LPS (1 mg/kg) at ZT0 or ZT12 for 1 hour before RNA extraction. (a) Spaghetti plot showing LPS vs Saline log2FoldChange at each timepoint, ZT0 and ZT12, for the BMAL1-dependent gateset. Colour indicates whether the log2FoldChange is more positive at ZT0, or ZT12. (b) Box-plot of BMAL1-dependent gated genes LPS vs Saline log2FoldChange at each timepoint, in each genotype (WT in green, BMAL1-KO in pink), against genes which show no timepoint-treatment interaction (WT gate padj > 0.05, coloured in grey).

To test whether the BMAL1-dependent gate set in BMAL1-KO macrophages shows a similar expression pattern to WT ZT0 or ZT12, I plotted the directionality of LPS vs Saline log2FC for the BMAL1-dependent gate set for each genotype/timepoint combination (Figure 3.10(b)). In the BMAL1-KO, the response of the BMAL1-dependent gated genes resembles WT ZT0. This indicates that the loss of BMAL1 results in the loss of a clock-mediated repression at ZT12.

The convergence of BMAL1-KO LPS responses toward a WT ZT0-like pattern indicated that BMAL1 is specifically required for the ZT12 phenotype. Given that LPS-induced fold-changes were reduced at ZT12 despite similar absolute expression, I hypothesised that elevated basal expression at ZT12 drives the gating phenotype. Heatmap analysis of normalised expression across all conditions showed that BMAL1-dependent gated genes exhibited elevated saline baseline at ZT12 but converged to similar levels following LPS stimulation (Figure 3.11).

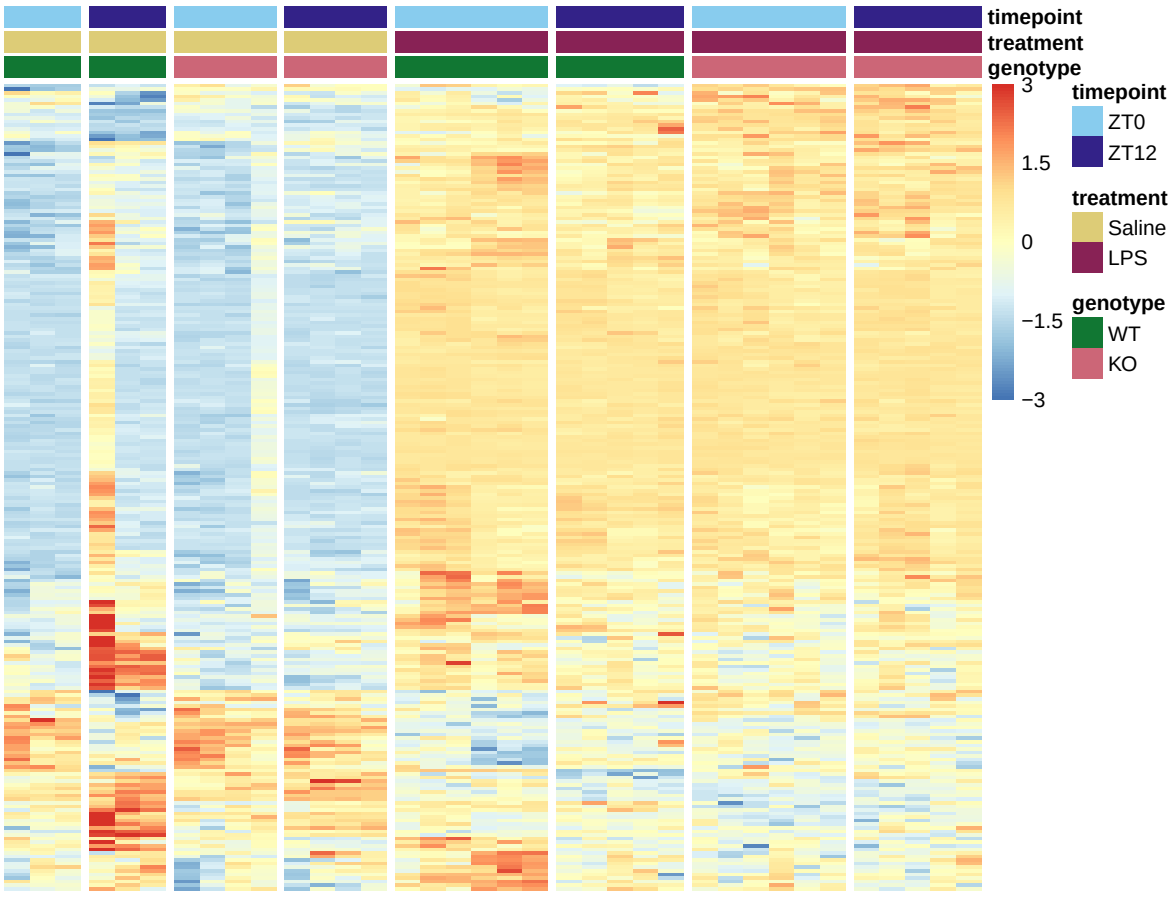

Figure 3.11: **Heatmap for the BMAL1-dependent gate of the LPS-response shows greater time-of-day difference in saline samples in WT only.**
Heatmap displays variance-stabilised expression (VST) of genes across samples, organised by timepoint, treatment, and genotype. Each row represents a gene, and values are Z-score normalised per gene (mean=0, SD=1) to highlight relative expression patterns across conditions. Genes were hierarchically clustered by correlation distance. Samples were manually ordered (not clustered) to group biological replicates and facilitate comparison across experimental conditions.

3.3.4 BMAL1-gated genes represent core inflammatory response pathways.

Having established that BMAL1-dependent gating operates through baseline pre-activation at ZT12, I next asked which biological processes are subject to this circadian control. I performed Gene Ontology (GO) enrichment analysis, using the enrichGO function from clusterProfiler. The 225 BMAL1-dependent gated genes were tested against a background of all LPS-responsive genes showing treatment x time interaction in wild-type mice (regardless of significance), with Benjamini-Hochberg correction for multiple testing.

BMAL1-gated genes were strongly enriched for canonical inflammatory pathways, including inflammatory response (GO:0006954, padj=6.8e-05), cytokine-mediated signalling pathway (GO:0019221, padj=3.5e-05), regulation of cell activation (GO:0050865, padj=6.8e-05), and cell chemotaxis (GO:0060326, padj=0.00051) (Figure 3.12). Additional enriched categories included response to lipid (GO:0033993), response to hormone (GO:0009725), circadian rhythm (GO:0007623), angiogenesis and vascular development (GO:0001525, GO:0001944), and regulation of apoptotic processes (GO:0043068). Molecular function analysis revealed enrichment for signalling receptor activity (GO:0038023) and DNA-binding TFs (GO:0140297; Figure 3.13), indicating that BMAL1 gates signal transduction and downstream transcriptional effectors. These enrichments demonstrate that BMAL1 does not indiscriminately gate all LPS-responsive genes at ZT12, but specifically controls pathways critical for inflammatory signalling amplification, and tissue remodelling. The inclusion of both pro-inflammatory pathways (chemotaxis, cytokine response) and tissue homeostatic processes (angiogenesis, vascular development) suggests that BMAL1-dependent gating balances inflammatory activation with tissue-protective mechanisms.

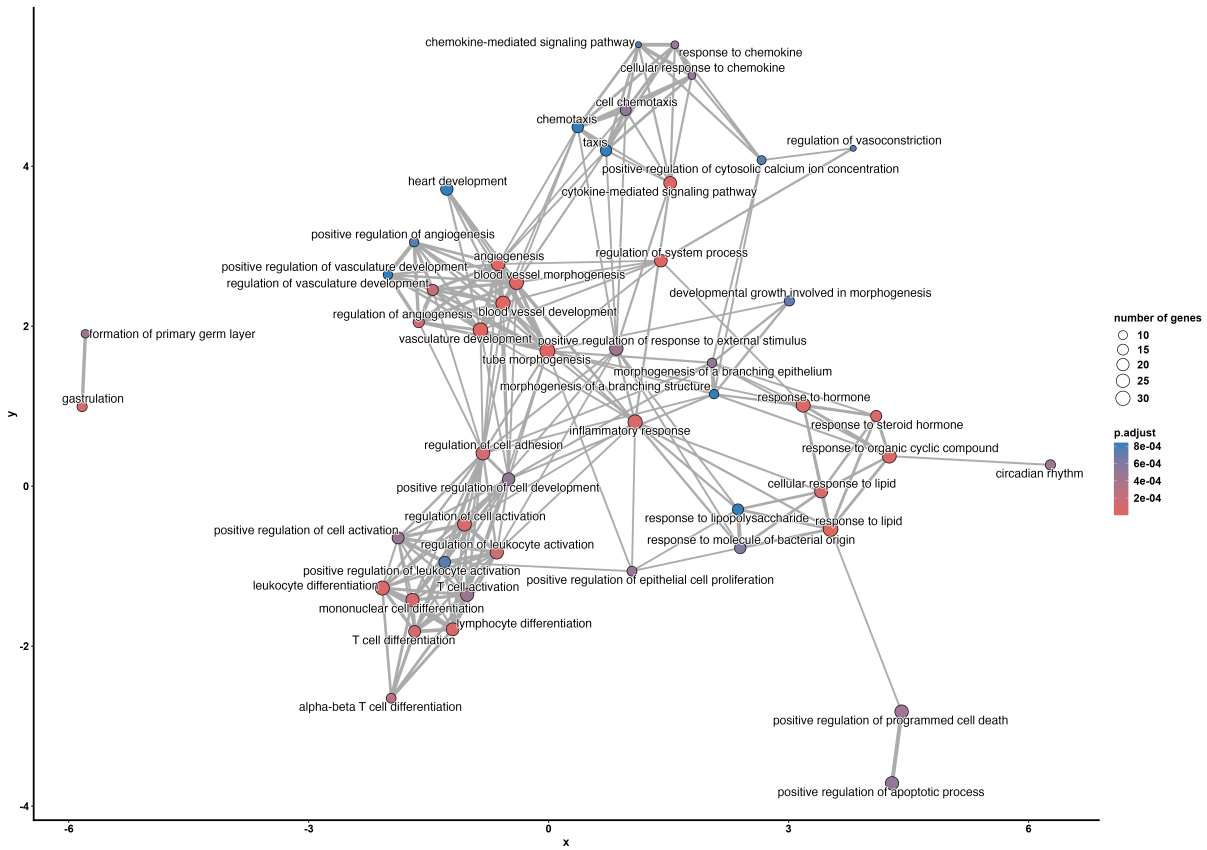

Figure 3.12: **Functional enrichment of the BMAL1-dependent gate set.**
Peritoneal macrophages from WT or BMAL1-KO mice were treated with saline, or LPS (1 mg/kg) at ZT0 or ZT12 for 1 hour, and transcriptomic analysis identified a set of 225 genes showing an interaction between timepoint and treatment in WT-only. The enrichment map shows a network of enriched pathways in BMAL1-dependent gated genes. Edges connect overlapping gene sets or pathways, so clusters are functionally related modules.

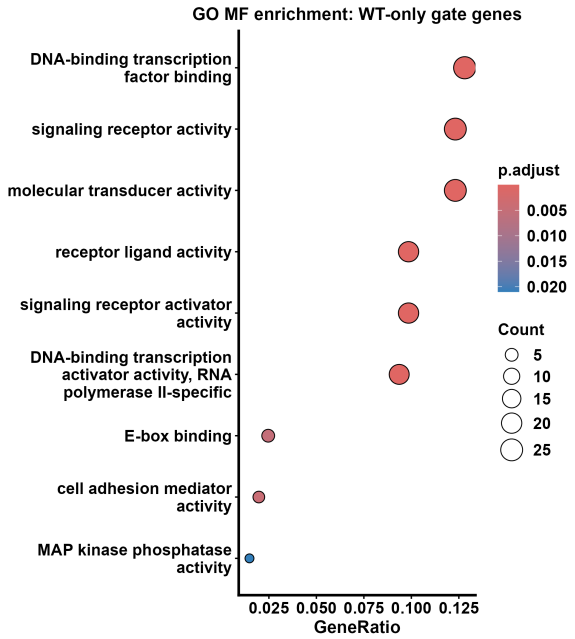

Figure 3.13: **Functional enrichment of the BMAL1-dependent gate set.**
Peritoneal macrophages from WT or BMAL1-KO mice were treated with saline, or LPS (1 mg/kg) at ZT0 or ZT12 for 1 hour, and transcriptomic analysis identified a set of 225 genes showing an interaction between timepoint and treatment in WT-only. The dotplot shows the top 12 enriched molecular functions for the BMAL1-dependent gated genes.

3.3.5 Transcription factors implicated in the BMAL1-mediated repression at ZT12.

Having established BMAL1-necessity for circadian gating of inflammatory genes (Hypothesis 1), I sought to identify molecular mechanisms by which BMAL1 regulates these genes (Hypotheses 3 and 4). I tested 1) TF expression and 2) TF and pathway activity inference to identify regulators active at ZT12 (the timepoint at which this gene set is repressed), and 3) chromatin accessibility between timepoints to test whether remodelling underlies gating.

The identification of a dampened acute response from a higher basal set-point strongly suggests that the clock engages transcriptional repressors at ZT12. To test this hypothesis, I first identified which TFs are downregulated in BMAL1-KO macrophages at ZT12 (Figure 3.14).

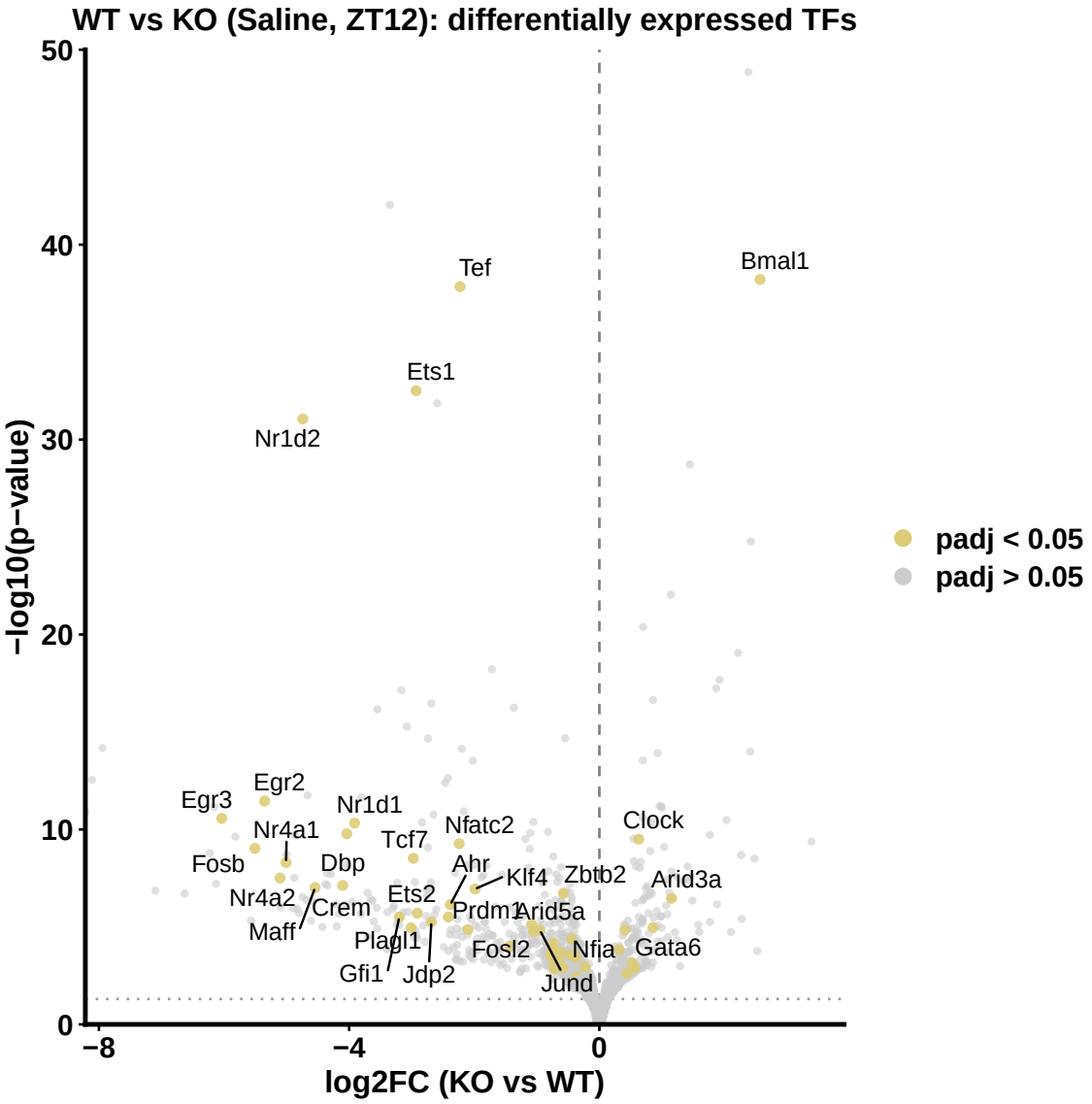
WT vs KO (Saline, ZT12): differentially expressed TFs
−log10(p−value)
log2FC (KO vs WT)
50
40
30
20
10
0
−8
−4
0
Tef
Bmal1
Ets1
Nr1d2
Egr3
Egr2
Nr1d1
Nr4a1
Tcf7
Nfatc2
Clock
Fosb
Dbp
Ahr
Klf4
Zbtb2
Arid3a
Nr4a2
Crem
Ets2
Prdm1
Arid5a
Maff
Plagl1
Fosl2
Nfia
Gata6
Gfi1
Jdp2
Jund
padj < 0.05
padj > 0.05

(a) Saline

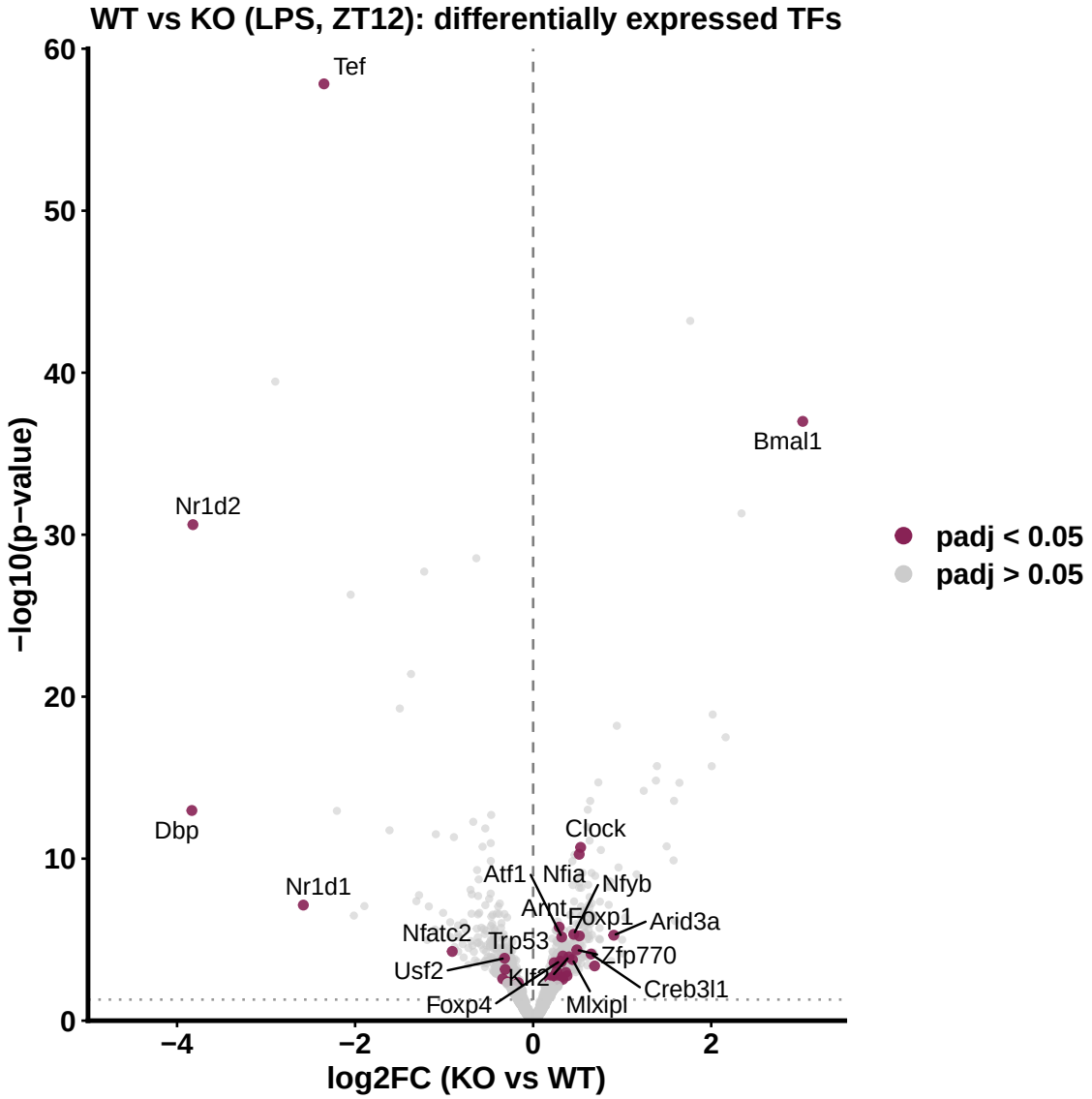

(b) LPS

Figure 3.14: **The effect of genotype on expression of TF transcripts at ZT12, in basal-state and LPS-stimulated macrophages.**
Volcano plots showing significant differentially expressed TFs, between WT and BMAL1-KO macrophages at ZT12 (a) Saline, (b) LPS-stimulated. TFs were identified using the JASPAR2024 Core non-redundant database. Coloured points indicate genes passing FDR < 0.05 (yellow in saline, magenta in LPS).

In basal-state macrophages at ZT12, BMAL1-deletion resulted in downregulation of 47 TFs, indicating BMAL1-dependent upregulation at ZT12. These included clock-associated factors *(Rora, Nr1d1, Nr1d2, Dbp)*, anti-inflammatory (M2-associated) TFs *(Nfe2l2 (*NRF2*)*, *Klf4, Prdm1, Gata3)*, and transcriptional regulators with known circadian or immunomodulatory functions *(Ets1, Usf2)*. Only 8 TFs were found to be upregulated in BMAL1-KO macrophages at ZT12: this pattern is consistent with the broader observation that BMAL1-dependent genes in basal-state macrophages are predominantly upregulated at ZT12. In LPS stimulated macrophages at ZT12, there were fewer differences between WT and BMAL1-KO for expressed TFs. 8 out of 27 TFs were downregulated in BMAL1-KO, while 19 were upregulated. The downregulated TFs were circadian/metabolic regulators (*Nr1d1/2, Dbp*), signal-dependent or activity-regulated TFs (*Usf2, Mef2c, Nfatc2*), and immune regulators (*Stat2, Ikzf1, Gfi1*).

Notably, *Bmal1* transcript itself was detectable and upregulated in BMAL1-KO compared to WT macrophages at ZT12. As previously reported for the LysM-Cre *Bmal1* conditional knock-out model, Cre-mediated excision of exon 8 results in expression of an arrhythmic, truncated *Bmal1* transcript in macrophages (Gibbs et al., 2012). This truncated transcript showed similar expression at both ZT0 and ZT12 in BMAL1-KO (with non-significant timepoint difference), whereas full-length *Bmal1* in WT macrophages showed significant ZT12 vs ZT0 differences, confirming loss of circadian rhythmicity of the core clock components (Figure 3.15).

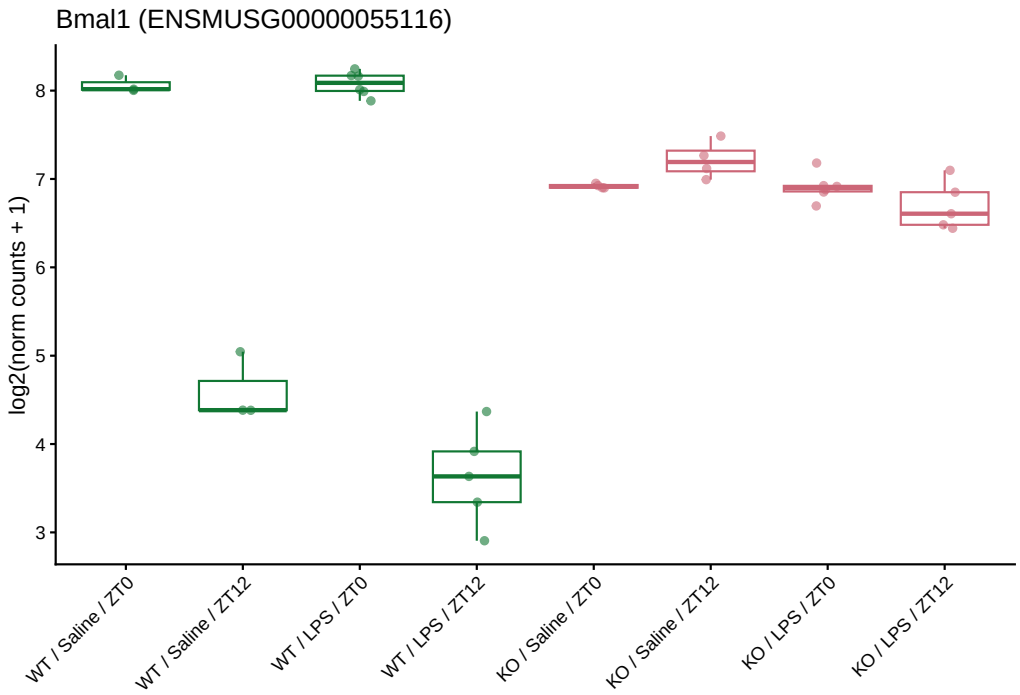

Figure 3.15: **Expression of *Bmal1* across experimental conditions.**
Log_2-normalised counts in WT and BMAL1-KO peritoneal macrophages, stratified by treatment (saline/LPS) and timepoint (ZT0/ZT12). Boxplots show median and IQR; points represent individual samples.

Five TFs were consistently upregulated in WT compared to BMAL1-KO between conditions: *Nr1d1, Nr1d2, Nfatc2* (promotes M2 macrophage polarisation), *Mef2c* (Myocyte enhancer factor 2 C, regulates macrophage polarisation), and *Gfi1* (known transcriptional repressor).

3.3.6 Inferred transcription factor activity implicates STAT/IRF pathways in ZT12 repression.

Having established that BMAL1 controls the abundance of mRNA for key immunoregulatory TFs at ZT12, I used expression patterns of TF target genes to identify which of these TFs are differentially active between ZT0 and ZT12, and between WT and BMAL1-KO.

Multiple statistical methods exist to infer upstream regulation from expression patterns of TF targets, which employ a variety of curated datasets of TF interactions. I analysed the WT gate

results using decoupleR with CollecTRI derived TF regulons, a collection of signed TF-gene interactions which outperforms other public collections of TF regulatory interactions (Müller-Dott et al., 2023). An alternative collection of regulon-interactions, DoRothEA, was used to cross-check. Very few gating effects were observed in the BMAL1-KO macrophages, reflecting the incoherence of the dataset and lack of significant gated LPS-response genes identified previously (Figure 3.9).

TF activity inference using two independent regulon databases (DoRothEA and CollecTRI) revealed strong concordance and identified distinct temporal profiles for inflammatory TFs. Most inferred TF activities for the WT gate have negative scores, indicating that activity is lower in the ZT12 LPS response relative to ZT0 (Figure 3.16). Classical inflammatory TFs including RelA, NFkB, Jun/JunD, Fos, SP1, HIF1A, Smad3, Cebpb, and Atf6 all showed reduced activity in the LPS response at ZT12 compared to ZT0.

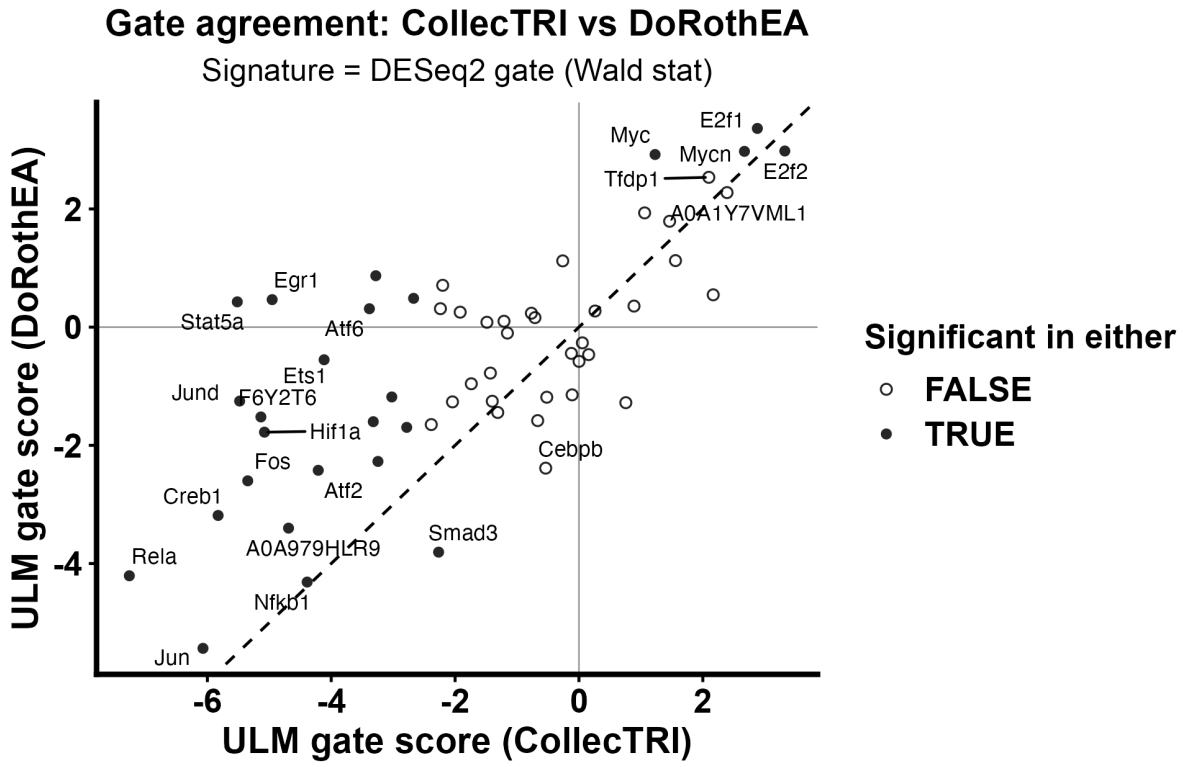

Figure 3.16: **TF activity inference for the BMAL1-dependent timepoint-treatment interaction tested through the WT-gate.**
TF activity was inferred from LPSvSaline Wald statistics for the timepoint-treatment interaction, or "gate", for each genotype using decoupleR with DoRothEA and CollecTRI regulons. Positive scores indicate TF activation in the LPS response at ZT12 relative to the response at ZT0. TFs with significant activity (FDR < 0.05 in either database) are highlighted.

Analysing TF activity within the LPS response at each timepoint, for each genotype, produced concordant results (Figure 3.17). Interferon-regulatory TFs STAT1 and IRF1 exhibited increased activity at ZT12 in WT macrophages (IRF1: ULM gate score ZT0 4.8, ZT12 5.7; STAT1 ZT0 5.6, ZT12 6.3). This temporal difference was BMAL1-dependent: BMAL1-KO macrophages showed similar STAT1 and IRF1 activity at both timepoints, losing the ZT12 enhancement observed in WT. The temporal gating of NFkB-related TFs was reduced and reversed in BMAL1-KO macrophages, which showed increased RelA activity at ZT12, where WT macrophages show increased RelA at ZT0.

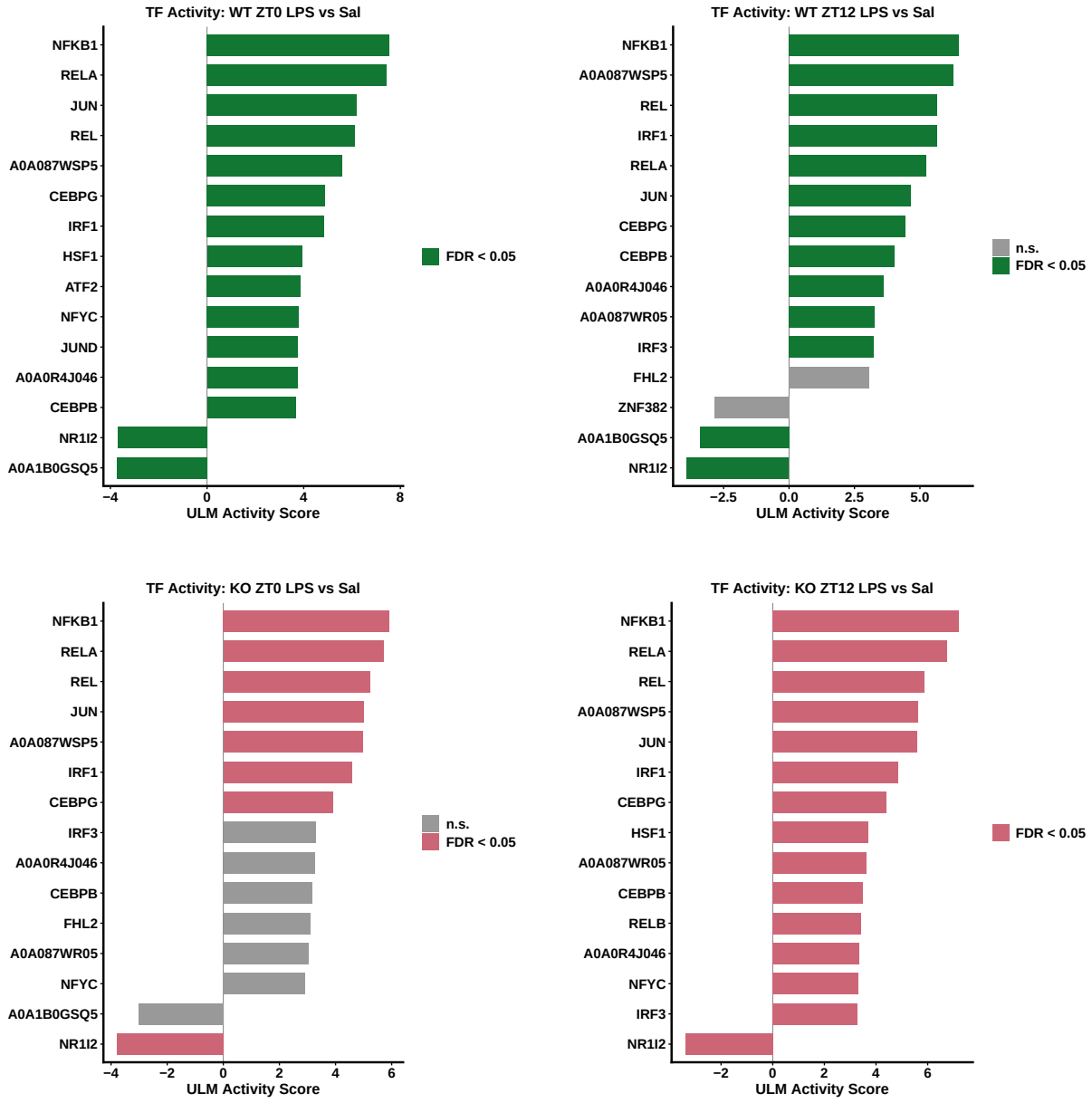

Figure 3.17: **The effect of timepoint and loss of BMAL1 on transcription factor activity in the LPS response.**
TF activity inference results for the LPS response (LPS vs Saline) in peritoneal macrophages at ZT0 and ZT12, for each genotype. TF activity was inferred for the LPS response at ZT0 and ZT12 for each genotype, inputting LPSvSaline Wald statistics into decoupleR with DoRothEA and CollecTRI regulons. Positive scores indicate TF activation by LPS treatment. TFs with significant activity (FDR < 0.05) are highlighted in green for WT and pink for BMAL1-KO; non-significant factors are shown in grey.

3.3.7 Pathway activity inference reveals increased JAK-STAT signalling at ZT12.

For both the WT and BMAL1-KO gates, the top pathways active at ZT12 vs ZT0 were inferred with decoupleR using PROGENy's multivariate linear model (MLM). Rather than inferring pathway activation via the expression of signalling molecules (through gene ontology analysis testing pathway components), PROGENy makes use of a database of perturbation experiments (capturing the response to stimulus) to extract signatures of pathway activation, assigning weights to genes in accordance with the effect of pathway activation on their expression (positive weighting indicates increased expression when pathway is active).

The negative score given to the NFkB pathway indicates greater activation of NFkB signalling in the ZT0 LPS response than the ZT12 LPS response in WT (Figure 3.18). This pattern is reversed in BMAL1-KO. The same reverse of direction by genotype is seen for JAK-STAT signalling, where activation is highest in the ZT12 LPS response in WT, and ZT0 in BMAL1-KO. The low score for the TNFa pathway shows minimal difference in activation between the two timepoints.

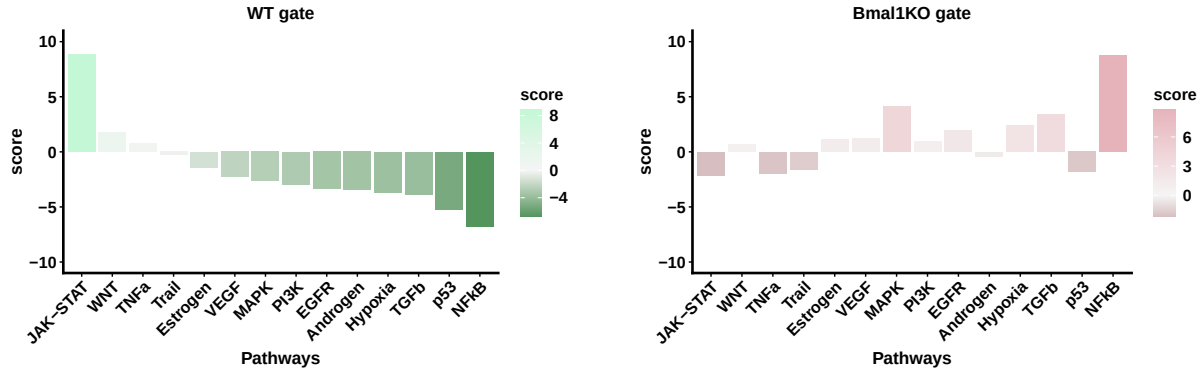

Figure 3.18: **BMAL1 deletion reverses the timepoint with greatest JAK-STAT and NFkB pathway activity in WT, and disrupts timepoint-dependence of non-inflammatory pathways.**
Pathway activity enrichment scores were inferred using decoupleR with PROGENy's multivariate linear model. Wald statistics for timepoint-treatment interaction from the WT-gate and KO-gate contrasts (WT n = 3-6, KO n = 3-6 per timepoint/treatment subgroup) served as input to score activity across 14 pathways. Positive scores indicate pathway activation at ZT12 relative to ZT0; negative scores indicate activation at ZT0. WT scores are shown in green; BMAL1-KO scores in pink.

To examine pathway-level coordination of the temporal LPS response, I plotted Wald statistics for timepoint-treatment interaction against PROGENy-derived pathway weights for target genes in the NFkB and JAK-STAT pathways (Figure 3.19). In WT macrophages, NFkB target genes with positive pathway weights predominantly showed negative Wald statistics, indicating stronger pathway activation in the ZT0 LPS response. This pattern was consistent with the reduced fold-changes observed for many inflammatory genes at ZT12. Conversely, JAK-STAT target genes with positive weights predominantly showed positive Wald statistics, indicating enhanced pathway activity specifically at ZT12 in WT macrophages.



Figure 3.19: **BMAL1 deletion disrupts the coordinated regulation of NFkB and JAK-STAT pathway target genes at ZT0 and ZT12, respectively.**
Wald statistics for timepoint-treatment interaction were calculated for each gene through the WT-gate and KO-gate separately (WT n = 3-6, KO n = 3-6 per timepoint/treatment subgroup) and used as input to decoupleR with PROGENy's multivariate linear model. For target genes in the NFkB and JAK-STAT pathways, Wald statistics are plotted against PROGENy-derived pathway weights. Negative Wald values indicate higher expression at ZT0; positive values indicate higher expression at ZT12. In WT mice (left), dark green points represent target genes whose expression patterns are consistent with pathway activation at ZT12 (positive correlation between Wald statistic and pathway weight), while light blue points indicate expression patterns suggesting pathway suppression at ZT12 (negative correlation). In BMAL1-KO mice (right), light pink indicates concordant pathway activation at ZT12, while dark pink indicates patterns suggesting pathway suppression at ZT12.

BMAL1 deletion disrupted both temporal patterns. In the KO-gate contrast, NFkB target genes showed predominantly positive Wald statistics, suggesting a reversal toward greater ZT12 responsiveness, although overall interaction effects were weak, as few genes showed significant timepoint-treatment interaction in BMAL1-KO macrophages. Similarly, JAK-STAT target genes in the KO-gate showed uniformly low Wald statistics, reflecting the loss of temporal gating. These findings demonstrate that BMAL1 orchestrates opposing temporal regulation of these two key inflammatory pathways: suppressing NFkB-mediated responses while specifically enhancing JAK-STAT signalling at ZT12.

3.3.8 Motif analysis reveals E-box and hormone response elements in promoters of BMAL1-dependent inflammatory genes.

To link the BMAL1-dependent transcription and modulation of activity of key regulatory TFs to the regulation of the gate, I next asked whether the promoters of the BMAL1-dependent gate set were enriched for motifs for these TFs.

To identify transcriptional mechanisms underlying BMAL1-dependent temporal gating, I performed HOMER motif analysis on promoter regions (-300bp to +50bp from TSS) of genes showing significant timepoint-treatment interaction in the WT-gate. Using LPS-responsive but non-gated genes as background, I found significant enrichment for E-box motifs, consistent with direct CLOCK:BMAL1 regulation of this gene set (Table 3.2).

Promoters were also enriched for hormone response elements (HREs), including both estrogen response elements (EREs) and glucocorticoid response elements (GREs). This hormonal regulatory architecture was corroborated by Gene Ontology analysis (Figure 3.12), which showed enrichment for steroid hormone response pathways. The convergence of circadian and hormonal regulatory elements in BMAL1-gated genes suggests potential crosstalk between these

systems in governing temporal inflammatory responses, a mechanism explored further in Chapter 4.

Rank	Motif (Family)	Target (%)	q-value
1	ERE (NR)	7.9	0.060
2	BMAL1 (bHLH)	34.2	0.060
3	GRE (NR)	5.9	0.795
4	Usf2 (bHLH)	12.9	0.795
5	ZNF467 (Zf)	32.2	0.795

Table 3.2: **Motif enrichment in promoter regions of BMAL1-dependent gated genes.** HOMER motif enrichment analysis. Target (%) indicates percentage of target sequences containing the motif.

3.3.9 ATAC-seq reveals few differentially-accessible regions between timepoints.

Circadian control of gene expression can arise from rhythmic enhancer activity and TF occupancy and/or time-varying recruitment of promoter co-regulators without large changes in chromatin accessibility. To test whether early LPS responses differ in chromatin accessibility between ZT0 and ZT12, I performed ATAC-seq in the LPS-stimulated WT peritoneal macrophage subgroups (Table 3.1). Reads were aligned to mm10, PCR duplicates and blacklist regions were removed, and sub-nucleosomal fragments were retained to enrich for TF binding sites. LanceoTron was used to call peaks, and the peak calls from each sample group (Male ZT0, Female ZT0, Male ZT12, Female ZT12) were used to build a consensus peak set consisting of 20,332 peaks. These peaks were enriched for promoters and as such, quality was a limiting factor in detecting subtle shifts to the chromatin landscape.

I first asked whether there were significant rearrangements in global chromatin accessibility between ZT0 and ZT12. Differential accessibility analysis was performed using edgeR, chosen due to its superior accuracy when analysing ATAC with low biological sample size (Gontarz et

al., 2020). I found no significantly differentially accessible regions of open chromatin (Figure 3.20).

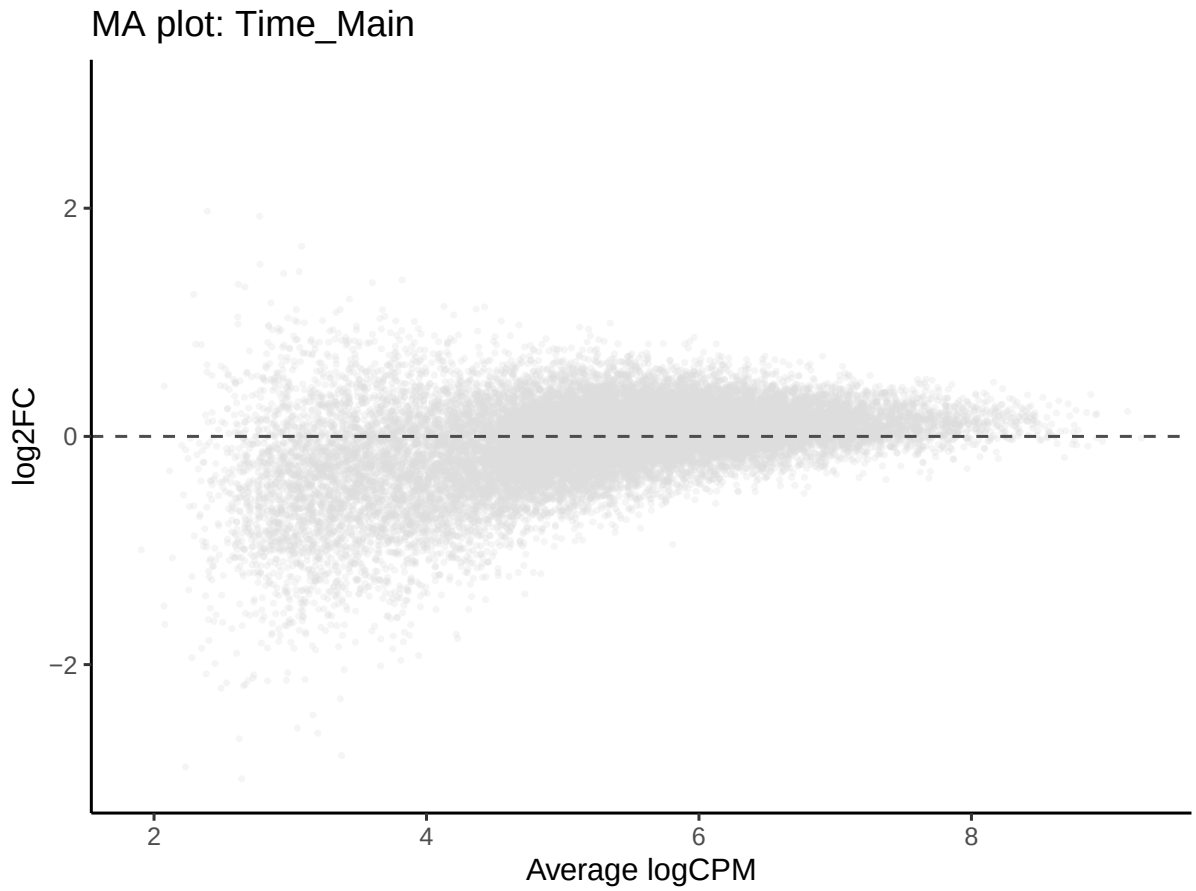

Figure 3.20: **Effect of timepoint on global chromatin accessibility in peritoneal macrophages.**
MA plot showing differential chromatin accessibility between ZT12 and ZT0 in LPS-stimulated WT peritoneal macrophages. Each point represents an accessible chromatin region, with log2FC (ZT12/ZT0) plotted against average log counts per million (logCPM). Differential accessibility was assessed using edgeR (ZT0 n = 5, ZT12 n = 6). All regions were found to be non-significant (FDR > 0.05) and are shown in gray.

This suggests that at 1 hour after LPS, large, global shifts in chromatin accessibility between ZT0 and ZT12 are not detectable: these results do not support Hypothesis 3, indicating that large-scale chromatin remodelling opening/closing enhancers is not the primary driver of BMAL1-dependent gating. I therefore moved to a gene set-biased enrichment strategy, as gating is more likely mediated through changes in TF availability or activity at the constitutively accessible chromatin landscape surrounding clock-gated genes.

3.3.10 Accessible chromatin regions are enriched within 50kb of BMAL1-dependent inflammatory genes.

Using the consensus peak set built from WT macrophages at ZT0/ZT12, and the consensus peak set built from WT ZT8 basal state macrophages (described in Section 3.3.12), I tested whether peaks are enriched near the BMAL1-dependent gate set using PEGS (Peak-set Enrichment of Gene-Sets) (Briggs et al., 2021). I analysed both the full BMAL1-dependent gate set, and two subsets split dependent on whether the response to LPS was amplified or repressed at ZT12. Three negative control sets of randomly selected non-clock gated genes which respond to LPS-stimulation (matched for gene set length) were tested alongside.

Across distance shells, I observed clear enrichment up to the 50kb region for the complete BMAL1-dependent gate set and for the *repressed* subset, where p-values lay below 1e-10 in both basal and LPS chromatin (Figure 3.21). Enrichment was weaker for the *activated* subset, consistent with its smaller size. This shows that BMAL1-dependent gated genes are in peak-dense neighbourhoods, in both basal-state and after 1 hour of LPS stimulation.



Figure 3.21: **Heatmap showing enrichment of accessible chromatin regions near BMAL1-dependent clock-gated inflammatory gene set.**
ATAC-seq was performed on peritoneal macrophages from WT male and female mice in basal (unstimulated, ZT8, n=5) and LPS-stimulated conditions (ZT0 n = 5, ZT12 n = 6). Consensus peak sets were generated, and Peak-set Enrichment in Gene Sets (PEGS) was used to test whether open chromatin regions were enriched at specified distances from transcription start sites (TSSs) of the target gene sets. The BMAL1-dependent gated genes are split into those genes repressed in their activation at ZT12, or amplified. Three negative control gene sets are composed of randomly selected non-clock gated genes which respond to LPS-stimulation (matched for gene set length with the BMAL1-dependent gate set). Colour intensity indicates -log(Pval), with darker colour indicating greater enrichment.

Having identified significant spatial association between BMAL1-dependent gate set and open chromatin regions (OCRs, putative regulatory regions), I identified potential regulators by performing motif enrichment analysis on the OCRs within 50kb of the BMAL1-dependent gated gene set.

In both basal and LPS macrophage chromatin, I observed enrichment for bZIP family motifs (ATF, AP-1, FOS/JUN), E-boxes (BMAL1, CLOCK, NPAS2), NFkB (RelA), and nuclear receptor motifs (RARα, ERRα, COUP-TFII; Table 3.3). However, the motif families did not reach statistical significance in basal chromatin after multiple test correction. LPS chromatin showed additional enrichment for STAT family motifs (STAT-1/3/4/6, q<0.05), consistent with JAK-STAT pathway activation at ZT12 (Section 3.3.7).

Motif family	Representative TFs	Basal q-value	LPS q-value
bZIP (AP-1)	ATF2/3/7, FOS, JUN	0.26	<**0.001**
bZIP (PAR)	NFIL3	0.26	**0.007**
E-box	BMAL1, CLOCK, NPAS2	0.26	**0.045**
NFκB	p65/RelA	0.26	**0.012**
STAT	STAT1/3/4/6	-	**0.004**
Glucocorticoid	GR	-	**0.004**
Nuclear receptor	RARα, ERRα, COUP-TFII	0.26	<**0.001**

Table 3.3: **Motif enrichment in open chromatin regions within 50kb of BMAL1-dependent gated genes.** HOMER motif enrichment analysis was performed on OCRs proximal to BMAL1-dependent gated genes. Minimum q-values (BH-corrected) across motifs within each family are reported. **Bold** indicates q<0.05. - indicates motif family not detected.

3.3.11 REV-ERBα is not required for the circadian gating of BMAL1-dependent inflammatory genes.

The BMAL1-dependent gating of the LPS response is defined by a repression acting at ZT12 (Figure 3.10). As many reports have indicated that anti-inflammatory clock-control is conferred through REV-ERBα activity, I tested the importance of REV-ERBα in shaping the peritoneal macrophage response to LPS through use of a myeloid-cell specific genetic deletion. I assessed

global changes in transcriptomics and chromatin accessibility compared to WT littermate controls. Both sexes were included; sample sizes per group are given in Table 3.4.

Group	Male	Female	Total
WT Saline	2	3	5
KO Saline	3	2	5
WT LPS	3	3	6
KO LPS	3	3	6

Table 3.4: **Summary of REV-ERBα experimental group sample sizes.** Animals per group split by sex.

Of the 10,275 transcripts passing the expression-level filter, REV-ERBα deletion perturbed basal gene expression more than expression after LPS-stimulation (Figure 3.22). There were 72 baseline DEGs, and 16 DEGs following LPS (FDR < 0.05), suggesting that inflammatory signalling largely overrode its regulatory effects.

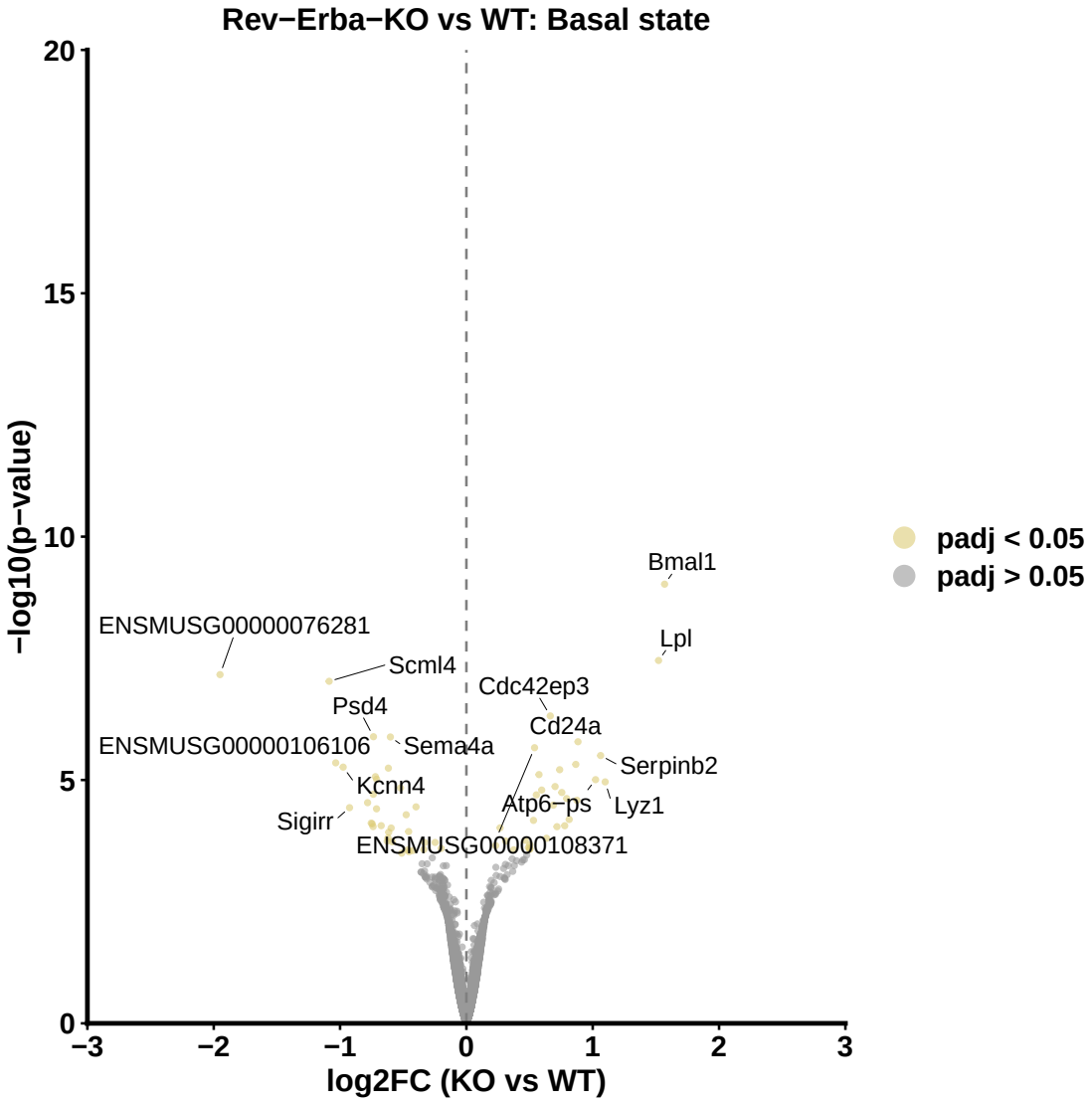

(a) Basal state

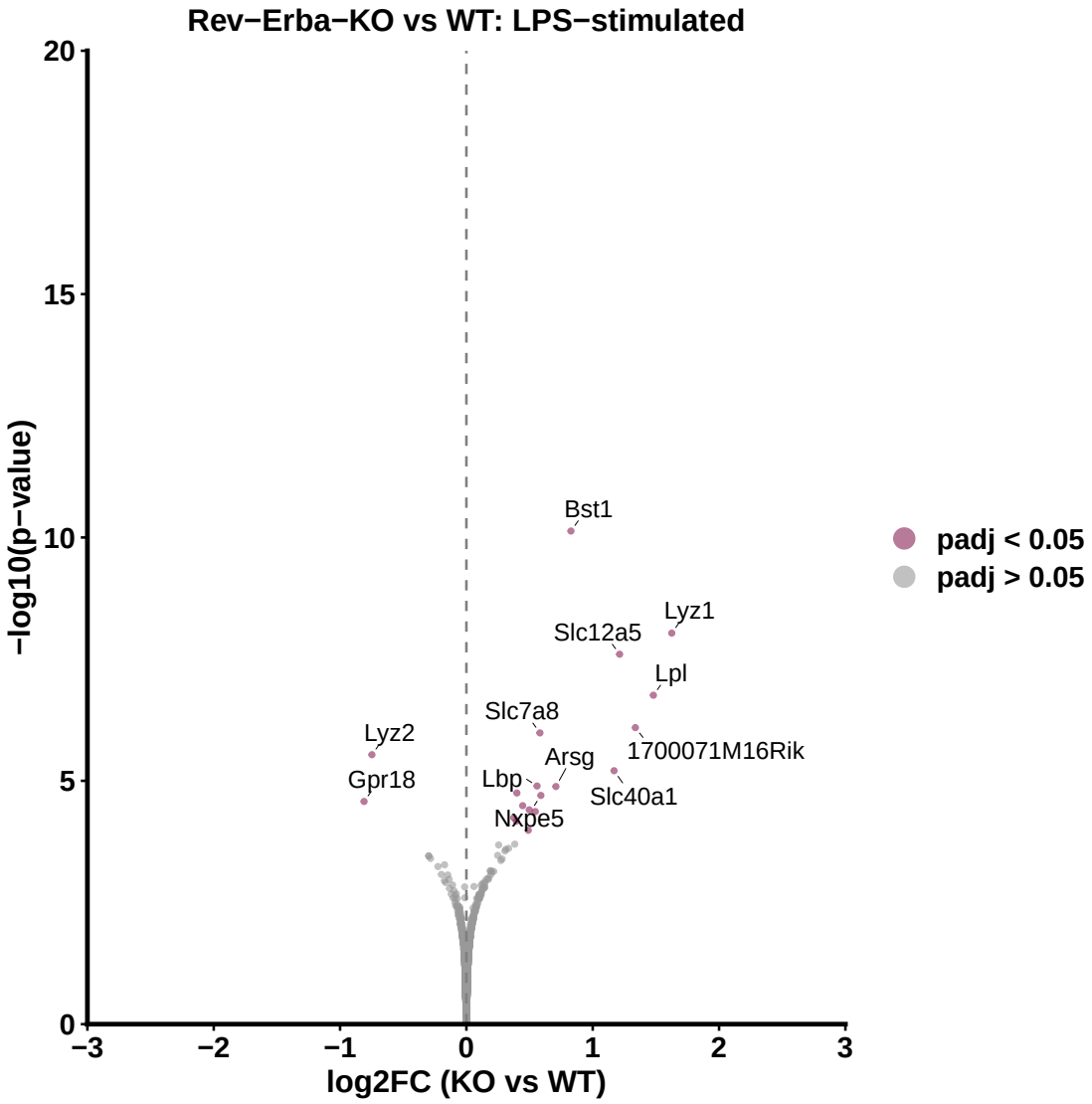

(b) LPS-stimulated

Figure 3.22: **REV-ERBα deletion has minimal impact on both basal and LPS-stimulated transcriptomes at ZT8.**
Volcano plots showing the effect of REV-ERBα deletion on peritoneal macrophage transcriptomes at ZT8 in (a) basal state and (b) LPS-stimulated conditions. Each point represents a gene, with log2FC (KO/WT) plotted against -log10 p-value. Genes with significant differential expression (FDR < 0.05) are highlighted in yellow for basal state and magenta for LPS-stimulated conditions; non-significant genes are shown in grey. Saline n = 5, LPS n = 6 per genotype.

In the basal state, there were 32 genes upregulated by REV-ERBα deletion and so representing repressive targets of the TF (Figure 3.22(a)). These included *Bmal1*, confirming disruption of the TTFL negative feedback loop, alongside lipid metabolism genes (*Lpl, Pla2g7, Fabp7*), immune regulators (*Nlrp3, Nfil3, Cxcl13, Ccrl2, Lyz1*), and hypoxia response factor *Egln3*. *Nlrp3* and *Nfil3* derepression is consistent with previous reports of REV-ERBα-mediated repression of the inflammasome and the transcriptional repressor NFIL3 (Duez et al., 2008; S. Wang et al., 2018). No significant pathway enrichments were detected among upregulated genes.

40 genes were downregulated in REV-ERBα-KO macrophages in the basal state, indicating positive regulation by REV-ERBα (direct or indirect). These included negative regulators of inflammation (*Sigirr*, which attenuates TLR4 and IL-1R signalling), inflammatory effectors (*Aif1, Lyz2, Itgal*), and signalling mediators (*Traf1, Kcnn4*). Enrichment analysis identified GO term GO:0042101 (T cell receptor complex; padj = 0.0028), driven by genes *Cd6, Cd3d, Cd3g*.

Critically, REV-ERBα deletion only minimally perturbs the LPS-stimulated macrophage transcriptome (Figure 3.22(b)). These results do not support Hypothesis 2: REV-ERBα-KO resulted in minimal transcriptional changes, indicating that the TF is not required for BMAL1-dependent gating of inflammatory genes, contrary to predictions based on its role as a circadian repressor in other systems.

The 16 DEGs included 14 upregulated by REV-ERBα deletion, including *Lpl, Lbp* (lipopolysaccharide-binding protein), *Slc40a1* (the iron transporter ferroportin), *Slc7a8* (amino acid transporter), and lysosomal protease *Ctsl*. No significant pathway enrichments were detected among upregulated genes. Only two genes were downregulated by REV-ERBα deletion: *Lyz2* and *Gpr18*.

Lyz2 was consistently downregulated across both conditions. The LysM Cre allele is itself a *Lyz2* loss-of-function knock-in; reduced *Lyz2* expression and promoter accessibility relative to

Cre-negative WT controls are expected consequences of the allele, independent of REV-ERBα

.

As the saline baseline showed greater perturbation, I next asked whether REV-ERBα-KO altered the magnitude and direction of fold-change of genes in response to LPS. LPS response in WT and REV-ERBα-KO macrophages is highly similar (Figure 3.23). The majority of LPS-responding genes had similar magnitude and direction fold-change between genotypes (pearson correlation r = 0.96). Very few genes were found to have different reactions to LPS (as identified by opposite signs of Log2FC). Genes passing FDR only in one genotype were identified as WT-only or REV-ERBα-KO-only LPS-response genes. These genes showed a pattern of regulation fitting within the pattern of regulation in the opposite genotype, and are likely sub-threshold responders.

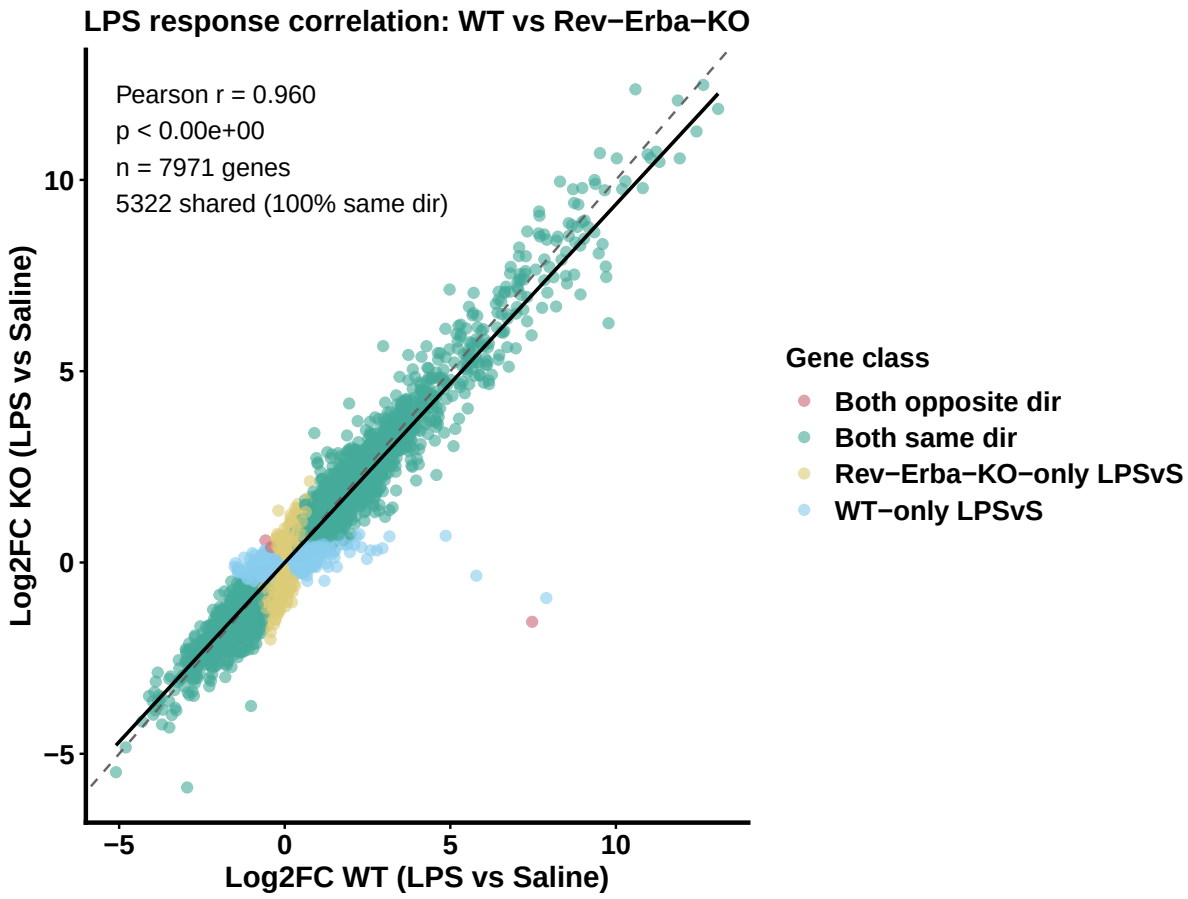

Figure 3.23: **The response to LPS is highly conserved between WT and REV-ERBα-KO peritoneal macrophages.**
Scatter plot comparing the log2FC in response to LPS (LPSvSaline contrast analysed using DESeq2) for both WT and REV-ERBα-KO. Saline n = 5, LPS n = 6 per genotype.

3.3.12 Chromatin accessibility is largely unaffected by REV-ERBα deletion in basal peritoneal macrophages.

REV-ERBα is a transcriptional repressor known to recruit co-repressors and histone deacetylases to enhancers. I performed ATAC-seq on the same peritoneal macrophages used for basal-state RNA-seq, to test whether REV-ERBα's contribution to LPS-response gating is driven by the pre-setting of basal state enhancer accessibility at clock-regulated genes in macrophages. I used the same cells used for basal RNA-seq to eliminate technical confounders, allowing me to ask whether expression differences co-occurred with accessibility changes at the relevant loci.

To test whether these changes in gene expression are accompanied by the changes to chromatin accessibility expected in line with REV-ERBα's role in recruiting epigenetic modifiers, I perfomed ATAC-seq on the basal-state macrophages to accompany the transcriptomic analysis. Using LanceoTron to call peaks, I found a consensus set of 70,628 peaks, 49,772 of which were kept after replicate-aware filtering to ensure reproducibility. Differential accessibility analysis was performed using edgeR.

I observed specific, locus-level de-repression (Figure 3.24). 33 DARs passed FDR control: 27 peaks which were more accessible in the REV-ERBα-KO, and 6 peaks more accessible in the WT, consistent with the loss of a transcriptional repressor. In either direction, the effect size is modest and centred near |log2FC| = 1.

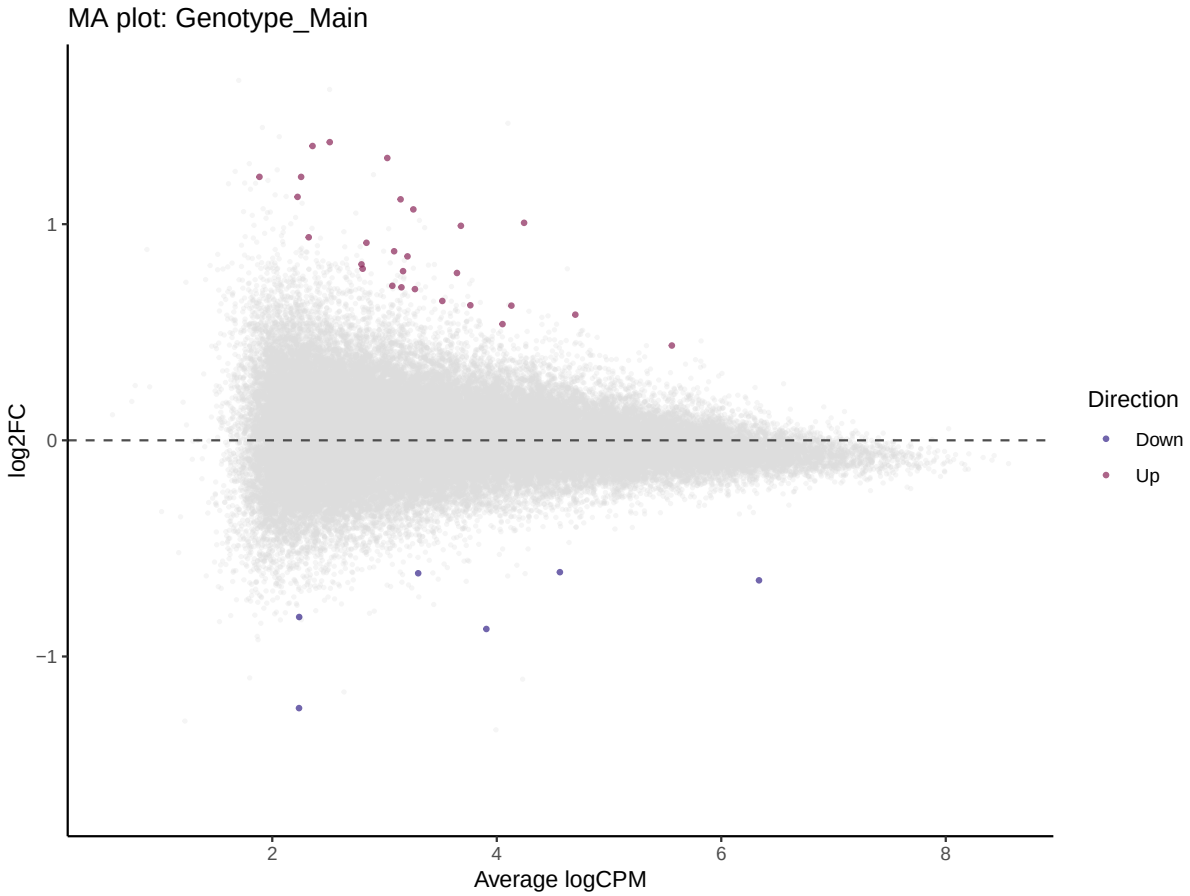

Figure 3.24: **Effect of REV-ERBα deletion on global chromatin accessibility in peritoneal macrophages.**
MA plot showing differential chromatin accessibility between REV-ERBα-KO and WT littermates in basal state WT peritoneal macrophages. Each point represents an accessible chromatin region, with log2FC (KO/WT) plotted against average log counts per million (logCPM). Differential accessibility was assessed using edgeR (n = 5). Significant regions (FDR < 0.05) are highlighted in purple where open in KO, and blue where open in WT; non-significant regions are shown in grey.

DARs were distributed across genomic features including promoters, introns, and distal intergenic regions. Among promoter-associated DARs, *Lpl, Efcab5, Gcnt2, Itgb7,* and *1700003M07Rik* showed increased accessibility in REV-ERBα-KO , while *Svop* and *Pgk1* showed reduced accessibility. Intronic DARs with increased accessibility in REV-ERBα-KO included regions within *Fbxl5, Lipg, Kcnn3, Plxdc2*, and *Usp7*, while *Cpsf6, Krt80,* and *Kcnip2* contained intronic regions less accessible in REV-ERBα-KO. Intergenic DARs more accessible in REV-ERBα-KO were proximal to *Lyz1, Cracr2a, Itpr2,* and *Trim72*, among others.

Several DARs corresponded directly to genes differentially expressed in the RNA-seq analysis. *Lpl*, a known REV-ERBα-KO target in adipose tissue, showed both increased promoter accessibility and transcriptional upregulation in REV-ERBα-KO macrophages under both basal and LPS-stimulated conditions. Similarly, *Lyz1* was upregulated in both states, with a corresponding intergenic DAR located 20 kb upstream of its TSS showing increased accessibility in REV-ERBα-KO macrophages.

REV-ERBα-KO increases accessibility in proximity to known circadian regulators (*Usp7, Cpsf6*) and clock-regulated genes (*Kcnip2, Lpl, Itpr2*). Usp7 (ubiquitin-specific protease 7) promotes the stability of CRYs through deubiquitination, and knock-down or inhibition shortens circadian period (Hirano et al., 2016).

Despite these locus-specifc changes, loss of REV-ERBα did not significantly remodel genome-wide chromatin accessibility at ZT8 in unstimulated peritoneal macrophages.

3.4 Discussion

3.4.1 The scope of BMAL1-dependent gating.

Circadian control of the macrophage transcriptome is extensive. (Collins et al., 2021) identified approximately 2800 rhythmic protein-encoding transcripts in BMDMs *in vitro*, falling in two temporally-separated waves. My results demonstrate the extent to which the circadian transcriptome, as measured at two timepoints ZT0 and ZT12, is BMAL1-dependent when macrophages are measured *in vivo*. Critically, BMAL1-dependent regulation of timepoint-dependent transcripts is context specific, with distinct biological processes regulated in basal-state macrophages versus LPS-activated macrophages.

Most genes showing ZT0 vs ZT12 differences were BMAL1-dependent in both saline (89%) and LPS-stimulated (72%) peritoneal macrophages. These results support Hypothesis 1, and confirm the necessity of the macrophage-intrinsic clock for the timepoint-dependent differences in the LPS response. There were 875 BMAL1-dependent genes in basal state macrophages, and 516 in LPS-stimulated, with minimal overlap in which genes were BMAL1-dependent in each condition (141 genes). This limited concordance is supported by multiple studies that have shown that pro-inflammatory modulators can remodel circadian control and dampen rhythmicity in output. In macrophages, the LPS-mediated dampening occurs through the changes to Reactive Oxygen Species (ROS) levels (Y. Wang et al., 2016), and through miR-155 binding to the 3'-UTR of *Bmal1* and suppressing subsequent mRNA and protein levels (Curtis et al., 2015). Most recently, comprehensive testing of pro- and anti-inflammatory modulators has revealed their counteractive effects on the macrophage clock, with multiple pro-inflammatory stimuli able to suppress Per2-Luciferase expression, suggesting a common downstream mech-

anism regardless of initial signalling event, which could involve the re-wiring of the metabolic state of the cell to a glycolysis-dominant phenotype (S. Chen et al., 2020).

There are fewer transcriptional differences between ZT0 and ZT12 at the early 1 hour post-LPS timepoint than in the basal state. These LPS-differences relate primarily to interferon responses and lipid metabolism rather than canonical cytokine production pathways. This disparity between early transcriptional changes and the substantial timepoint-dependent differences in downstream protein production observed by others reflects both the timing of sampling and the extensive post-transcriptional regulation in the inflammatory response. The 1 hour timepoint captures the immediate-early transcriptional response before complex feedback loops develop. Importantly, (Collins et al., 2021) found that few rhythmic proteins in BMDMs had correspondingly rhythmic transcripts, and (Hurley et al., 2018) demonstrated that the rhythmic proteome in *Neurospora* was determined primarily by energy availability and translational regulation rather than transcriptional rhythms. The observed enrichment for altered lipase activity between ZT0 and ZT12 may reflect the metabolic transition from oxidative phosphorylation in the light phase to glycolysis in the dark phase. The absence of classic inflammatory pathway enrichment (for example, GO terms relating to cytokine signalling) in the LPS BMAL1-dependent set suggests that dominant effects of BMAL1 gating LPS responses are mediated through control of upstream regulators or metabolic pathways that modulate inflammatory capacity (including via post-transcriptional control), rather than direct action at the regulatory elements of a wide-ranging set of clock-controlled inflammatory genes.

Supporting this model, I observed enrichment of GO terms relating to defense against protozoans in the ZT12-upregulated LPS-BMAL1-dependent ZT0 vs ZT12 DEGs, driven by presence of guanylate-binding proteins (GBPs). GBPs are a family of interferon-inducible GTPases acting as cytosolic LPS sensors and promote host defense against intracellular gram-negative

bacteria in part through facilitating recognition of LPS by the noncanonical caspase-4 inflammasome. Critically, this timepoint is the time at which the GO term type II interferon production is enriched in saline-BMAL1-dependent ZT0 vs ZT12 DEGs. This suggests that autocrine IFN-γ could be elevated at ZT12 in peritoneal macrophages, priming the induction of ISGs including GBPs.

The active phase typically involves increased environmental exploration, which brings an increased probability of injury and of exposure to environmental pathogens. It is possible that this IFN-primed state observed at ZT12 may have been selected for the ancestral environment as it would position macrophages for enhanced responses to intracellular pathogens encountered at the onset of the active period.

Metabolic programming likely contributes to the ZT12 pro-inflammatory priming. (Collins et al., 2021) demonstrated that BMDMs in opposing circadian phases exhibit distinct metabolic phenotypes: rest phase macrophages are anti-inflammatory and oxidative phosphorylation-dominant, whereas active phase macrophages favour glycolysis and are pro-inflammatory. At ZT12, positioned at the transition to the active period, macrophages would be increasingly glycolytic: a metabolic state that supports inflammatory activation and creates conditions permissive for HIF1α stabilisation. ZT12 priming could also be explained through action of other clock factors. PER1/2 have been shown to suppress basal and LPS-induced *Tnfa* and *Il-1b* expression (T. Wang et al., 2016; H. Xu et al., 2014). CRY negatively regulates the cAMP-PKA-NFkB pathway, suppressing *Il6, Tnfa,* and *iNos* (Narasimamurthy et al., 2012).

Metabolic status is defined by nutrient availability alongside intrinsic clock action. In basal macrophages, I identified a set of 31 genes showing upregulation at ZT12 in WT, and upregulation at ZT0 in BMAL1-KO, enriched for pro-inflammatory GO terms like inflammatory response. This set may reflect the integration of BMAL1-dependent and BMAL1-independent

temporal cues. The "flipped" genes include *Il-1b*, shown to be under clock control via BMAL1's diurnal regulation of ROS, allowing HIF-1a activation and induction of *Il-1b* (Early et al., 2018).

3.4.2 BMAL1-dependent repression of the ZT12 LPS response.

To examine clock-regulation of the LPS response, rather than simply timepoint differences in baseline or LPS-stimulated states, I asked whether the clock promotes or represses LPS-induced expression at the two timepoints, and how this LPS responsiveness relates to basal timepoint differences in inflammatory genes. I identified a set of 225 genes that were predominantly upregulated in response to LPS, and whose upregulation was attenuated at ZT12. Importantly, this attenuation was driven by elevated basal expression of these genes at ZT12, with similar expression levels reached at both timepoints after 1 hour of LPS.

ZT12 is the timepoint at which peritoneal macrophages produce higher concentrations of cytokine proteins (Gibbs et al., 2012). The paradox of ZT12 responses having lower transcriptional fold-changes but higher ultimate protein output could be explained by a two-phase model where BMAL1-dependent IFN priming establishes elevated basal transcription while simultaneously positioning post-transcriptional amplification machinery. At the 1 hour timepoint examined in this study, the immediate-early transcriptional response to LPS has occurred, but insufficient time has elapsed for the full development of secondary feedback loops and post-transcriptional regulation. The elevated baselines at ZT12 may reflect constitutive interferon signalling that pre-positions inflammatory machinery in an activated state, reducing the transcriptional amplitude required for functional responses while enabling rapid protein production through translational and post-translational mechanisms.

The BMAL1-dependent gated gene set is composed of both pro-inflammatory mediators and negative regulators of inflammation, including *Dusp1* and *Il10*. This balanced composition sug-

gests that ZT12 priming prepares macrophages not only for rapid inflammatory initiation but also for efficient resolution. At ZT12, positioned at the transition to the active phase when pathogen encounter is more probable, this coordinated elevation of both activation and resolution machinery would enable rapid, controlled responses. In contrast, at ZT0 at the start of the rest phase when pathogen exposure is less likely, maintaining this primed state would be energetically costly and potentially damaging to the host. Instead, ZT0 macrophages may rely on higher-amplitude transcriptional responses that develop more slowly, with delayed engagement of post-transcriptional amplification and resolution pathways.

3.4.3 Transcription factors mediating BMAL1 effects.

The shift in inflammatory signalling from NFkB-dominant at ZT0 to JAK-STAT-dominant at ZT12 provides insight into how BMAL1 gates the inflammatory response through control of upstream transcriptional programs. In WT macrophages, I observed a clear temporal shift: ZT0 LPS responses are characterised by NFkB signalling, while ZT12 responses show dominant JAK-STAT pathway activity. This shift is BMAL1-dependent: in BMAL1-KO macrophages, NFkB and JAK-STAT signalling remain similar at both timepoints, with the LPS response largely invariant across the timepoints.

Other evidence also points to STAT and IRF activity mediating the shift in inflammatory signalling. Using decoupleR, I identified that STAT1, IRF1, and IRF3 activity is higher at ZT12 compared to ZT0 in WT peritoneal macrophages responding to LPS. This elevated STAT/IRF activity at ZT12 is consistent with the IFN-primed state suggested by the enrichment of type II interferon production genes in basal ZT12 macrophages. Together, these results support a model where BMAL1-dependent control of autocrine IFN-γ signalling establishes constitutive STAT1 and IRF activity at ZT12, altering the transcriptional response to LPS from an NFkB-dominated

acute response to a JAK-STAT-dominated interferon-amplified response.

The differential expression of TFs themselves supports this shift in BMAL1-dependent control of upstream transcriptional programs. At ZT12, basal state WT peritoneal macrophages show elevated expression of both pro- and anti-inflammatory TFs compared to BMAL1-KO, including *Nrf2* (which suppresses ROS and HIF1a-driven Il-1b production), *Klf4* (which promotes M2 polarisation), and clock-TFs *Rora* and *Nr1d1/2*. This coordinated elevation of regulatory TFs with opposing inflammatory roles, rather than a simple pro-inflammatory skewing, is consistent with the balanced priming model where ZT12 macrophages position both inflammatory initiation and resolution machinery in the basal state.

How BMAL1 mechanistically controls this transcriptional switch remains an open question, with multiple mechanisms likely contributing. Importantly, BMAL1 functions as a transcriptional activator, and so apparent repression of inflammatory programs at ZT0 likely occurs indirectly through activation of anti-inflammatory regulators. BMAL1 could activate repressors of interferon pathway genes at ZT0. BMAL1 may also act indirectly through control of metabolic intermediates that modulate STAT signalling: BMAL1 was previously found to regulate STAT3 activation through control of glycolytic enzyme PKM2 (Timmons et al., 2021), linking metabolic state to inflammatory signalling capacity. As a consequence of BMAL1-mediated changes to TF activity (whether through, direct transcriptional activation or secondary effects on metabolic status), effects on chromatin-mediated mechanisms may then propagate the program of inflammatory effects, as observed by Oishi et al. who found that BMAL1 deletion increased H3K27 acetylation at enhancers of inflammatory genes (Oishi et al., 2017). Oishi et al. attributed the mechanism to reduced expression of REV-ERBs, whereby BMAL1 activation of REV-ERBs enables their recruitment of co-repressor complexes to inflammatory enhancers, although my results indicate REV-ERBα alone is insufficient for this repression.

To help distinguish these potential mechanisms, I examined chromatin accessibility and the contribution of REV-ERBα to inflammatory gating.

3.4.4 Chromatin accessibility results indicate chromatin remodelling does not drive gating.

To investigate whether chromatin remodelling contributes to clock-gating of macrophage inflammatory responses, I examined the chromatin accessibility landscape of LPS-stimulated peritoneal macrophages at ZT0 and ZT12 using ATAC-seq. Surprisingly, I detected no differentially accessible regions (DARs) between timepoints in either basal state or LPS-stimulated macrophages. This absence of timepoint-dependent chromatin remodelling contrasts sharply with the extensive transcriptional differences observed and suggests that the macrophage-accessible chromatin landscape is largely stable between the two timepoints examined. This stability is consistent with a model where lineage-determining TFs maintain macrophage enhancers in a constitutively accessible, "poised" state, while circadian-regulated TFs modulate enhancer activity through differential binding. In this model, clock-regulated TFs bind poised enhancers, recruiting co-activators such as p300. The resulting histone acetylation and initiation of transcription is a consequence of TF recruitment (rather than a cause). The observation by Oishi et al., 2017 that BMAL1 deletion increases H3K27ac at inflammatory enhancers likely reflects an altered program of TF activity rather than direct BMAL1 chromatin-regulatory function.

My PEGS analysis showing stable enrichment of accessible chromatin up to 50 kb around BMAL1-dependent genes in both basal and LPS-stimulated states is consistent with this model: the regulatory elements are constitutively open, but their activity is modulated by rhythmic TF recruitment and so histone modifications, rather than by changes in accessibility.

It is also possible that chromatin changes occur on timescales not captured by the 12-hour

interval examined, or that changes manifest as peak broadening or narrowing rather than complete opening or closing alterations that current peak-calling algorithms cannot detect without dedicated peak shape analysis. ATAC does not provide the resolution required to observe the changes in TF binding dynamics happening at enhancers. However, the biological interpretation remains that developmental or tissue-specific gene regulation, which requires establishing new chromatin landscapes, operates differently from circadian regulation. Timepoint differences in inflammatory gene expression do not require chromatin remodelling but instead rely on variable TF activity and enhancer activation states at constitutively accessible regulatory elements.

Motif enrichment analysis provided insight into the regulatory logic operating at these stable chromatin regions. In proximal promoters of BMAL1-dependent genes, I observed enrichment for E-box motifs (direct CLOCK:BMAL1 binding sites) and hormone response elements, consistent with the enrichment of "response to hormone/steroid" pathways in this gene set. In distal regulatory elements within 50 kb of BMAL1-dependent genes, nuclear receptor (NR) and bZIP motifs were enriched in both basal and LPS-stimulated states, while STAT motifs showed enrichment specifically in LPS-stimulated distal elements. The enrichment of nuclear receptor motifs alongside E-boxes at distal enhancers suggests potential coordination between CLOCK:BMAL1 and clock-controlled nuclear receptors in regulating enhancer activity, consistent with the mechanism proposed by (Oishi et al., 2017), though my study suggests these are nuclear receptors other than REV-ERBα.

3.4.5 REV-ERBα does not mediate the repression of the LPS response at ZT12.

The enrichment of nuclear receptor motifs alongside E-boxes at distal regulatory elements in my dataset supported the hypothesis that REV-ERBα, a known circadian transcriptional repressor

found to regulate inflammatory genes in macrophages, would be necessary for the BMAL1-dependent gating of LPS responses I had observed. Surprisingly, REV-ERBα deletion had minimal effect on both basal state and LPS-stimulated macrophages, and the effects on basal gene expression (72 DEGs) were greater than the effect on LPS-stimulated macrophages (16 DEGs). This asymmetry suggests inflammatory signalling overrides basal REV-ERBα effects, and that REV-ERBα is not essential for inflammatory gating.

In the basal state, REV-ERBα deletion did produce effects consistent with its known repressive function. 32 genes were upregulated, including *Bmal1* (confirming disruption of the TTFL negative feedback loop), *Nlrp3* (consistent with reported REV-ERBα -mediated inflammasome repression), and *Nfil3* (a known REV-ERBα target). Lipid metabolism genes *(Lpl, Pla2g7, Fabp7)* and the hypoxia response factor *Egln3* were also derepressed, consistent with the reported role of REV-ERBα as a regulator of lipid metabolism in other tissues. 40 genes were downregulated in REV-ERBα-KO basal macrophages, including the negative regulator of TLR4 signalling *Sigirr*, suggesting REV-ERBα can function as both direct repressor and indirect activator in resting macrophages. However, none of these basal-state changes translated into substantial alterations in the LPS response.

The 16 genes altered by REV-ERBα deletion in LPS-stimulated macrophages were predominantly involved in lipid metabolism *(Lpl, Lbp)*, iron transport *(Slc40a1)*, and amino acid transport *(Slc7a8)* rather than canonical inflammatory pathways. No significant inflammatory pathway enrichments were detected. Critically, the core inflammatory response remained intact in REV-ERBα-KO macrophages.

The results do not support Hypothesis 2 and instead suggest that in this *in vivo* peritoneal macrophage model, REV-ERBα alone is surprisingly not necessary for the circadian gating of the inflammatory response. In a LysM-Cre model where only the DNA-binding domain of

REV-ERBα is deleted, Pariollaud found no differences in cytokine levels in bronchoalveolar fluid following inhaled LPS challenge, with only minimal increases in *Il6, Ccl2,* and *Cxcl5* expression in whole lung tissue (Pariollaud et al., 2018). Together with my results, this suggests that REV-ERBα is neither necessary nor sufficient to drive the clock-mediated modulation of acute LPS responses in macrophages.

There are several possible explanations for the unexpected finding that REV-ERBα is not important in the circadian regulation of LPS responses in peritoneal macrophages. Inflammatory phenotypes have been observed previously in global REV-ERBα-KO models, which show disrupted behaviour and feeding rhythms, systemic perturbations which may affect macrophage function indirectly (Hunter et al., 2020). Beyond the methodological difference of using a myeloid-specific knockout in this study, there may be functional redundancy with REV-ERBβ, which would require double knockout studies to reveal the full extent of REV-ERB-mediated regulation with the caveat that this would disrupt the TTFL and perturb other clock TFs expression. Additionally, multiple reports of REV-ERBα's anti-inflammatory functions have drawn on the potent effects of REV-ERBα agonists on inflammatory disease models, but highly significant off-target effects have been noted for commonly used agonist SR9009, particularly cross-reactivity with LXR (Dierickx et al., 2019; Trump et al., 2013).

The dynamics of REV-ERBα expression argue against it being the primary regulator of clock-imposed anti-inflammatory function. REV-ERBα is downregulated in response to LPS, and so least available when anti-inflammatory gene expression would be needed, suggesting it is unlikely that it was naturally selected by evolution as the key anti-inflammatory arm of clock-regulation. REV-ERBα may still contribute to the basal inflammatory tone. The myeloid-specific knockout might reveal stronger effects at a later stage of the LPS response in this acute model, or in chronic inflammatory contexts where REV-ERBα expression is sustained.

Despite small numbers of locus-specific accessibility changes, the minimal transcriptomic impact of REV-ERBα deletion suggests REV-ERBα does not gate macrophage LPS response by priming basal-state chromatin. Future work should focus on other clock components, such as BMAL1, which has been demonstrated to act independently of REV-ERBα in modulating phagocytic pathways (Kitchen et al., 2020).

Together, these results indicate BMAL1 primarily gates macrophage inflammatory responses through the regulation of upstream TF programs, rather than through direct action at inflammatory gene loci or through REV-ERBα-mediated repression. By establishing an elevated expression of pro- and anti-inflammatory regulators at ZT12, macrophages are positioned for rapid inflammatory responses at the onset of the active period. Alongside, the altered activity of the STAT/IRF axis helps establish the inflammatory set points seen at ZT0 versus ZT12. The model is more complex than previous REV-ERBα-centric frameworks (Figure 3.25).

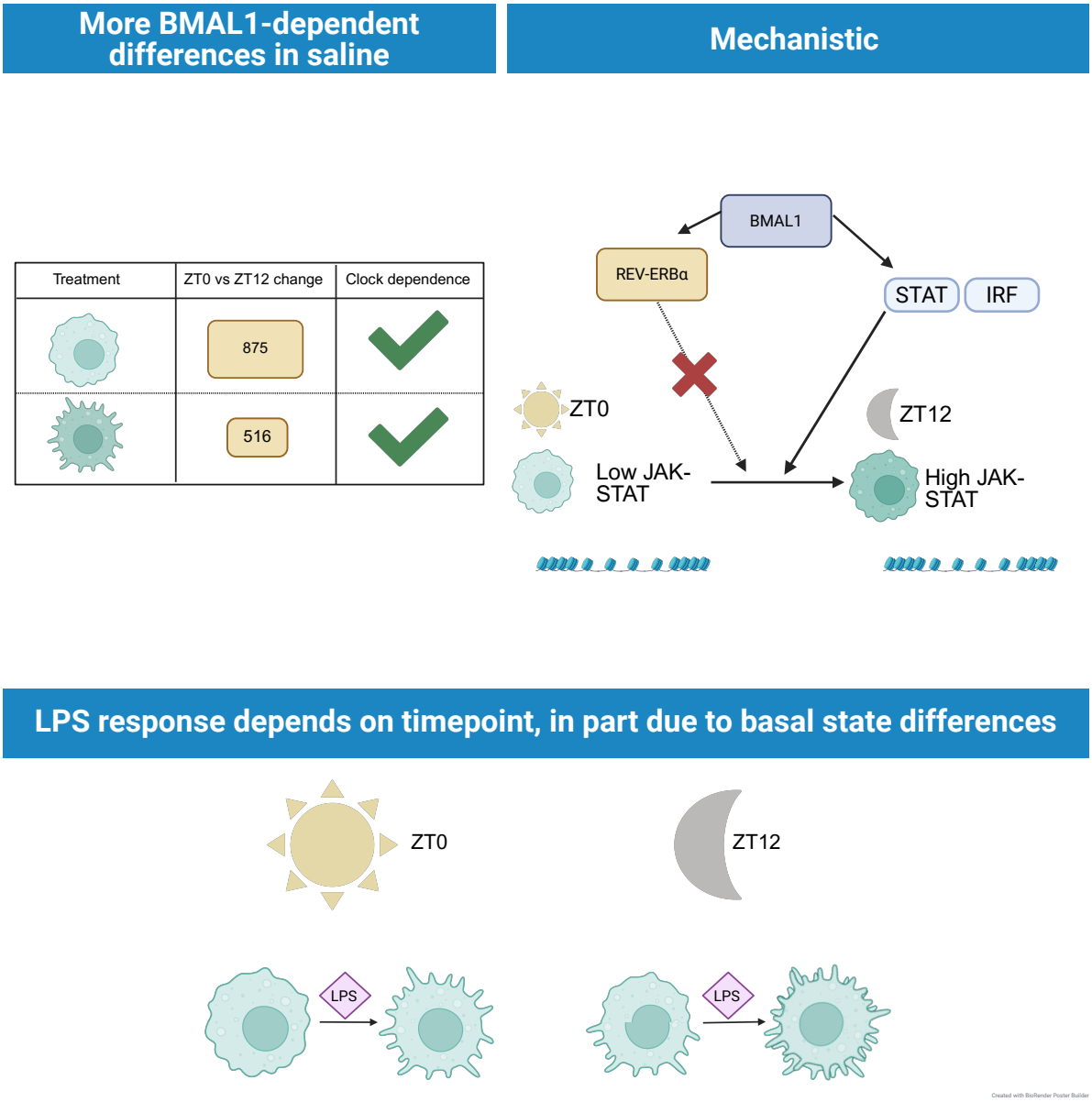

Figure 3.25: **Summary of results from Chapter 3.**
Top left: there are more BMAL1-dependent timepoint differences in saline, basal-state peritoneal macrophages than there are in LPS-treated. Bottom: The LPS response interacts with timepoint. Peritoneal macrophages are primed for inflammatory responses in the basal state at ZT12. Top right: REV-ERBα-mediated repression is not necessary for BMAL1-mediated anti-inflammatory function. Chromatin accessibility is similar between timepoints, and a broad program of TFs vary in both expression and activity between timepoints. The LPS response at ZT12 is characterised by higher JAK-STAT activity than at ZT0, with this difference lost with BMAL1-deletion. Created in https://BioRender.com

3.4.6 Limitations and future directions.

By capturing transcriptomes at a single timepoint post-LPS (1 hour), I was able to capture immediate-early transcriptional responses unaffected by downstream feedback loops, and avoid most changes to the peritoneal macrophage population that occur in the macrophage disappearance reaction upon LPS exposure. However, this means I have not tested the hypothesis that the basal-state ZT12 priming leads to post-transcriptional amplification by capturing the time-course of the LPS response, which I would expect (in accordance with previous reports that this timepoint results in higher cytokine protein levels (Gibbs et al., 2012)). By examining only ZT0 and ZT12, this study cannot capture the dynamics of inflammatory responses across the full 24-hour cycle. (Collins et al., 2021) identified two temporally-separated waves of circadian gene expression in macrophages; sampling at additional timepoints would clarify whether the ZT0 and ZT12 states represent stable phases or transition points, and whether inflammatory gating exists at other circadian times. Additionally, (Collins et al., 2021) found that few rhythmic proteins in BMDMs have correspondingly rhythmic transcripts, and (Kitchen et al., 2020) found that BMAL1-KO inhibits appropriate post-translational phosphorylation events. My transcriptomic data signals how the bulk inflammatory response is poised, but I cannot directly assess whether STAT and IRF proteins show elevated activity (inferred computationally and by expression levels), and whether negative regulators elevated at ZT12 baseline (*Dusp1, Il10*) show concordant functional protein.

Similarly, future work should validate IFN-γ protein levels in basal WT and BMAL1-KO peritoneal macrophages throughout the 24-hour period, to assess whether there is an elevated interferon baseline (as my work computationally predicts), and whether any circadian-regulated autocrine-signalling functionally primes acute inflammatory responses by time-of-day.

Whether IFN priming occurs uniformly across the peritoneal macrophage population or reflects circadian variation in monocyte recruitment remains unknown. While MACS purification ensured analysis of the same population at each timepoint, and the 1-hour LPS treatment minimises complications from monocyte influx that occurs with prolonged inflammation, single-cell approaches would be necessary to determine whether all macrophages are IFN-primed at ZT12 or whether a primed subpopulation dominates the bulk transcriptional signal. Similarly, the flipped genes showing directional reversal in BMAL1-KO could reflect altered proportions of metabolically distinct subpopulations rather than uniform transcriptional reprogramming.

ATAC-seq reveals open chromatin but does not indicate whether regulatory elements are actively engaged or physically interacting with target promoters. Chromosome conformation capture approaches (3C and variants) would determine whether promoter-enhancer looping differs between timepoints despite stable accessibility. This is a possibility given that REV-ERBα has been reported to regulate loop formation through co-repressor recruitment (Y. H. Kim et al., 2018). Determining whether enhancers are differentially acetylated (H3K27ac), methylated (H3K4me1/3), or bound by specific TFs requires orthogonal approaches such as CUT&RUN for histone marks and TF occupancy. ChromVAR analysis would provide more sensitive inference of TF activity variation than motif enrichment analysis alone and could reveal subtle changes in TF binding masked by stable chromatin accessibility patterns.

Finally, the inflammatory gating observed at ZT0 and ZT12 may not extend to all circadian times, LPS doses, or inflammatory stimuli. My results establish BMAL1-dependent gating at opposing circadian phases with a single LPS dose (1 mg/kg) and stimulation duration (1 hour), but whether similar mechanisms operate at intermediate timepoints, with varying pathogen loads, or with other TLR ligands remains to be determined. The context-dependence of BMAL1's effects - regulating distinct gene sets in basal versus LPS-stimulated states - suggests that in-

flammatory gating may be stimulus-specific, with different temporal control mechanisms for different classes of pathogens or inflammatory triggers, as recently reviewed in the context of clinically relevant bacterial pathogens (Mo et al., 2025).

4 | Sex differences in circadian programs in inflammatory macrophages

4.1 Introduction

Despite strong sex biases in many immune pathologies, including autoimmune disorders and susceptibility to infection, sex has often not been included as a factor in immunological studies. There is strong evidence at multiple scales of biology that sex is important in regulating immunity, including evolutionarily-conserved evidence of sexual dimorphisms in the immune system present in diverse species ranging from insects/birds/lizards to mammals suggesting an adaptive advantage (Klein & Flanagan, 2016). In humans, a trade-off is evident: females generally mount more robust immune responses but experience higher rates of autoimmune conditions while males show worse infectious disease outcomes (Silva & Iwasaki, 2024). There is increasing mechanistic evidence *in vitro* that sex hormones regulate gene expression, and inflammatory function, of immune cell types such as macrophages.

In Chapter 1, I summarised the emerging evidence that sex and circadian rhythms interact at multiple regulatory levels. Whether these findings extend to immune cells remains largely untested, although several observations suggest they might. Recent epidemiological studies have shown sex-specific effects of circadian disruption on inflammatory disease, with shift work increasing asthma exacerbation risk in women but not men (Maidstone et al., 2025). However, the cellular and molecular mechanisms of this interaction are undefined.

Sex and the circadian clock independently regulate the macrophage transcriptome. As peritoneal macrophages show the most sex-dimorphism in tissue-resident immune cells, they are a

promising subset in which to look for sex-clock interactions (Gal-Oz et al., 2019). Sex differences in this population are clinically relevant: female mice have improved outcomes in models of bacterial peritonitis (Bain et al., 2020), and in humans the incidence and severity of sepsis and post-surgical infections is markedly lower in women than men (Cohen et al., 2013).

In Chapter 3, I established that BMAL1 gates the early transcriptional response to LPS-stimulation in mixed-sex populations. However, in accordance with the significant sex-dimorphism in this population, principal component analysis revealed sex to explain more transcriptional variance than timepoint or genotype, suggesting that the effects of sex may be dominant and/or interactive with clock function.

4.1.1 Hypothesis and Aims

Based on previous studies and my investigation in Chapter 3, I hypothesised that sex modifies how the circadian clock regulates inflammatory macrophages, creating sex-specific circadian programs.

Competing, testable hypotheses were:

1. Sex and clock regulate programs independently, with BMAL1-necessity for ZT0 vs ZT12 differences equivalent in males and females
2. Sex modifies which genes are clock-controlled, with BMAL1-dependent gene sets differing between males and females

Mechanistically, I hypothesised that LPS-stimulated macrophages would show sex-specific changes in TF availability and/or activity between timepoints, mediating the sex-dependent effects.

4.1.1.1 Aims

Test whether sex modifies BMAL1-dependent circadian gating *in vivo*.

- Compare the transcriptomes of male and female WT and BMAL1-KO peritoneal macrophages 1 hour after LPS-stimulation at ZT0 and ZT12.
- Quantify BMAL1-dependent ZT12 vs ZT0 DEGs within each sex, and identify sex-specific BMAL1-dependent genes.
- Test for sex-timepoint interaction using DESeq2 within each genotype.

Contingent on the finding that sex-specific circadian programs exist:

Identify which TFs could be mediating sex-differences in clock-dependent LPS-stimulated macrophage transcriptomes.

- Infer TF activity and measure TF expression between timepoints for each sex.
- Identify TFs showing sex-specific time-of-day regulation.
- Analyse differential pathway activity between timepoints for each sex.

4.2 Methods

The same experiment was analysed as in Chapter 3, and so experimental design is as described in Chapter 3 and Methods 2. However, sex-stratified saline groups lacked power for reliable differential expression testing, and so I analysed sex differences within the LPS-stimulated peritoneal macrophages only, as sex-dimorphism extends beyond basal-state gene expression in macrophages: a variety of tissue-resident macrophages from male and female mice consistently showed transcriptional sexual dimorphism, which increased after interferon stimulation (Gal-

Oz et al., 2019).

I analysed time-of-day differences independently within each sex (male and female) by comparing ZT12 vs ZT0 in LPS-stimulated macrophages (sample sizes are in Table 4.1). Genes were classified as BMAL1-dependent if they showed significant time-of-day differences in wild-type mice (padj < 0.05) but not in BMAL1-KO mice (padj ≥ 0.05).

Group	Sample size
WT ZT0 Male	3
KO ZT0 Male	3
WT ZT0 Female	3
KO ZT0 Female	3
WT ZT12 Male	3
KO ZT12 Male	2
WT ZT12 Female	2
KO ZT12 Female	3

Table 4.1: **Summary of LPS only experimental group sample sizes.**

I tested for statistical interaction between zeitgeber time (ZT12 vs ZT0) and sex (male vs female) using DESeq2. A significant interaction (padj < 0.05) indicates that the magnitude or direction of the timepoint-induced fold-change differs between males and females. For example, a gene may show high timepoint variance, peaking at ZT12, in males but with lower timepoint variance in females, indicating that sex *gates* the magnitude of clock-control for that gene. I classified an interaction as BMAL1-dependent if it was statistically significant in wild-type mice (padj < 0.05) but not in BMAL1-KO mice (padj ≥ 0.05), indicating that BMAL1 is necessary for sex-dependency of the timepoint-regulation of that gene.

4.3 Results

4.3.1 BMAL1-dependent gene expression shows pronounced sexual dimorphism.

In Chapter 3, I found that the intrinsic macrophage clock regulated timepoint-dependent differences in inflammatory macrophages. To identify which of these differences are dependent on sex, I first identified BMAL1-dependent changes to gene expression between ZT0 and ZT12 in LPS-stimulated peritoneal macrophages stratified by sex. Genes showing time-of-day differences in WT but not in BMAL1-KO mice represent BMAL1-dependent differences. Differential expression of core-clock components *Bmal1, Clock, Nr1d1/2, Per1/2/3, Cry1/2* between ZT12 vs ZT0 in LPS-stimulated macrophages stratified by sex was highly similar between males and females, indicating that the effect of LPS on the clock mechanism was similar (Figures 4.1 and 4.2).

In male WT LPS-stimulated macrophages, 623 genes showed time-of-day differential expression (padj < 0.05) (Figure 4.1(a)). Of these, 388 were upregulated at ZT12, and 235 upregulated at ZT0. In BMAL1-KO macrophages, only 45 genes showed time-of-day differences (Figure 4.1(b)). 22 genes showed time-of-day differential expression in both conditions, leaving 23 genes changing only in BMAL1-KO macrophages and 601 BMAL1-dependent genes (96% of WT changes). This is an increase when compared to the result from the mixed-sex analysis in Chapter 3, where 516 genes (72%) showed BMAL1-dependent differences in LPS-stimulated macrophages. The directionality is consistent with mixed-sex analysis, with most genes under clock-control showing upregulation at ZT12.

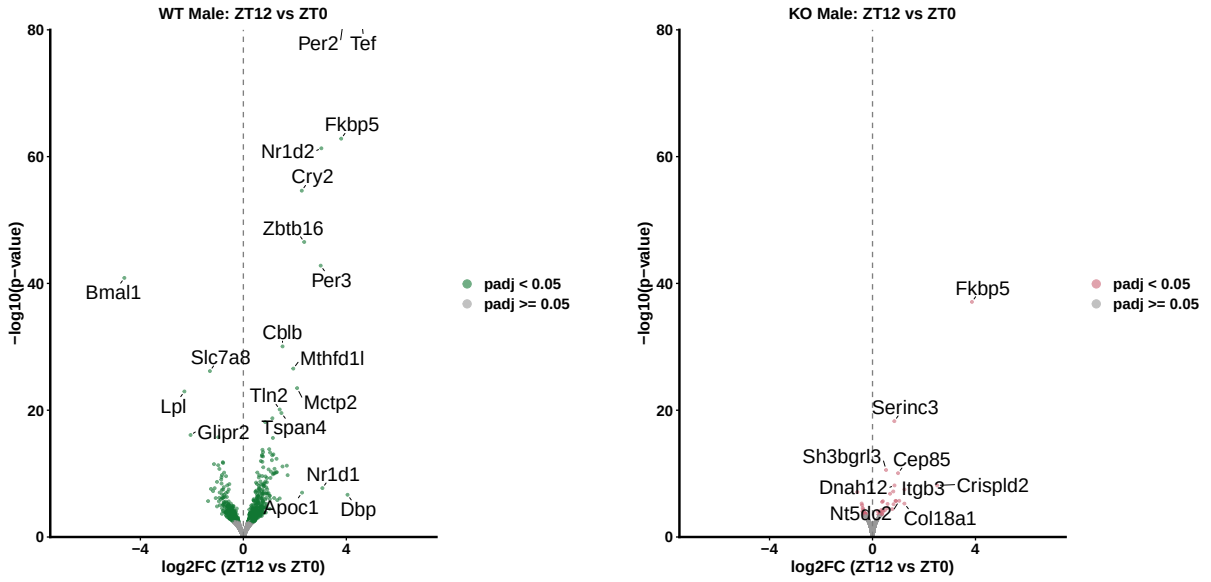

(a) Wild-type (WT) Male

(b) BMAL1-KO (KO) Male

Figure 4.1: **The effect of myeloid-specific BMAL1-KO on ZT12 vs ZT0 differential expression in peritoneal macrophages, after 1 hour of LPS stimulation (1 mg/kg).**
DEGs were identified using DESeq2, at BH-adjusted < 0.05. WT $n = 3$, BMAL1-KO $n = 2$–3. The top-ranked DEGs (by Wald statistic) are labelled. Panel (a) shows WT DEGs (green), and panel (b) shows BMAL1-KO DEGs (pink).

In female WT LPS-stimulated macrophages, fewer genes showed timepoint-dependence (Figure 4.2). 208 genes were differentially expressed between ZT0 and ZT12, with 102 upregulated at ZT12 and 106 upregulated at ZT0 (Figure 4.2(a)). In BMAL1-KO macrophages, 68 genes showed timepoint-dependence, with 61 of these genes timepoint-dependent only in BMAL1-KO and 7 genes sharing timepoint-dependence with WT female macrophages (Figure 4.2(b)). This leaves 201 BMAL1-dependent DEGs in females: 96% of WT timepoint-differences.

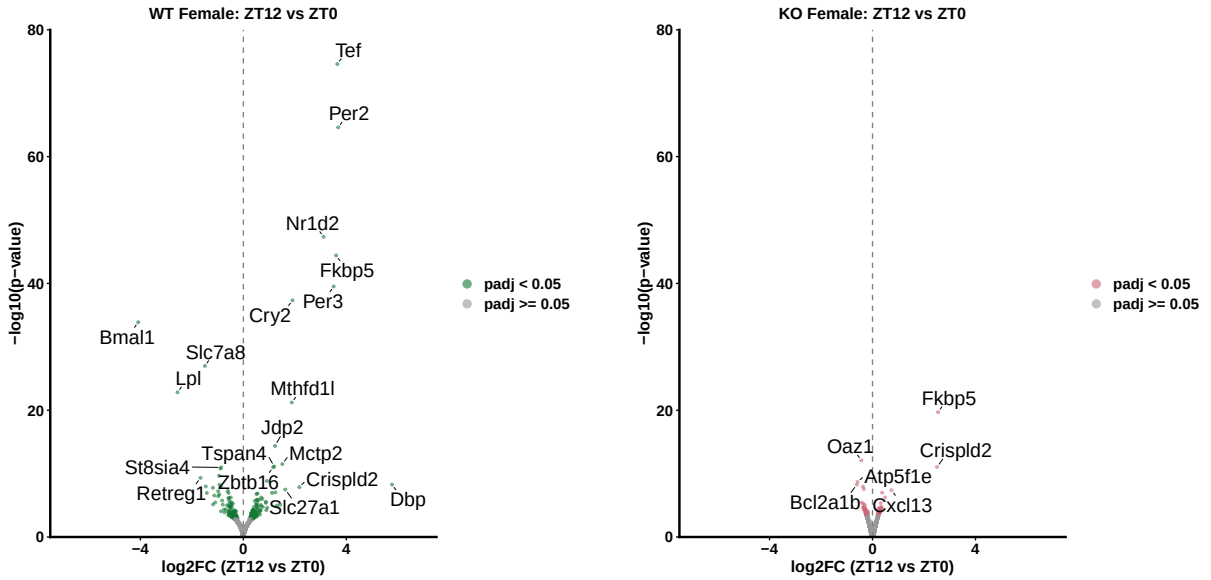

(a) Wild-type (WT) Female

(b) BMAL1-KO (KO) Female

Figure 4.2: **The effect of myeloid-specific BMAL1-KO on ZT12 vs ZT0 differential expression in peritoneal macrophages, after 1 hour of LPS stimulation (1 mg/kg).**
DEGs were identified using DESeq2, at BH-adjusted < 0.05. WT $n = 3$, BMAL1-KO $n = 2$–3. The top-ranked DEGs (by Wald statistic) are labelled. Panel (a) shows WT DEGs (green), and panel (b) shows BMAL1-KO DEGs (pink).

In both males and females the proportion of BMAL1-dependence exceeded the 72% observed in the mixed-sex analysis (Chapter 3), suggesting i) greater variability in the ZT12 vs ZT0 contrast in mixed sex detecting fewer differences overall, ii) that the power-increase of pooling BMAL1-KO sexes allows detection of a greater number of timepoint-differences, or iii) a combination of both. Equally, the effect of BMAL1-KO may differ by sex, and so defining BMAL1-dependence across mixed-sex groups may not be appropriate.

In both males and females, genes sharing timepoint-dependence in both BMAL1-KO and WT macrophages include *Fkbp5*, a glucocorticoid responsive gene encoding a co-chaperone modulating glucocorticoid receptor (GR) activity, and negative regulator of HIF-1a, and *Crispld2*, a glucocorticoid responsive in epithelial cells (Himes et al., 2014). This indicates BMAL1-independent differences in GR activity by timepoint, likely modulated through the systemic rhythmicity of circulating glucocorticoid.

4.3.2 The majority of sex-specific clock-regulation is male-specific, enriched for inflammatory terms.

I next defined sex-specific BMAL1-dependent ZT12 vs ZT0 genes, identifying them as genes found to be significant through the sex-specific BMAL1-dependence test, and not found to pass the BMAL1-dependence test in the macrophages from the opposite sex (i.e. WT padj ≥ 0.05 or BMAL1-KO padj < 0.05). 106 genes were BMAL1-dependent in both sexes, while 84 genes showed female-specificity and 487 genes showed male-specificity (Figure 4.3).

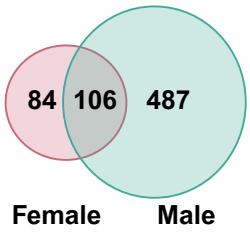

Figure 4.3: **There are more male-specific BMAL1-dependent differences than female.** WT and myeloid-specific BMAL1-KO mice were stimulated with LPS for 1 hour at ZT0 or ZT12, before isolation of peritoneal macrophages. ZT12 vs ZT0 differential expression was analysed using DESeq2. BMAL1-dependent timepoint differences were defined as genes which passed WT padj < 0.05 and BMAL1-KO padj ≥ 0.05, in each sex. Sex-specific genes were genes which were found to be significant through the sex-specific BMAL1-dependence test, and not found to pass the BMAL1-dependence test in the macrophages from the opposite sex. Female-specific genes in red, male-specific genes in teal. WT $n = 3$, BMAL1-KO $n = 2$–3

.

Female-specific genes (Figure 4.4) included DNA replication licensing factors *Mcm2/3/4*, *Fos*, acyl-CoA-binding protein *Dbi*, and metabolic regulators which included ceramide synthases *Cers2/6* and regulators of HMGCR *Insig1* and *Amfr* (E3-ubiquitin ligase involved in ubiquitination of HMGCR).

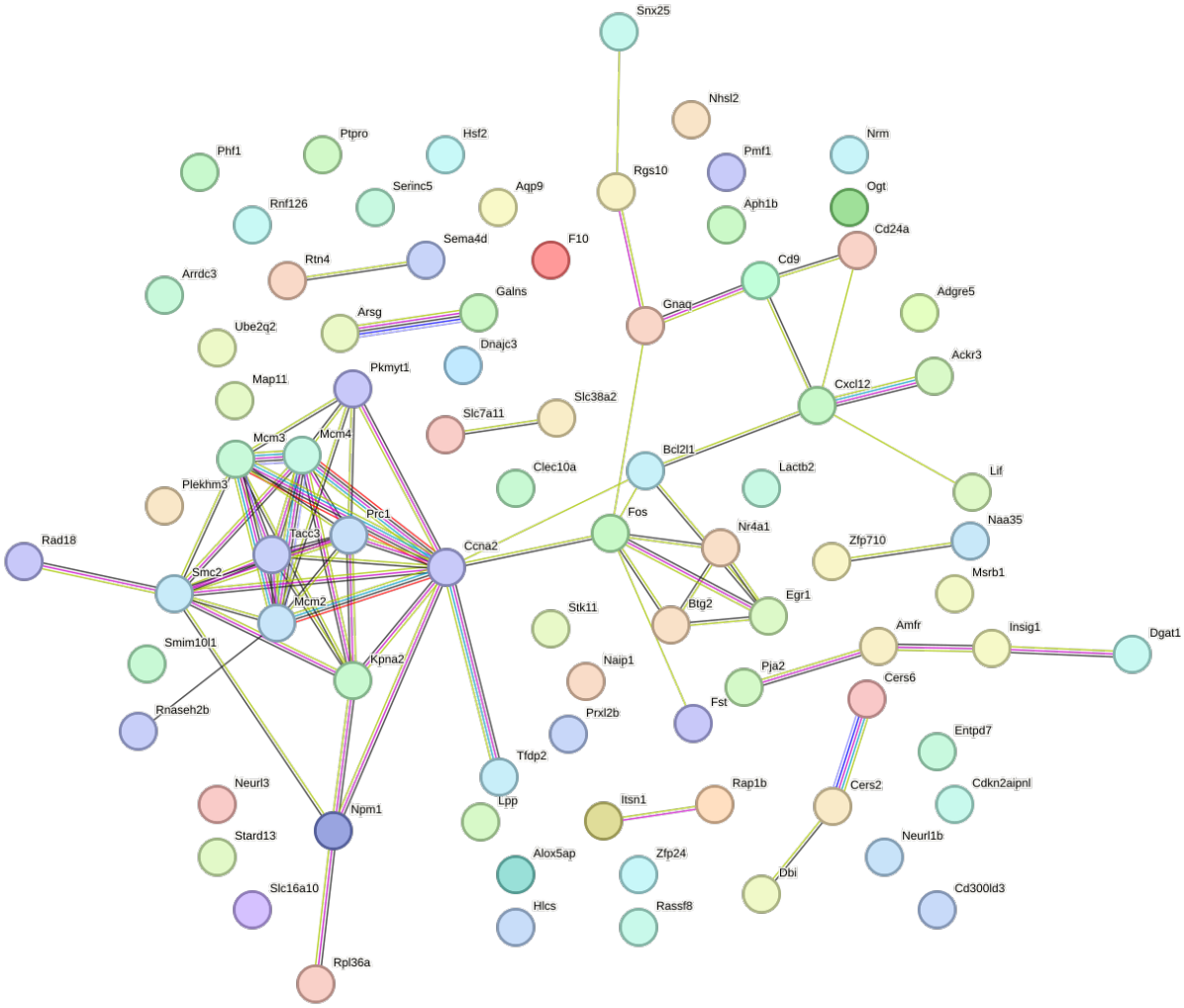

Figure 4.4: **The set of 84 female-specific BMAL1-dependent ZT12 vs ZT0 differences, in LPS-stimulated macrophages.**
Predicted functional protein association network (STRING) for female-specific BMAL1-dependent DEGs. BMAL1-dependent timepoint-differences were defined by the inclusion of significant ZT12 vs ZT0 DEGs in WT, excluding any significant ZT12 vs ZT0 DEGs in BMAL1-KO macrophages. Female-specificity was defined where genes were found to be significant through the BMAL1-dependence test in females, and not found to pass the BMAL1-dependence test in males.

Male-specific genes (Figure 4.5) included pro-inflammatory markers *Tnf, Tlr2, Ccl2/3/4, Cxcl1/10/14, Atf6, Ptgs2, Lbp, Stat4*, Guanylate-binding proteins *Gbp5/7/9*, markers of peritoneal macrophage sexual dimorphism *Timd4, Cd209b*, and regulators of stress-responses such as the post-translational regulator of HIF proteins *Egln3*, and *Nr3c2*, encoding mineralocorticoid receptor.

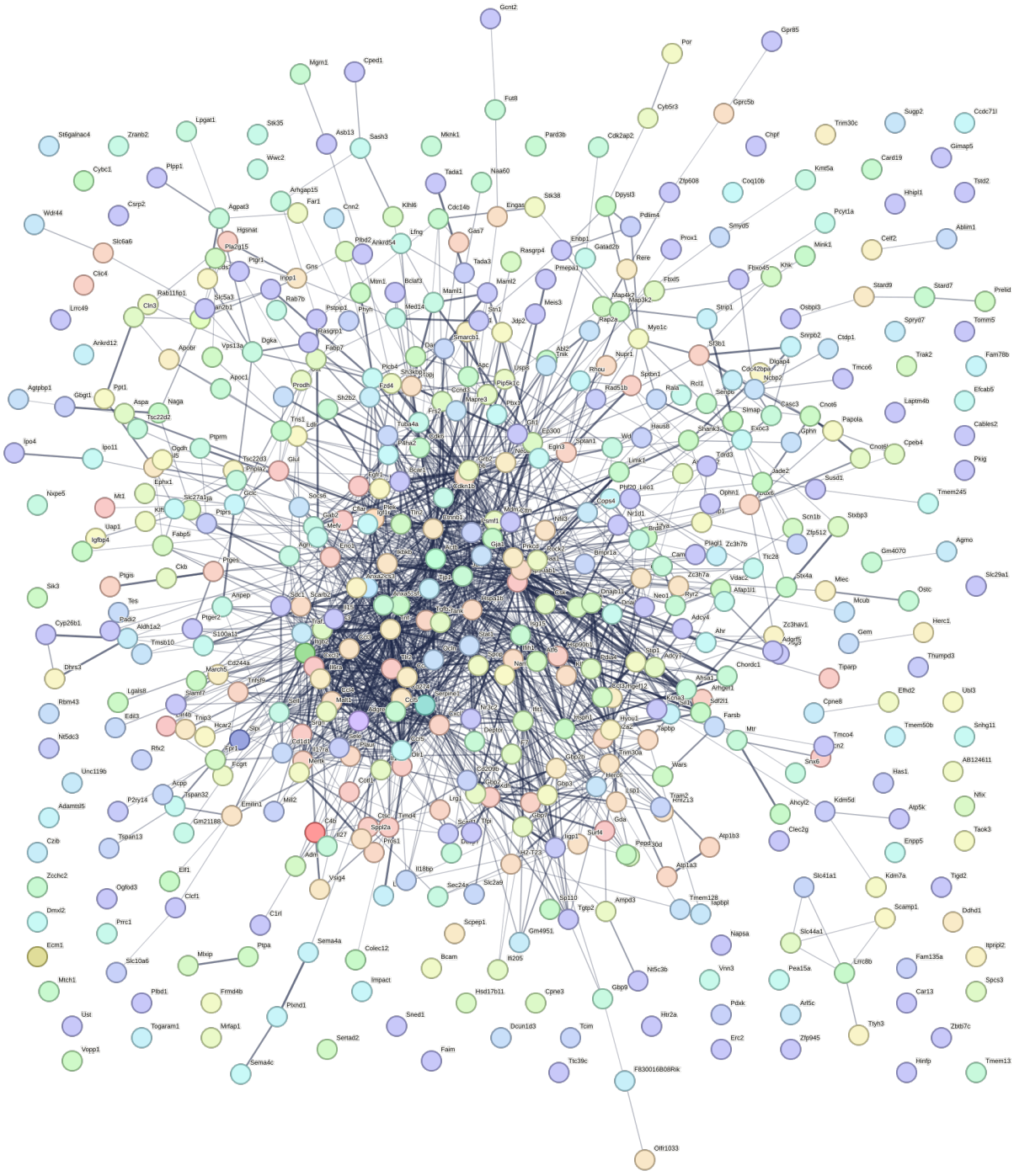

Figure 4.5: **The set of 487 male-specific BMAL1-dependent ZT12 vs ZT0 differences, in LPS-stimulated macrophages.**
Predicted functional protein association network (STRING) for male-specific BMAL1-dependent DEGs. BMAL1-dependent timepoint-differences were defined by the inclusion of significant ZT12 vs ZT0 DEGs in WT, excluding any significant ZT12 vs ZT0 DEGs in BMAL1-KO macrophages. Male-specificity was defined where genes were found to be significant through the BMAL1-dependence test in males, and not found to pass the BMAL1-dependence test in females.

Genes regulated by BMAL1 in both males and females included core circadian components *Bmal1, Nr1d1/2, Per2/3, Cry1/2, Tef, Dbp*, cytokine *Il12b* and metalloproteinases *Adam17, Mmp9*, transcriptional regulators *Mlxipl, Ezh1, Jund*, and metabolic genes *Lpl, Sod1, Slc7a8*.

Having defined these sex-specific, clock-dependent gene sets, I next asked whether the biological functions enriched differed by sex.

I performed GO enrichment analysis using a background of the WT female ZT12 vs ZT0 or WT male ZT12 vs ZT0 contrasts respectively. Two GO terms were enriched in the female-specific BMAL1-regulated genes: GO:0099536, synaptic signalling (padj = 0.0206, q value = 0.0184), and GO:0023061 signal release (padj = 0.0398, q value = 0.0355) (Figure 4.6). The 13 genes driving this enrichment were *Rap1b, Slc7a11, Cd24a, Gnaq, Rtn4, Nr4a1, Slc38a2, Rgs10, Dbi, Egr1, Aph1b, Kpna2,* and *Bcl2l1*. In macrophages, these genes reflect shared receptor machinery with neurons, including genes involved in G-protein coupled receptor signalling *(Gnaq, Rgs10, Rap1b)* and corresponding transcriptional responses *(Nr4a1, Egr1)*. The genes also regulate metabolic/redox control (*Slc7a11*, a solute carrier whose expression promotes glutathione levels, keeping ROS low and increasing resistance of cells to ferroptosis, *Dbi*, acyl-coenzyme A binding protein, and *Slc38a2* a glutamine transporter). The enrichment of amino-acid transporters in BMAL1-dependent gene sets is consistent with literature finding amino-acid metabolism is upregulated in response to the dysregulation of energy metabolism and increased oxidative stress that occurs with BMAL1-deletion in macrophages (Alexander et al., 2020).

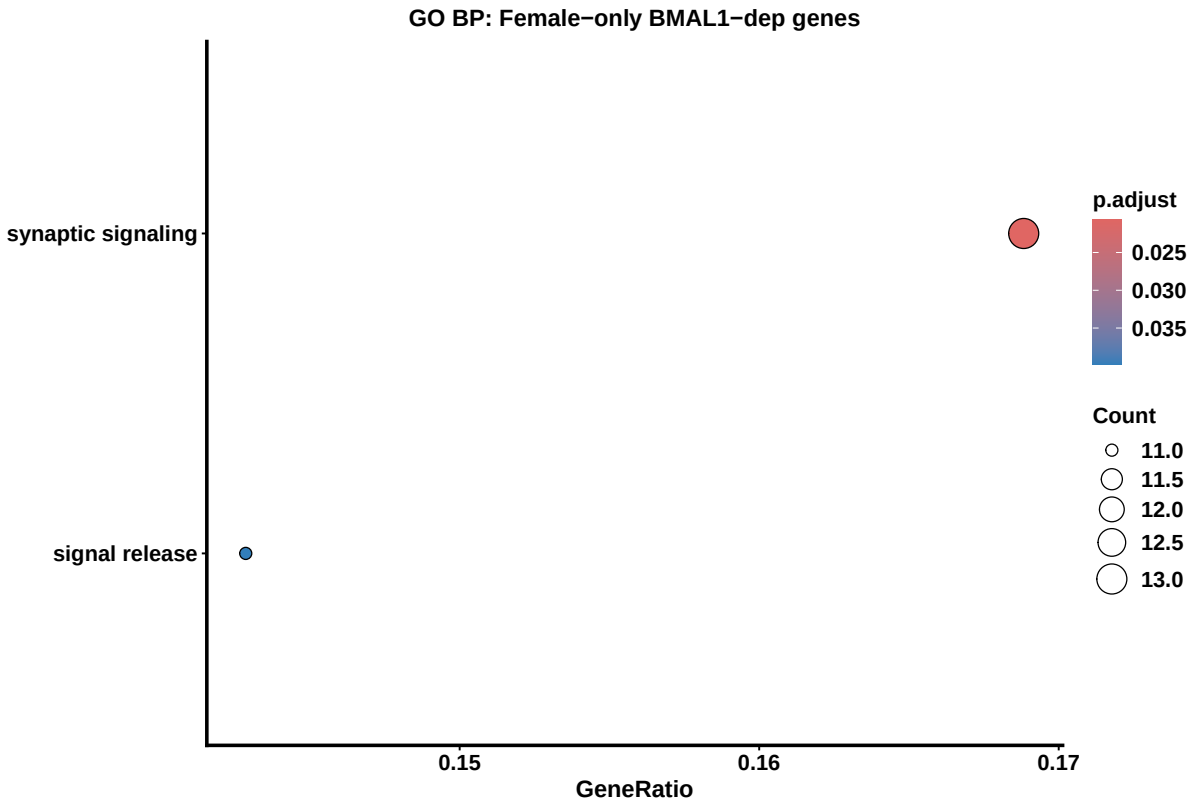

Figure 4.6: **Enriched GO terms in the female-specific BMAL1-dependent ZT12 vs ZT0 differences, in LPS-stimulated macrophages.**
BMAL1-dependent timepoint-differences were defined by the inclusion of significant ZT12 vs ZT0 DEGs in WT, excluding any significant ZT12 vs ZT0 DEGs in BMAL1-KO macrophages. Female-specificity was defined where genes were found to be significant through the BMAL1-dependence test in females, and not found to pass the BMAL1-dependence test in males. GO over-representation analysis was performed using clusterProfiler with hypergeometric testing. Background gene universe comprised all genes with valid statistical tests (non-NA p-values) in the WT female ZT12 vs ZT0 contrast. BH FDR correction was applied (padj < 0.05, q value < 0.05). Enriched terms were simplified to remove redundancy (similarity cutoff = 0.5), retaining the most significant term per cluster.

There was significant enrichment of multiple GO terms in male-specific BMAL1-dependent genes. This included cell-cell adhesion (GO:0098609, padj 2.20e-05, q value 1.7e-05), vasculature development (GO:0001944, padj 6.6-05, q value 5.0e-05), regulation of MAPK cascade (GO:0043408, padj 7.2e-05, q value 5.5e-05), positive regulation of cytokine production (GO:0001819, padj 1.0e-04, q value 7.9e-05), inflammatory response (GO:0006954, padj 0.00018814, q value 0.000143882) (Figure 4.7). MAPK activation occurs in MyD88-dependent TLR signalling, resulting in expression of M1-type pro-inflammatory cytokines.

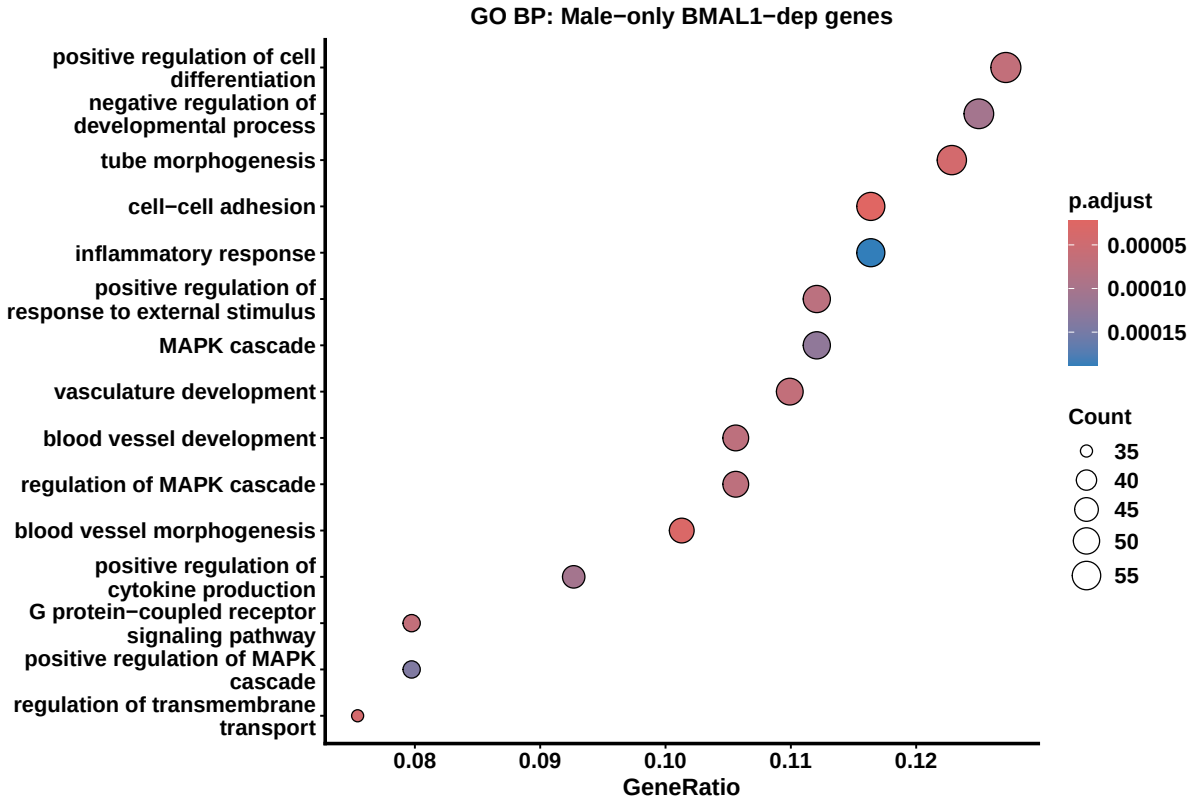

Figure 4.7: **Top 15 enriched GO terms in the male-specific BMAL1-dependent ZT12 vs ZT0 differences, in LPS-stimulated macrophages.**
BMAL1-dependent timepoint-differences were defined by the inclusion of significant ZT12 vs ZT0 DEGs in WT, excluding any significant ZT12 vs ZT0 DEGs in BMAL1-KO macrophages. Male-specificity was defined where genes were found to be significant through the BMAL1-dependence test in males, and not found to pass the BMAL1-dependence test in females. GO over-representation analysis was performed using clusterProfiler with hypergeometric testing. Background gene universe comprised all genes with valid statistical tests (non-NA p-values) in the WT male ZT12 vs ZT0 contrast. BH FDR correction was applied (padj < 0.05, q value < 0.05). Enriched terms were simplified to remove redundancy (similarity cutoff = 0.5), retaining the most significant term per cluster.

The GO term vasculature development is driven by *Tgfb2, Bmp2, Fzd4,* and *Prox1*. The cytokines and chemokines driving enrichment of activation/adhesion terms included *Tnf, Ccl2, Cxcl10, Il6ra*. Inflammatory modulators included prostaglandin-signalling genes *Ptgs2, Ptger4,* and *Ptgis*, alongside *Serpine1*, PAI-1 (an inhibitor of fibrinolysis) and *F3* (main initiator of coagulation, important in sepsis).

4.3.3 Sex modulates amplitude of BMAL1-dependent programs.

The identification of functionally-distinct sex-specific programs raised a question: are these functional programs truly unique to one sex, or are they regulated by the clock in both sexes but with insufficient power to detect? To test this, I used gene set enrichment analysis (GSEA) to ask whether the "male-unique" inflammatory gene signature showed any evidence of coordinated regulation in females, and vice-versa. Specifically, whether the identified male/female-specific gene sets (Figure 4.3) were significantly enriched at either end of the total ranked DEGs between ZT12 vs ZT0 in the opposite sex. To do this, the gene sets were split into subsets upregulated at either ZT0 or ZT12, so the concordance with directional changes in the other sex could be seen.

Male-unique BMAL1-dependent ZT12 vs ZT0 DEGs are significantly enriched within the female ranked ZT12 vs ZT0 genes, and at the same timepoint: genes upregulated at ZT12 in males are similarly upregulated in females at ZT12 (Figure 4.8).

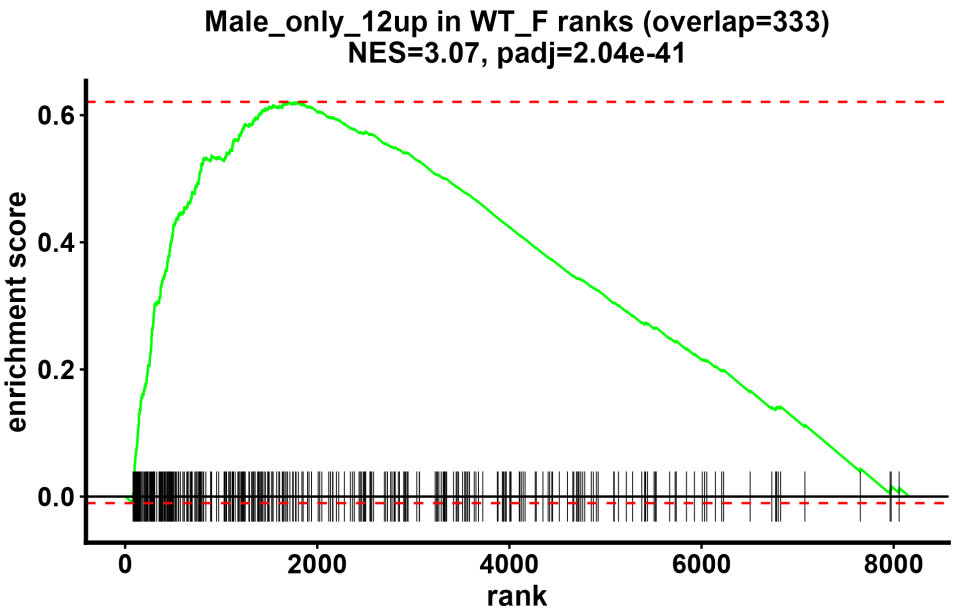

(a) Male ZT12 up

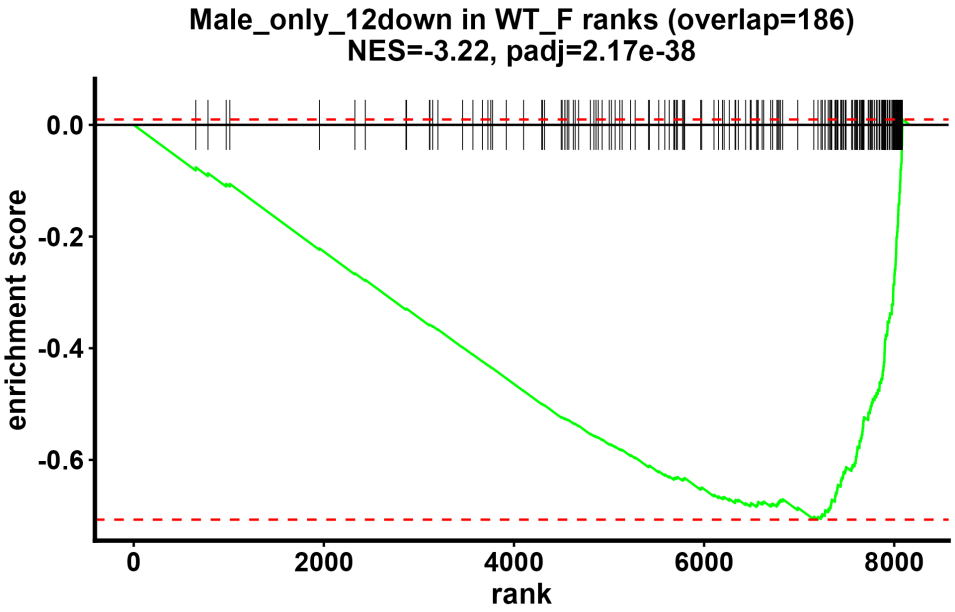

(b) Male ZT12 down

Figure 4.8: **Male-specific BMAL1-dependent genes are similarly enriched in wild-type female macrophages.**
Gene Set Enrichment Analysis (GSEA) testing whether male-specific BMAL1-dependent genes show coordinated expression changes in female samples. Genes were ranked by DESeq2 Wald statistic (ZT12 vs ZT0) for WT female macrophages, with ZT12-upregulated genes on the left and ZT0-upregulated genes on the right. The running enrichment score (green line) reflects the cumulative over- or under-representation of gene set members as the algorithm moves through the ranked list. Vertical black lines (barcode) indicate positions of individual gene set members within the ranked list. The red dashed line marks the peak enrichment score, corresponding to the leading edge (the subset of genes driving the enrichment signal). Positive normalised enrichment score (NES) indicates enrichment among ZT12-upregulated genes; negative NES indicates enrichment among ZT0-upregulated genes. Custom gene sets were compiled from male-specific ZT12-upregulated (n = 333) and ZT12-downregulated (n = 186) genes. Enrichment was tested using fgseaMultilevel (minSize = 5).

Similarly, the female-specific BMAL1-dependent ZT12 vs ZT0 DEGs are significantly enriched within the female ranked ZT12 vs ZT0 genes, at the same timepoint (Figure 4.9). Normalised enrichment score (NES) for female-specific BMAL1-dependent ZT12 vs ZT0 DEGs are smaller than those for male-specific, which likely reflects the statistical testing using smaller gene sets.

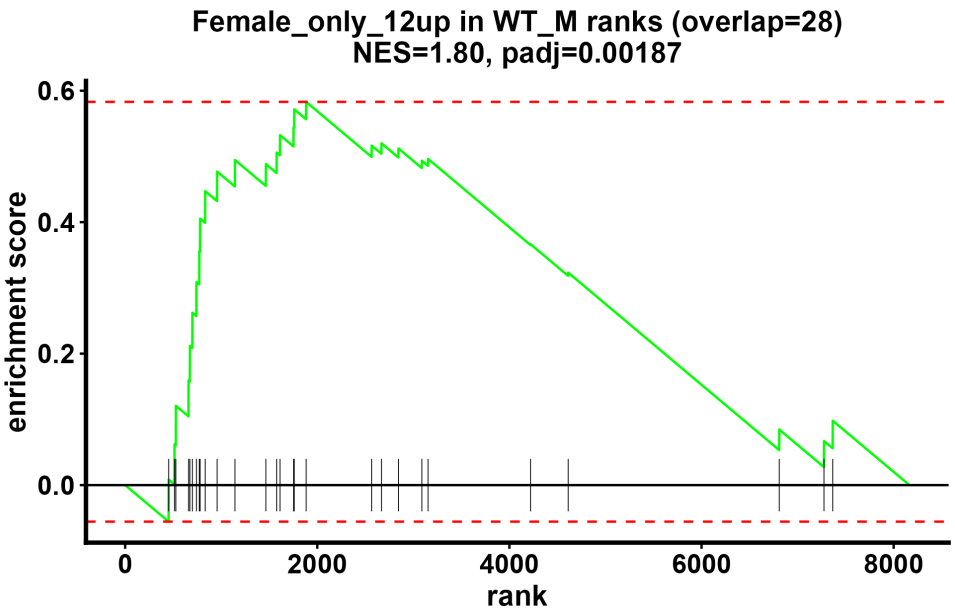

(a) Female ZT12 up

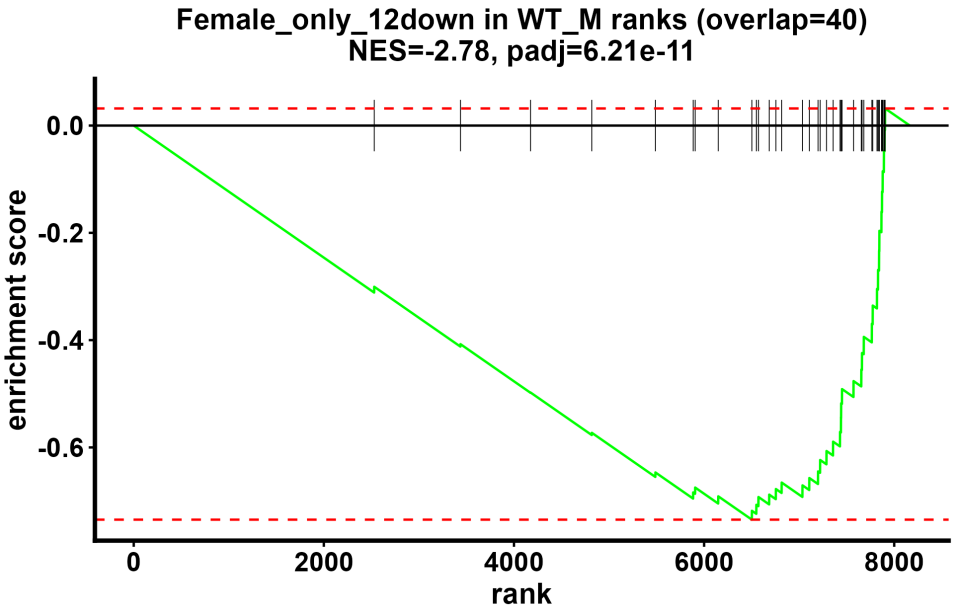

(b) Female ZT12 down

Figure 4.9: **Female-specific BMAL1-dependent genes are similarly enriched in wild-type male macrophages.**
Gene Set Enrichment Analysis (GSEA) testing whether female-specific BMAL1-dependent genes show coordinated expression changes in male samples. Genes were ranked by DESeq2 Wald statistic (ZT12 vs ZT0) for WT male macrophages, with ZT12-upregulated genes on the left and ZT0-upregulated genes on the right. The running enrichment score (green line) reflects the cumulative over- or under-representation of gene set members as the algorithm moves through the ranked list. Vertical black lines (barcode) indicate positions of individual gene set members within the ranked list. The red dashed line marks the peak enrichment score, corresponding to the leading edge (the subset of genes driving the enrichment signal). Positive normalised enrichment score (NES) indicates enrichment among ZT12-upregulated genes; negative NES indicates enrichment among ZT0-upregulated genes. Custom gene sets were compiled from female-specific ZT12-upregulated (n = 28) and ZT12-downregulated (n = 40) genes. Enrichment was tested using fgseaMultilevel (minSize = 5).

While male to female enrichment was robust for both directions (as indicated by comparable NES values) (Figure 4.8), female to male enrichment was asymmetric (Figure 4.9). ZT12-downregulated genes showed strong enrichment in males, but ZT12-upregulated genes showed weaker enrichment, suggesting the subset may represent genuinely sex-specific regulation (rather than amplitude differences).

The set of female-specific ZT12-upregulated genes contains genes involved in DNA replication such as licensing factors, *Mcm2/3/4*, *Smc2* (Structural maintenance of chromosomes protein 2, component of condensin, required for conversion of interphase chromatin to mitotic chromosomes), and *Rad18* (E3 ubiquitin-ligase involved in DNA repair).

4.3.4 Transcription factor activity differs qualitatively between sexes.

The results of Chapter 3 suggest BMAL1 gates inflammatory macrophages through control of master regulators of inflammation. Having established that sex modifies the amplitude of shared BMAL1-dependent programs enriched for inflammatory functions, I next asked which upstream regulators might establish different amplitudes. To identify the transcription factors (TFs) driving these sex-biased responses, TF activity and pathway enrichment was inferred using decoupleR.

TF activity inference revealed qualitatively distinct regulatory signatures between sexes (Figure 4.10). The TFs with conserved directionality of activity in both sexes included CLOCK and BMAL1, active at ZT12 (Figure 4.10(a), 4.10(b)). TFs predicted to be active at ZT0 were BHLHE41, MECP2, and DBP (MECP2 and DBP non-significant in males).

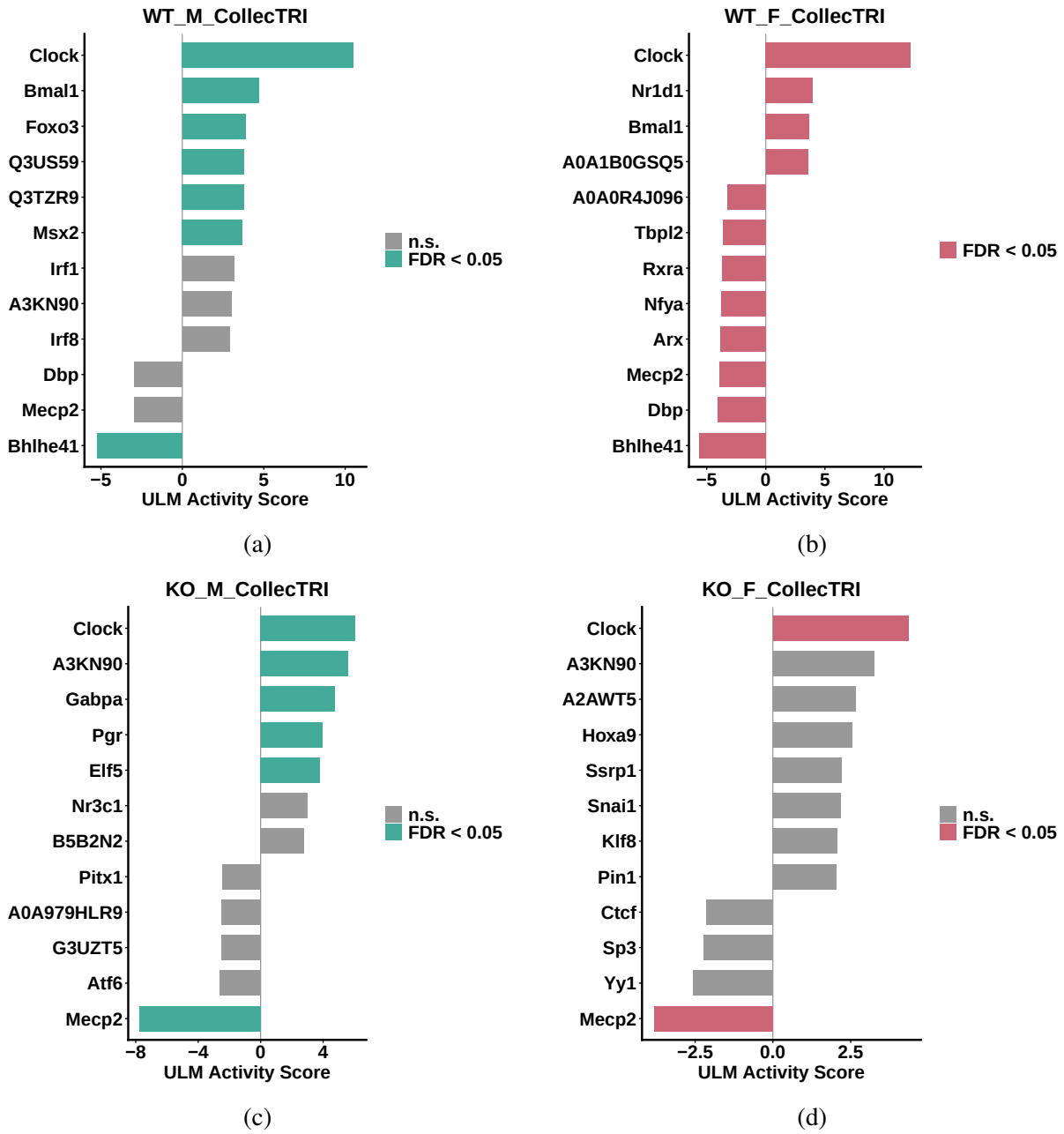

Figure 4.10: **The effect of sex and loss of BMAL1 on differential transcription factor activity between ZT0 and ZT12 in LPS-stimulated macrophages.**
TF activity inference results for the ZT12 vs ZT0 contrast in LPS-stimulated peritoneal macrophages, for each sex and genotype combiniation. TF activity was inferred by inputting ZT12vsZT0 Wald statistics into decoupleR with CollecTRI regulons. Positive scores indicate TF activation at ZT12, and negative scores activation at ZT0. (a) WT Male, (b) WT Female, (c) BMAL1-KO Male, (d) BMAL1-KO Female. TFs with significant activity (FDR < 0.05) are highlighted in green for males and pink for females; non-significant factors are shown in gray.

TFs with predicted differential ZT12 vs ZT0 activity in females only were NR1D1 and HDAC9 (active at ZT12), and Arx, Nfya, Rxra, Tbpl2, ROR-γ (active at ZT0). TFs predicted to act differentially between ZT12 vs ZT0 only in males were FOXO3, IRF-1/8 (nonsignificant but concordant with results from Chapter 3), and ATF7 (active at ZT12).

In BMAL1-KO, TFs changing by timepoint in the same direction, (even if non-significant in one sex), were MECP2, CLOCK, Mineralocorticoid receptor, and PGR (Figure 4.10(c), 4.10(d)).

4.3.5 Males drive the JAK-STAT activation observed in mixed-sex analysis.

The differential TF activity between sexes (Figure 4.10) suggested distinct upstream signalling cascades. To test this hypothesis at the pathway level, I used decoupleR using PROGENy's multivariate linear model (MLM) to infer sex-specific pathway activity between ZT12 and ZT0.

In both sexes, PI3K signalling is more active at ZT0 (Figures 4.11 and 4.12). Phosphoinositide-3-kinases (PI3Ks) are central metabolic regulators, and activation is important in relaying extracellular stimuli and in limiting pro-inflammatory responses in LPS-mediated TLR4 activation.

In males only, the hypoxia, JAK-STAT and androgen pathways are more active at ZT12 (with padj < 0.1) (Figure 4.11). Pathway activation differs in females, with both p53 and TGFβ signalling more active at ZT0, and Wnt signalling more active at ZT12 (Figure 4.12).

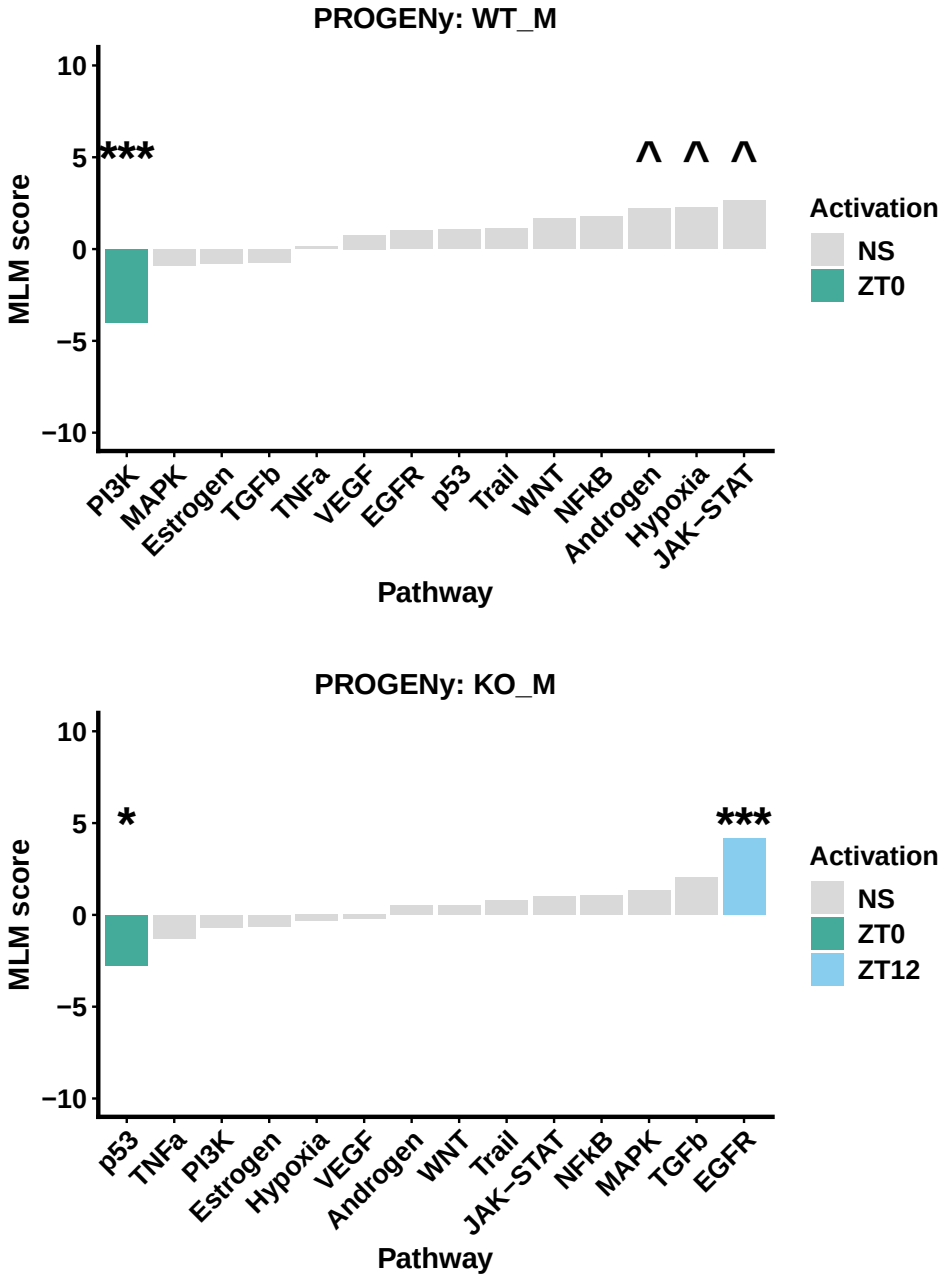

Figure 4.11: **BMAL1 deletion disrupts timepoint-dependence of inflammatory pathways in male LPS-stimulated macrophages.**
Pathway activity enrichment scores were inferred using decoupleR with PROGENy's multivariate linear model. Wald statistics for the WT and BMAL1-KO male ZT12 vs ZT0 contrasts (WT n = 3, KO n = 2-3 per timepoint subgroup) served as input to score activity across 14 pathways, in LPS-stimulated macrophages. Positive scores indicate pathway activation at ZT12 relative to ZT0; negative scores indicate activation at ZT0. *** = padj < 0.001, ** = padj < 0.01, * = padj < 0.05, ∧ = padj < 0.1.

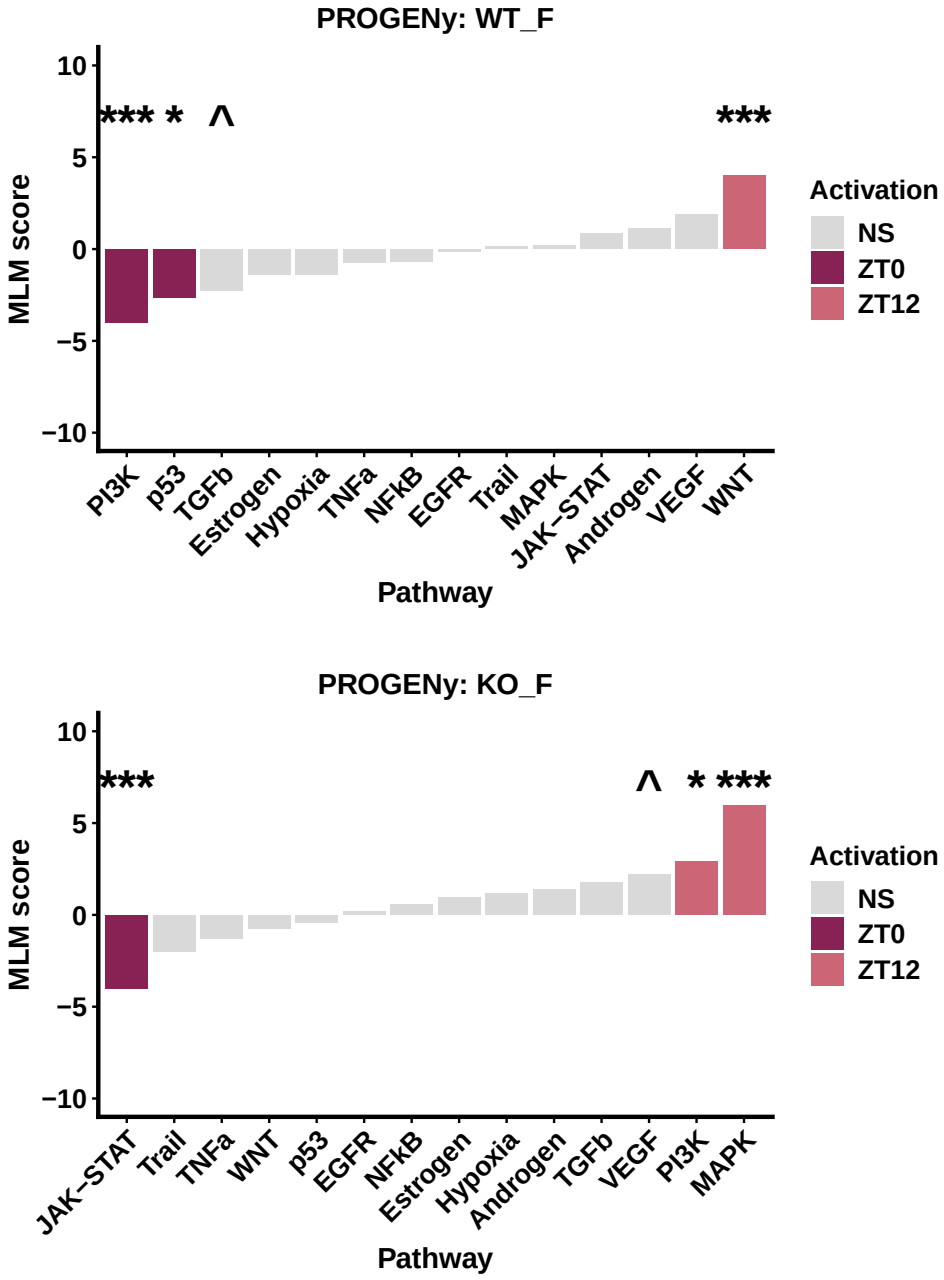

Figure 4.12: **BMAL1 deletion disrupts timepoint-dependence of inflammatory pathways in female LPS-stimulated macrophages.**
Pathway activity enrichment scores were inferred using decoupleR with PROGENy's multivariate linear model. Wald statistics for the WT and BMAL1-KO female ZT12 vs ZT0 contrasts (WT n = 2-3, KO n = 3 per timepoint subgroup) served as input to score activity across 14 pathways, in LPS-stimulated macrophages. Positive scores indicate pathway activation at ZT12 relative to ZT0; negative scores indicate activation at ZT0. *** = padj < 0.001, ** = padj < 0.01, * = padj < 0.05, ∧ = padj < 0.1.

This analysis differs from that performed in Chapter 3 in important ways: in Chapter 3, I examined pathway activity in the LPS response (LPS vs Saline contrast) to reveal which pathways are differentially active in response to stimulation at each timepoint. Here, I compare pathway activity *within* LPS-stimulated macrophages between timepoints, which reveals differences in absolute pathway state at the 1-hour endpoint rather than characteristics of the response. The approaches are complementary: Chapter 3 showed increased JAK-STAT activation in the LPS response at ZT12. Here, I tested whether the absolute JAK-STAT activity within LPS-stimulated macrophages also differs by timepoint, and whether this differs by sex. I found that the absolute activity is increased at ZT12 in males only.

To identify which genes drive this male-specific circadian regulation of the JAK-STAT pathway, I examined individual gene contributions weighted by their pathway membership (Figure 4.13). Genes with positive PROGENy weights showed greater ZT12 vs ZT0 changes (Wald stat values) in males than females. This suggests that the Chapter 3 observation that JAK-STAT activation is greater in the LPS-response at ZT12 than ZT0 is predominant in males, resulting in greater JAK-STAT activity 1-hour post LPS at ZT12 in males only.

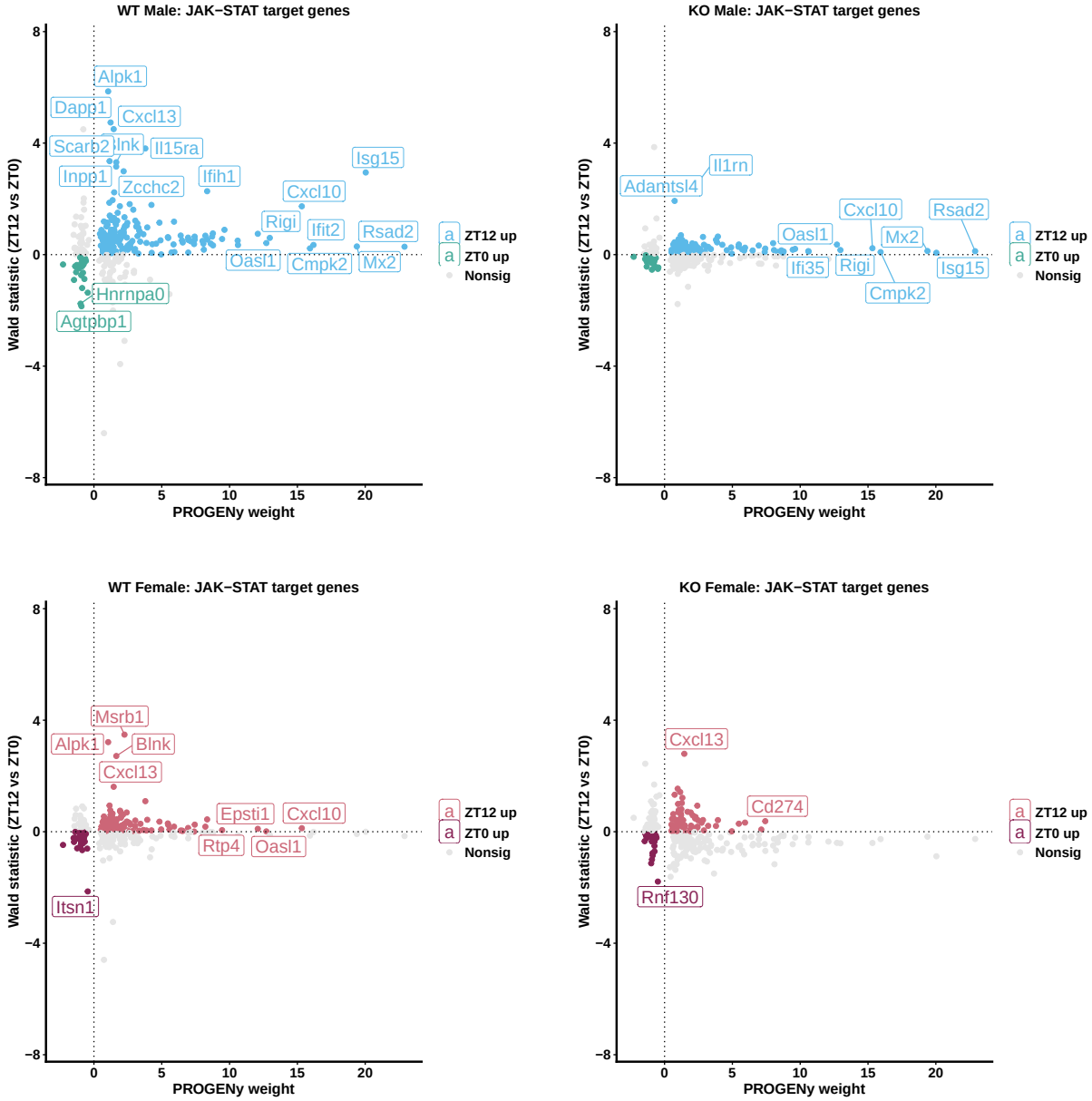

Figure 4.13: **BMAL1 deletion disrupts the coordinated regulation of JAK-STAT pathway target genes in males and females, respectively.**
Wald statistics for ZT12 vs ZT0 contrasts were calculated for each gene for each sex/genotype combination separately (WT Male n = 3, WT Female n = 2-3, BMAL1-KO Male n = 2-3, BMAL1-KO Female n = 3 per timepoint subgroup) and used as input to decoupleR with PROGENy's multivariate linear model. For target genes in the JAK-STAT pathways, Wald statistics are plotted against PROGENy-derived pathway weights. Negative Wald values indicate higher expression at ZT0; positive values indicate higher expression at ZT12. In male mice, light blue points represent target genes whose expression patterns are consistent with pathway activation at ZT12 (positive correlation between Wald statistic and pathway weight), while teal points indicate expression patterns suggesting pathway suppression at ZT12 (negative correlation). In female mice, pink indicates concordant pathway activation at ZT12, while dark pink indicates patterns suggesting pathway suppression at ZT12.

4.3.6 There is a small, but significant BMAL1-dependent sex-timepoint interaction.

The convergent evidence from differential gene sets, TF activity, and pathway analysis pointed to a fundamental interaction between sex and time-of-day in shaping LPS responses. To formally test whether sex modifies circadian gating, I fit an interaction model (sex-timepoint, within each genotype) to definitively identify genes whose clock-gating is significantly different between the sexes.

In WT macrophages, there were 46 significant genes showing sex-timepoint interaction (Figures 4.14 and 4.15), with only 3 significant genes in BMAL1-KO macrophages which showed no consistent biological function: *Oaz1* (antizyme, regulating polyamine homeostasis), *Rps5* (ribosomal protein), and *Cep85* (centrosomal protein).

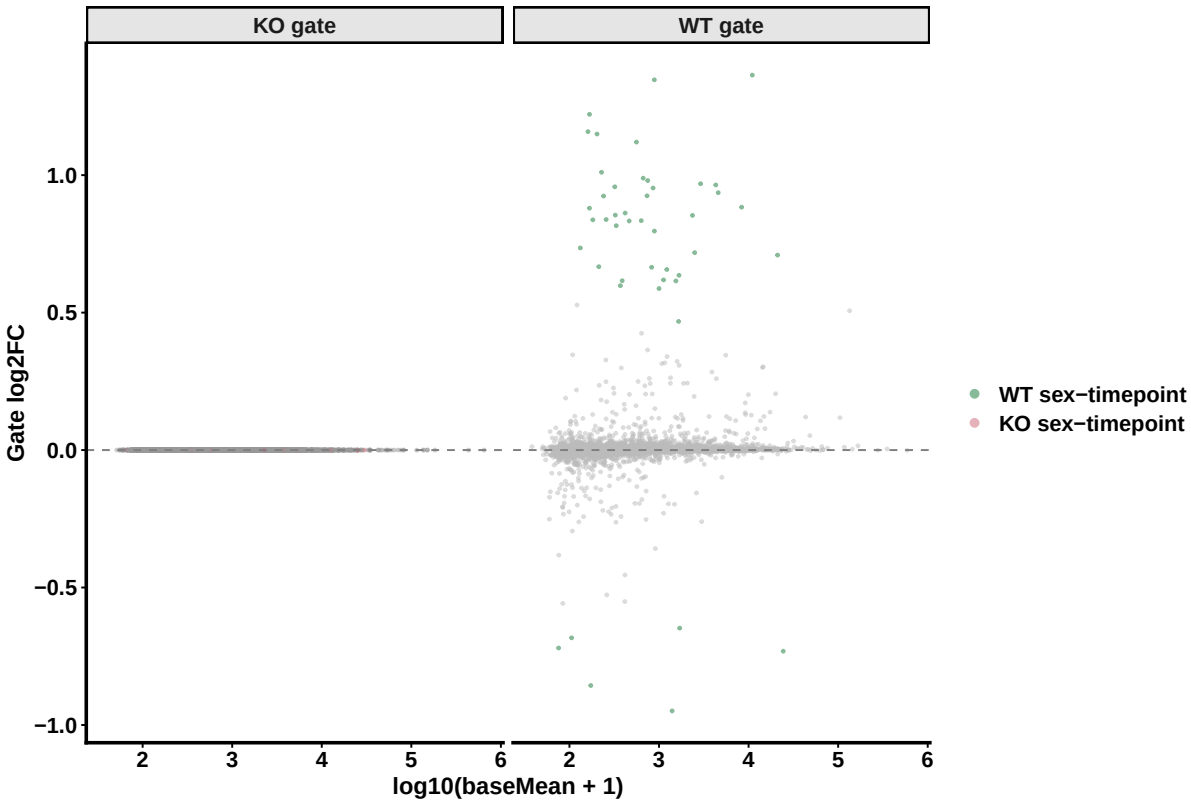

Figure 4.14: **Myeloid-specific BMAL1 is necessary for sex-timepoint interactions in LPS-stimulated peritoneal macrophages.**
This interaction term defines which genes show dependence on sex (male or female) for their expression at ZT0 relative to ZT12. DEGs were identified using DESeq2, where BH-adjusted p-values < 0.05. (WT Male n = 3, WT Female n = 2-3, BMAL1-KO Male n = 2-3, BMAL1-KO Female n = 3 per timepoint subgroup) WT DEGs in green, BMAL1-KO DEGs in pink.

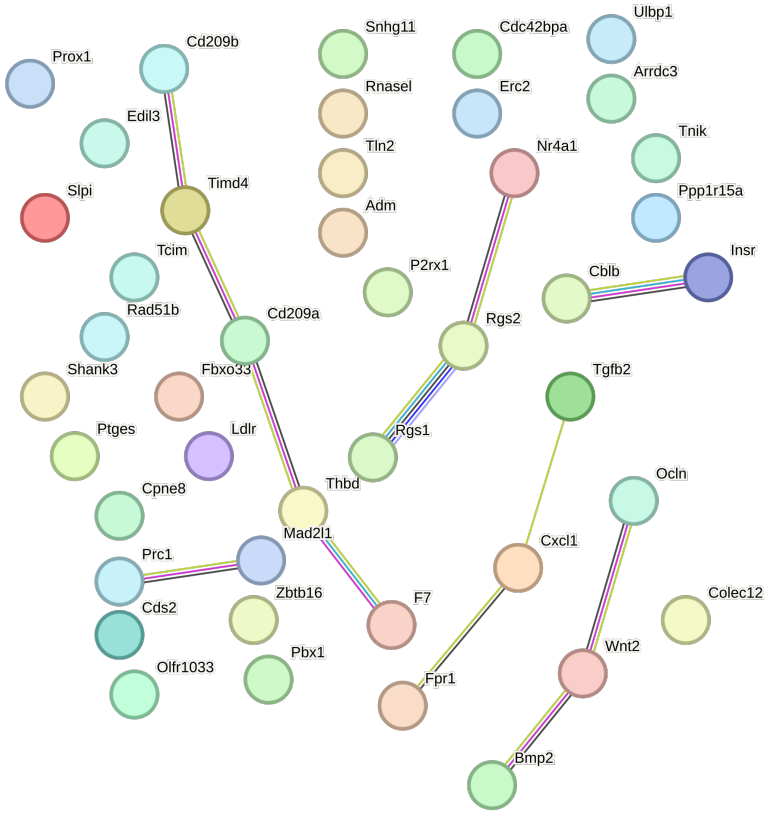

Figure 4.15: **The genes showing a BMAL1-dependent sex-timepoint interaction in LPS-stimulated macrophages.**
Predicted functional protein association network (STRING) for the significant sex-timepoint interacting genes, identified using DESeq2, where BH-adjusted p-values < 0.05. BMAL1-dependent interactions were defined by the exclusion of any significant sex-timepoint interacting genes in BMAL1-KO macrophages.

To identify the biological processes governed by this BMAL1-dependent sex-time interaction, I performed functional enrichment analysis on the 46 genes showing sex-time interaction in WT macrophages only (Figure 4.16).

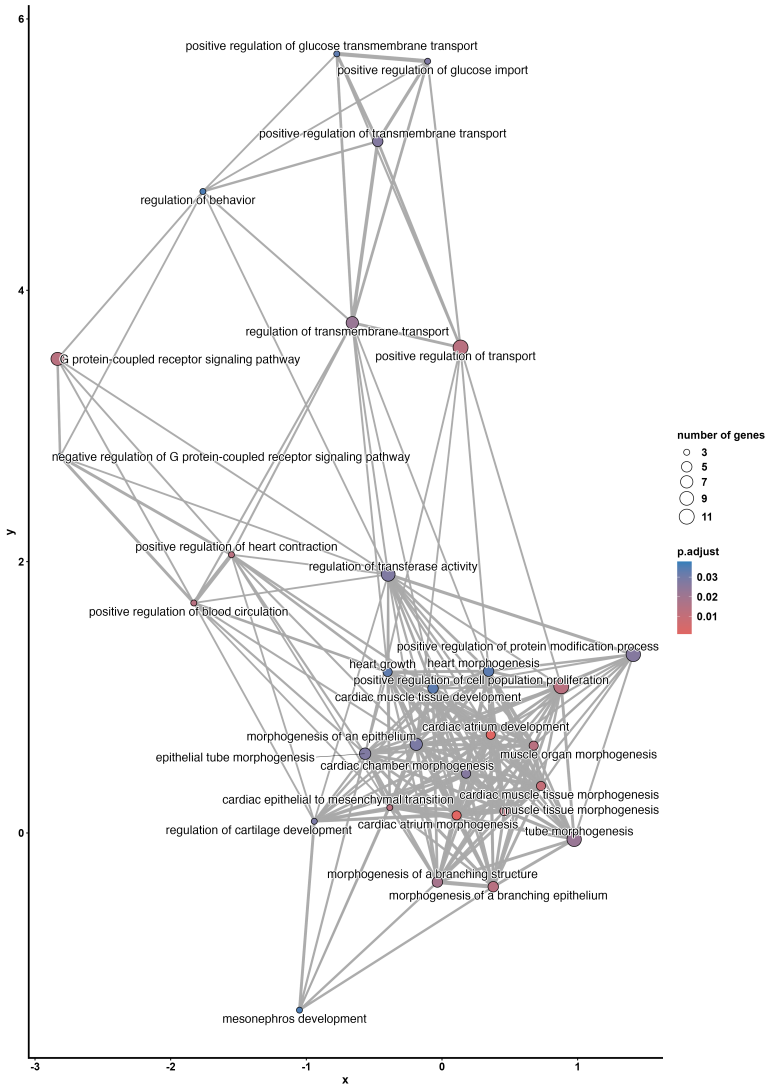

Figure 4.16: **Functional enrichment of the genes showing a BMAL1-dependent sex-timepoint interaction in LPS-stimulated macrophages.**
Peritoneal macrophages from WT or BMAL1-KO mice were treated with LPS (1 mg/kg) at ZT0 or ZT12 for 1 hour, and transcriptomic analysis identified a set of 46 genes showing an interaction between sex and timepoint in WT-only. Enrichment map showing network of enriched pathways in BMAL1-dependent interaction term genes. Edges connect overlapping gene sets or pathways, so clusters are functionally-related modules.

BMAL1-dependent sex-timepoint interaction shows unexpected enrichment of cardiac terms (atrium morphogenesis, development, contraction), driven by *Wnt2, Bmp2, Tgfb2,* and *Prox1*. PROX1 is a known circadian modulator, repressing transcription of ROR-α and ROR-γ (Takeda & Jetten, 2013). The gene set is also enriched for transmembrane transport and G-protein coupled receptor signalling. *Cd209a, Cd209b, Timd4,* and *Colec12* were previously identified as sex-dimorphic in peritoneal macrophages, with *Cd209b* conferring resistance to bacterial infection (Bain et al., 2020).

With GO enrichment for vasculature development in the male-specific gene set and cardiac terms enriched in the sex-timepoint interaction set, it might be expected that vascular leak or clotting is more dependent on circadian phase in males.

The majority of the BMAL1-dependent sex-timepoint interaction shows greater amplitude of ZT12 vs ZT0 difference in males than in females (Figure 4.17). This reflects the findings that there are more "male-unique" BMAL1-dependent ZT12 vs ZT0 DEGs (Figure 4.3).

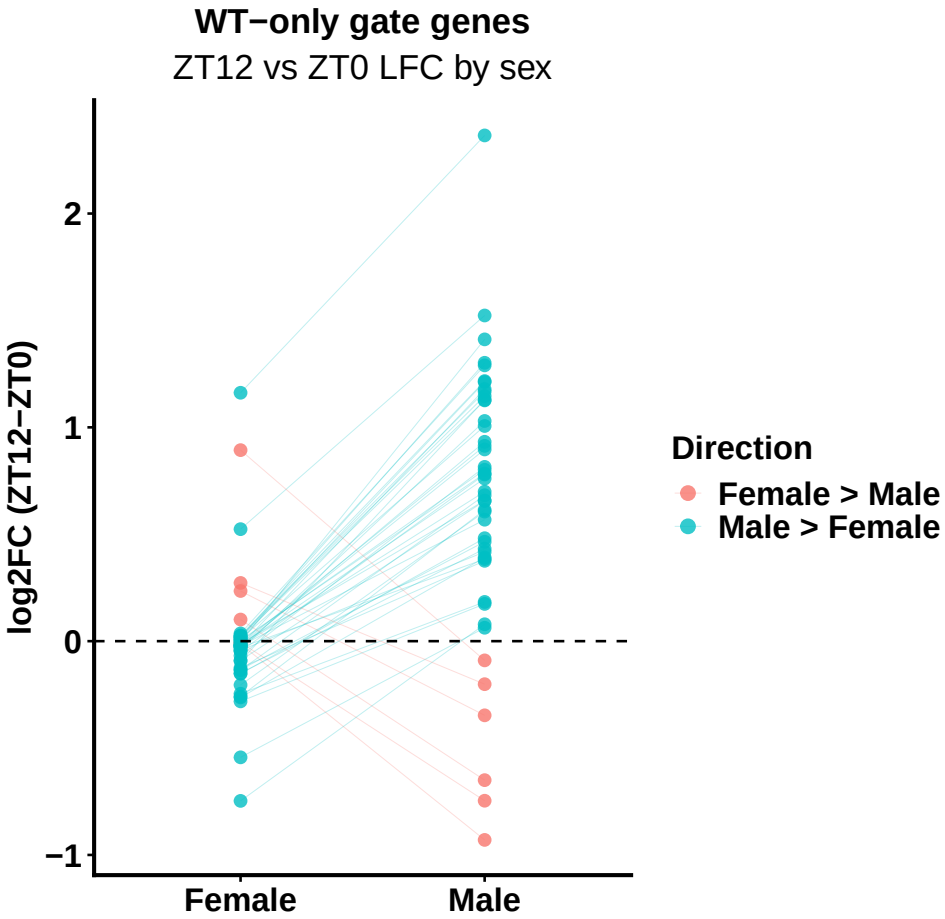

Figure 4.17: **The sex-timepoint interaction set show greater magnitude of change, and are largely upregulated at ZT12, in male macrophages.**
Peritoneal macrophages from WT or BMAL1-KO mice were treated with LPS (1 mg/kg) at ZT0 or ZT12 for 1 hour before RNA extraction. Spaghetti plot showing ZT12 vs ZT0 log2FoldChange for each sex, males and females, for the sex-timepoint interaction set identified by DESeq2 with an interaction term, where BH-adjusted p-values < 0.05. Colour indicates whether the log2FoldChange is amplified more at ZT0, or ZT12.

4.3.7 Sex-specific oscillation of key transcription factor expression.

The interaction gene set was characterised by larger-amplitude ZT12 vs ZT0 changes in males, with a majority of genes showing sign-flipped regulation between sexes. Of the 46 genes, 11 were amplitude differences with the same directionality. 29 were upregulated in males at ZT12 and females at ZT0. The functions of these 29 genes included pattern recognition and regulation of phagocytosis (*Cd209a/b, Timd4*, adhesion (*Tln2*), metabolic programs (*Insr, Ldl2, Cds2*) and ROR-regulator *Prox1*). There were also genes involved in tissue remodelling, such as *Has1* (hyaluronan synthase 1 - hyaluronan synthesis contributes to extracellular matrix structure and cellular adhesion/migration as well as fibrotic responses (Siiskonen et al., 2015)), *Bmp2/Wnt2*, and *Areg* (amphiregulin, a ligand for epidermal growth factor receptor EGFR (Y. Xu et al., 2016)).

Four genes were upregulated in males at ZT0 and females at ZT12: *F7* (factor VII), a coagulation factor, two genes relating to cell-cycle processes (*Prc1*, protein regulator of cytokinesis 1), protein present at high levels during S, G2/M phases of mitosis, and *Mad2l1* (mitotic arrest deficient-like 1, a spindle checkpoint protein), and *Ulbp1* (UL16 binding protein 1), and an MHC Class I-like molecule which activates natural killer cells.

To identify transcriptional regulators that might establish these sex-divergent oscillation amplitudes, I examined which TFs were themselves differentially expressed between ZT12 and ZT0 in each sex. This analysis revealed that males show broader timepoint-dependent TF regulation than females, with key inflammatory and metabolic regulators showing reciprocal sex-specific oscillation patterns (Figure 4.18).

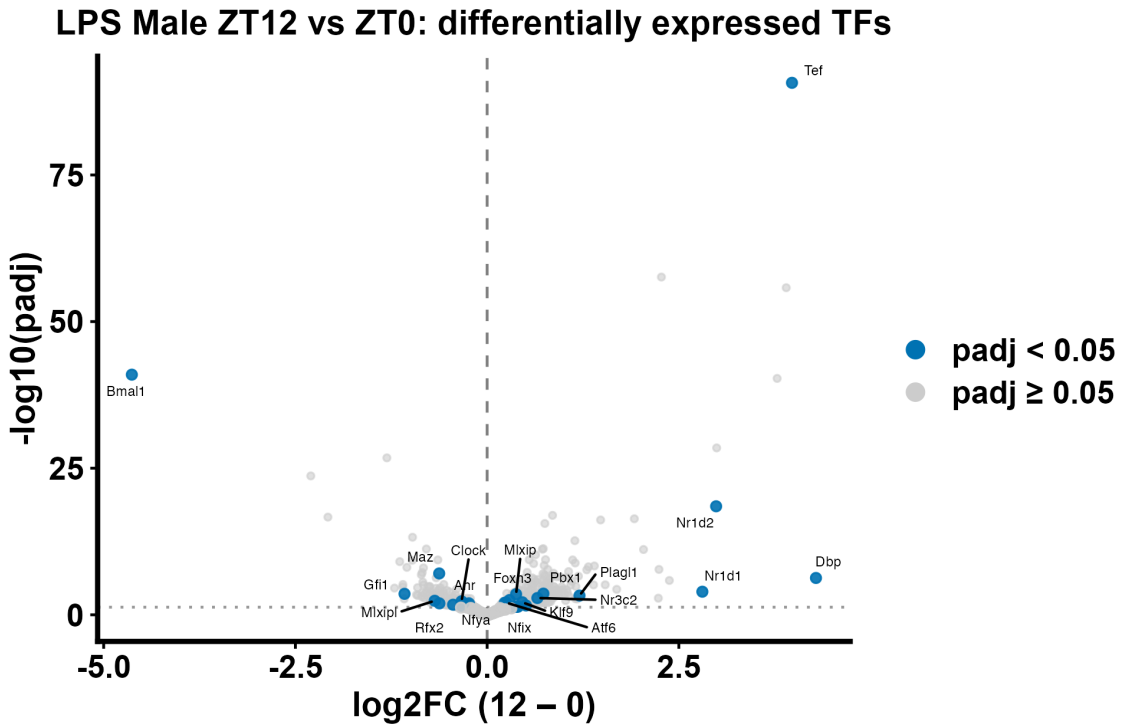

(a) Male

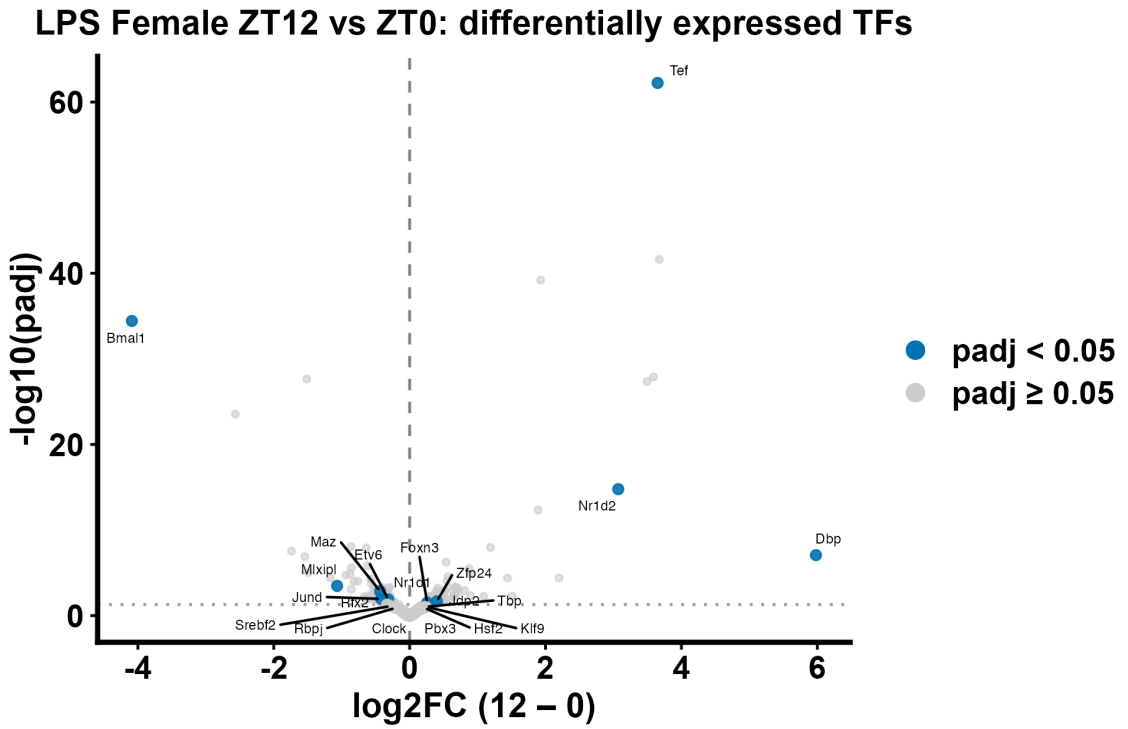

(b) Female

Figure 4.18: **The effect of timepoint on expression of transcription factor transcripts in WT macrophages, in males and females separately.**
Volcano plots showing significant differentially expressed TFs, between ZT12 and ZT0 LPS-stimulated WT macrophages (a) Male, (b) Female. TFs were identified using the JASPAR2024 Core non-redundant database. Blue points indicate genes passing FDR < 0.05.

In WT male macrophages, there were 29 TFs showing timepoint dependence between ZT0 and ZT12. Zinc-finger protein-encoding transcript *Gfi1* was downregulated at ZT12 in males only, and was identified as a TF downregulated in BMAL1-KO (Chapter 3), and so is likely under clock-control for its expression, seemingly in males only. Gfi1 inhibits *Nlrp3* transcription directly and indirectly as a transcriptional repressor interfering with NFkB activity, inhibiting IL-1β production (Zhu et al., 2014). The downregulation of an anti-inflammatory TF at ZT12 is consistent with the observed increase in genes enriched for cytokine production/inflammatory response GO terms at ZT12, in male-specific BMAL1-dependent genes. Only 10 TFs showed differential expression in females, including *Srebf2*, reported to be a target of REV-ERB-mediated repression that associates with RORγ to activate the cholesterol biosynthesis program (Cai et al., 2019; Sitaula et al., 2017).

There was a strong concordance between TF activity scores (Figure 4.10) and TF expression (Figure 4.18): STAT1 and IRF1 were both more active and more highly expressed at ZT12 in males, while SREBF2 showed reduced activity and expression at ZT12 in females. This suggests transcriptional regulation of TFs as one mechanism underlying sex-specific circadian gating. These changes by timepoint in expression or activity are not seen in the BMAL1-KO (for SREBF2, STAT1, IRF1), in either sex or pooled (where there is greater power to detect variance between timepoints).

To visualise how these key TFs differ between sexes across the circadian cycle, I plotted normalised expression of *Srebf2* (and target gene *Hmgcr*) *Stat1/Irf1*, and *Prox1* across conditions (Figure 4.19).

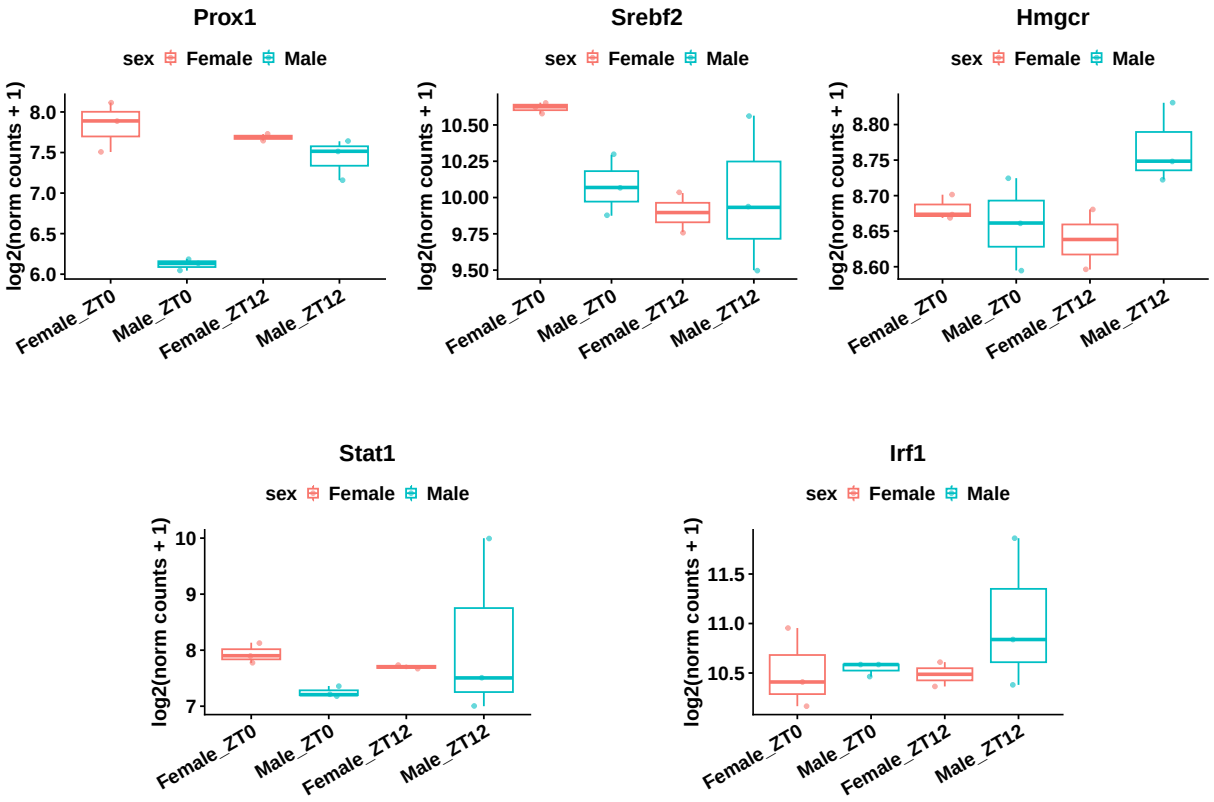

Figure 4.19: **Boxplots for the expression of key TFs which vary across timepoints differently in males and females, respectively.**
Log2normalised counts were plotted for each gene for each sex/timepoint combination separately (WT Male n = 3, WT Female n = 2-3 per timepoint subgroup). Male points in teal, female in pink.

PROX1 is a co-repressor of RORα/γ present in the BMAL1-dependent sex-timepoint interaction gene set. Males and females differ in PROX1 expression at ZT0: expression is constitutively high in females, suggesting PROX1 is a potential TF coordinating inflammatory-metabolic trade-off in males.

Srebf2 was identified as differentially expressed between ZT12 and ZT0 in females only, and is downregulated at ZT12 relative to ZT0. Females have higher expression at ZT0, which drops to male levels by ZT12. The *Srebf2* target and rate-limiting enzyme in the mevalonate pathway is *Hmgcr*, which shows flipped directionality between sexes (higher in females at ZT0 and males at ZT12) with greater peak expression in males at the timepoints covered.

STAT1/IRF1 show the inverse pattern to PROX1: constitutively low in females, with peak expression in males at ZT12. This is consistent with the observed JAK/STAT activation at ZT12 in males only (Figure 4.11).

4.4 Discussion

In this Chapter, I analysed the transcriptomes of male and female peritoneal macrophages from mice given 1 mg/kg LPS for 1 hour at ZT0 and ZT12. I compared the ZT12 vs ZT0 contrasts from WT and BMAL1-KO mice to establish which timepoint-differences were BMAL1-dependent for each sex, and compared results to identify sex-specific BMAL1-dependent genes. I found that the majority of sex-specific changes were weakly present in the other sex, indicating that the major effect of sex is modifying the amplitude of a shared circadian program as opposed to regulating distinct transcriptional programs.

4.4.1 Sex predominantly modulates amplitude, not directionality.

I hypothesised that the circadian clock governs sex-specific programmes in inflammatory macrophages. The two contrasting hypotheses were: i) Sex and clock regulate programs independently, with BMAL1-necessity for ZT0 vs ZT12 differences equivalent in males and females; ii) Sex modifies which genes are clock-controlled, with BMAL1-dependent gene sets differing between males and females. I found that sex modifies amplitude, not directionality of BMAL1-dependent gene expression in this model of early transcriptional responses to LPS in peritoneal macrophages, supporting the second hypothesis.

Strikingly, the male:female ratio of BMAL1-dependent genes is approximately 3:1, reflecting a greater number of ZT12 vs ZT0 differences. GSEA showed that the same genes change between ZT12 vs ZT0 in males and females at different thresholds, indicating coordinated regulation between sexes, with timepoint directionality preserved for most genes. There were only 46 statistically significant sex-timepoint interactions, and of these 35 genes where directionality is reversed by sex. This gene set contains *Cd209a/b, Timd4,* and *Colec12*, all previously found to show significant sex-dimorphism in peritoneal macrophages (Bain et al., 2020).

The GTEX project in humans (where gene expression rhythms were identified in 46 tissues from 914 donors), identified that the number of rhythmic genes was twice as high in females in a majority of tissues, but especially in liver and adrenal gland (Talamanca et al., 2023). However, the tissue most comparable to this analysis of macrophages, spleen, showed more rhythmic genes in males than females, consistent with my findings.

Talamanca et al. found that targets of the glucocorticoid receptor showed increased rhythmicity in female adrenal glands, perhaps reflecting increased sensitivity to glucocorticoid autocrine signalling in females. In my results, I found BMAL1-KO female macrophages show a greater

number of ZT12 vs ZT0 differences than male BMAL1-KO macrophages, which might reflect greater dependence on glucocorticoid rhythms (Talamanca et al., 2023).

4.4.2 Inflammatory gating is amplified in males.

Male macrophages showed amplified BMAL1-dependent timepoint differences. GO enrichment in male-specific BMAL1-dependent genes, not present in female-specific, included the inflammatory response, cytokine production, and vasculature development.

The absolute JAK-STAT activity is increased at ZT12 in males only. This suggests the ZT12 JAK-STAT-driven LPS-response identified in Chapter 3 may also be a male-specific effect, but warrants further investigation with basal state macrophage sex-differences.

Hypoxia signalling showed timepoint-dependence in males only, with greatest activity at ZT12. BMAL1 forms transcriptionally active heterodimers with HIF1$1\alpha/2\alpha$ (Wu et al., 2017). Circadian modulation of hypoxic responses has been established in cardiac tissue, and the importance of hypoxia in inflammatory diseases means this may be a clinically significant sex-difference. For example, perturbing the clock may have more severe cardiac outcomes in males, where clock-control of inflammatory macrophages is more important (at transcriptional level). In accordance with this, aged male CLOCK-$\Delta19/\Delta19$ mice develop severe cardiomyopathy compared to WT controls, and females are protected despite similar heart structure and function when compared to WT at 18 months old. Ovariectomy in female CLOCK-$\Delta19/\Delta19$ mice induces the phenotype seen in males, indicating that ovarian hormones protect females from the effects of clock-disruption (Alibhai et al., 2018). This sex-specific cardiac vulnerability to clock disruption in males is consistent with my observation that male macrophages show greater BMAL1-dependence of inflammatory programs than females.

Atf6, encoding an ER stress sensor activated in the unfolded protein response (UPR), showed

male-specific regulation by BMAL1. ER stress and the UPR are increasingly being recognised as drivers of pro-inflammatory signalling, with crosstalk with NFkB signalling pathways (W. Li et al., 2022). This male-specific clock control of cellular stress pathways may contribute to the observed amplified inflammatory gating with an enhanced pro-inflammatory state at ZT12 in males.

At the TF level, males showed ZT12-specific activity of FOXO3 and trends toward IRF-1/8 activation. *Gfi1*, encoding a repressor of NLRP3 and NFkB activity, was downregulated at ZT12 in males only, suggesting clock-dependent transcriptional-regulation of the increased inflammatory response at ZT12.

Overall, male macrophages showed amplified BMAL1-dependent timepoint differences in pro-inflammatory pathways compared to females, indicating greater reliance on the cell-intrinsic clock for inflammatory gating.

4.4.3 Lipid metabolic gating is prioritised in females.

Female-specific BMAL1-dependent genes showed weak enrichment for GO terms, with significance only for synaptic signalling. This contrasts with the coherent enrichment seen in the male BMAL1-dependent gene set, suggesting broad homeostatic processes rather than focused inflammatory pathways are most dependent on the clock in females.

The clearest female-specific circadian program involves lipid metabolism. *Srebf2*, the regulator of cholesterol and fatty acid synthesis, showed ZT0-specific upregulation in females, dropping to male baseline levels by ZT12. Beyond lipid homeostasis, SREBPs have context-dependent effects on inflammation: in the basal state restraining the type I interferon response, while augmenting pro-inflammatory polarisation in the late-phase responses to TNF (Kusnadi et al., 2019). This study did not include sex as biological variable, leaving uncertain whether SREBP's

activity in inflammation is consistent between sexes. Female-specific circadian control of *Srebf2* may represent sex-specific clock control of this metabolic-inflammatory axis, with implications for diseases where cholesterol metabolism is dysregulated like atherosclerosis.

Hmgcr (the rate-limiting enzyme for cholesterol biosynthesis and downstream target of SREBP2) showed corresponding ZT0 elevation. Surprisingly, *Hmgcr* showed reversed rhythmicity between sexes: elevated at ZT0 in females and at ZT12 in males. This may have implications for atherosclerosis, where there are notable sex-differences in its prevalence: females are protected relative to males, until after menopause. Males show peak *Hmgcr* coincident with their peak pro-inflammatory state at ZT12, while for females the *Hmgcr* peak is separated temporally. Coincident pro-inflammatory states with greater cholesterol synthesis would potentially favour foam cell formation, which is characterised by the disruption of lipid homeostasis and cholesterol accumulation (Chistiakov et al., 2016).

HMGCR deletion in hepatocytes induces ER stress (De Giorgi et al., 2020). Female macrophages might show circadian variation in cholesterol synthesis out of phase with males (as suggested by *Hmgcr* reversed directionality), which could create sex-dimorphic ER stress dynamics. Sex-specific circadian cholesterol homeostasis might elevate ER stress in different phases in males and females.

The sex-divergent circadian programs I have observed in peritoneal macrophages are consistent with evolutionarily conserved patterns of sexual dimorphism in innate immunity. In a pan-immune survey of immune sexual dimorphism, female macrophages showed upregulated genes relating to lipid and lipoprotein metabolism (Gal-Oz et al., 2019). Consistent with this, the BMAL1-dependent female-specific genes were enriched for lipid metabolism (*Cers2/6, Dbi*), and *Srebf2* showed female-specific ZT0 upregulation. These pathways are regulated by sex hormones (X. Wang et al., 2011).

4.4.4 Sex-timepoint interaction term consists of a small subset of genes with reversed directionality between sexes.

The 46 sex-timepoint interaction gene set contains genes with roles modulating inflammatory responses in macrophages, and is enriched for GO terms relating to cardiac function. PROX1 represses ROR-α and ROR-γ, core clock components which regulate lipid metabolism and ROR-α has anti-inflammatory function in macrophages (Moharrami et al., 2018). In males, PROX1 oscillates (low at ZT0, high at ZT12), which potentially permits ROR-driven anti-inflammatory function and lipid metabolism at ZT0 while suppressing it at ZT12 to prioritise inflammation. Constitutively high PROX1 in females may maintain ROR suppression. PROX1 heterozygous mice have defective lymphatic vasculature and lymphatic leakage, and impaired lymph drainage affects inflammatory responses (Herrada et al., 2022). *Prox1*+/- heterozygotes were found to be protected from DSS colitis, which was attributed to lymph leakage, but intrinsic effects in macrophages might contribute.

The interaction set contains genes previously identified to connect to sexually dimorphic disease outcomes. *Has1* (hyaluronan synthase 1) was upregulated at ZT12 in males, and ZT0 in females. *Has1* is induced by inflammatory stimuli, and elevated in models of murine atherosclerosis, infectious lung disease, and human arthritis (Siiskonen et al., 2015). In smooth muscle cells, *Has1* expression is suppressed by estradiol via estrogen receptor signalling, suggesting hormonal regulation of this clock-sex interaction (Freudenberger et al., 2011). The same opposing pattern of expression is seen for *Areg* (amphiregulin). AREG promotes tissue repair following inflammatory damage through EGFR signalling (Y. Xu et al., 2016). Additionally, AREG shows marked sex-differences in the response to influenza A virus. Male lungs express higher AREG in response to virus, enabling faster recovery and reduced post-viral pathology

compared to females, independent of the anti-inflammatory effects of testosterone (Vermillion et al., 2018). The circadian regulation of these two genes may contribute to sex-differences in effects of clock-disruption on inflammatory pathologies.

However, the sex-timepoint interaction term identified is small (46 genes), and amplitude dampening of the ZT12 vs ZT0 program is the dominant effect of sex. Between sexes, the circadian program is broadly similar, which is consistent with the mixed-sex analysis (Chapter 3) finding consistent ZT12 vs ZT0 differences with the male-dominant program found in this chapter, including enhanced cytokine production at ZT12 which is in agreement with protein-level cytokine secretion at this timepoint (Gibbs et al., 2012). In my sex-stratified pathway activity analysis, I found that PI3K (Phosphoinositide-3-kinase) signalling is more active at ZT0 in both sexes. Activation of PI3Ks have been implicated in limiting pro-inflammatory responses in LPS-mediated TLR4 activation (Sharif et al., 2019), and integrating nutrient signals and TLR4-signals. PI3K activity at ZT0 is clock-dependent (not seen in BMAL1-KO macrophages). The core findings for this chapter are summarised in Figure 4.20.

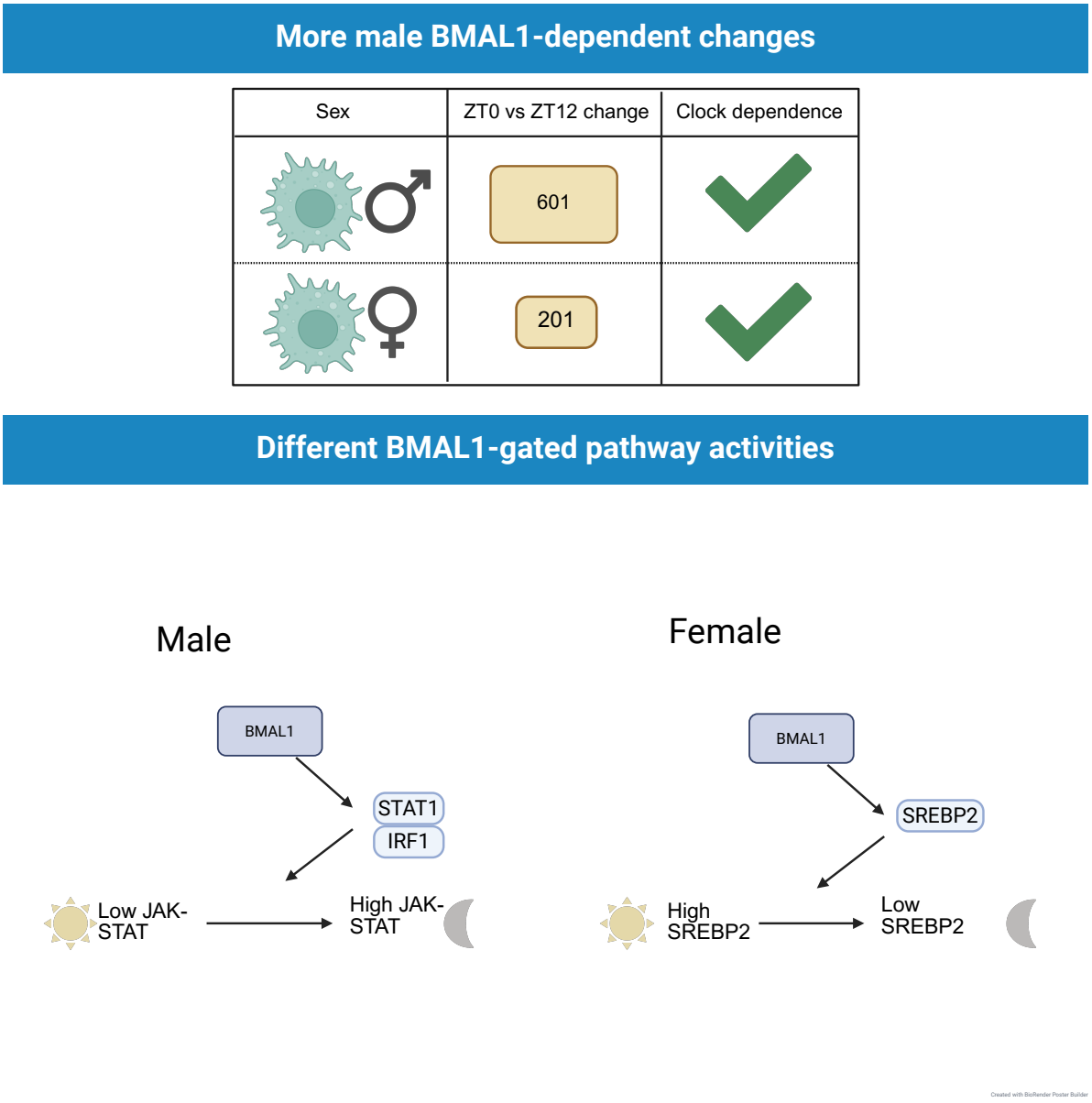

Figure 4.20: **Summary of results from Chapter 4.**
Top: There are more BMAL1-dependent timepoint differences in male, LPS-treated peritoneal macrophages than in female. This is a difference in magnitude: similar changes were observed in females, only more weakly. Bottom: However, some programs were found to be very sexually dimorphic. Male ZT12 inflammatory macrophages were characterised by higher JAK-STAT activity than at ZT0, with this difference lost in females and with BMAL1-deletion. Female ZT12 inflammatory macrophages were characterised by lower SREBP2 activity than at ZT0, with this difference lost in males and with BMAL1-deletion. Created in https://BioRender.com

4.4.5 Limitations and future directions.

My study examines an early timepoint, 1 hour, in the transcriptional response to LPS, and as such it is difficult to make predictions on what functional changes might occur in the hours following (as macrophages mediate the resolution of inflammation). Here, inflammatory male macrophages show greater differences between ZT0 and ZT12 than female macrophages, and these differences are BMAL1-dependent. This would suggest a greater importance of clock-dependent transcriptional regulation in male macrophages, and so greater pathological consequences to clock-disruption. However, predicting functional significance is complicated by the disconnect between rhythmic mRNA and protein or post-translational modifications. Additionally, tissue context strongly influences macrophage function in chronic inflammatory disease. Moreover, different pathogens elicit distinct inflammatory responses in acute inflammatory disease. These considerations make extrapolation to infection and disease model outcomes difficult, and are all limitations that highlight areas of interest for future research.

To address the mRNA-protein disconnect, it will be important to first establish how sex influences clock regulation of macrophage cytokine production, phagocytosis, and inflammasome activation. Phagocytosis shows sex-dimorphism, with female macrophages generally exhibiting greater phagocytic ability (Scotland et al., 2011). Given my finding that males show more BMAL1-dependent inflammatory programs, I would predict that phagocytic capacity shows greater time-of-day variation in males, with females maintaining a more consistent (potentially higher baseline) activity.

The design of this study captured only ZT0 and ZT12. There has been some indication from gene expression in other tissues (such as cardiac sex differences (X. Zhang et al., 2025)) that male and female circadian programs vary in phase, and so the two-timepoint design in my study

may have undersampled female rhythms if they peak in inflammatory program expression at different phases. To address this, a time-course of sampling across ideally 48 hours would enable comparison of rhythm amplitude across sexes.

Mechanisms of sex-clock interactions are unclear in the tissues/organs where they have been demonstrated. Sex differences in immune function are mediated by both sex hormones and X-chromosomal linked dosage. In this study, mice were not staged by estrous cycle, leaving uncertainty as to whether females at particular estrous stages show "male" rhythms. Gonadectomy controls would be needed to examine the influence of sex hormones on time of day acute infection outcome, alongside single nuclei experiments to distinguish bulk RNA-seq changes mediated by altered clock-dependent monocyte recruitment dynamics throughout the time period. Investigation of tissue-resident macrophages in different tissues is important to distinguish whether the tissue environment signals alter sex-clock interactions.

The translational relevance of my findings seem likely to be in pathologies with significant crosstalk between inflammation and lipid metabolism. Macrophages are important mediators of tissue-repair and remodelling, and disruption of circadian rhythms drives atherosclerosis in multiple models, driven by dysfunctional endothelium and macrophage number/activation in lesions. There are various indications from my data that macrophage-regulated fibrotic processes may have sex-differences in circadian-regulated pathology. The sex-timepoint interaction gene set included *Areg, Bmp2/Wnt2, F7,* and *Thbd*. All of these are involved in fibrotic processes, and are regulated in opposite directions in males vs females by the macrophage clock. TGFβ signalling (also invovled in fibrosis) was differentially active in females (more active at ZT0) only.

Atherosclerosis model ApolipoproteinE-deficient mice with chronic jet-lag exacerbated atherosclerosis in female and not male mice. This was attributed to increased atherogenic VLDL/LDL

particles, as no changes in feeding-fasting cycles were observed (Chalfant et al., 2023). Sex-specificity was dependent on the model of circadian disruption used: the same group previously found that ApoE-deficient males but not females had increased atherosclerosis in constant lighting conditions (where some mice became arryhthmic) (Chalfant et al., 2020). In general, females show greater pathology resulting from perturbation of the clock in atherosclerotic models of hyperlipidemia (Chalfant et al., 2023; Schilperoort et al., 2020). These findings raise the possibility that an intact circadian system contributes to the relative protection females show against atherosclerosis.

My data suggest female macrophages rely less on cell-intrinsic clock control of inflammatory programs, and that circadian disruption may more severely affect males under normal conditions, as shown by the CLOCK-$\Delta 19/\Delta 19$ model where males are more severely affected (Alibhai et al., 2018). Females appear more vulnerable with the addition of hyperlipidaemic stress (Chalfant et al., 2023). This may reflect the female-specificity of the SREBF program: disruption of circadian cholesterol homeostasis may increase ER stress, driving pro-inflammatory signalling through NFkB cross-talk (W. Li et al., 2022). However, these models involve multiple cell types (including cardiomyocytes and endothelial cells), so macrophage-specific contributions have yet to be determined.

The sex-differences observed in early transcriptional responses in this study may manifest differently in acute versus chronic inflammatory contexts. Sex-differences (both occurrence and severity) have been observed in both acute and chronic contexts, from sepsis having worse outcomes in males, to the greater risk of autoimmune inflammatory diseases like rheumatoid arthritis in females. Disease-specific investigation is therefore necessary to understand contributions of clock-sex interactions to these divergent patterns.

To increase the translational relevance of our emerging evidence on circadian-sex interactions,

we must learn more about how sex-differences impact diseases where circadian pathology has been demonstrated. Asthma, psoriasis, rheumatoid arthritis and IBD all show sex differences in prevalence, with much higher rates of autoimmune conditions in females. Clinical data is rarely accurately time-stamped, and of the time-stamped data, rarely analysed by sex. Recent reports suggest that the circadian system differentially regulates chronic inflammatory disease occurrence by sex, but we lack mechanistic information on where sex-differences lie: in the cell-types affected, and/or in the systemic circadian signals received (Maidstone et al., 2025). Chronobiology and chrono-inflammation literature is largely sex-neutral. The data presented here highlight the importance of including sex as a biological variable in circadian-inflammation studies: we may find the relevance of macrophage clocks to different diseases differs by sex.

5 | Pharmacological modulation of the macrophage circadian clock

5.1 Introduction

Pharmacological manipulation of the circadian clock is an attractive strategy across diverse areas of medicine, from inflammatory and metabolic diseases to cancer: circadian timing influences cellular state, tissue physiology, and treatment responses. Converging epidemiological and experimental data associate altered clock parameters, especially amplitude and phase alignment, to disease risk and therapeutic efficacy. The potential for improving health outcomes via clock-manipulation has motivated the search for small molecules that tune clock outputs in a controlled, mechanism-informed manner.

Additionally, as genetic knock-out models targeting core circadian components have limitations for understanding circadian biology, pharmacological tools offer advantages over genetic approaches to improve our understanding of the clock system. In contrast to most genetic manipulations, pharmacological tools can be used at a precise timepoint, are not permanent, and as such have no developmental effects on physiology.

Much early-stage discovery work has focused on ligands for nuclear receptors (REV-ERBs, RORs). Many compounds developed do not achieve criteria necessary as high-quality tools, with issues such as off-target effects (Dierickx et al., 2019). Pharmacokinetic profiles have generally been poor, meaning there is limited proof of concept data from animal models.

Direct pharmacological control of BMAL1, particularly via its PAS-B domain, has remained an unachieved target of the field. This has limited our ability to test BMAL1-centric hypotheses

in primary immune cells, where genetic perturbations can be confounded by developmental effects.

A novel compound Core Circadian Modulator (CCM) was developed by collaborators at the target discovery institute (TDI), who have previously identified multiple synthetic compounds able to modulate PAS-domain containing bHLH-PAS transcription factors (TFs) (Figure 5.1). CCM has specificity for the PAS-B domain of BMAL1, causing it to expand and providing dose-dependent thermal stabilisation. CCM therefore provides the opportunity to regulate BMAL1 and examine the downstream consequences to cells, and further our understanding of the role of BMAL1 as a TF and clock component.

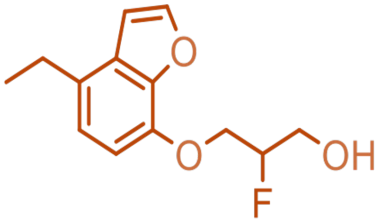

Formula	$C_{13}H_{15}FO_3$
M.W.	*238.26*
SPR K_D *(μM)*	*4.30 ±0.26*

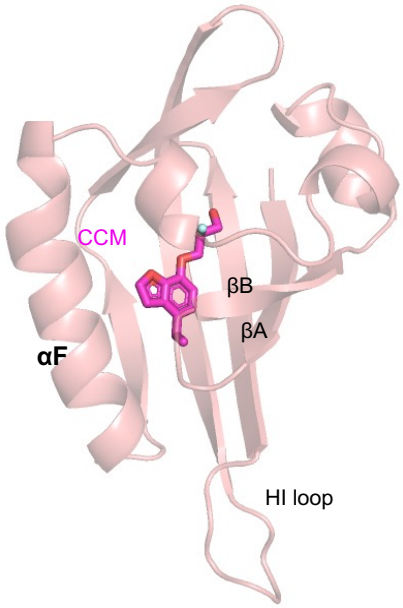

Figure 5.1: **CCM is a novel synthetic ligand of the BMAL1 PASB domain.**
Left: Chemical structure of CCM and dissociation constant (K_d) determined by surface plasmon resonance, a technology detecting molecular interactions by measuring refractive index changes on a metallic surface. Right: Crystal structure of BMAL1(PASB) in complex with CCM. Figures reproduced from (Pu et al., 2025).

As established in Chapter 3, macrophages vary in function by time of day in a BMAL1-dependent manner. Macrophages therefore represent an ideal system to test effects of CCM, as BMAL1-dependence has been established.

5.1.1 Hypothesis and Aims

Chapter 3 demonstrated that BMAL1 gates macrophage inflammatory responses, with loss of BMAL1 eliminating time-of-day differences in LPS responses.

Based on previous studies and my investigation in (Chapter 3), I hypothesised that using a compound that thermally stabilises and induces conformational change in BMAL1 would perturb the anti-inflammatory effect of BMAL1 on macrophage inflammatory responses.

Mechanistically, I hypothesised that CCM-treated macrophages would show changes in TF availability and/or activity in accordance with BMAL1-dependent changes observed in peritoneal macrophages *in vivo*.

5.1.1.1 Aims

Peritoneal macrophages were used for luminometry as they retain *in vivo* synchronisation without the confounding effects of serum (needed for BMDM culture) on circadian phase. BMDMs were used for transcriptional and functional experiments due to higher cell yields, minimising animal numbers.

Investigate the effects of CCM on circadian oscillations in peritoneal macrophages.

- Compare the luminometry traces of PER2::Luciferase peritoneal macrophages treated with a range of concentrations of CCM.
- Quantify changes to oscillation parameters, and corresponding effects on viability at each concentration.

Investigate the effects of CCM on gene expression in basal state and LPS-activated bone–marrow derived macrophages.

- Compare the transcriptomes of WT and BMAL1-KO BMDMs with and without CCM, with and without LPS-stimulation.
- Identify BMAL1-dependent CCM-responsive genes in basal and LPS-stimulated states.

Identify which TFs could be mediating CCM effects in WT bone-marrow derived macrophage transcriptomes.

- Infer TF activity between CCM vs control contrasts.
- Analyse differential pathway activity between CCM vs control contrasts.

Investigate effects of CCM on morphology and motility in bone-marrow derived macrophages.

- Compare morphology of BMDMs, with and without CCM treatment.
- Compare motility of BMDMs, with and without CCM treatment.
- Compare phagocytic ability of BMDMs, with and without CCM treatment.

5.1.2 Contributions in this chapter

This chapter draws from work published in "Pharmacological targeting of BMAL1 modulates circadian and immune pathways" (Pu et al., 2025), of which the full publication is attached in the Appendix. The TDI collaborators performed all experiments developing and characterising CCM biochemically. Maria Voronkov (Ray lab) cultured and treated the BMDMs, and I performed all RNA extractions for sequencing by Novogene. I analysed the resulting data. I then supervised FHS student Jack Gamblin with the help of Siyu Chen (Ray lab), who produced images and analysis of effects of CCM on macrophage morphology. Kacper Kurzyp (Greaves lab, Dunn School of Pathology) performed the gentamycin survival assay on cells I had prepared.

5.2 Methods

BMDMs were used in all experiments for this chapter (except luminometry) due to the high number of cells needed to test each condition (CCM in basal and LPS-stimulated state) in each biological replicate.

5.2.1 Luminometry

Peritoneal macrophages were isolated from both male and female PER2::Luc mice (12-19 weeks old). Peritoneal exudate cells (PECs) were isolated via peritoneal lavage with ice-cold PBS and placed immediately on ice. PECs were spun at 500 x G for 10 minutes at 4°C. Cells were resuspended in 1 ml of recording medium (DMEM/F12 without phenol red (ThermoFisher 11039021) supplemented with 2% B27 (Gibco 17504044) and 1% penicillin/streptomycin (Gibco 15140-122) and cells were counted and plated for 90 min at a density of 1 x 10^5 per well in a 96-well white-walled cell culture plate (Greiner, 655083). Non-adherent cells were removed through washing with PBS. Plastic adherence is a commonly used technique to enrich peritoneal macrophages, typically yielding macrophage-enriched cultures in the approximate range of 80–90% purity (Davies & Gordon, 2004).

Macrophages were then immediately treated with CCM at various concentrations (10/30/50/100μM) or vehicle (0.1% DMSO) in pre-warmed recording medium containing luciferin added to concentration 1 μl/ml (Promega, E1602). The plate was sealed with vacuum grease and parafilm, before being placed in a CLARIOstar Plus platereader (BMG Labtech) with atmospheric control (5% CO2).

Luminescence was recorded every half an hour for 4-5 days. In every experiment, three independent wells were measured from each condition. The parameters period, phase and amplitude,

were then calculated for each well individually and technical replicates were averaged, with statistical analysis performed on biological replicates. Representative traces shown in figures were combined from two biological replicates to display the full range of CCM concentrations analysed. Data were first processed in MultiCycle (Actimetrics) and then smoothed with second-order smoothing, 10 neighbor (GraphPad Prism version 10.0.3).

5.2.2 Analysis of parameters

The rhythmicity of raw luminometry data was tested in BioDare2 (https://biodare2.ed.ac.uk/). No linear detrending was used. The test method selected was BD2 eJTK (the BioDare2 implementation of Empirical JTK-CYCLE with asymmetry search) (Zieliński et al., 2022). The analysis presets (the set of pattern curves against which the comparison test is run) selected were eJTK Classic. Samples were excluded from amplitude/period/phase analysis where they were not found to be rhythmic (Benjamini-Hochberg correction padj > 0.05). For period analysis: raw data were analysed using default settings in BioDare2 software with the fast Fourier transform-nonlinear least squares (FFT-NLLS) algorithm. Options *Phases by Fit, zero* and *circadian* were enabled during the process. For phase and amplitude analysis: values were reported using a phase by fit method: one cosine function having period matching the estimated data period is fitted to the data. The fitting procedure finds phase and amplitude parameters of the cosine that follow the data the most closely and reports those values as phase and amplitude. Phase was reported relative to zero (as data are periodic and phase has been estimated, it is possible to back-calculate the data to zero). Phase was reported in circadian units (the circadian unit is 1/24 of the free running period, and it allows comparison of peaking times independently of the period).

5.2.3 ATP viability assay

To assess cell viability after treatment with CCM, an ATP viability assay (CellTiter-Glo; Promega, G7570) was carried out on peritoneal macrophages after the 5 days of luminometry recording according to manufacturer's instructions. In brief, the addition of a homogenous reagent induces cell lysis and generation of luminescent signal proportional to the amount of ATP present, which signals presence of metabolically active cells and is directly proportional to number of cells present in culture (Crouch et al., 1993).

5.2.4 RNA-seq

BMDMs were prepared as described in Chapter 2. Cells were treated for 6 hours with one of four conditions: vehicle control (0.1% DMSO), 100 nM LPS, 100 μM CCM and 100 nM LPS/100 μM CCM. Following treatment, cells were lysed for RNA extraction and processed for RNA-seq as described in the general methods.

Due to sample availability, there were 3 biological replicates for WT compared to 5 for KO. The imbalanced design (WT n=3, KO n=5) creates differential statistical power that complicates direct cross-genotype comparisons. I therefore analysed genotypes separately and defined BMAL1-dependent genes conservatively: significant in WT (despite lower n) AND non-significant in KO (despite higher n). This approach minimises false positives from the power asymmetry, though it may underestimate the true number of BMAL1-dependent effects. Genes were identified to be regulated by CCM in the basal state by comparing CCM to vehicle alone, and to be CCM-responsive in an inflammatory state by comparing CCM+LPS to LPS alone.

5.2.5 Downstream analyses for RNA-seq

5.2.5.1 Epigenetic Landscape In Silico Deletion Analysis

To identify potential upstream TFs responsible for the observed gene expression changes, the Lisa (v2) web server was used (Qin et al., 2020). The analysis was performed using a single gene set of interest, in which genes were previously identified as being repressed by CCM and LPS in a BMAL1-dependent manner. The analysis was set to the Mus musculus (mm10) genome build. The default Lisa sampling of 3000 background genes was used for statistical comparison. Lisa evaluates potential regulators using two complementary methods, both of which were used in this analysis: CistromeDB TF ChIP-seq Analysis: This method ranks TFs based on the enrichment of their binding sites, as determined by public TF ChIP-seq experiments in the CistromeDB, near the transcription start sites (TSS) of the input gene set. The model integrates the regulatory potential (RP) of TF binding peaks with the in-silico deletion effect of those peaks on chromatin accessibility (DNase-seq) and active enhancer (H3K27ac) signals. Cistrome Motif Analysis: This method identifies enriched TF motifs in the regulatory regions of the input genes. It then ranks TFs by modelling the effect of in-silico deleting (knocking out) these motif sites on local DNase-seq and H3K27ac signals. The ranked lists of TFs from both the CistromeDB ChIP-seq analysis and the Cistrome motif analysis were extracted. The top-ranked TFs from these lists were reported as the most probable transcriptional regulators for the gene set.

5.2.6 Morphology

Cell preparation and fixation: BMDMs were prepared as described in Chapter 2. BMDMs were seeded on glass coverslips in 24-well plates and treated for 6 or 24 hours with vehicle (0.1% DMSO), 100 μM CCM, 100 nM LPS, or 100 nM LPS + 100 μM CCM (n=3 biological

replicates for 6-hour treatment, n=2 for 24-hour treatment). Following treatment, media was removed, cells were washed once with PBS and fixed with 4% paraformaldehyde (400 μL/well) for 15 minutes at room temperature. Cells were washed twice with PBS and could be stored in PBS at 4°C until staining.

Immunofluorescence staining: Fixed cells were permeabilised with 0.1% Tween-20 in PBS (500 μL/well) for 10 minutes at room temperature, then washed twice with PBS. F-actin was labelled with Alexa Fluor 488-conjugated phalloidin (1:1000 in 1% BSA; 500 μL/well) for 2 hours at room temperature in the dark. Following three PBS washes, nuclei were counterstained with DAPI (1:100 in PBS; 500 μL/well) for 10 minutes at room temperature in the dark, then washed three times with PBS. Coverslips were mounted cell-side down on glass slides using 50 μL mounting medium, allowed to cure for 1–2 hours in the dark, and stored at 4°C until imaging.

Image acquisition: Images were acquired on a Leica TCS SP8 confocal microscope using 405 nm (DAPI) and 488 nm (phalloidin) excitation wavelengths. Acquisition parameters were: 16-bit depth, 1024 x 1024 format, 1x zoom. To minimise sampling bias, four fields of view were captured per condition (one per quadrant of each coverslip). Z-stacks were acquired for every other 2D image to enable cell height quantification. Laser intensity and detector gain were maintained constant across all images to ensure comparable fluorescence intensities.

Analysis: Cell area and height were quantified in ImageJ (version 1.54p). Cell boundaries were manually outlined from phalloidin-stained images to measure cross-sectional area. Cell height was determined from Z-stack projections by identifying the uppermost and lowermost planes where cell signal was visible.

5.2.7 Motility

BMDMs were prepared as described in Chapter 2. BMDMs were treated for 24 hours with vehicle (0.1% DMSO), 100 μM CCM, 100 nM LPS, or 100 nM LPS + 100 μM CCM, then harvested and replated at 5 x 10^4 cells/well in 96-well plates. Due to equipment limitations restricting simultaneous multi-well recording, only wild-type BMDMs were analysed. To enable visualisation, cells were labelled with a lipophilic carbocyanine membrane dye: 5 μL of BioTracker 490 (Sigma-Aldrich SCT106) was added to each 1 ml of media, incubation period of 20 minutes at 37°C, followed by two washes with warm media).

Time-lapse imaging was performed using a Nikon Eclipse Ti inverted microscope with environmental control (37°C, 5% CO2). Images were captured every 3 seconds for 1 hour (1,200 frames per well). Cell tracking was performed using the TrackMate plugin (v2.1.0 in ImageJ, analysing only cells that remained within the field of view for the entire recording period.

5.2.8 Phagocytosis assay

BMDM preparation: Cryopreserved bone marrow cells were thawed, washed in DMEM, and resuspended in differentiation medium (DMEM supplemented with 10% FBS, 10% L929-conditioned medium, and 1% penicillin/streptomycin). L929-conditioned medium was used as a source of M-CSF for macrophage differentiation. Cells (1 mL suspension) were plated in 10 cm Petri dishes containing 7 mL differentiation medium and incubated at 37°C, 5% CO2. On day 5, cells were fed by removing 3 mL medium and adding 5 mL fresh differentiation medium. On day 6, non-adherent cells were removed by aspiration, and adherent macrophages were harvested by scraping in PBS, pelleted by centrifugation, and resuspended in complete DMEM (DMEM + 10% FBS). Cells were counted, adjusted to 5 x 10^5 cells/mL, and seeded

at 1 x 10^5 cells/well (200 μL/well) in 96-well plates. Cells were incubated overnight to allow adherence.

Bacterial preparation: *Escherichia coli* strain DH5α was streaked on LB agar plates on day 5 of BMDM differentiation. A single colony was inoculated into liquid LB medium and grown overnight at 37°C with shaking (180 rpm). On the day of infection, mid-log phase bacteria were prepared by diluting overnight culture 1:50 in fresh LB medium and incubating for 2 hours 15 minutes at 37°C, 180 rpm. Bacterial density was estimated by measuring OD600, and inocula were prepared at a multiplicity of infection (MOI) of 20 in complete DMEM containing either 100 μM CCM or 0.1% DMSO vehicle control.

Infection and quantification: Macrophages were washed once with PBS, then 200 μL bacterial inoculum was added per well. Bacteria were centrifuged onto cells (200 x G, 4 minutes) and co-incubated for 1 hour at 37°C. Aliquots of each inoculum were serially diluted (neat to 1:15,625 in 5-fold steps) and plated on LB agar as input controls. Following infection, cells were washed three times with PBS and incubated with complete DMEM containing 100 μg/mL gentamicin for 30 minutes to kill extracellular bacteria. Cells were washed three times with PBS, then lysed with 1% saponin for 10 minutes. Lysates were serially diluted in LB (neat to 1:625 in 5-fold steps) and plated on LB agar in duplicate. Plates were incubated overnight at 37°C, and colony-forming units (CFU) were enumerated the following day.

Data analysis: CFU counts were performed on the lowest dilution that yielded reliably countable colonies. Technical duplicate values were averaged and converted to CFU/mL in the original lysate. Data were normalised within each biological replicate as: (1) percentage of recovery relative to DMSO-treated cells, and (2) percentage of recovery relative to wild-type cells within each genotype. Data were analysed both as raw CFU values and following both normalisation

strategies.

5.2.9 Statistical analysis for morphology, motility, and phagocytosis

Data normality was assessed using the Shapiro-Wilk test. As the assumption of normality was violated ($p < 0.05$), differences between experimental groups were evaluated using the non-parametric Kruskal-Wallis test followed by Dunn's post-hoc test for pairwise comparisons. Statistical significance was set at $\alpha = 0.05$. All analyses were performed using GraphPad Prism (version 10.0.3).

5.3 Results

5.3.1 CCM alters circadian rhythm dynamics in peritoneal macrophages.

The target of CCM, BMAL1, is a core, non-redundant component of the circadian clock. I first investigated the effects of this compound on circadian parameters for measured bioluminescence in peritoneal macrophages. I isolated peritoneal macrophages from male and female PER2::Luc mice, treated them with varying concentrations of CCM, and monitored luminescence intensity over the course of 5 days to capture 4-5 circadian cycles to enable robust estimation of parameters amplitude, phase, and period (Figure 5.2).

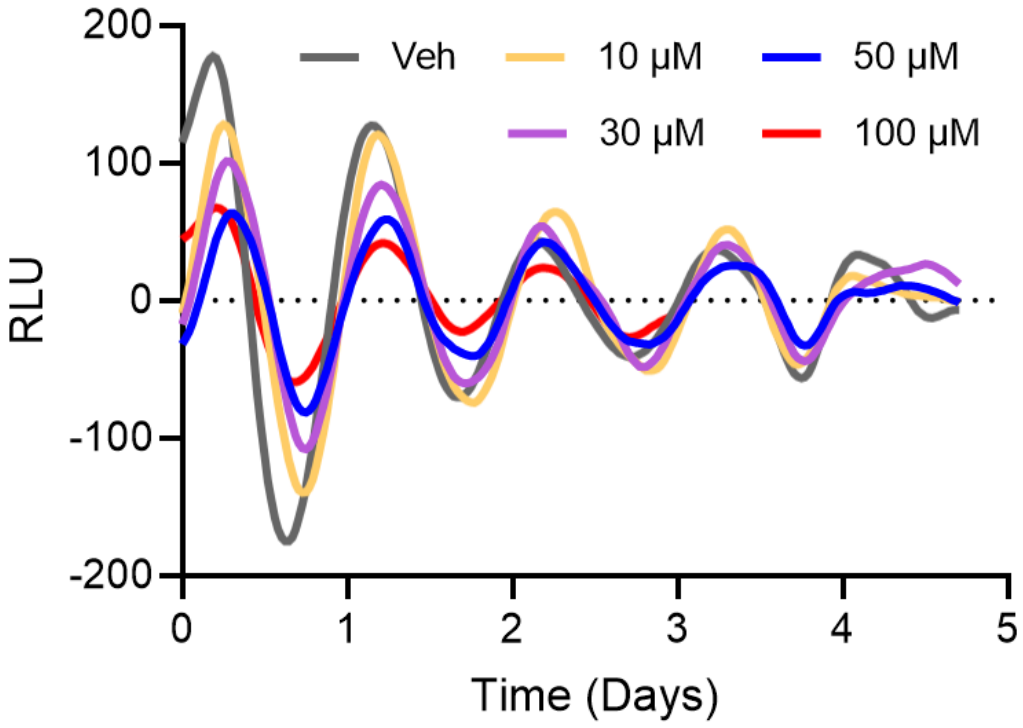

Figure 5.2: **Dose-dependent modulation of PER2 oscillations by CCM.**
Real-time luminometry traces from peritoneal macrophages isolated from male and female PER2::Luc mice and treated with vehicle or varying concentrations of CCM (10/30/50/100μM). Luminescence was recorded every half an hour for 4-5 days.$n = 3$–6 per concentration. Modified from (Pu et al., 2025).

CCM significantly dampened oscillation amplitude in a dose-dependent manner (Figure 5.2). In a linear mixed-effects model with concentration as a factor (0 μM vehicle, concentrations 10/30/50/100 μM CCM) and replicate as a random intercept, the omnibus test for concentration was significant (p = 0.0009) (Figure 5.3(a)). Relative to vehicle, amplitude was lower at 50 μM (Dunnett-adjusted p = 0.0048) and 100 μM (Dunnett-adjusted p = 0.0037). Viability remained unaffected, with no evidence of a concentration effect (mixed-effects p = 0.4504) (Figure 5.3(d)). Period was reduced by CCM (mixed-effects p = 0.0008); vs vehicle (100 μM Dunnett-adjusted p = 0.0003) (Figure 5.3(b)). There was a marked phase delay (mean = 1.8 h at 100 μM; mixed-effects p < 0.0001) (Figure 5.3(c)). The pairwise comparison of each concentration with vehicle was significant: 10 μM (p = 0.0641), 30/50/100 μM < 0.0001 (Dunnett-adjusted). These findings demonstrate that CCM alters circadian dynamics in macrophages, supporting its activity as a BMAL1-targeting compound.

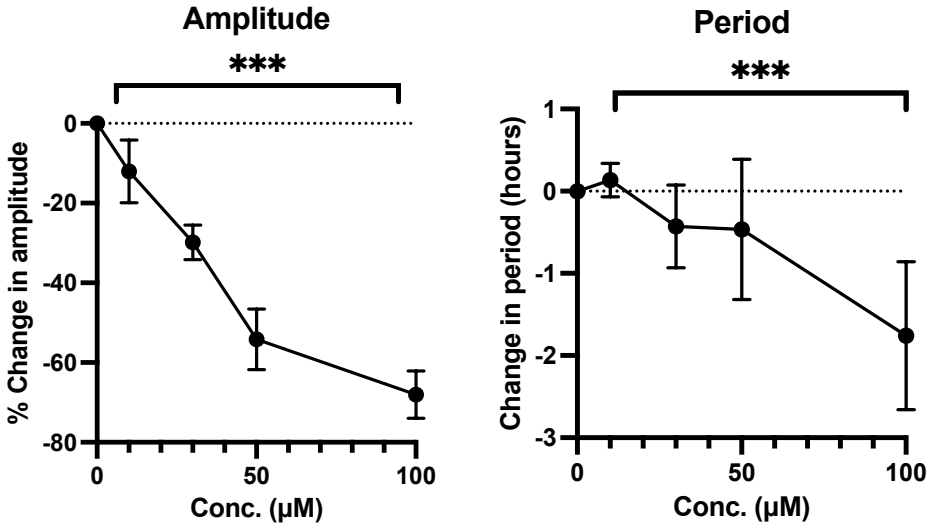

(a) Percentage change in amplitude

(b) Change in period (hours)

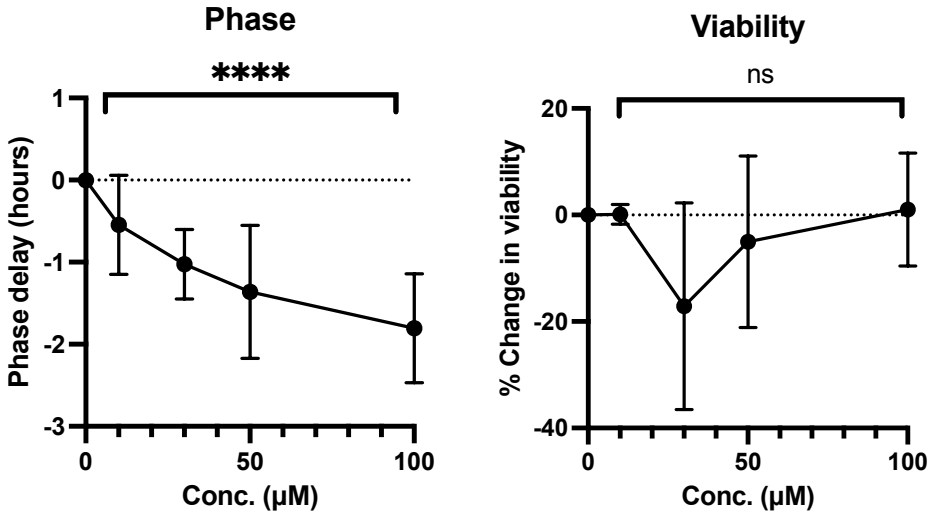

(c) Phase delay (hours)

(d) Percentage change in viability

Figure 5.3: **CCM significantly reduced amplitude of PER2 oscillations in a dose-dependent manner.**
Analysis of real-time luminometry traces from peritoneal macrophages isolated from PER2::Luc mice and treated with vehicle or varying concentrations of CCM (10/30/50/100 μM). Luminescence was recorded every 30 minutes for 4-5 days. Panels: (a) amplitude change, (b) period change, (c) phase delay, (d) viability change. For each independent experiment, three wells per condition were measured. Parameters were computed per well and averaged; data represent $n = 3$–6 independent experiments per concentration, pooled from male and female mice. Mixed-effects ANOVA with Dunnett multiple comparisons to vehicle control. * $p < 0.05$, ** $p < 0.01$, *** $p < 0.001$, **** $p < 0.0001$, ns $p > 0.05$. Modified from (Pu et al., 2025).

5.3.2 CCM promotes anti-inflammatory gene expression profiles in BMDMs.

The amplitude dampening and phase delay caused by CCM suggests altered BMAL1 activity. To investigate how CCM might be modulating BMAL1 to create these altered rhythm dynamics and any changes in BMAL1-regulated genes, I used a myeloid-cell specific BMAL1-knockout model. This allowed the separation of the BMAL1-dependent component of CCM's transcriptional effects from BMAL1-independent actions.

To capture the net transcriptional consequences of the altered BMAL1-activity, I performed RNA-seq on unsynchronised BMDMs after 6 hours of CCM treatment. As the effects of CCM on macrophage transcription were unknown, unsynchronised cultures were used to capture major BMAL1-dependent effects independent of circadian phase, while the 6-hour timepoint provides sensitivity to both primary and secondary transcriptional responses. BMDMs were chosen as BMAL1's transcriptional effects are well characterised in this model, particularly in inflammation (Curtis et al., 2015).

Cells were treated with 100 μM CCM, the highest concentration showing pronounced effects while maintaining viability (Figure 5.3). Transcriptional effects were assessed in basal state (CCM versus vehicle) and LPS-stimulated conditions (CCM + LPS versus LPS alone) (Figure 5.4).

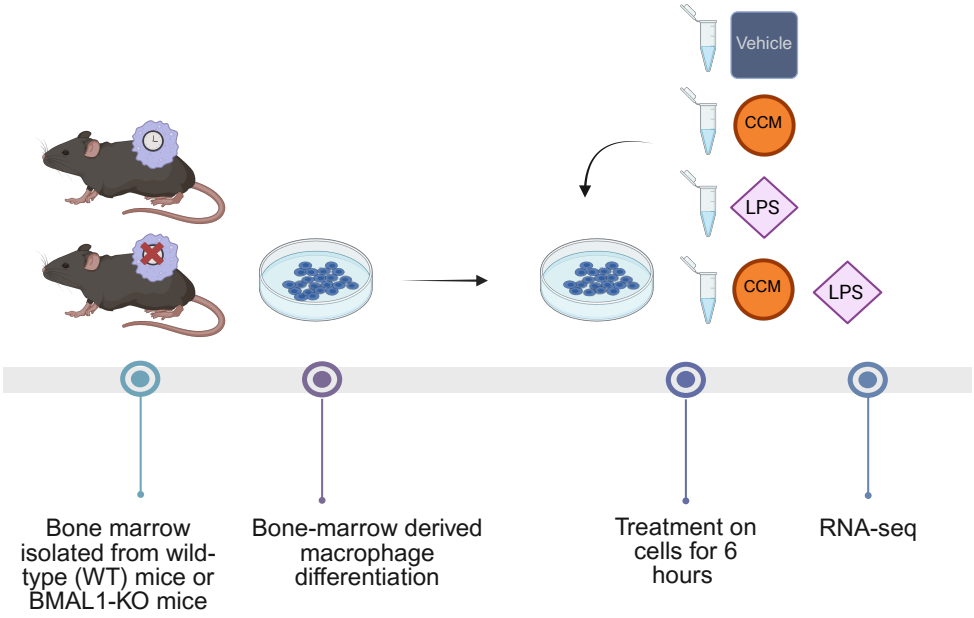

Figure 5.4: **Design of experiment testing effects of CCM on BMDM gene expression.** BMDMs from WT and myeloid specific BMAL1-KO female mice were prepared as described in Chapter 2. Unsynchronised BMDM cells were treated for 6 hours with one of four conditions: vehicle control (0.1% DMSO), 100 nM LPS, 100 μM CCM and 100 nM LPS + 100 μM CCM. Following treatment, cells were lysed for RNA extraction and processed for RNA-seq. Due to sample availability, there were 3 biological replicates for WT and 5 for BMAL1-KO. Created in https://BioRender.com

5.3.2.1 Effects of CCM in basal state macrophages.

I first examined the global transcriptional landscape to identify CCM-responsive genes, then dissected which effects require intact BMAL1. Genes were identified to be regulated by CCM in the basal state by comparing CCM to vehicle alone. Effects of CCM in the basal state were modest: 167 genes were upregulated and 140 downregulated (Figure 5.5). Core clock components (*Clock, Per1/2/3, Cry1/2, Nr1d1/2, Dbp, Tef*) showed no significant changes with CCM treatment under basal conditions.

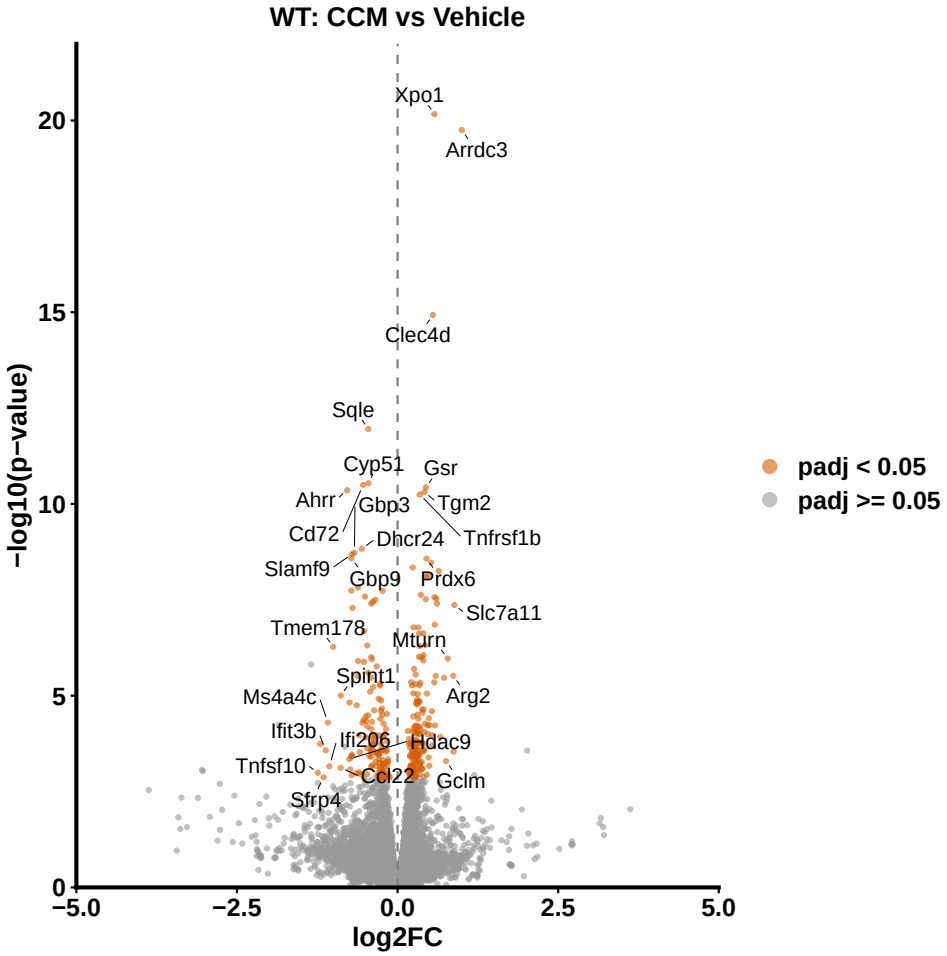

Figure 5.5: **The genes perturbed by CCM in the basal state show modest effect sizes.** BMDMs from WT female mice ($n = 3$ were treated for 6 hours with one of four conditions: vehicle control (0.1% DMSO), 100 nM LPS, 100 μM CCM and 100 nM LPS + 100 μM CCM. DEGs for the CCM vs vehicle contrast were identified using DESeq2, at BH-adjusted < 0.05. The top-ranked DEGs (by Wald statistic) are labelled.

Amongst the top hits by fold-change and p-value in the CCM-responsive upregulated genes

in the basal state are regulators of inflammation *Tnfaip2, Ikbkg* (modulates NFkB activity by mediating degradation of inhibitor complexes), *Arg2* (arginase-2, regulates NOS via arginine bioavailability), and recognition of PAMPs (TLRs *Tlr7* and *Tlr8*, and C-type lectins, *Clec4d* and *Clec4n*). Also upregulated are the divalent metal ion transporter *Slc11a1* (regulates oxidative stress via ROS production, and so mediates defense against intracellular pathogens), *Slc7a11, Slc3a2, Slc36a1* (amino acid transporters), and lipid metabolic gene *Sgms2* (sphingomyelinsynthase).

CCM downregulated genes in several coherent functional categories: cholesterol/sterol biosynthesis (*Hmgcs1, Lss, Idi1, Fdft1*), lipid metabolism (*Fasn, Fabp3*), cytoskeletal organisation (*Actb, Actg1, Actr2/3*, multiple tubulins), and inflammatory mediators (*Ccl2, Tlr1, Ptgs1*). Notably, *Ccl2* has previously been shown to be upregulated in genetic BMAL1-deletion models (K. D. Nguyen et al., 2013), and the interferon-responsive guanylate-binding proteins (*Gbp2/3/7/9*) downregulated here were among genes elevated at ZT12 in Chapter 3.

To ask which pathways are enriched in CCM-regulated genes in basal state, I performed GO enrichment analysis separately for the genes upregulated and downregulated by CCM, using a background of the CCM vs Vehicle contrast. Upregulated genes were enriched for signal transduction, cholesterol transport, and development/angiogenesis (Figure 5.6).

Downregulated genes were enriched for cholesterol biosynthesis, phagocytosis, actin cytoskeleton organisation, and interferon response (Figure 5.7).

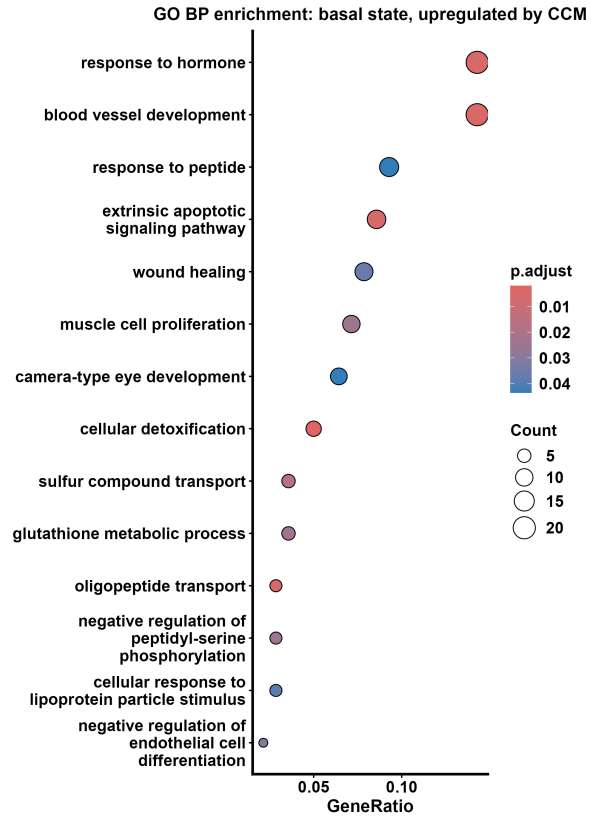
GO BP enrichment: basal state, upregulated by CCM
response to hormone
blood vessel development
response to peptide
extrinsic apoptotic signaling pathway
wound healing
muscle cell proliferation
camera-type eye development
cellular detoxification
sulfur compound transport
glutathione metabolic process
oligopeptide transport
negative regulation of peptidyl-serine phosphorylation
cellular response to lipoprotein particle stimulus
negative regulation of endothelial cell differentiation
p.adjust
0.01
0.02
0.03
0.04
Count
5
10
15
20
0.05
0.10
GeneRatio

(a)

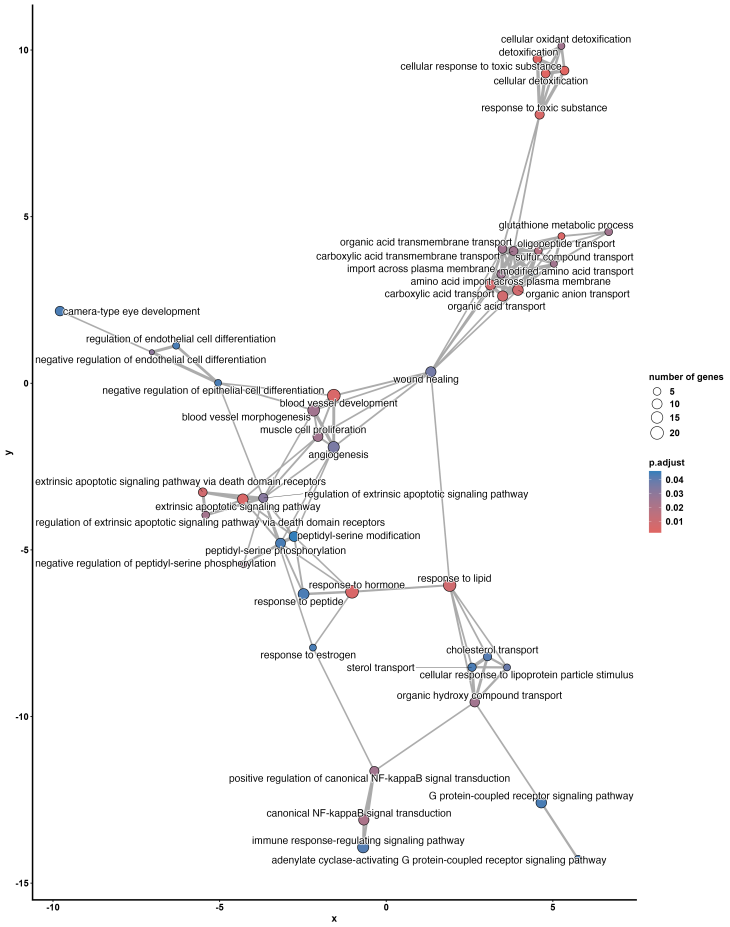
cellular oxidant detoxification
detoxification
cellular response to toxic substance
cellular detoxification
response to toxic substance
glutathione metabolic process
organic acid transmembrane transport
oligopeptide transport
carboxylic acid transmembrane transport
sulfur compound transport
import across plasma membrane
neutral amino acid transport
amino acid import across plasma membrane
carboxylic acid transport
organic anion transport
organic acid transport
camera-type eye development
regulation of endothelial cell differentiation
negative regulation of endothelial cell differentiation
wound healing
negative regulation of epithelial cell differentiation
blood vessel development
blood vessel morphogenesis
muscle cell proliferation
angiogenesis
extrinsic apoptotic signaling pathway via death domain receptors
regulation of extrinsic apoptotic signaling pathway
extrinsic apoptotic signaling pathway
regulation of extrinsic apoptotic signaling pathway via death domain receptors
peptidyl-serine modification
peptidyl-serine phosphorylation
negative regulation of peptidyl-serine phosphorylation
response to lipid
response to hormone
response to peptide
response to estrogen
cholesterol transport
sterol transport
cellular response to lipoprotein particle stimulus
organic hydroxy compound transport
positive regulation of canonical NF-kappaB signal transduction
G protein-coupled receptor signaling pathway
canonical NF-kappaB signal transduction
immune response-regulating signaling pathway
adenylate cyclase-activating G protein-coupled receptor signaling pathway
number of genes
5
10
15
20
p.adjust
0.04
0.03
0.02
0.01
y
x
10
5
0
-5
-10
-15
-10
-5
0
5

(b)

Figure 5.6: **CCM upregulates transport and signalling pathways in WT macrophages.** GO Biological Process over-representation analysis for genes upregulated by CCM treatment (CCM vs vehicle) in WT female BMDMs ($n = 3$). DEGs were identified using DESeq2 at BH-adjusted < 0.05. GO analysis was performed using clusterProfiler with hypergeometric testing against all genes with valid statistical tests. Enriched terms were simplified to remove redundancy (similarity cutoff = 0.5). (a) Dotplot showing top enriched terms; dot size indicates gene count, colour indicates adjusted p-value. (b) Enrichment map showing network of enriched pathways; edges connect gene sets with overlapping members, forming functionally related clusters.

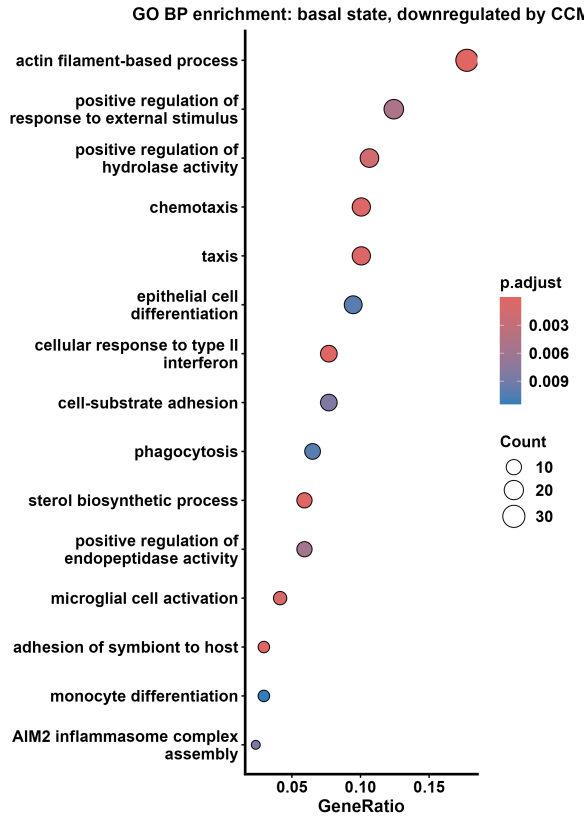

(a)

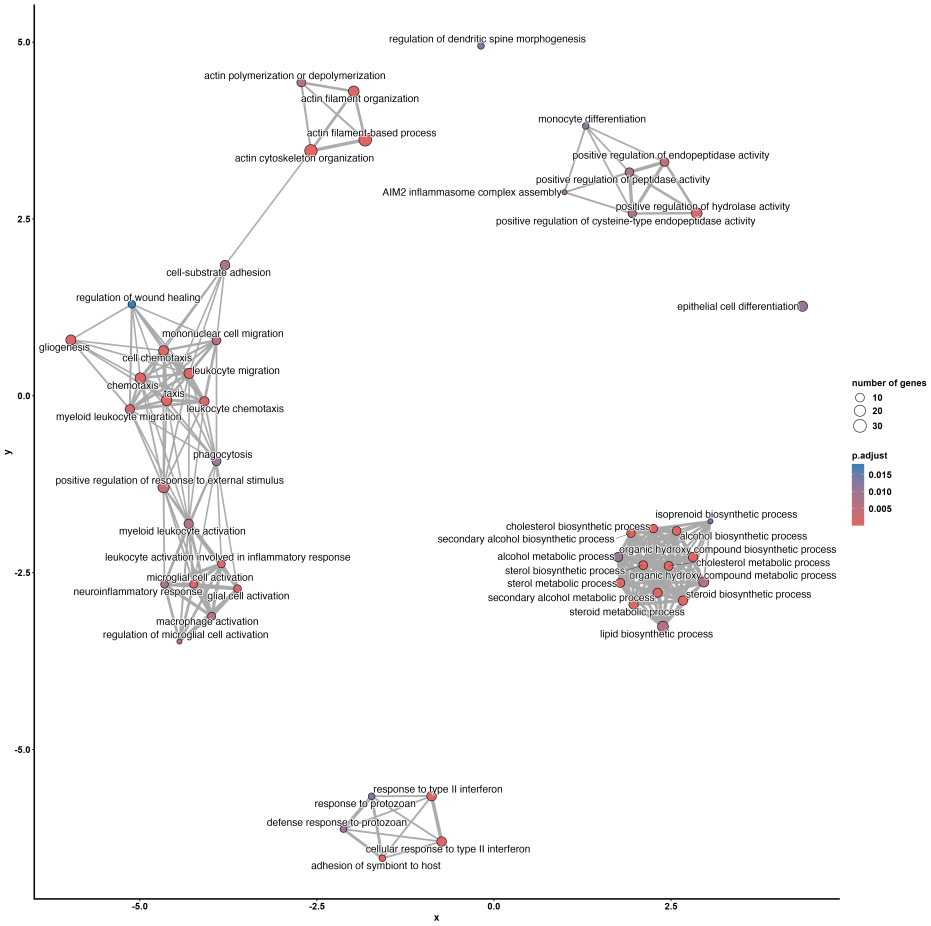

(b)

Figure 5.7: **CCM downregulates cytoskeletal organisation, and inflammatory response pathways.**
GO Biological Process over-representation analysis for genes downregulated by CCM treatment (CCM vs vehicle) in WT female BMDMs ($n = 3$). DEGs were identified using DESeq2 at BH-adjusted < 0.05. GO analysis was performed using clusterProfiler with hypergeometric testing against all genes with valid statistical tests. Enriched terms were simplified to remove redundancy (similarity cutoff = 0.5). (a) Dotplot showing top enriched terms; dot size indicates gene count, colour indicates adjusted p-value. (b) Enrichment map showing network of enriched pathways; edges connect gene sets with overlapping members, forming functionally related clusters.

5.3.2.2 BMAL1-dependency of CCM effects in basal state macrophages.

To determine which CCM effects are mediated specifically through BMAL1 versus potential off-target mechanisms, I contrasted CCM responses in WT against those in BMAL1-KO macrophages.

Genes were defined as BMAL1-dependent where they show significant differences in WT (padj < 0.05) and were not identified as significantly altered in the KO (padj ≥ 0.05). The gating approach (requiring significance in WT with lower power, and non-significance in KO with higher power) is conservative: BMAL1-dependent genes must show a CCM response in WT despite smaller sample size, while failing to show this response in KO despite greater statistical power. This minimises false positives resulting from the power asymmetry from the imbalanced design.

It should be noted that the BMAL1-KO shows incomplete penetrance: examination of RNA-seq coverage at the floxed locus showed that approximately one-third of WT-level *Bmal1* transcript remained detectable at exon 8 in the KO (Figure 5.8), consistent with the variable recombination efficiency reported for LysM-Cre (Clausen et al., 1999). This hypomorphic phenotype likely explains why some BMAL1-dependent effects are attenuated rather than abolished in BMAL1-KO macrophages.

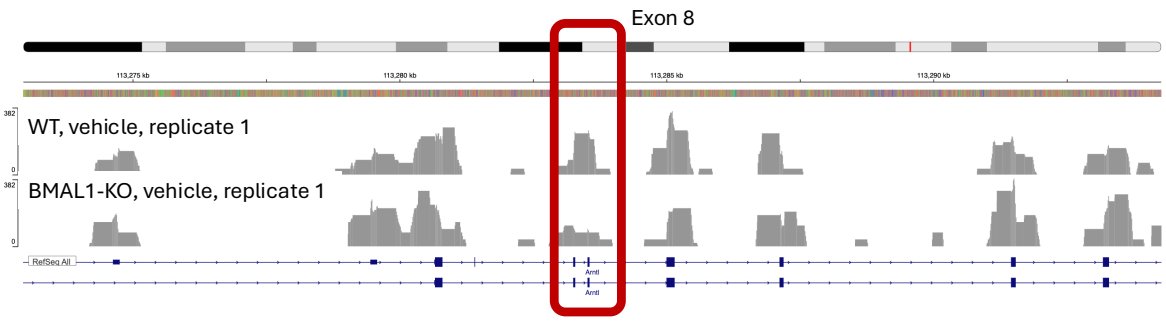

Figure 5.8: **Residual *Bmal1* expression at the floxed exon 8 confirms incomplete penetrance of the myeloid BMAL1-KO.** RPKM-normalised RNA-seq coverage across the *Arntl* (*Bmal1*) locus (mm10, chr7) in basal-state BMDMs treated with vehicle control from WT and myeloid-specific BMAL1-KO (*Bmal1*$^{fl/fl}$; LysM-Cre) female mice. Tracks were group-autoscaled to a shared data range (0–382) to permit direct comparison; one representative replicate per genotype is shown (WT $n = 3$, BMAL1-KO $n = 5$). The floxed exon 8 (encoding the bHLH DNA-binding domain; circled) shows markedly reduced coverage in the KO, while flanking exons remain comparable between genotypes, indicating locus-specific excision rather than global downregulation. Across replicates, mean coverage at exon 8 was reduced from 241 RPKM (WT) to 78 RPKM (BMAL1-KO), to approximately one-third of WT levels. Residual signal is consistent with incomplete LysM-Cre–mediated recombination.

Most CCM effects were BMAL1-dependent: 242 DEGs in WT-only, 65 shared between WT and BMAL1-KO, and 54 in BMAL1-KO only (Figure 5.9).

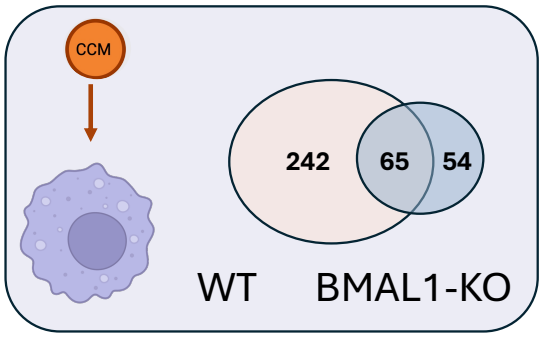

Figure 5.9: **Most CCM-effects are BMAL1-dependent in basal state macrophages.** BMDMs from WT and BMAL1-KO female mice were treated for 6 hours with one of four conditions: vehicle control (0.1% DMSO), 100 nM LPS, 100 μM CCM and 100 nM LPS + 100 μM CCM. DEGs for the CCM vs vehicle contrast were identified using DESeq2, at BH-adjusted < 0.05. The top-ranked DEGs (by Wald statistic) are labelled. (WT $= 3$, BMAL1-KO $= 5$). BMAL1-dependent CCM-effects were identified as WT-only CCM vs vehicle DEGs.

GO terms were consistent with the full WT basal results, indicating no significant variance from core programs in the BMAL1-KO (consistent with BMAL1-KO incomplete penetrance) (Figure 5.10). The top term was phagocytosis (GO:0006909, q-value = 0.011), driven by the

downregulation of *Pparg* and *Aif1*, and other terms present in the CCM-downregulated enrichment (response to type II interferon (GO:0034341, q-value = 0.02), actin filament organisation (GO:0007015, q-value = 0.02). Also included terms upregulated by CCM, angiongenesis (GO:0001525, q-value = 0.018), and wound healing (GO:0042060, q-value = 0.019).

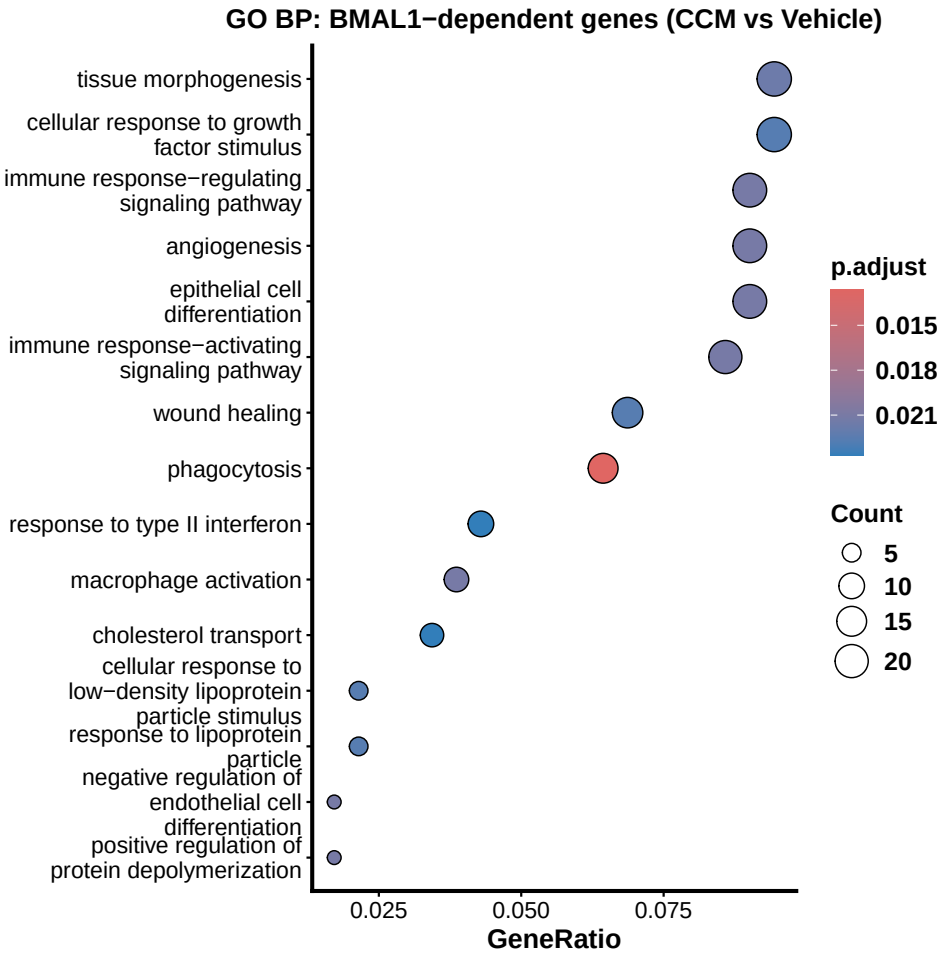

Figure 5.10: **BMAL1-dependent CCM effects in basal state macrophages relate to macrophage activation.**
BMDMs from WT and BMAL1-KO female mice were treated for 6 hours with one of four conditions: vehicle control (0.1% DMSO), 100 nM LPS, 100 μM CCM and 100 nM LPS + 100 μM CCM. DEGs for the CCM vs vehicle contrast were identified using DESeq2, at BH-adjusted < 0.05. The top-ranked DEGs (by Wald statistic) are labelled. (WT $= 3$, BMAL1-KO $= 5$). BMAL1-dependent CCM-effects were identified as WT-only CCM vs vehicle DEGs. GO over-representation analysis was performed using clusterProfiler with hypergeometric testing. Background gene universe comprised all genes with valid statistical tests (non-NA p-values) in the WT CCM vs vehicle contrast. BH FDR correction was applied (p-value < 0.05, q-value < 0.05). Enriched terms were simplified to remove redundancy (similarity cutoff = 0.5), retaining the most significant term per cluster.

To identify upstream regulators of CCM-responsive genes, I inferred TF activity using decou-

pleR with CollecTRI regulons. TF activity inference identified several regulators with significantly altered activity following CCM treatment (Figure 5.11). CCM increased activity of NFE2L2/NRF2 (padj = 9.4e7), PPARD (padj = 0.034), and ELK3 (padj = 0.047). CCM decreased activity of SRF (padj = 0.002), ZFP202 (padj = 0.008), E2F3 (padj = 0.047), and SPI1 (padj = 0.047). The reduced SRF activity is consistent with the observed downregulation of cytoskeletal genes, as SRF is a master regulator of actin-cytoskeletal transcription. NFKB1 activity was downregulated (padj = 0.052).

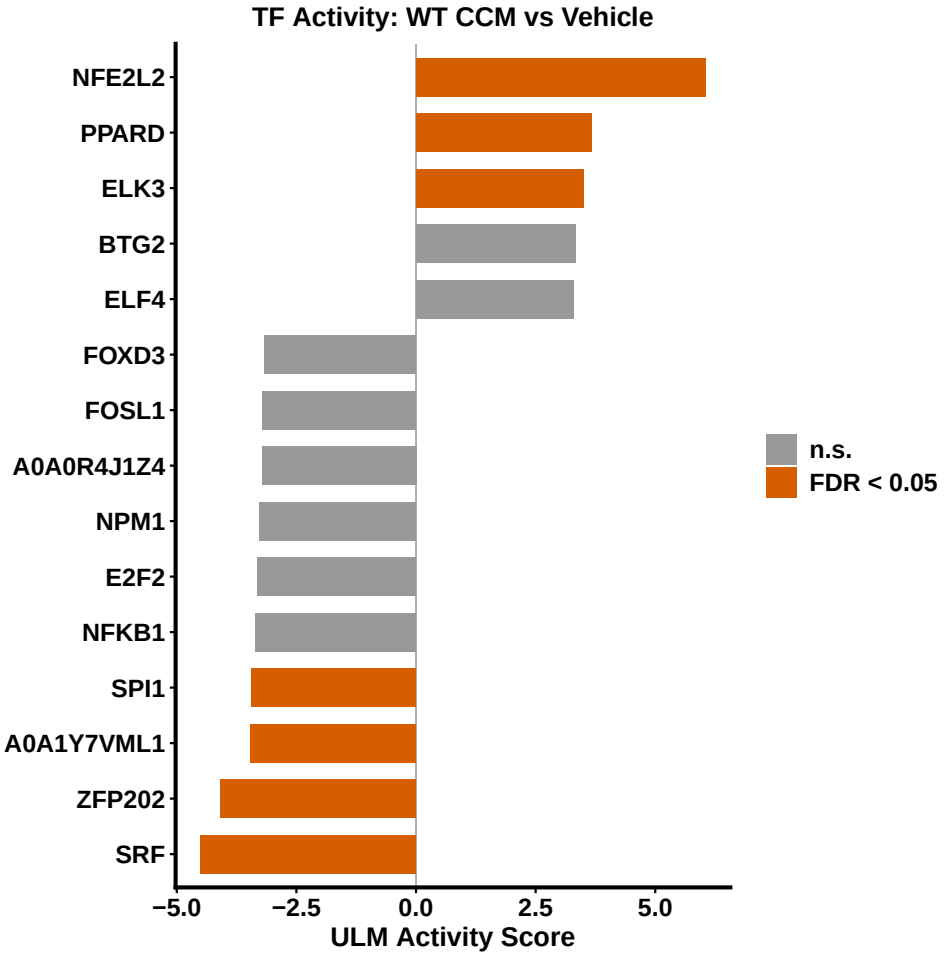

Figure 5.11: **The effect of CCM on transcription factor activity in basal state macrophages.** TF activity inference results for the CCM vs vehicle contrast in WT female BMDMs treated for 6 hours (n = 3). TF activity was inferred by inputting CCM vs vehicle Wald statistics into decoupleR with CollecTRI regulons. Positive scores indicate TF activation by CCM treatment. TFs with significant activity (FDR < 0.05) are highlighted in orange; non-significant factors are shown in grey.

I inferred which signalling pathways are affected by CCM with decoupleR using PROGENy's

multivariate linear model (MLM). The pathways EGFR (padj = 5.9e-12), JAK-STAT (padj = 7.9 e-7), estrogen (padj = 6.0e-4), TRAIL (padj = 0.0016) were less active with CCM treatment in the basal state (Figure 5.12). CCM increased the activity of both the p53 (padj = 2.0e-4) and VEGF (padj = 0.0087) pathways.

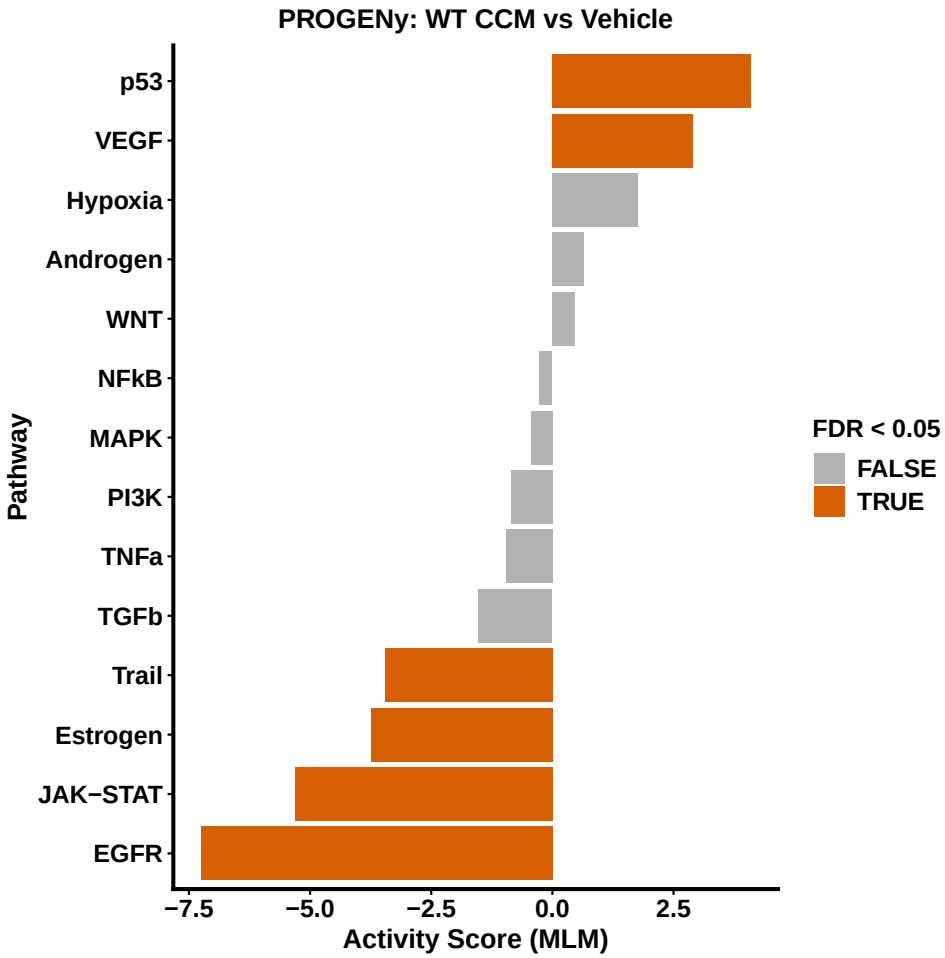

Figure 5.12: **The effect of CCM on pathway activity in basal state macrophages.** Pathway activity enrichment scores were inferred using decoupleR with PROGENy's multivariate linear model. Wald statistics for the CCM vs vehicle contrast in WT female BMDMs treated for 6 hours (n = 3) served as input to score activity across 14 pathways. Positive scores indicate pathway activation with CCM relative to vehicle; negative scores indicate decreased pathway activity with CCM. Pathways with significant activity (FDR < 0.05) are highlighted in orange; non-significant pathways are shown in gray.

Overall, despite modest effect sizes, CCM induces coordinated effects on coherent functional programs in the basal state, which include NRF2-mediated anti-inflammatory effects and effects on cholesterol metabolism.

5.3.2.3 Effects of CCM in LPS-stimulated macrophages.

Having characterised CCM effects in basal macrophages, I next examined whether CCM modulates the transcriptional response to inflammatory stimulation by comparing CCM/LPS co-treatment to LPS alone. Strikingly, under LPS-stimulation the effects of CCM are much greater than in basal state conditions, consisting of 566 upregulated and 1219 downregulated DEGs (Figure 5.13). Expression levels of core clock components (*Clock, Per1/2/3, Cry1/2, Nr1d1/2, Dbp, Tef*) showed no significant changes with CCM treatment under LPS-stimulated conditions.

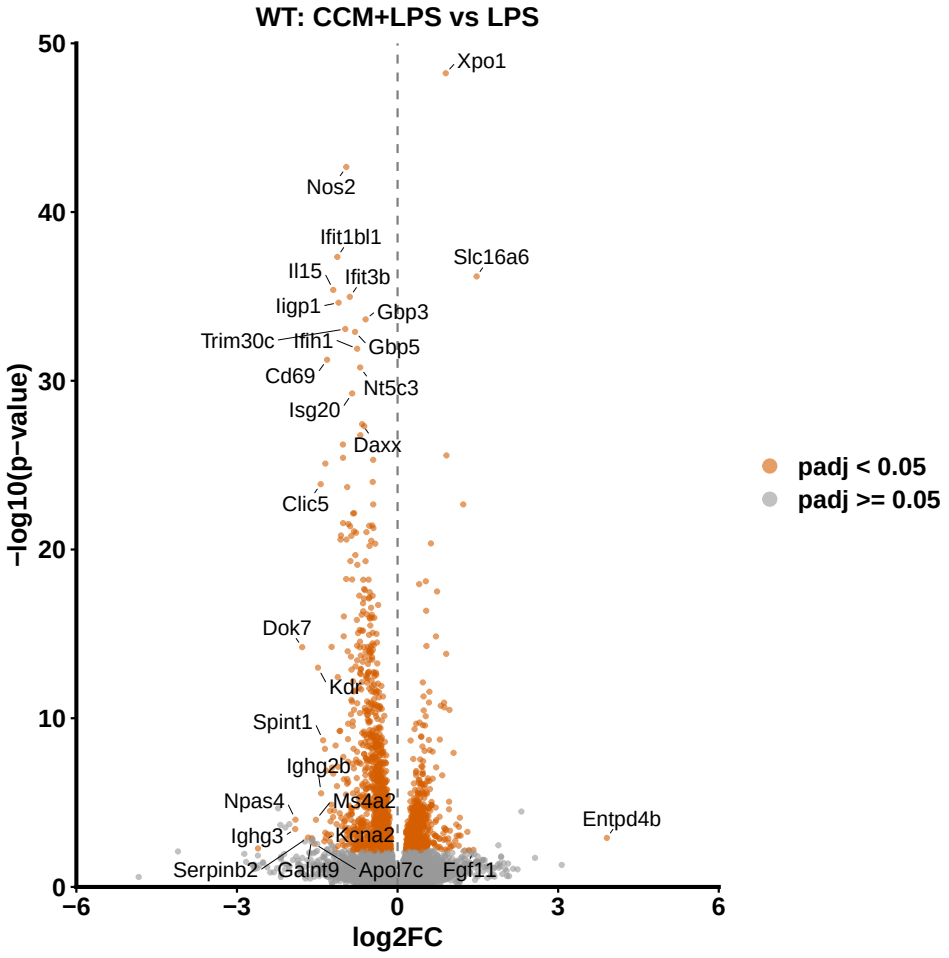

Figure 5.13: **The dominant effect of CCM is downregulation of gene expression in LPS-stimulated macrophages.**
BMDMs from WT female mice ($n = 3$ were treated for 6 hours with one of four conditions: vehicle control (0.1% DMSO), 100 nM LPS, 100 μM CCM and 100 nM LPS + 100 μM CCM. DEGs for the CCM + LPS vs LPS contrast were identified using DESeq2, at BH-adjusted < 0.05. The top-ranked DEGs (by Wald statistic) are labelled.

To ask whether the same pathways are enriched in CCM-regulated genes in LPS-stimulated macrophages compared to basal state, I performed GO enrichment analysis, splitting gene sets by direction of regulation by CCM. There were distinct functional programs: upregulated genes were enriched for endocytosis, metabolic processes, and cholesterol efflux (Figure 5.14).

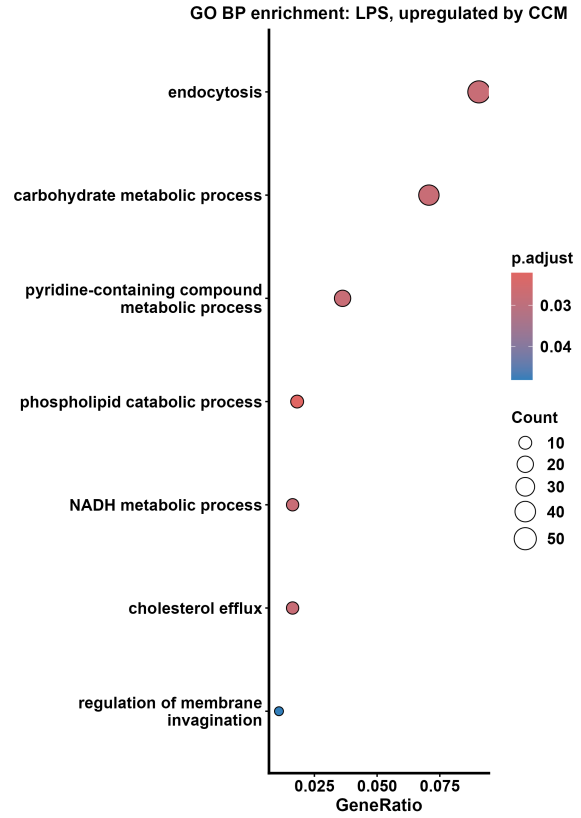
GO BP enrichment: LPS, upregulated by CCM
endocytosis
carbohydrate metabolic process
pyridine-containing compound metabolic process
phospholipid catabolic process
NADH metabolic process
cholesterol efflux
regulation of membrane invagination
0.025
0.050
0.075
GeneRatio
p.adjust
0.03
0.04
Count
10
20
30
40
50

(a)

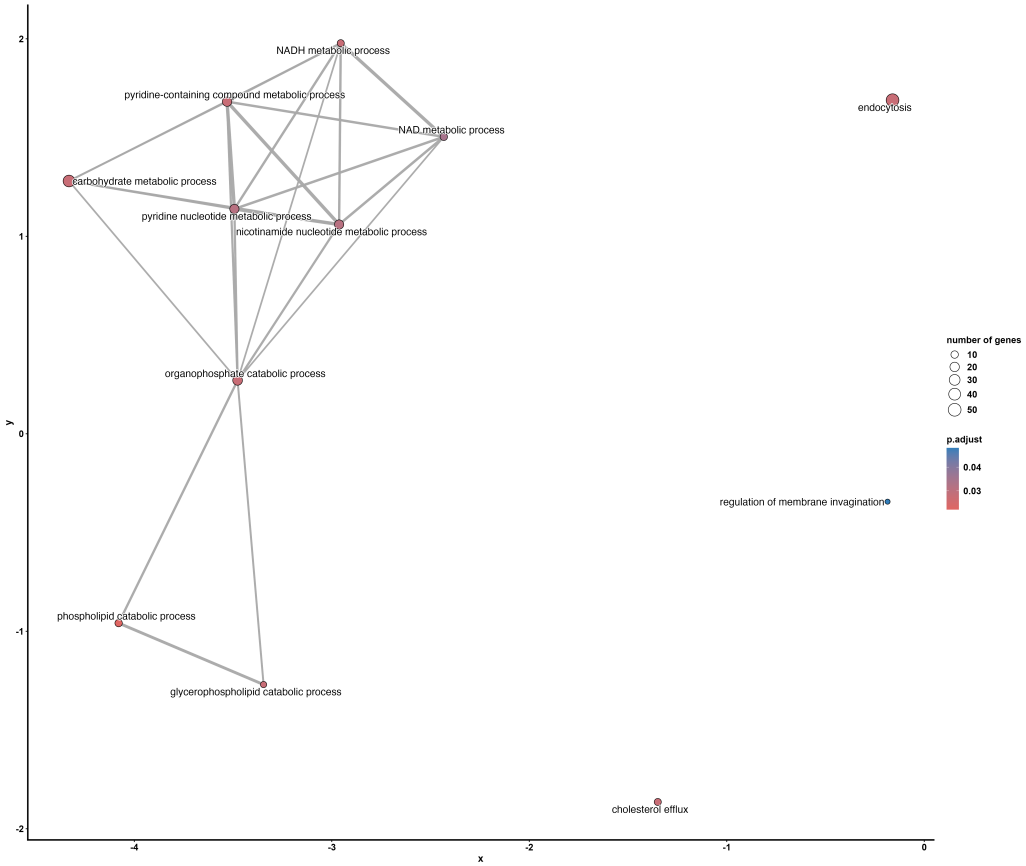
NADH metabolic process
pyridine-containing compound metabolic process
NAD metabolic process
carbohydrate metabolic process
pyridine nucleotide metabolic process
nicotinamide nucleotide metabolic process
organophosphate catabolic process
phospholipid catabolic process
glycerophospholipid catabolic process
endocytosis
regulation of membrane invagination
cholesterol efflux
x
y
number of genes
10
20
30
40
50
p.adjust
0.04
0.03

(b)

Figure 5.14: **CCM upregulates endocytosis and vesicle-mediated transport pathways in LPS-stimulated macrophages.**
GO Biological Process over-representation analysis for genes upregulated by CCM co-treatment (CCM+LPS vs LPS) in WT female BMDMs ($n = 3$). DEGs were identified using DESeq2 at BH-adjusted < 0.05. GO analysis was performed using clusterProfiler with hypergeometric testing against all genes with valid statistical tests. Enriched terms were simplified to remove redundancy (similarity cutoff = 0.5). (a) Dotplot showing top enriched terms; dot size indicates gene count, colour indicates adjusted p-value. (b) Enrichment map showing network of enriched pathways; edges connect gene sets with overlapping members, forming functionally related clusters.

Downregulated genes were enriched for pro-inflammatory response terms, including regulation of cytokine production and inflammasome-signalling (Figure 5.15).

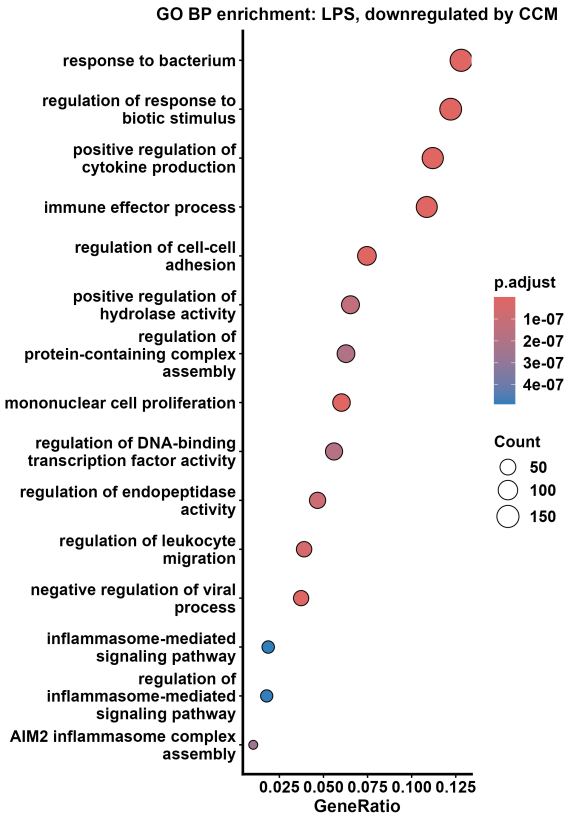

(a)

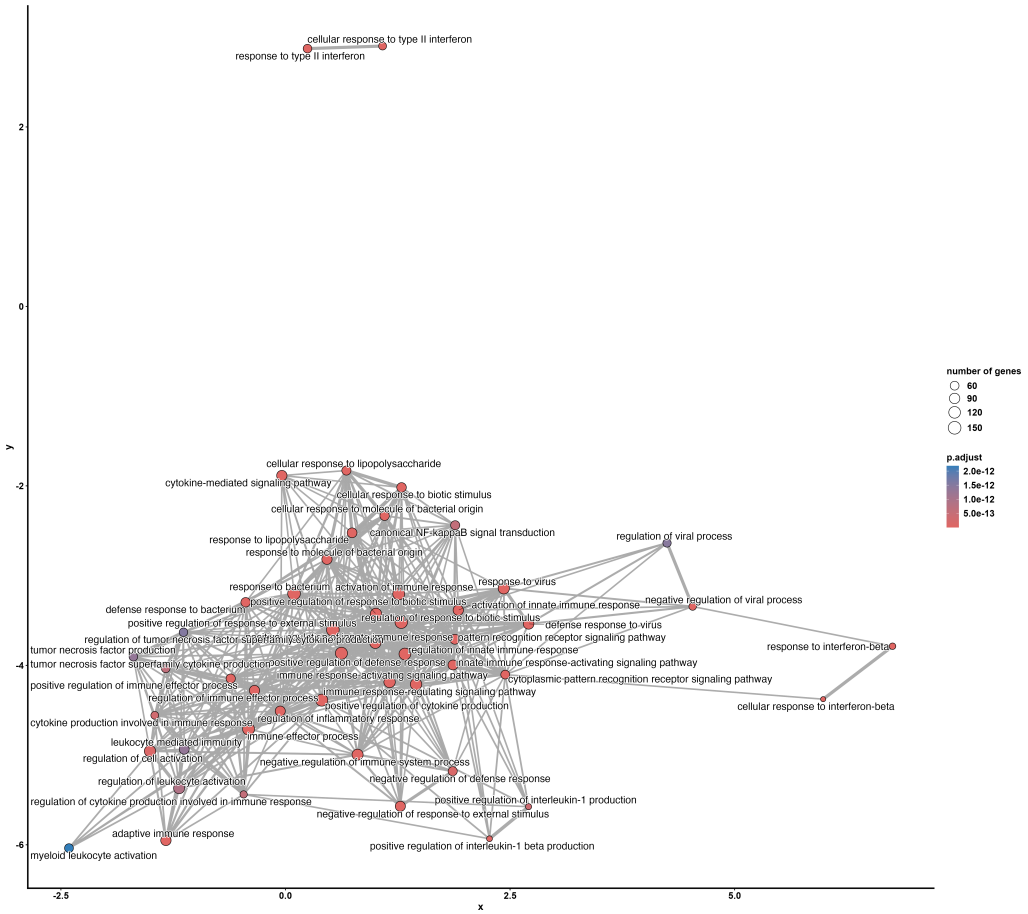

(b)

Figure 5.15: **CCM downregulates pro-inflammatory response pathways in LPS-stimulated macrophages.**
GO Biological Process over-representation analysis for genes downregulated by CCM co-treatment (CCM+LPS vs LPS) in WT female BMDMs ($n = 3$). DEGs were identified using DESeq2 at BH-adjusted < 0.05. GO analysis was performed using clusterProfiler with hypergeometric testing against all genes with valid statistical tests. Enriched terms were simplified to remove redundancy (similarity cutoff = 0.5). (a) Dotplot showing top enriched terms; dot size indicates gene count, colour indicates adjusted p-value. (b) Enrichment map showing network of enriched pathways; edges connect gene sets with overlapping members, forming functionally related clusters.

5.3.2.4 BMAL1-dependency of CCM effects in LPS-stimulated macrophages.

As in basal, unstimulated macrophages, I contrasted CCM responses in WT against those in BMAL1-KO macrophages, defining genes as BMAL1-dependent where they show significant differences in WT (padj < 0.05) and were not identified as significantly altered in the KO (padj $\geq$ 0.05). In LPS-stimulated macrophages, CCM perturbed the transcriptomes of both WT and BMAL1-KO cells (Figure 5.16). Despite reduced power in WT samples, 855 DEGs were identified as BMAL1-dependent (altered in WT-only). 884 DEGs were shared between WT and BMAL1-KO, and there were 784 DEGs in BMAL1-KO only. This is consistent with the observed incomplete penetrance noted above. Of the BMAL1-dependent effects, CCM upregulated 334 genes and downregulated 521 genes. Dividing the BMAL1-dependent CCM effects in LPS by direction of CCM-regulation, I performed GO enrichment analysis.

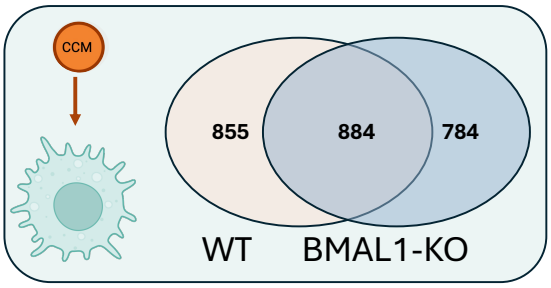

Figure 5.16: **A majority of CCM-effects are BMAL1-dependent in LPS-stimulated macrophages.**
BMDMs from WT and BMAL1-KO female mice were treated for 6 hours with one of four conditions: vehicle control (0.1% DMSO), 100 nM LPS, 100 μM CCM and 100 nM LPS/100 μM CCM. DEGs for the CCM/LPS vs LPS contrast were identified using DESeq2, at BH-adjusted < 0.05. The top-ranked DEGs (by Wald statistic) are labelled. (WT $= 3$, BMAL1-KO $= 5$). BMAL1-dependent CCM-effects were identified as WT-only CCM/LPS vs LPS DEGs.

The BMAL1-dependent CCM-mediated activation showed enrichment for GO terms cholesterol efflux (GO:0033344, q-value = 0.0017), membrane invagination (GO:0010324, q-value = 0.0081), positive regulation of autophagosome assembly (GO:2000786, q-value = 0.027), and development of primary female sexual characteristics (GO:0046545, q-value = 0.032) (Figure

5.17(a)). Genes driving these enrichments include *Pparg, Abca1/2/3, Pip4k2b/c, Foxo3, Ahr, Ptger4, Brca2*.

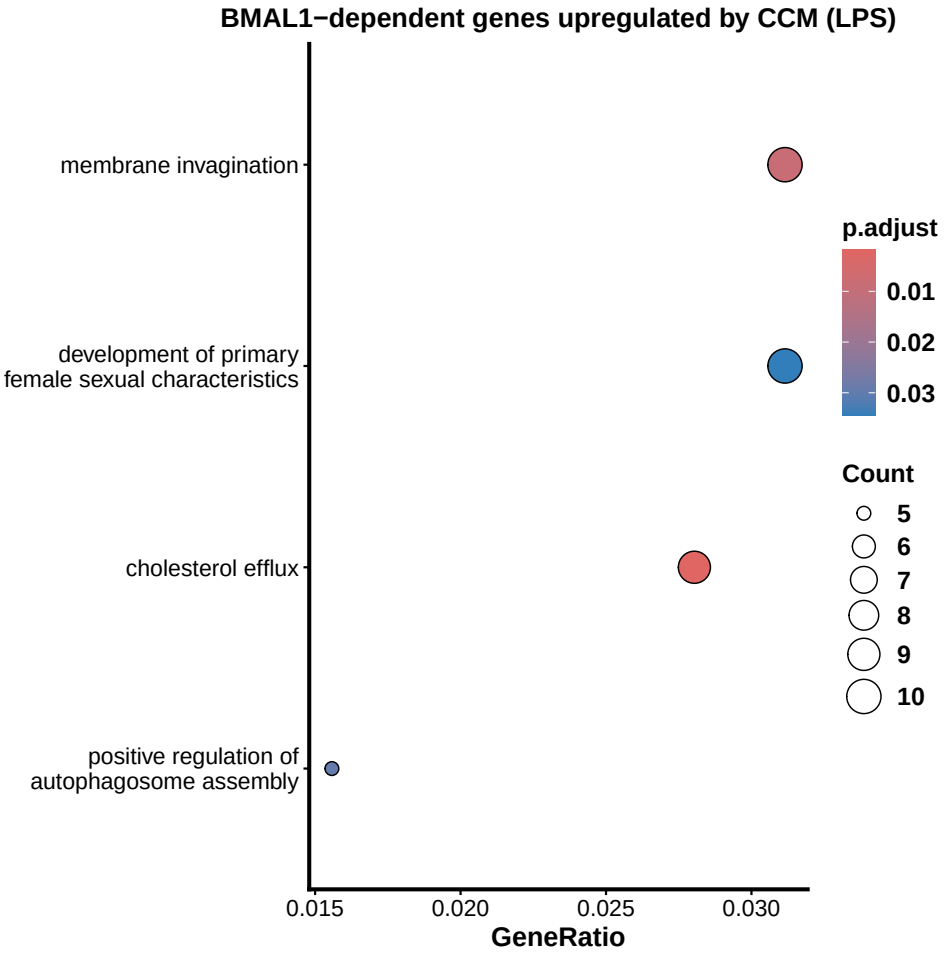

(a) Up-regulated

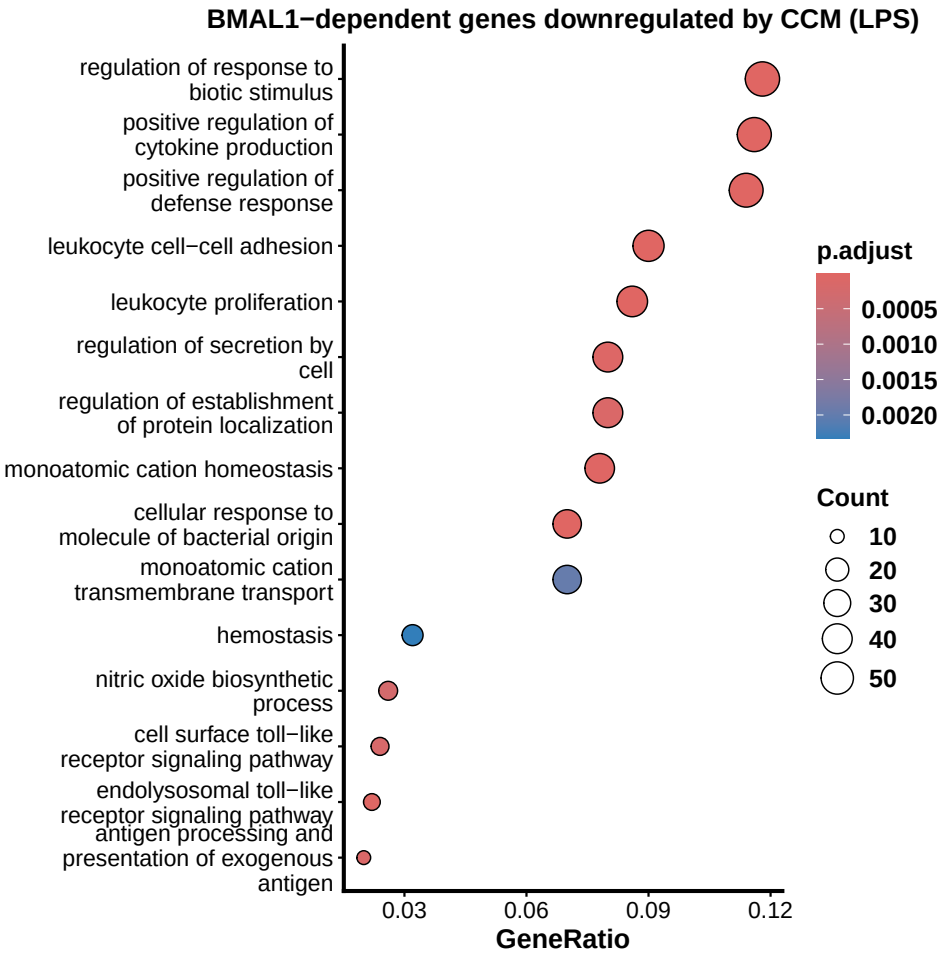

(b) Down-regulated

Figure 5.17: **In LPS-stimulated macrophages, BMAL1-dependent effects of CCM are to upregulate endocytosis pathways while downregulating pro-inflammatory response terms.** BMDMs from WT and BMAL1-KO female mice were treated for 6 hours with one of four conditions: vehicle control (0.1% DMSO), 100 nM LPS, 100 μM CCM and 100 nM LPS + 100 μM CCM. DEGs for the CCM/LPS vs LPS contrast were identified using DESeq2, at BH-adjusted < 0.05. The top-ranked DEGs (by Wald statistic) are labelled. (WT $= 3$, BMAL1-KO $= 5$). BMAL1-dependent CCM-effects were identified as WT-only CCM/LPS vs LPS DEGs. GO over-representation analysis was performed using clusterProfiler with hypergeometric testing. Background gene universe comprised all genes with valid statistical tests (non-NA p-values) in the WT CCM/LPS vs LPS contrast. BH FDR correction was applied (p-value < 0.05, q-value < 0.05). Enriched terms were simplified to remove redundancy (similarity cutoff = 0.5), retaining the most significant term per cluster.

The larger set of genes representing BMAL1-dependent CCM-mediated repression showed enrichment for more terms, dominated by pro-inflammatory response (Figure 5.17(b)). Top-enriched term was positive regulation of cytokine production (GO:0001819, q-value = 2.3e-12), driven by expression of cytokines *Il-1b, Tnf, Il6,* and inflammatory-regulators such as *Stat1, Ccl5, Aif1,* and TLRs 1/2/6/9. Guanylate-binding proteins (*Gbp2/3/5*) drove enrichment of pyroptosis (GO:0070269, q-value = 0.0021). Tripartite motif (TRIM) protein transcripts (*Trim12c/13/30b*) and interferon-stimulated genes *Oas1a/1b/1g* drove enrichment of the negative regulation of viral process (GO:0048525, q-value = 0.0021).

Principal component analysis using fragments per kilobase of transcript per million mapped reads (FPKM) from WT macrophages only revealed that the first principal component of variance in these samples is driven by the major effects LPS has on the macrophage transcriptome (Figure 5.18). CCM/LPS co-treatment samples cluster in between the control and LPS group on this axis, suggesting that CCM treatment can partially revert the gene expression profile of LPS-treated cells towards the baseline profile of vehicle-treated controls. CCM alone does not significantly alter the gene expression profile compared to the control.

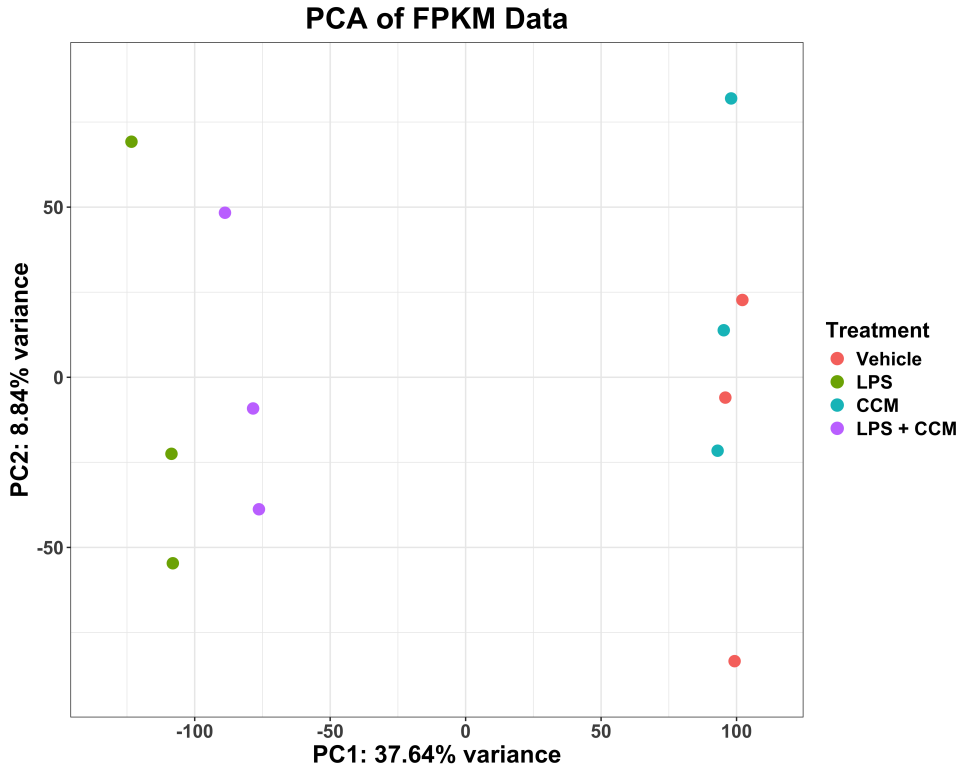

Figure 5.18: **CCM acts by inhibiting activation in response to LPS.**
BMDMs from WT and BMAL1-KO female mice were treated for 6 hours with one of four conditions: vehicle control (0.1% DMSO), 100 nM LPS, 100 μM CCM and 100 nM LPS + 100 μM CCM. Shown is a principal component analysis of the WT samples only.(WT $= 3$).

I then asked which upstream regulatory TFs may be responsible for effects in LPS-stimulated macrophages using decoupleR with CollecTRI/DoRothEA. decoupleR predicted decreased activity of 63 TFs at FDR < 0.05 (Figure 5.19). These included IRFs (IRF1 (padj = 1.7e-37), IRF2 5.3e-10), IRF9 8.2e-9), STAT1 (A0A087WSP5) (padj = 1.6e-17), NFkB mediators (NFKB1 (padj = 6.9e-24), RELA (padj = 4.1e-19), REL, 7.8e-11), and SPI1 (padj = 2.2e-08).

There were few predicted increased TF activities, but these included ZNF143, HDAC4/9, SKIL, NAB2 (a predicted regulatory of co-transcriptional splicing).

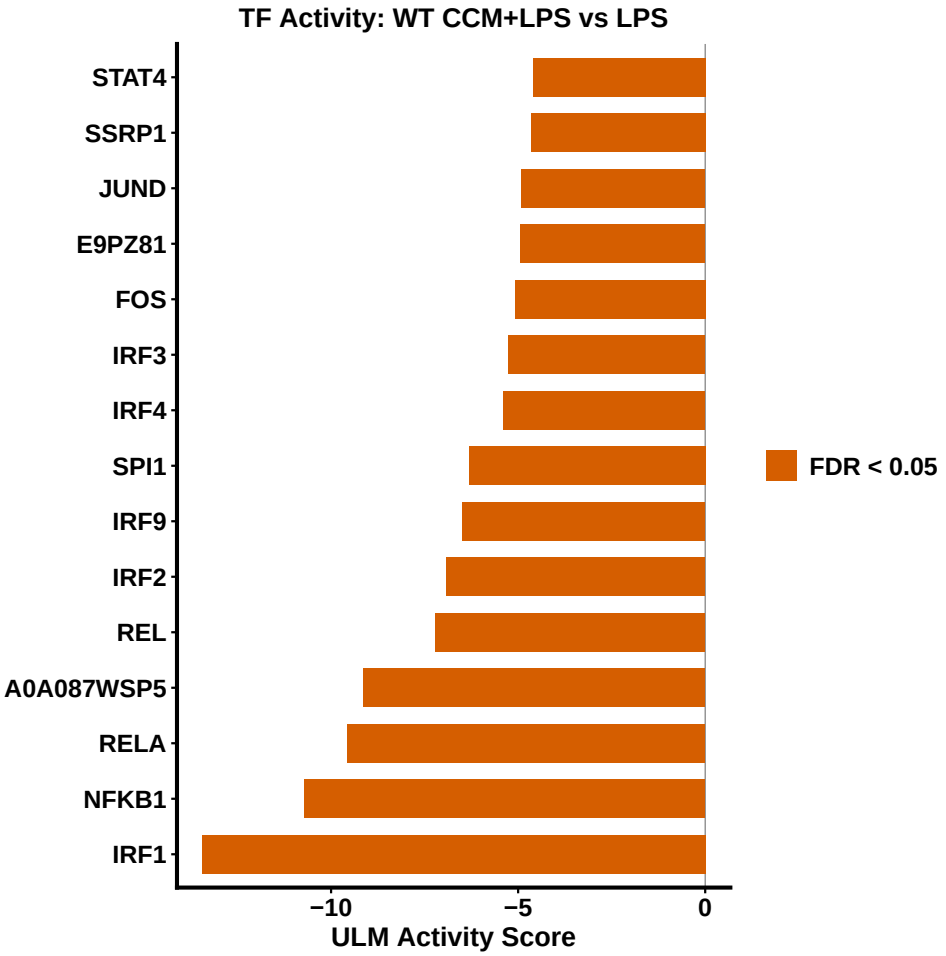

Figure 5.19: **The effect of CCM on transcription factor activity in LPS-stimulated macrophages.**
TF activity inference results for the CCM/LPS vs LPS contrast in WT female BMDMs treated for 6 hours (n = 3). TF activity was inferred by inputting CCM/LPS vs LPS Wald statistics into decoupleR with CollecTRI regulons. Positive scores indicate TF activation by CCM treatment. TFs with significant activity (FDR < 0.05) are highlighted in orange; non-significant factors are shown in grey.

To ask whether the same pathways are inferred as active in CCM-regulated genes in LPS-stimulated macrophages compared to basal state, I performed pathway activity enrichment using decoupleR with PROGENy. The JAK/STAT pathway was most significantly affected, with the largest score for decreased activity after CCM co-treatment (padj = 3.0e-60), followed by NFkB (padj = 2.5e-15), p53 (padj = 2.6e-5), EGFR, (padj = 0.011), TRAIL (padj = 0.018), PI3K (padj = 0.027) (Figure 5.20). This is concordant with results from Chapter 3, where the JAK-STAT pathway showed significant macrophage clock dependent activation at ZT12 *in vivo*.

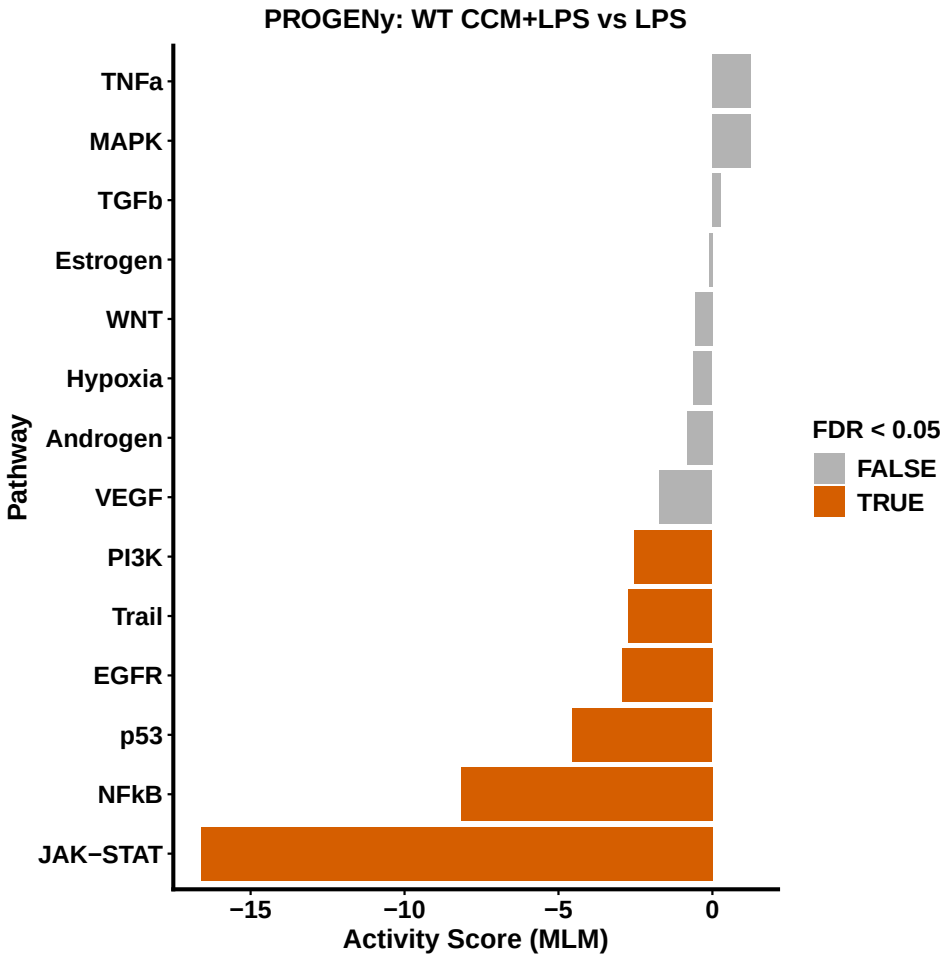

Figure 5.20: **The effect of CCM on pathway activity in LPS-stimulated macrophages.** Pathway activity enrichment scores were inferred using decoupleR with PROGENy's multivariate linear model. Wald statistics for the CCM/LPS vs LPS contrast in WT female BMDMs treated for 6 hours (n = 3) served as input to score activity across 14 pathways. Positive scores indicate pathway activation with CCM relative to LPS baseline; negative scores indicate decreased pathway activity with CCM. Pathways with significant activity (FDR < 0.05) are highlighted in orange; non-significant pathways are shown in grey.

The BMAL1-dependent downregulated genes showed strong functional coherence, suggesting coordinated regulation. To identify potential upstream regulators of this gene set, I used Lisa, which incorporates DNase-seq and H3K27ac ChIP data to construct chromatin models and identify relevant TFs. Lisa outperforms alternative methods for gene set-based regulator inference (Qin et al., 2020). Lisa analysis of BMAL1-dependent CCM-repressed genes identified STAT and IRF family members as the top-ranked predicted regulators (Figure 5.21). Additional high-ranking TFs included RELA, SPI1, REL, JUNB, CEBPA, and PRDM1, TFs central to inflammatory gene expression programs.

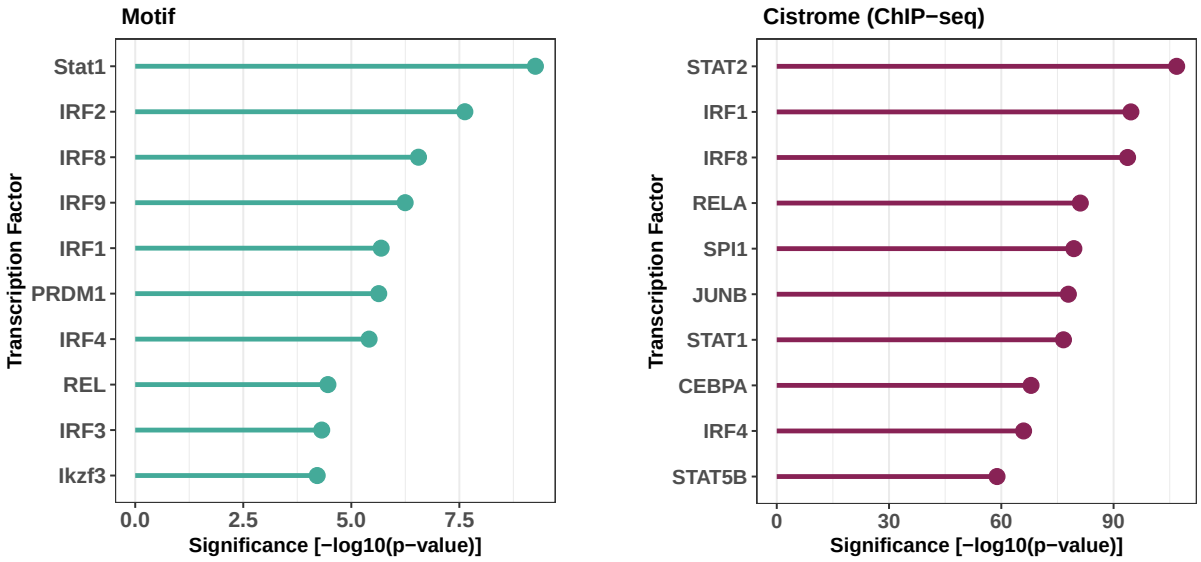

(a) (b)

Figure 5.21: **Predicted transcriptional regulators of BMAL1-dependent CCM-repressed genes are enriched for STAT/IRF proteins.**
BMDMs from WT female mice ($= 3$) were treated for 6 hours with one of four conditions: vehicle control (0.1% DMSO), 100 nM LPS, 100 μM CCM and 100 nM LPS + 100 μM CCM. DEGs for the CCM/LPS vs LPS contrast were identified using DESeq2, at BH-adjusted < 0.05. BMAL1-dependent CCM-effects were identified as WT-only CCM/LPS vs LPS DEGs. Lisa (mm10 genome build) was used to predict transcriptional regulators of the BMAL1-dependent CCM-repression of gene expression in LPS-stimulated macrophages. Lisa uses two complementary methods: (a) Cistrome Motif Analysis, which ranks TFs by enrichment of their binding motifs in regulatory regions; and (b) CistromeDB ChIP-seq Analysis, which ranks TFs based on enrichment of experimentally-determined binding sites (from public ChIP-seq data) near transcription start sites of input genes.

I next tested the hypothesis that CCM drives differential transcription of these TFs through

BMAL1 transactivation. To test this, I identified STAT/IRF genes within the BMAL1-dependent CCM-effects. *Stat1/2/3/5a* and *Irf1/2/8* were significantly downregulated by CCM in WT but not BMAL1-KO macrophages, identifying these pro-inflammatory TFs as BMAL1-dependent CCM targets (Figure 5.22). These TFs showed non-significant but same directionality changes in BMAL1-KO, likely explained by the incomplete penetrance of the genetic knock-out.

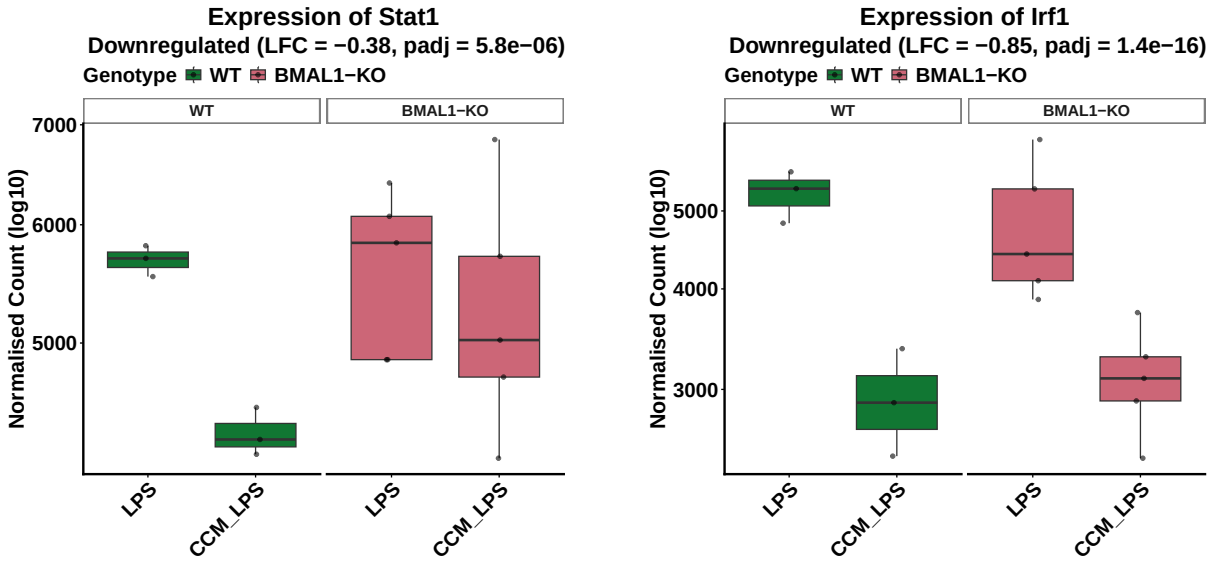

(a) (b)

Figure 5.22: **Expression of STAT1 and IRF1 is significantly downregulated by CCM in a BMAL1-dependent manner.**
BMDMs from WT and BMAL1-KO female mice were treated for 6 hours with one of four conditions: vehicle control (0.1% DMSO), 100 nM LPS, 100 μM CCM and 100 nM LPS + 100 μM CCM. DEGs for the CCM/LPS vs LPS contrast were identified using DESeq2, at BH-adjusted < 0.05. BMAL1-dependent CCM-effects were identified as WT-only CCM/LPS vs LPS DEGs. Normalised counts are plotted for WT and BMAL1-KO. (WT $= 3$, BMAL1-KO $= 5$).

To determine whether CCM affects the same genes that show clock-dependent regulation of LPS responses *in vivo*, I examined CCM effects on genes identified in Chapter 3 as showing BMAL1-dependent timepoint-treatment interactions in peritoneal macrophages. CCM treatment resulted in predominantly negative log2FC values for both gene sets, indicating repression of clock-gated genes irrespective of their time-of-day regulation pattern *in vivo* (Figure 5.23).

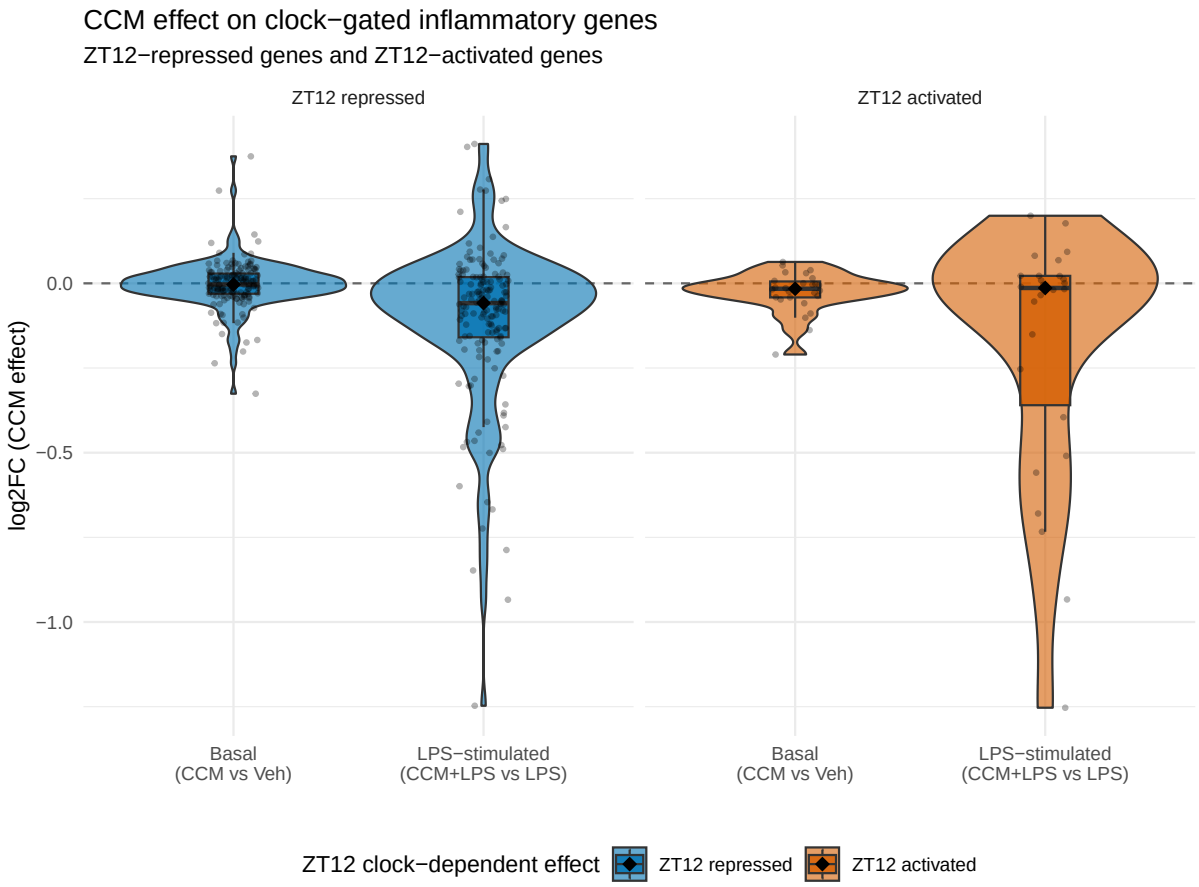

Figure 5.23: **The effect of CCM on BMAL1-dependent inflammatory response genes identified in peritoneal macrophages.**
Genes identified in peritoneal macrophages as showing BMAL1-dependent interaction between timepoint (ZT0 or ZT12) and treatment (Saline or LPS (1 mg/kg)) for their expression were identified using DESeq2, with sex as covariate, where BH-adjusted p-values < 0.05. Saline WT n=3, BMAL1-KO n=3-4. LPS WT, BMAL1-KO n=5-6. The effect of CCM on this gene set, split by whether the magnitude of their expression in response to LPS is greater at ZT12 or ZT0, is plotted as log2FC of the CCM/LPS vs LPS contrast in BMDM (WT, n=3).

Overall, despite modest per-gene effect sizes, CCM has substantial impact on inflammatory programs, with approximately 15% of the LPS-responsive transcriptome affected.

5.3.3 CCM attenuates LPS-effects on macrophage phenotypes.

The transcriptional signatures pointed to CCM-mediated regulation of cytoskeletal organisation and phagocytosis pathway, both BMAL1-dependent processes in macrophages (Figure 5.10). Phagocytosis requires coordinated cytoskeletal rearrangement, and BMAL1 inhibits activation of RhoA, a major regulator of the actin cytoskeleton in resting conditions (Kitchen et al., 2020). I therefore tested whether CCM's transcriptional effects translate to observable changes in macrophage morphology.

5.3.3.1 Morphology.

BMDMs were exposed to CCM for 6 or 24 hours in the presence of LPS. CCM inhibited LPS-induced changes to macrophage morphology (Figure 5.24). At both 6 and 24 hours, LPS increased projected cell area and reduced cell height, consistent with an activated/spread morphology. CCM attenuated these LPS-induced changes after 24 h treatment (Kruskal-Wallis test, Dunn's test pairwise comparisons) (Figure 5.24).

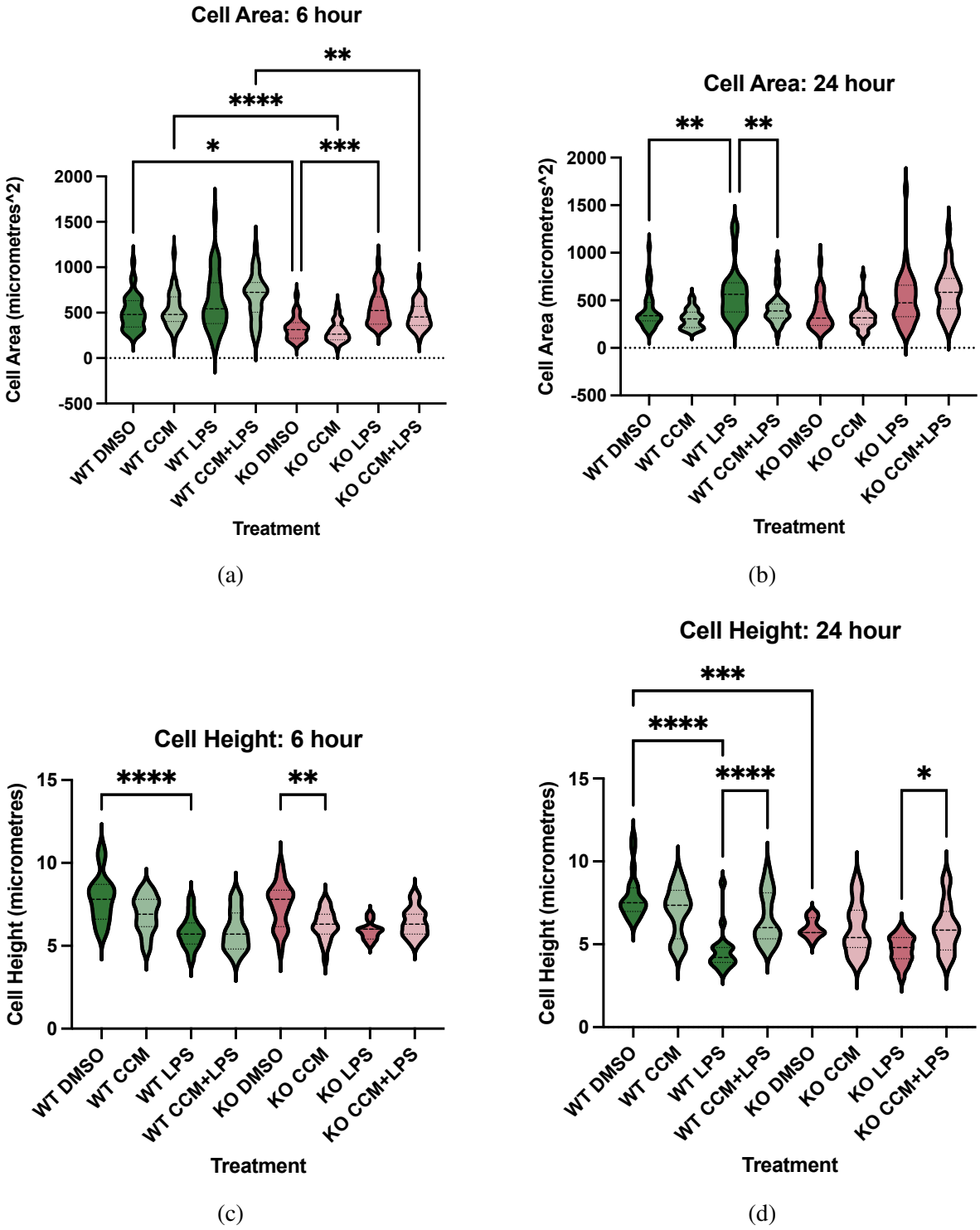

(a) (b) (c) (d)

Figure 5.24: **CCM significantly reduces effect of LPS on cell area and height.** BMDMs from WT female mice were seeded on glass coverslips and treated for 6 hours (n=3) or 24 hours (n=2) with vehicle (0.1% DMSO), 100 μM CCM, 100 nM LPS, or 100 nM LPS + 100 μM CCM. Cells were fixed with 4% paraformaldehyde, stained with Alexa Fluor 488-phalloidin (F-actin) and DAPI (nuclei), and imaged on a Leica TCS SP8 confocal microscope. Four fields of view were captured per condition. Cell area was measured by manual outlining in ImageJ; cell height was determined from Z-stack projections.(a) Cell area, 6 hours. (b) Cell area, 24 hours. (c) Cell height, 6 hours. (d) Cell height, 24 hours. Statistical analysis: Kruskal-Wallis test with Dunn's post-hoc comparisons. * $p < 0.05$, ** $p < 0.01$, *** $p < 0.001$, **** $p < 0.0001$, ns $p > 0.05$.

Consistent with incomplete penetrance, similar attenuation of LPS-induced morphological changes was observed in BMAL1-KO BMDMs, albeit with smaller effect sizes, mirroring the RNA-seq result that many CCM responses are shared between genotypes while a subset is BMAL1-dependent.

5.3.3.2 Motility.

Macrophage morphology is intrinsically linked to motile behaviour, with BMAL1-deletion resulting in more rounded, and more motile cells (Kitchen et al., 2020). Given CCM's effects on cell-spreading and cytoskeletal gene expression, I also assessed whether CCM impacts macrophage motility in a preliminary single-replicate experiment. In this replicate, CCM increased spontaneous motility of macrophages compared to LPS alone (Figure 5.25), consistent with the observed attenuation of LPS-effects on morphology.

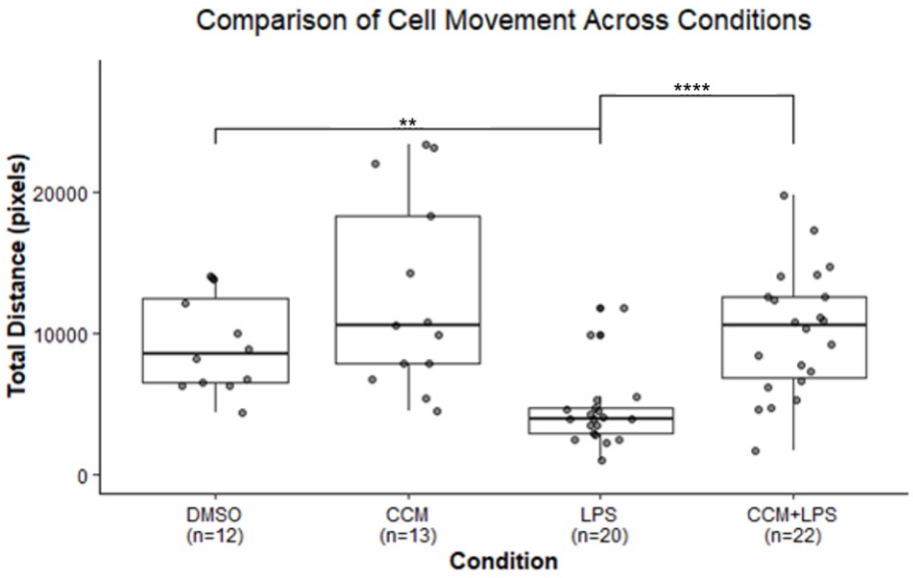

Figure 5.25: **CCM significantly increases spontaneous motility, reducing the effect of LPS.** BMDMs from WT female mice were treated for 24 hours with vehicle (0.1% DMSO), 100 μM CCM, 100 nM LPS, or 100 nM LPS + 100 μM CCM, then replated and labelled with BioTracker 490 membrane dye. Time-lapse imaging was performed on a Nikon Eclipse Ti microscope (37°C, 5% CO) with images captured every 3 seconds for 1 hour. Cell tracking was performed using TrackMate (ImageJ). Data shown are from a single preliminary experiment (n=1). Statistical analysis: Kruskal-Wallis test with Dunn's post-hoc comparisons. * $p < 0.05$, ** $p < 0.01$, *** $p < 0.001$, **** $p < 0.0001$, ns $p > 0.05$.

5.3.3.3 Phagocytosis.

Both morphology and motility are coupled to macrophage phagocytic ability, and the phagocytosis GO term was enriched in the genes downregulated by CCM in basal state (Figure 5.10). The attenuated LPS-induced spreading seen in CCM-treated macrophages, and resulting increased motility, suggests reduced substrate adhesion. I therefore tested whether CCM influences bacterial uptake.

In a gentamicin protection assay (1-h infection), CCM decreased intracellular *E. coli* colony-forming units (CFU) recovered from WT macrophages (Sidak's-adjusted p = 0.019) from 42,517 to 22,633 (Figure 5.26). In line with reduced but not absent BMAL1, the KO similarly showed decreased recovery of CFU (Sidak's-adjusted p = 0.027) from 30,833 to 11,958. However, this assay cannot resolve whether this observed effect is due to reduced uptake, enhanced intracellular killing, or both.

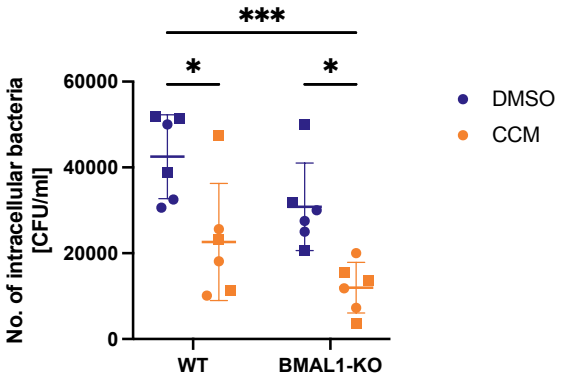

Figure 5.26: **CCM significantly reduces number of intracellular bacteria as a measure of phagocytic uptake.**
BMDMs from WT and BMAL1-KO male and female mice were infected with *E. coli* DH5α (MOI 20) in the presence of vehicle (0.1% DMSO) or 100 μM CCM for 1 hour. Extracellular bacteria were killed with gentamicin (100 μg/mL, 30 minutes), cells were lysed, and intracellular bacteria were enumerated by colony-forming unit (CFU) counts on LB agar. Circles represent BMDMs from male mice, and squares represent BMDMs from female mice. Statistical analysis: two-way ANOVA with Sidak's post-hoc comparisons. * $p < 0.05$, ** $p < 0.01$, *** $p < 0.001$, **** $p < 0.0001$, ns $p > 0.05$.

Together, these functional assays demonstrate that CCM's transcriptional suppression of cy-

toskeletal and phagocytic programs translate to measurable, coherent changes in macrophage phenotype. Reduced LPS-induced spreading corresponds to increased motility, and a possible decrease in bacterial uptake. This is consistent with a model where CCM enhances BMAL1's role maintaining macrophages in a quiescent state (Kitchen et al., 2020).

5.4 Discussion

Pharmacological modulation of the circadian clock has therapeutic potential, and small-molecule modulators exist for REV-ERBs, CRYs, and RORs. However, BMAL1 (the core positive regulator of the clock) has lacked a targeted compound. CCM fills this gap, enabling acute perturbation of BMAL1 biology without the confounding effects of genetic deletion on development. In this chapter, I characterised CCM's effects on macrophage circadian rhythms, transcriptional programs, and cellular function.

5.4.1 CCM alters circadian dynamics in macrophages.

CCM significantly dampened amplitude, shortened period, and induced a phase delay in peritoneal macrophages in a dose-dependent manner, while leaving viability (as measured through ATP levels) unaffected.

Other clock-modulatory compounds show comparable effects on circadian dynamics. The CRY stabiliser KL001 lengthens period and reduces amplitude through prevention of CRY-degradation, amplifying negative-feedback in the core clock TTFL (Hirota et al., 2012). Conversely, a compound inhibiting CRY function reduced amplitude and delayed phase (Jang et al., 2018). CCM's actions of decreasing amplitude, shortening period, and delaying phase, resemble CRY-inhibition more than CRY-stabilisation.

These alterations in circadian parameters suggested CCM affects BMAL1 function, prompting investigation of downstream transcriptional consequences of CCM treatment.

5.4.2 CCM promotes anti-inflammatory transcriptional programs through BMAL1.

The effects of CCM were amplified in LPS-stimulated macrophages relative to basal, with 307 DEGs in basal, and 1785 DEGs in LPS (FDR < 0.05). This pattern parallels observations in other tissues, where clock perturbations through genetic deletion have minimal phenotypic consequences under basal conditions and need metabolic or inflammatory challenges to reveal them (Hunter et al., 2020).

BMAL1-dependent CCM effects were 242/307 (79%) of basal, and 855/1785 (48%) of LPS effects. The incomplete penetrance I observed explains an amount of BMAL1-KO shared changes with WT. However, off-target effects of the compound are also possible as CCM targets a protein domain that is conserved across multiple TFs.

The effects of CCM in basal state macrophages are functionally coherent, with coordinated upregulation of genes encoding anti-inflammatory TFs like NRF2. *Gsr* and *Slc7a11* are targets of NRF2: overexpression of BMAL1 has been shown to activate NRF2 signalling, resulting in reduced intracellular reactive oxygen species release and the inhibition of inflammatory responses (Zeng et al., 2025). The stabilisation of BMAL1 by CCM resulting in increased NRF2 activity is concordant with this finding. Increased arginase-2 (ARG2) promotes the resolution of inflammation in macrophages.

Transcriptomic analysis suggested CCM altered cholesterol metabolism in both basal state and LPS-stimulated macrophages: in the basal state, cholesterol synthesis genes were downregu-

lated. Consistently, in the LPS-stimulated state, cholesterol efflux was one of few GO terms enriched in BMAL1-dependent activation by CCM. A recent study has found that myeloid-specific BMAL1-deficient mice showed higher cholesterol accumulation in macrophages due to deficiencies in cholesterol efflux capabilities (Pan et al., 2025). The authors show that BMAL1 regulates *Abca1* (cholesterol efflux protein), with reduction of *Bmal1* reducing expression, and overexpression of BMAL1 increasing expression of *Abca1*. CCM appears to mimic BMAL1-overexpression through the increased expression of *Abca1*. In my data, ZFP202 was predicted to have lower activity with CCM treatment in basal macrophages. ZFP202 is a repressor controlling tissue-specific expression of *Abca1*, and Pan et al showed ZFP202 binding at the *Abca1* promoter was enhanced after knock-down of *Bmal1*, indicating BMAL1 regulates cholesterol efflux in part through effects through ZFP202. In summary, my evidence shows that CCM's effects resemble BMAL1 overexpression (the opposite of genetic knockout of BMAL1). CCM upregulation of cholesterol-efflux gene programmes warrants exploration of CCM in models of atherosclerosis, where cholesterol accumulation in subendothelial macrophages contributes to disease.

In LPS-stimulated macrophages, I observed broad suppression of inflammatory response in line with known BMAL1-macrophage biology. Downregulation of pro-inflammatory GO terms indicates a stabilisation of the anti-inflammatory arm of clock's regulation of macrophages, mediated through altered BMAL1 activity. In models where BMAL1 is targeted for genetic deletion, macrophages exhibit pro-inflammatory states and increased cytokine production (Alexander et al., 2020; Curtis et al., 2015; Oishi et al., 2017). Here, too, CCM's effects are in the opposite direction, indicating an alteration of BMAL1 activity similar to activation, and providing a new tool to perturb BMAL1 biology with effects countering genetic knock-out.

In both states, the changes to expression are low amplitude (small log2FoldChanges CCM vs

control), in line with findings that BMAL1-occupancy was not significantly altered at key loci in U2OS cells treated with CCM (Pu et al., 2025).

5.4.3 CCM's effects concord with *in vivo* clock-gating mechanisms.

CCM repressed LPS-response genes that were previously identified as clock-gated in peritoneal macrophages *in vivo* (Chapter 3), regardless of whether those genes showed induction or repression at ZT12.

The same TF families (STAT1, IRF1, and related interferon-response regulators) emerged as predicted upstream mediators of both clock-dependent gating (Chapter 3) and CCM effects (this chapter). This concordance validates CCM as recapitulating physiological BMAL1 function: CCM-BMAL1 suppresses interferon/STAT signalling, matching the observation that BMAL1 loss elevates STAT/IRF activity at ZT12. CCM can therefore serve as a tool for studying BMAL1 biology without genetic manipulation.

5.4.4 Mechanism of action.

Pu et al. found that CCM does not alter BMAL1 levels (Appendix Figure 5c), localisation (Appendix Figure 5b), or heterodimerisation with CLOCK (Appendix Figure 5a) (Pu et al., 2025). but does alter the interaction of BMAL1 with histone H2A. H2A emerged from RIME as a candidate protein whose interaction with BMAL1 was altered by CCM. In agreement, the structural study of CCM-BMAL1 revealed a shift in the αF helix, which has been shown to be crucial for CLOCK:BMAL1 binding to chromatin and robust, rhythmic gene expression (Michael et al., 2023).

RNA-seq data were generated by Novogene, who also performed bioinformatics analysis including alternative splicing quantification. Their analysis, reported in (Pu et al., 2025) identi-

fied increased alternative splicing events with CCM treatment specifically in WT macrophages. This finding suggests altered BMAL1 transcriptional dynamics. Together, the evidence suggests CCM exerts effects by modulating BMAL1's interaction with chromatin rather than its abundance or formation of complexes. However, the precise mechanism through which CCM perturbs BMAL1 biology remains to be determined.

5.4.5 Functional consequences.

CCM inhibited the effect of LPS on macrophage morphology and motility. RNA-seq shows broad dampening of LPS-responsive modules, consistent with reduced phagocytic activation. CCM reduced the number of intracellular bacteria internalised in a gentamycin survival assay. This result suggests that CCM caused reduced uptake, or increased bacterial killing, or both. However, the transcriptional data shows broad dampening of inflammatory activation which suggests an action mechanism of reduced uptake capacity rather than enhanced bacterial killing. To disambiguate mechanisms and distinguish killing from uptake, uptake kinetics of pHrodo *E. coli* should be directly quantified in future.

The broad anti-inflammatory effects of CCM suggest therapeutic uses to restrain hyper-inflammatory responses and subsequent tissue-damage. Many antibiotics have immunomodulatory properties: ciprofloxacin, doxycycline, and erythromycin appear to lower bacterial phagocytosis through interference with TLR signalling (Silva Lagos et al., 2022). Daily low-doses of erythromycin are used to treat chronic airway diseases (Reijnders et al., 2020). CCM could offer similar benefits, without the risk of antimicrobial resistance through antibiotic prescription. However, like other immunosuppressants, CCM could increase susceptibility to infections. The most appropriate use-cases may therefore be conditions with excessive inflammation but limited infection risk.

A summary of the findings in this chapter is presented in Figure 5.27.

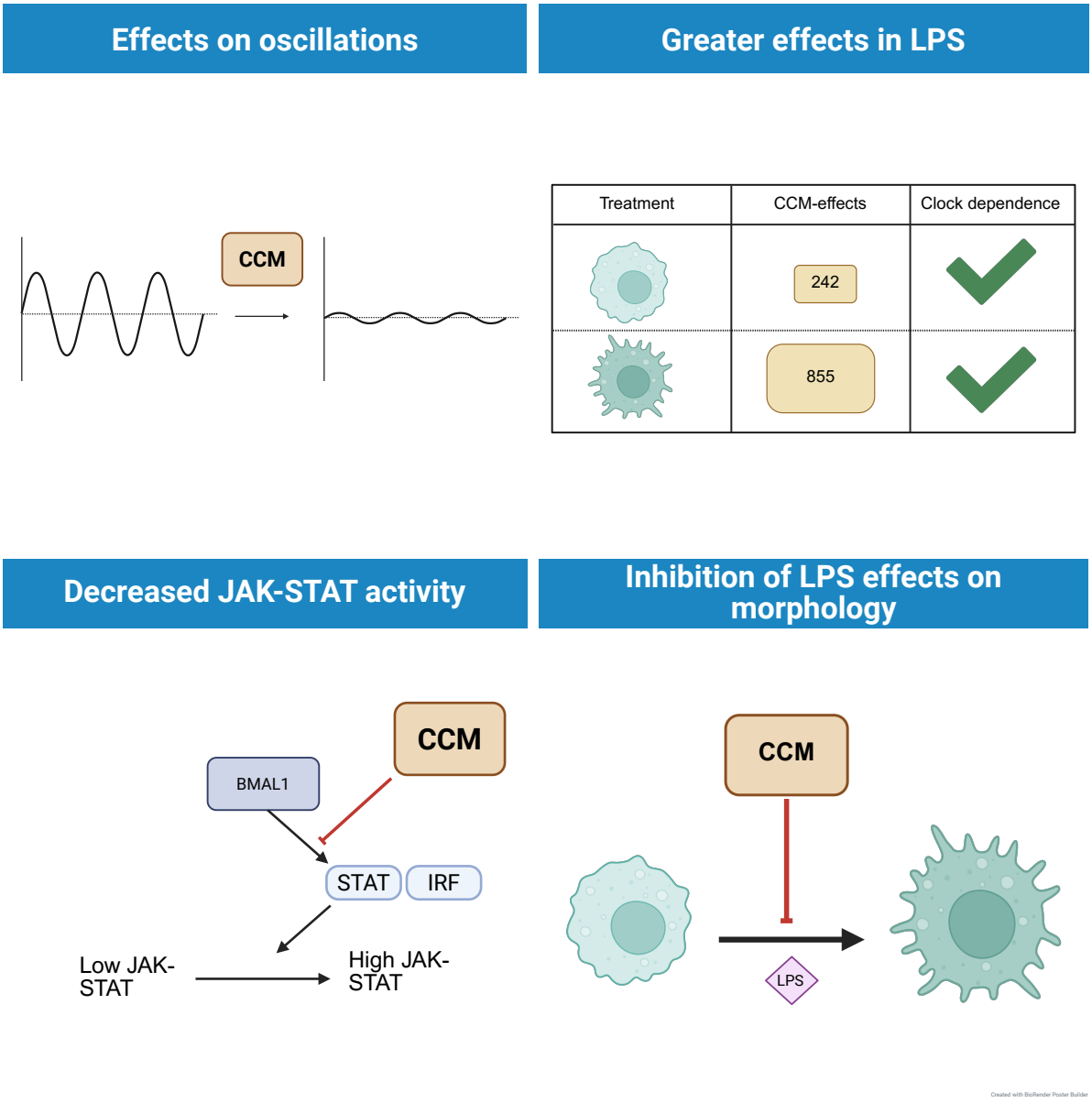

Figure 5.27: **Summary of results from Chapter 5.**
Top left: CCM significantly alters the parameters of circadian oscillations, with large reductions in amplitude, in peritoneal macrophages. Top right: there are more BMAL1-dependent effects of CCM in LPS-treated BMDMs than in basal state, vehicle-treated BMDMs. Bottom left: the BMAL1-dependent effects of CCM in inflammatory BMDMs are characterised by lower JAK-STAT activity than controls. Bottom right: CCM inhibits functional changes to macrophage morphology induced by LPS. Created in https://BioRender.com

5.4.6 Limitations and future directions

RNAseq was performed at a single timepoint only. Clock-dependent regulation of inflammatory gene expression differs dependent on point in the cycle: for example, I identified repressive effects at ZT12 in peritoneal macrophages (see Chapter 3). The use of single-timepoint profiling in this Chapter may underestimate CCM's impact on clock-controlled genes whose expression we sampled at a bulk-average of trough or peak.

It will be necessary to define the genomic mechanism of action of CCM, using ATAC and BMAL1-ChIP-seq before and after treatment, to determine how changes to chromatin accessibility and binding dynamics correlate with alterations to transcriptional responses observed in this study. Additionally, ChIP-seq would allow examination of CCM effects on histone modifications (such as H3K27Ac for transcriptionally active chromatin). BMAL1-KO increases enhancer acetylation (Oishi et al., 2017), and so depending on how CCM-BMAL1 interacts with DNA and histone-modifiers, we might expect decreased enhancer acetylation which could mediate the observed reduction in inflammatory gene transcription.

The significant number of BMAL1-KO-only CCM effects in LPS-conditions reflects the incomplete penetrance of the genetic deletion of BMAL1 in the knock-out (Figure 5.8), alongside any off-target effects of CCM. We could use overexpression of BMAL1 to increase target abundance, and so validate on-target effects in these conditions. Formally quantifying recombination efficiency would strengthen interpretation of this study. Three complementary readouts would be informative: genomic qPCR spanning the floxed region to quantify deletion at the DNA level; immunoblot for BMAL1 protein to confirm loss at the protein level; and single-cell RNA-seq. Single-cell RNA-seq would distinguish between two interpretations of incomplete penetrance: partial deletion within all cells (true hypomorph) versus a mosaic of fully wild-type and fully

deleted cells.

The BMDMs used in this study were female, and so it remains to be seen if effects of perturbing BMAL1 biology with CCM differ in male and female macrophages (with the prediction of greater effects on inflammatory response in males (Chapter 4), with and without sex hormones present.

Future molecules targeting BMAL1 need improved pharmacokinetic qualities to be used *in vivo*. Use under physiological conditions will inform firstly how CCM might regulate the master pacemaker (SCN), and so whole-organism metabolic and behavioural measurements will be needed. For peripheral clocks, pharmacological manipulation of BMAL1 in the context of inflammation will be necessary to validate anti-inflammatory effects on gene expression observed in this study. Given CCM's suppression of JAK-STAT signalling, inflammatory models with prominent IFN signatures such as mouse models of rheumatoid arthritis, or imiquimod-induced skin inflammation, would be appropriate for *in vivo* validation of CCM's anti-inflammatory effects.

The circadian clock regulates and is regulated by multiple complex systems, and as such an increase or decrease in amplitude is not necessarily consistently desirable across time, tissue, or system. Perturbation in one direction (enhancing BMAL1 activity with CCM) may be beneficial in acute infection, by limiting potential for host damage, but may trade off with limiting clearance of the pathogen.

6 | Discussion

6.1 Summary of analysis

Many biological processes in diverse species are regulated through the 24-hour timing system imposed by circadian clocks. In mammals, the core transcription-translation feedback loop (TTFL), centred on BMAL1, confers rhythms to tissue-specific programs of downstream target genes. Many immune processes are recognised to show circadian regulation, including inflammatory responses in both acute and chronic disease settings. Macrophages are important innate immune sentinel and effector cells driving inflammatory responses. When macrophages detect threats, they remodel transcriptional programs to respond appropriately, such as through the production of pro-inflammatory cytokines. Previous work has shown that these pro-inflammatory transcriptional programs are circadian-regulated, and that macrophages produce greater levels of these cytokines at the start of the active period in mammals, when exposure to pathogens may have been most likely in the ancestral environment (C. Wang et al., 2022).

However, much of the work characterising circadian macrophage inflammatory responses has been performed *in vitro* (where effects of extrinsic signals on clock function cannot be assessed), in male macrophages only, and by using only genetic knock-out models to study the function of BMAL1. This leaves many unanswered questions about the mechanisms and therapeutic implications of circadian inflammatory control.

Chapter 3: Intrinsic macrophage clock. Tissue-resident macrophages are exposed to many extrinsically rhythmic signals (from glucocorticoids and metabolites to output from the nervous system), all of which are recognised to modulate pro-inflammatory activation of macrophages.

To define the importance of the intrinsic macrophage clock in the inflammatory response in tissue-resident (peritoneal) macrophages *in situ*, I compared transcriptomes of macrophages after 1 hour of intraperitoneal saline or LPS given at antiphasic timepoints ZT0 and ZT12, isolated from WT and myeloid-specific BMAL1-KO mice.

I discovered that almost all timepoint-differences were BMAL1-dependent in this study. The basal state macrophages showed greater BMAL1-dependent timepoint differences. I found a subset of BMAL1-dependent LPS-response genes which show an interaction between timepoint and treatment, which show a lower LPS response at ZT12 (relative to ZT0). Inflammatory stimuli have been shown to modulate clock function (S. Chen et al., 2020): consistent with this, I found that distinct biological processes showed BMAL1-dependent time-of-day regulation in basal state macrophages relative to LPS-activated macrophages. The smaller number of BMAL1-dependent differences in LPS-activated macrophages showed functional enrichment for interferon responses, despite the 1-hour timepoint used capturing immediate-early transcriptional responses without time for secondary IFN-producing signalling to exert full effects. Guanylate binding proteins (GBPs) drove this enrichment and were upregulated in LPS-BMAL1-dependent differences at ZT12 relative to ZT0. GBPs are promoters of inflammasome activation and so the effect is consistent with previous observations that inflammasome activation peaks at the start of the active period (O'Siorain et al., 2024; Tretina et al., 2019).

How BMAL1 regulates inflammatory responses via regulation of gene expression is an active area of research. One such mechanism may be the contribution of chromatin remodelling to time-of-day regulation. I used ATAC (Assay for Transposase Accessible Chromatin) to assess this, and found few differences between LPS-stimulated chromatin at ZT0 and ZT12. This negative result must be interpreted with caution, however, as ATAC lacks the resolution to capture transient accessibility changes induced by signal-dependent TF binding. Even still, the

absence of large-scale chromatin remodelling suggests that clock-mediated changes to transcription factor activity and/or availability by timepoint may be a more important contributor to this mechanism. I inferred transcription factor activity between timepoints, identifying a BMAL1-dependent activation of STAT1, IRF1, and IRF3 at ZT12. Pathway activity analysis showed the expected increase in JAK-STAT signalling at ZT12 relative to ZT0. By analysing differential expression of TFs themselves in the basal state, I found that at ZT12 (the timepoint of WT-specific baseline priming of pro-inflammatory expression), deletion of BMAL1 resulted in downregulation of a program of both pro- and anti-inflammatory TFs, including characterised BMAL1-targets like NRF2, despite the ZT12 timepoint being close to the trough of NRF2 expression over the 24-hour period (Early et al., 2018). This suggests that components of the macrophage clock are not simply priming pro-inflammatory responses at the start of the active phase, as macrophages also seem primed for resolution of inflammation.

Consistent with this, I found a subset of genes in which the response to LPS was timepoint-dependent, with no such interaction in BMAL1-KO macrophages. Most of this subset showed a reduced activation in response to LPS at ZT12 relative to ZT0, indicating some transcriptional repression or absence of activation in these primary response genes enriched for pro-inflammatory functions. I tested the role of REV-ERBα, noted to have direct repressive effects on inflammatory gene expression in previous macrophage models (Gibbs et al., 2012), and found that in my *in vivo* model of inflammation, REV-ERBα-deletion did not modulate the BMAL1-dependent LPS-response gating, in agreement with findings in lung model of inflammation that it was REV-ERBα-deletion in non-myeloid cell types which drove the significant anti-inflammatory phenotype *in vivo* (Pariollaud et al., 2018).

These findings reinforce our understanding of BMAL1 to have pleiotropic effects on cellular states in many tissues. Here, the regulation of key upstream regulators in basal state sets up

different programs at ZT0 vs ZT12.

Chapter 4: Sex differences in macrophage circadian programs. We are now aware that circadian programs show sex-specificity in a variety of tissues, with consequences for health outcomes (Lok et al., 2024; Talamanca et al., 2023). In Chapter 3, I identified evidence that sex regulates clock-programs from the enrichment of response to hormone/steroid GO terms in the BMAL1-dependent LPS-response set, and from the enrichment of hormone response elements in the promoters of this set. There is a lack of data in the field as to whether macrophage-clocks show sex-specificity, so I decided to test for sex-specific BMAL1-dependent transcriptional programs in my dataset. In activated, LPS-stimulated macrophages, there were fewer BMAL1-dependent timepoint differences in females than in males. Sex-specific BMAL1-dependent genes showed different functional enrichments, with males showing greater BMAL1-dependent differences in cytokine production and pro-inflammatory terms, similar to the mixed-sex analysis in Chapter 3. However, the genes identified as showing sex-specific BMAL1-dependence in fact showed a coordinated direction of regulation in the other sex, with the effects not passing the significance threshold. In this study of LPS-stimulated macrophages, sex predominantly modified the amplitude and not directionality of BMAL1-dependent gene expression, with greater amplitude differences in males. However, I identified a subset of genes where directionality was reversed between sexes, which included important metabolic regulatory genes involved in cholesterol homeostasis. This aligns with GTEx analysis showing spleen has more male-specific rhythmic genes, unlike most tissues (Talamanca et al., 2023). Together, these findings indicate that sex should be considered as a biological variable in studies of macrophage clock function.

Chapter 5: Pharmacological clock modulation. To avoid the confounding effects of BMAL1-loss on development when using a genetic-deletion model, I used the novel compound CCM to perturb BMAL1 biology. I confirmed CCM-action on BMAL1 by first demonstrating that CCM modulates circadian parameters, decreasing PER2-luciferase amplitude, in a dose-dependent manner. I then used CCM to examine macrophage transcriptomes after 6 hours of treatment. In the basal state, CCM upregulates anti-inflammatory regulators, concordant with BMAL1's role in suppressing inflammatory responses. I found that CCM exerts its effects most strongly in the presence of LPS and broadly inhibits expression of pro-inflammatory genes. Predicted upstream regulators include IRF/STATs, and the JAK-STAT pathway was downregulated with CCM treatment. This supports previous work and my other findings here that the clock regulates IRF/STAT activity. Talamanca et al. found IRF/STAT activity peaked early in the night in a survey of rhythmically-expressed genes in 46 tissues (in humans), indicating this regulation is not macrophage-specific (Talamanca et al., 2023). In humans, this peak activity is early in the rest phase, which corresponds to early in the light phase for mice. However, I observed peak IRF/STAT activity at the beginning of the dark phase. The precise phase relationship between median IRF/STAT activation in diverse human tissues and mouse macrophages requires further investigation.

CCM regulated cholesterol homeostasis gene networks in both resting and activated macrophages, with CCM inhibiting cholesterol synthesis and promoting cholesterol efflux. These effects are opposite to those observed in BMAL1-KO macrophages, which show increased lipid stores and greater atherosclerosis in mice (Pan et al., 2025). In accordance with the well-documented inhibitory effects of the macrophage clock on transcription of pro-inflammatory genes, CCM acted to inhibit macrophage responses to LPS and Gram-negative bacteria: preventing the modulation of motility and morphology that occur with stimulation, and reducing internalised bacte-

ria number in a phagocytosis assay. CCM phenocopying enhanced rather than reduced BMAL1 function is consistent across inflammatory and metabolic programs, supporting the interpretation that CCM augments BMAL1 transcriptional activity.

Summary. Inflammatory responses must balance robust responses to pathogens with the need to minimise tissue damage through pro-inflammatory action. Together, these findings indicate the circadian clock (through BMAL1) pre-sets macrophage baseline readiness for inflammatory responses through regulation of TF availability rather than chromatin remodelling, as ATAC-seq revealed minimal accessibility differences between timepoints. The field has focused on BMAL1-modulation of specific inflammatory factors, and yet transcriptomic shifts are broad and cannot be restricted to a few focal genes. At ZT12, BMAL1-intact macrophages have elevated expression of both pro-inflammatory (STAT/IRF-dependent) and anti-inflammatory (NRF2-mediated) programs. This is lost with BMAL1-deletion, and CCM treatment resulted in repression of STAT/IRF action and activation of NRF2-mediated programs, recapitulating the anti-inflammatory action of the positive arm of the clock (CLOCK:BMAL1 heterodimer action) that is lost at ZT12 when CLOCK:BMAL1 levels are low. Sex modulates the amplitude of this program: males showed stronger STAT/IRF oscillations and corresponding oscillations in inflammatory-response pathways. As shown in peritoneal macrophages and in CCM-treated BMDMs, the clock also regulates cholesterol homeostasis. This regulation may show sex-specificity, with the rate-limiting cholesterol synthesis enzyme *Hmgcr* peaking in expression at opposing timepoints between sexes. BMAL1 coordinates broad transcriptional programs, across multiple inflammatory and metabolic pathways, rather than acting on a few specific target genes. Across the experimental approaches (genetic BMAL1-deletion, sex-stratified analysis, and pharmacological manipulation of BMAL1) STAT/IRF TF activity emerged as the key mediator: elevated at ZT12 in a BMAL1-dependent manner (Chapter 3), showing male-biased

amplitude (Chapter 4), and suppressed by CCM (Chapter 5).

6.1.1 Strengths and limitations

Model systems. Most studies of the circadian clock in primary macrophages have used male macrophages, often BMDMs. BMDM clock function *in vitro* may not reflect physiological clock function, where exposure to rhythmic extrinsic signals will influence signal integration and clock function. This work uses peritoneal macrophages, a well-studied population of macrophages with roles modulating peritoneal inflammation. This is especially important when studying the LPS response: the complete signalling context will determine the response to LPS/NFkB signalling.

Studying macrophages from a global BMAL1-KO may result in non-generalisable evidence. BMAL1-KO animals show multiple systems are affected, which may result in altered metabolic flux and therefore affect the potential for activation of the study macrophage population. Global deletion of other clock genes such as REVERB-α may have similar consequences, especially as macrophage biology is commonly driven by the signalling potential of nearby cells. For example, in epithelial cells, REVERB-α-KO has a strong effect on the lung inflammatory response (Pariollaud et al., 2018). The common alternative is to use Cre-driven recombination of a clock gene flanked with loxP sites. As noted in Chapter 5, Cre-drivers may cause incomplete recombination of the floxed allele. The implications of incomplete recombination, and the experimental approaches needed to formally assess it, are discussed in Chapter 5 (5.4.2) with reference to the BMAL1-flox line. The REV-ERBα-flox line used in Chapter 3 has not been similarly characterised in this study; formal assessment of recombination efficiency at the protein level, and complementary single-cell approaches, would clarify whether the minimal transcriptomic phenotype observed in REV-ERBα-KO peritoneal macrophages reflects genuine functional re-

dundancy or partial recombination. Despite this caveat, Cre-driven conditional deletion remains the most selective available approach for restricting clock gene deletion to the myeloid lineage, limiting unintended effects on the organ systems affected by global clock disruption. Although the peritoneal cavity contains a dominant macrophage population, I used magnetic-activated cell sorting (MACS) to ensure a consistent study population in each condition.

The pharmacological work in Chapter 5 used BMDMs rather than peritoneal macrophages, for two reasons. First, the cell numbers required to test CCM across multiple conditions (basal, LPS-stimulated, and with CCM) in each biological replicate exceeded what could be obtained from peritoneal lavage. Second, the use of BMDMs enabled direct comparison with published work on BMAL1 modulators and BMAL1-dependent macrophage biology, most of which has used BMDMs. The limitations noted above apply: BMDM clock function may not fully reflect the rhythmic signalling context of tissue-resident macrophages, and the CCM findings reported here therefore require validation in primary tissue-resident populations and *in vivo*, conditional on a CCM formulation with appropriate pharmacokinetic properties.

Experimental constraints. Studying the early transcriptional response to LPS allows the disentanglement of primary clock effects on transcription from clock-mediated modulation of secondary feedback loops. However, I cannot assess the role of the clock on the LPS response timecourse and how the resolution of inflammation is perturbed by clock-disruption. I have identified poised pro-inflammatory transcriptomes at ZT12, but would need to assess protein levels to address whether the transcriptional priming translates to altered cytokine production and resolution of inflammation, although published work shows high correspondence of mRNA to protein level for key cytokines at ZT12 (Gibbs et al., 2012). Bulk-sequencing methods also limit the ability to define molecular mechanisms: whether IFN-responses are uniform across the already-heterogenous peritoneal macrophage population, and so whether clock-mediated

anti-inflammatory effects are macrophage-type specific. Additionally, by capturing the two antiphasic timepoints chosen for maximal difference in macrophage clock-regulated activity, including cytokine production and phagocytosis, the results can only be interpreted as timepoint-differences and would not capture phase differences in BMAL1-dependent programs between sexes. When interpreting sex-stratified results, a key limitation is that there has been no control for the stage of estrous cycle, which may affect LPS-responsiveness and so the timepoint comparison.

Technical limitations. The time-of-day ATAC performed in LPS-stimulated macrophages was dominated by promoter signals, which limits my ability to conclude that chromatin remodelling is not essential for clock dependent-LPS response as small intergenic changes may not have been detected. Due to the overall similarity between timepoints, it seems likely that there are no large genome-wide remodelling events. Additionally, we do not have appropriate peak-calling tools to define subtle changes to peak shape (rather than appearances or disappearances between conditions), which would enable better motif-enrichment analyses.

6.1.2 Future directions

Mechanisms for BMAL1-dependent regulation of inflammatory genes. As there were no large-scale genome-wide differences between ZT0 and ZT12 (ATAC-seq results in Chapter 3), I would prioritise investigation of DNA-looping and altered enhancer activity via regulatory histone modifications. REV-ERBα regulates promoter-enhancer loop formation through recruitment of a co-repressor complex (Y. H. Kim et al., 2018). The ATAC-seq used in this study revealed few differences with REV-ERBα-deletion, but loop formation may show clock-regulation. The strength of enhancers is not well-predicted by -omics data. Enhancer activity, assessed via histone modification and eRNA production, and promoter-enhancer looping war-

rant further investigation with *in vitro* validation wherever possible (Galouzis & Furlong, 2022). TF activity and availability appear clock-modulated for a wide program of TFs: as localisation and activation status define activity, I would investigate where in the inflammatory-signalling cascade regulators are clock-regulated with both spatial and temporal resolution. Single cell approaches would enhance the study of clock-regulatory logic. Cell-type and cell-state matter for circadian rhythmicity (C. Y. Tong et al., 2025). Considering the peritoneal macrophage population heterogeneity, it is important to understand whether rhythmicity is the same in other tissue-resident macrophages, and in both sexes, at the level of macrophage subtypes.

Sex differences. This study was not originally designed to perform sex-stratified analysis, and as such animals were not assessed for estrus cycle stage, providing potentially confounding hormonal effects on inflammatory macrophages. To distinguish hormonal vs chromosomally-mediated effects on the macrophage clock, a combination of gonadectomised controls and exogenous hormonal supplementation could be used, after initial tests on *in vitro* WT and BMAL1-KO macrophages with hormone supplementation first.

CCM. Conditional on a new version of CCM with improved pharmacokinetic qualities for use *in vivo*, I would test effect of BMAL1-modulation in infection outcomes and models of chronic inflammation. To decipher the mechanism of action of CCM and gain a greater understanding of BMAL1's action as a TF, I would use ChIP-seq to see how BMAL1 binding and histone modifications are altered with CCM in macrophages.

6.1.3 Translational outlook for chronobiology

Effective chronotherapy requires the understanding of immune cell behaviour at multiple levels. The cells must be localised to the right tissue at the right time, with the relevant recep-

tors expressed, and in a permissive cellular state to respond to treatment. My findings indicate that the intrinsic macrophage clock establishes inflammatory states by timepoint, in part due to STAT/IRF priming at ZT12. Circadian disruption may perturb this regulation of IFN-enhanced inflammatory responses, contributing to the constitutively pro-inflammatory state seen in BMAL1-KO mice macrophage models and increased incidence of inflammatory disorders in shiftworkers (Maidstone et al., 2025).

The therapeutic relevance of clock-regulated JAK-STAT signalling is already evident clinically. My finding that JAK-STAT activity peaks at ZT12 in a BMAL1-dependent manner aligns with evidence that timed JAK inhibitor administration improves outcomes in rheumatoid arthritis, which like many autoimmune diseases is often characterised by IFN signatures (Miyamoto et al., 2022). In mice, JAK-STAT inhibition at ZT0 (when, conversely in my study, pathway activity is lower) improved arthritis scores relative to ZT12 administration (Yaekura et al., 2020). A recent non-randomised trial found nocturnal baricitinib administration resulted in better clinical endpoints than standard dosing, consistent with a long history of successful timed glucocorticoid administration for morning symptoms (Hashimoto et al., 2025). Evidence of circadian pathway dynamics may help us find the the most promising targets for chronotherapy. However, optimal dosing time of drugs will not necessarily correspond to peak pathway activity (due to drug-specific pharmacokinetics and mechanisms of action), so optimising chronotherapy protocols will require integration of pharmacokinetic modelling with circadian pathway dynamics.

As an example, clock modulation of IFN signalling has implications for pathogen-specific treatment timing. Type I IFN is protective against some bacteria (e.g., *pneumococci*) but promotes infection by others (e.g., *Mycobacterium tuberculosis*) (Adler & Adler, 2021). Understanding how the macrophage clock regulates IFN responses by time of day may therefore inform pathogen-specific chronotherapy strategies. My findings suggest that in infections where type

I IFN is detrimental, pharmacological enhancement of BMAL1 activity (as seen with CCM treatment) could suppress IFN signalling and improve outcomes. In contrast, where infections require robust IFN responses, inhibiting BMAL1 through stabilisation of the negative arms of the clock (e.g., CRY stabilisation) could enhance IFN production.

6.2 Final conclusions

Overall, the data presented show:

- Circadian gating of macrophage inflammatory responses *in vivo* depends on the intrinsic macrophage clock, operating through TF activity rather than chromatin remodelling.
- REV-ERBα does not mediate the widespread effects of the clock modulating LPS responses.
- BMAL1 establishes IFN-primed baseline states in unstimulated macrophages at ZT12.
- Sex modulates the amplitude of BMAL1-dependent programs.
- The novel compound CCM recapitulates physiological macrophage-BMAL1 function, validating it as a tool for acute BMAL1 perturbation.

Together, these findings show that BMAL1 coordinates macrophage inflammatory readiness through broad regulation of TF programs, particularly the STAT/IRF axis, with sex-specific amplitude modulation, and demonstrate that this function can be pharmacologically recapitulated.

nature chemical biology

Article

https://doi.org/10.1038/s41589-025-01863-x

Pharmacological targeting of BMAL1 modulates circadian and immune pathways

Received: 24 March 2024

Accepted: 14 February 2025

Published online: 25 March 2025

Check for updates

Hua Pu[1], Laura C. Bailey[2,3], Ludwig G. Bauer[1,4], Maria Voronkov[2,3], Matthew Baxter[2,3], Kilian V. M. Huber[1,4], Sepideh Khorasanizadeh[1], David Ray[2,3] & Fraydoon Rastinejad[1]

The basic helix–loop–helix PER-ARNT-SIM (bHLH-PAS) proteins BMAL1 and CLOCK heterodimerize to form the master transcription factor governing rhythmic gene expression. Owing to connections between circadian regulation and numerous physiological pathways, targeting the BMAL1–CLOCK complex pharmacologically is an attractive entry point for intervening in circadian-related processes. In this study, we developed a small molecule, Core Circadian Modulator (CCM), that targets the cavity in the PASB domain of BMAL1, causing it to expand, leading to conformational changes in the PASB domain and altering the functions of BMAL1 as a transcription factor. Biochemical, structural and cellular investigations validate the high level of selectivity of CCM in engaging BMAL1, enabling direct access to BMAL1–CLOCK cellular activities. CCM induces dose-dependent alterations in PER2–Luc oscillations and orchestrates the downregulation of inflammatory and phagocytic pathways in macrophages. These findings collectively reveal that the BMAL1 protein architecture is inherently configured to enable the binding of chemical ligands for functional modulation.

Circadian rhythms, oscillations with an approximately 24-h period, govern a wide array of physiological and behavioral functions. At the cellular level, these rhythms are controlled by transcription–translation feedback loops (TTFLs)[1–5]. The central element of this circuitry involves brain and muscle arnt-like 1 (BMAL1, also known as ARNTL or MOP3) and circadian locomotor output cycles kaput (CLOCK), which heterodimerize to form a transcription factor[6–9]. BMAL1–CLOCK drives expression of two feedback loops. The first comprises *Periods* (*PER1–3*) and *Cryptochromes* (*CRY1/2*), which form complexes to repress the transcriptional activity of BMAL1–CLOCK. In addition, BMAL1–CLOCK transactivates nuclear receptor subfamily 1 group D (*NR1D1/2*, also known as *REV-ERBs*), and retinoic acid receptor–related orphan receptors (*RORs*), which compete to repress or activate *BMAL1* transcription, respectively[10–12]. The circadian clock is entrained to light cycles through a central pacemaker located in the suprachiasmatic nucleus, which is innervated from the retina, but the circadian TTFL clock in mammals is largely cell autonomous[13].

Circadian dysregulation has been implicated in a spectrum of diseases, spanning cardiometabolic disorders, psychiatric conditions, autoimmune diseases, cancers and neurodegenerative disorders[14–21]. Pharmacological interventions targeting circadian rhythms hold promise for addressing these disorders. Although small molecules targeting CLOCK, CRYs, RORs and REV-ERBs have been reported[22–25], the direct targeting of BMAL1 via a defined protein pocket has remained unexplored. Given its more central role in circadian regulation, the pharmacological targeting of the BMAL1–CLOCK complex could have broad-reaching effects beyond the core clock machinery. This approach offers an entry point to intervene in the fundamental transcription control underlying circadian processes while also facilitating deeper insights into the connections between circadian regulation and physiological pathways.

[1]Nuffield Department of Medicine, Target Discovery Institute, University of Oxford, Oxford, UK. [2]Radcliffe Department of Medicine, Oxford Centre for Diabetes, Endocrinology and Metabolism, University of Oxford, Oxford, UK. [3]NIHR Oxford Biomedical Research Centre, John Radcliffe Hospital, Oxford, UK. [4]Nuffield Department of Medicine, Centre for Medicines Discovery, University of Oxford, Oxford, UK. e-mail: fraydoon.rastinejad@ndm.ox.ac.uk

Within the TTFL circuitry, BMAL1 emerges as the only non-redundant component[6,26]. Although NPAS2 can partially compensate for CLOCK function in peripheral tissue clocks, BMAL1, particularly in mice, appears indispensable, with *BMAL2* expression reliant on BMAL1 (ref. 27). BMAL1, CLOCK and their paralogs all belong to the mammalian basic helix–loop–helix PER-ARNT-SIM (bHLH-PAS) family of transcription factors, where crystal structures of their bHLH–PASA–PASB segments have been described in some cases[2,28–32]. In the case of CLOCK, a previous study based on a docking approach identified the small molecule CLK8 binding to its bHLH segment[22].

Our previous work explored the internal pockets located in the PASA and PASB domains of mammalian bHLH-PAS transcription factors, including BMAL1–CLOCK, finding that those domains could accommodate small molecules[29]. Such pockets may have evolved to accommodate endogenous ligands, as shown for aryl-hydrocarbon receptor (AhR) and hypoxia-inducible factor-3alpha (HIF3α)[31,33,34]. Synthetic compounds can bidirectionally modulate the transcriptional activities of AhR and HIF2α through their PAS domain pockets[35–37]. In the present study, we focused on the BMAL1 PASB domain (referred to as BMAL1(PASB)) to identify a ligand and evaluate whether the pocket could be leveraged to modulate BMAL1–CLOCK transcriptional activities.

Results

Compound discovery, engagement and selectivity studies

Using recombinant human BMAL1(PASB) protein and a high-throughput protein thermal shift (PTS) assay, which measures changes in protein stability in response to ligand binding[38], we identified an initial hit (designated hit01, **1**) within our fragment libraries that showed promising evidence of direct binding. The screening results are contained in Supplementary Data 1. Subsequently, through hit expansion and hit-to-lead optimization, we obtained analog 190 (A190, **2**) and analog 304 (A304, **3**). Based on the structure–activity relationship, we then developed a more potent lead compound, Core Circadian Modulator (CCM, **4**) (Fig. 1a and Extended Data Fig. 1a,b). The nuclear magnetic resonance (NMR) peak listings of compounds A190, A304 and CCM are provided in the Methods section; the quality control information (NMR and mass spectrometry (MS)) and purity assessments (by high-performance liquid chromatography (HPLC)) are in Supplementary Figs. 1–3; and syntheses are described in Supplementary Fig. 4. CCM binding significantly stabilizes BMAL1(PASB) protein, as evidenced by an increased melting temperature (Tm value) of 9.7 °C, demonstrating saturable dose-dependent binding (Fig. 1b and Extended Data Fig. 1a).

We confirmed the direct binding of CCM to BMAL1(PASB) through multiple methods, including isothermal titration calorimetry (ITC). Figure 1c shows that the binding process is enthalpically driven, with an ΔH of −29.67 ± 0.826 kJ mol^{-1} and a ΔG of −31.99 kJ mol^{-1}. Entropy ($\Delta S = 7.924$ J (mol·K)$^{-1}$) contributes only 7.3% to the Gibbs free energy. The equilibrium binding constant (K_d) measured was 1.99 ± 0.38 μM. Additionally, surface plasmon resonance (SPR) studies shown in Fig. 1d and Extended Data Fig. 1c corroborated this finding, revealing a similar K_d of 4 μM. The results from PTS, ITC and SPR established the thermodynamic basis for robust binding of CCM to the BMAL1(PASB) protein.

To determine the engagement of CCM with BMAL1 within cells, we used a BMAL1(PASB) construct with a HiBiT tag on its N-terminus and expressed it in HEK293T cells. This construct enabled the use of a cellular thermal shift assay (CETSA) to examine the dose-dependent binding and thermal stabilization of BMAL1 by CCM in the context of cellular proteins, employing split Nano Luciferase methodology[39]. Our findings revealed that CCM increased the thermal denaturation temperature of BMAL1(PASB) by 9 °C at 200 μM (Fig. 1e, left). This thermal stabilization exhibited dose dependency, with a half-maximal effective concentration (EC_{50}) value of 10.3 μM (Fig. 1e, right), in line with the biochemical binding affinity (K_d) range of 2–4 μM described earlier (Fig. 1c,d).

To validate that CCM binding was responsible for the cellular thermal stabilization of BMAL1, we used a BMAL1(PASB) construct with mutations replacing Tyr340 and Tyr404 with phenylalanine. These tyrosines were chosen based on their positions within our crystallographic complex with CCM, as discussed in the subsequent section. When using the double mutant, we observed no CCM-induced thermal stabilization in the mammalian cell CETSA experiment with HiBiT–BMAL1(PASB) (Fig. 1e and Extended Data Fig. 2a–c). Therefore, these internal cavity tyrosines play a crucial role in mediating the high degree of specificity for CCM binding to BMAL1(PASB).

After establishing that CCM directly engages BMAL1(PASB) in the context of whole U2OS cell proteome, we sought to evaluate the binding selectivity of CCM for BMAL1 compared to BMAL2 and other closely related PASB domains, including those of aryl hydrocarbon receptor nuclear translocator (ARNT), ARNT2 and the BMAL1 (PASA). We conducted additional CETSA studies and found no detectable binding to these PAS domains (Extended Data Fig. 2d,e).

To evaluate the proteome-wide target landscape of CCM, we conducted thermal profiling using quantitative MS in U2OS cell lysate[40,41]. Employing CCM concentrations of 50 μM and 200 μM, which are well above the K_d required for BMAL1(PASB) target engagement, allowed us to identify potential off-targets, including those with weak binding to CCM (Fig. 1f and Extended Data Fig. 2f). Encouragingly, very few proteins exhibited notable thermal stabilization in response to CCM, none of which is known to be involved in circadian control. As a positive control, HiBiT–BMAL1(PASB) itself showed clear evidence of CCM binding in the same cells (Fig. 1g). These data suggest that CCM displays a high degree of selectivity for BMAL1(PASB). Endogenous BMAL1 protein was not detected in these cells because of its low abundance. We also cannot exclude other potential off-targets, if their low abundance prevented their detection in this experiment.

Ligand binding site and induced conformational shifts

To visualize how CCM binds to human BMAL1(PASB), we used crystals of this protein for X-ray diffraction studies, resulting in refined structures at 1.83-Å resolution for the ligand-free (apo) state and 2.16-Å resolution for the CCM-bound BMAL1(PASB) complex. Details of the crystallographic data are in Extended Data Table 1. CCM occupies the central pocket in the BMAL1 PASB domain (Fig. 2a). In the apo structure, the central cavity houses three water molecules that interact with each other and residues Tyr340, His344, Tyr404, Ser436 and Asn438 (Fig. 2b and Extended Data Fig. 3a). Upon CCM binding, these water molecules are displaced, creating room for the compound's 2-fluoropropanol tail moiety ('tail') (Fig. 2b). The tail's primary hydroxyl group forms hydrogen bonds with residues engaged in stabilizing the water molecules in the apo structure. Trp420 and the surrounding residues create a favorable space to accommodate the benzofuran moiety of CCM. Replacing the benzene ring of hit01 with a benzofuran in CCM enables the additional π–π interactions with Tyr374 and His389, accounting for the latter's improved binding affinity. The ethyl group and the fluorine atom of CCM, absent in A190 and A304, respectively, each occupy a small cavity in Bmal1(PASB), thereby enhancing binding affinity.

CCM features a chiral center at the C2 position of its tail. While the rigid benzofuran moiety of CCM remains stationary, the tail exhibits both *S* and *R* configurations within the pocket, binding in slightly different modes (Fig. 2b and Extended Data Fig. 3b,c). Comparison of the apo and CCM-bound structures reveals overall and locally induced changes. When looking at the details of protein, repositioning of several side chains and shifts in portions of the main chain can be found (Fig. 2c and Extended Data Fig. 3d,e). These movements include displacing His389 and shifting the position of the αF helix, where His389 is located. Induced repositioning of those and other amino acids by CCM expands the volume of the resident PASB pocket three-fold (Fig. 2d).

Our structural analysis of the interactions of CCM within the pocket explains its selective binding affinity for BMAL1(PASB) over

https://doi.org/10.1038/s41589-025-01863-x

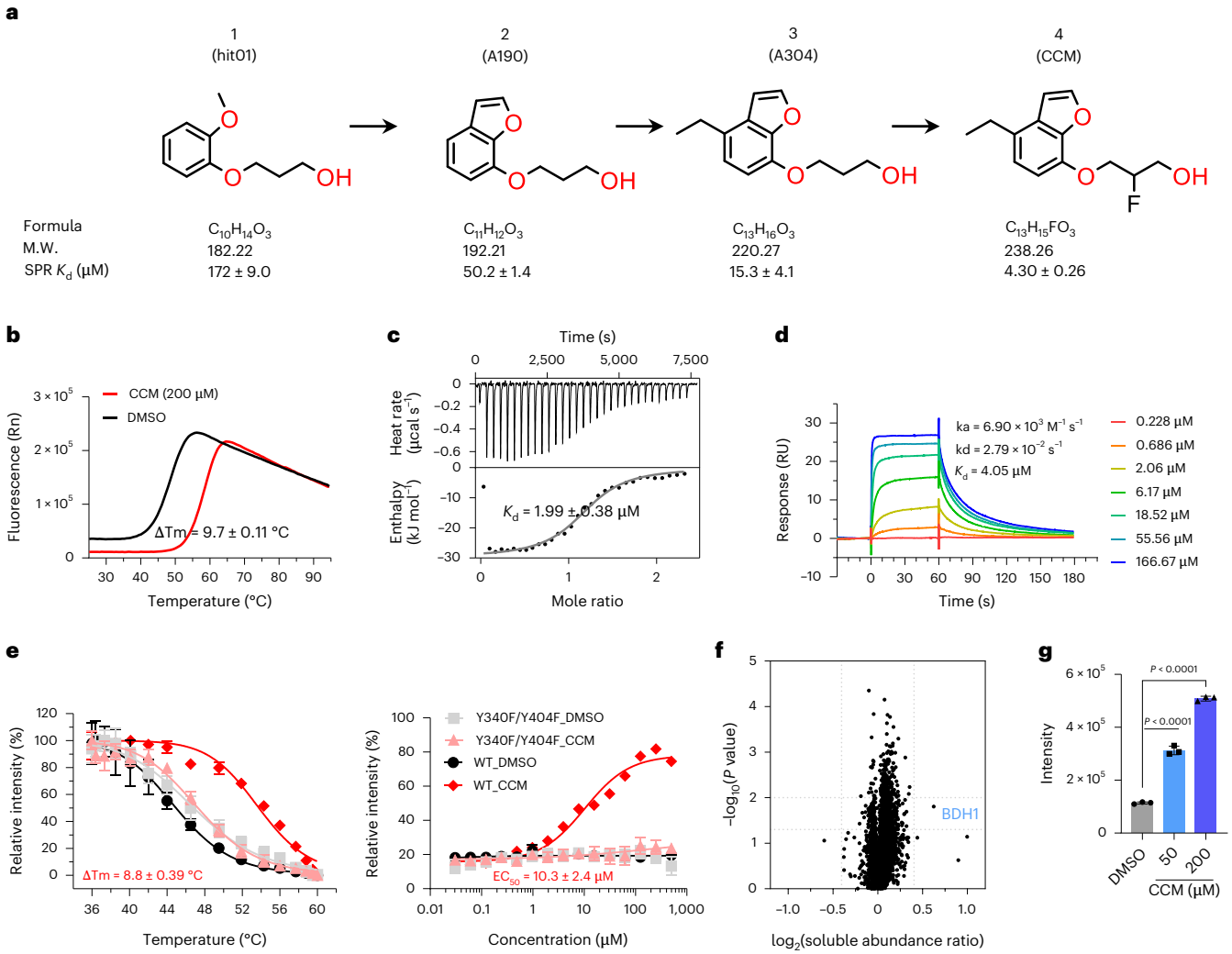

Fig. 1 | Characterization of CCM binding to human BMAL1(PASB). a, Hit-to-lead optimization of BMAL1 ligand. The K_d values for SPR were determined using equilibrium analysis. **b**, CCM enhances the Tm of hBMAL1(PASB) by 9.7 °C in a PTS assay. **c**, ITC detects CCM binding to hBMAL1(PASB) protein with K_d of 1.99 ± 0.38 μM, stoichiometry (n) value of 1.201 ± 0.028 and enthalpy (ΔH) of −29.67 ± 0.826 (kJ mol^{-1}). **d**, SPR demonstrates the binding of CCM to hBMAL1(PASB) with affinity of 4.05 μM calculated from kinetic analysis. **e**, CCM stabilizes WT hBMAL1(PASB) but not Y340F/Y404F double mutant in CETSA (left). Isothermal dose–response curves of the effects of CCM on both WT and double mutant at 48 °C to obtain EC_{50} values reveal key residues necessary for compound stabilization (right). Four technical replicates were applied. Data are presented as mean values ± s.d. **f**, Volcano plot displays the thermal profile of the U2OS proteome with CCM treatment (50 μM) compared to DMSO treatment. U2OS cell lysate (n = 3) was heated at a temperature gradient (37–60.9 °C) for 3 min, and then denatured proteins were removed by centrifugation. The combined stabilization of the proteins in the supernatant across the heat gradient was detected by MS. The P value was generated by two-tailed t-test. **g**, CCM stabilization of HiBiT–hBMAL1(PASB) in the same U2OS cells as in **f**. The y axis shows its remaining protein levels after heating/denaturation steps, detected via the intensity of the Nano-Glo HiBiT signal. Error bars denote the mean ± s.d., and unpaired two-tailed t-test was used for statistical analyses. M.W., molecular weight; Rn, normalized reporter value.

highly related PASB domains. For instance, the lack of conservation in residues Tyr340 and His344 in BMAL2(PASB) explains the lack of binding (Extended Data Fig. 4a,b). Similarly, the absence of conserved residues Trp420, Tyr374 and His389 in ARNT(PASB) and ARNT2(PASB), which recognize CCM's benzofuran group, explains the inability to bind CCM (Extended Data Fig. 4a,b). Additionally, more substantial amino acid differences between BMAL1's PASA and PASB account for the lack of binding to the PASA domain.

The effects of CCM on peripheral clock components

Our biochemical and cellular findings position CCM as a highly specific pharmacological tool for understanding the consequences of targeting this pocket in BMAL1–CLOCK functions. To assess the impact of CCM on known downstream targets within the TTFL circuitry, we conducted quantitative reverse transcription polymerase chain reaction (RT–qPCR) analysis in U2OS cells. All primers are listed in Supplementary Table 1. CCM treatment resulted in decreased expression levels of core TTFL components *CRY1*, *CRY2*, *PER2* and *PER3* while modestly increasing levels of *NR1D1*, *RORA* and *RORB* (Fig. 3a). However, *PER1*, *NR1D2* and *RORC* levels showed no significant changes with CCM treatment. Notably, the expression level of *BMAL1* itself remained unchanged after CCM treatment.

We observed dose-dependent reductions in the expression of certain BMAL1 target genes, exemplified by *CRY1* and *PER2* in Fig. 3b. Knocking down *BMAL1* attenuated the effects of CCM on these target genes (Fig. 3c), supporting the mechanism of action for requiring BMAL1. Furthermore, we compared the overall gene expression patterns induced by CCM with those resulting from *BMAL1* small

https://doi.org/10.1038/s41589-025-01863-x

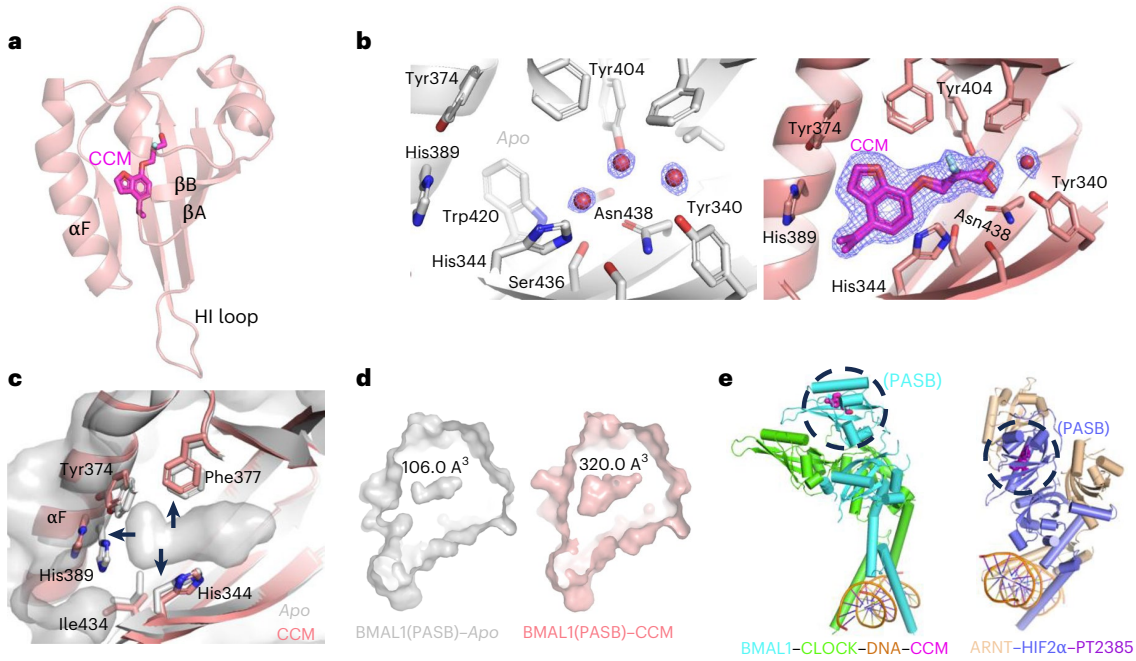

Fig. 2 | Structural basis for CCM binding to human Bmal1(PASB) and induced conformational changes. a, Crystal structure of BMAL1(PASB) in complex with CCM. **b**, Electron density maps in the central cavity of BMAL1(PASB), showing three water molecules in the apo structure (left) and the CCM molecule bound in the complex (right). The *R* versus *S* isomers of CCM are shown together. **c**, CCM binding repositions residues in BMAL1(PASB). **d**, CCM expands the central pocket volume three-fold. The accessible cavity size (when CCM is removed in the complex and waters are removed in the apo structure) was calculated in PyMol with PvVOL. **e**, Location of PASB domains of BMAL1 and HIF2α in their respective complexes. Structures used here are from PDB IDs 4F3L, 4H10, 4ZPK and 6E3S. The position of CCM in the complex was added manually based on the BMAL1(PAS) complex structure determined in this study.

interfering RNA (siRNA) knockdown in the same cells (Fig. 3a). The BMAL1 and CLOCK siRNA was validated by western blot (Fig. 3d). Interestingly, the impact of CCM across these genes was distinct from the effects of *BMAL1* knockdown. Examples include *CRY1* and *CRY2*, which are increased with knockdown of *BMAL1* but decrease with CCM. Examples further include *NR1D1*, which is reduced with knockdown but increased with CCM (Fig. 3a).

Although the preceding experiments exclusively assessed CCM-induced alterations in gene expression in unsynchronized cells, we considered that CCM might also affect the amplitude and/or periods of gene expression patterns. To evaluate these potential effects on circadian gene expression patterns, we initially used synchronized peritoneal macrophages directly isolated from Per2–Luc mice. CCM significantly modified the amplitude, period and phase of the core circadian oscillator in a distinctly dose-dependent manner (Fig. 3e and Extended Data Fig. 5a). Most noteworthy were the pronounced effects on amplitude of oscillations, which were not attributable to any toxicity effects from CCM (Fig. 3e,f).

After dexamethasone-induced synchronization, we examined the CCM broader impact on circadian genes in the U2OS cell line using RT–qPCR. CCM reduced the amplitudes of *CRY1*, *CRY2*, *PER2* and *PER3* gene expression oscillations (Fig. 3g), consistent with our findings of reduced overall levels of *CRY1/2* and *PER2/3* expressions in unsynchronized cells. Interestingly, the effects of CCM remained selective for gene targets, as shown by the relatively minor changes in the cyclical expressions of other genes (Extended Data Fig. 5b).

The effects of CCM on the macrophage gene expression signature

Numerous immune cell types, including macrophages, monocytes and neutrophils, have intrinsic circadian clock-regulated activities[42–44]. Macrophages, in particular, harbor a robust endogenous clock closely tied to their inflammatory signaling pathways[45]. Previous research demonstrated that deletion of the core clock protein BMAL1 heightened macrophage immune functions, indicating that BMAL is an immune system regulator governing phagocytic responses after infection[45]. The amino acid sequence identity of mouse and human full-length BMAL1 is 97%, and, for the BMAL1(PASB) portion, the identity is 100%. Therefore, the compound is expected to be equally effective when used with mouse macrophages as with human-derived cell lines.

In pursuit of a comprehensive understanding of the effects of CCM on macrophage gene expression under both basal and stimulated conditions, we employed an unbiased approach using purified bone marrow–derived macrophages (BMDMs) and RNA sequencing (RNA-seq) analysis (Fig. 4a). Under unstimulated conditions, CCM addition resulted in minimal alterations in gene expression, with only a limited number of genes showing statistical significance. Notably, among these genes was *NPAS4*, previously implicated in photonic entrainment and circadian behavior in mice[46]. However, upon stimulation of macrophages with lipopolysaccharide (LPS), the effects of CCM were significantly amplified, leading to a broader spectrum of gene expression changes. In this context, CCM inhibited a greater number of genes than it stimulated (Fig. 4a). In phenotypic evaluation, CCM alone does not have significant effect on macrophages, but CCM treatment could partially revert the gene expression profile of LPS-treated cells (M1) toward the baseline profile of vehicle-treated controls (M0) (Extended Data Fig. 6).

Although our CETSA mass spectrometric studies in U2OS cells suggested very few potential off-targets for CCM in that cell type, we seized the opportunity to further evaluate the target selectivity of CCM in macrophages. By comparing the effects of CCM on primary macrophages from wild-type (WT) mice versus BMAL1-null (*LysM-*$^{Bmal1-/-}$) mice, we observed extensive regulation of multiple genes in WT macrophages, whereas a considerably smaller set of genes was affected in BMAL1-null mice, highlighting substantial target selectivity (Fig. 4b).

https://doi.org/10.1038/s41589-025-01863-x

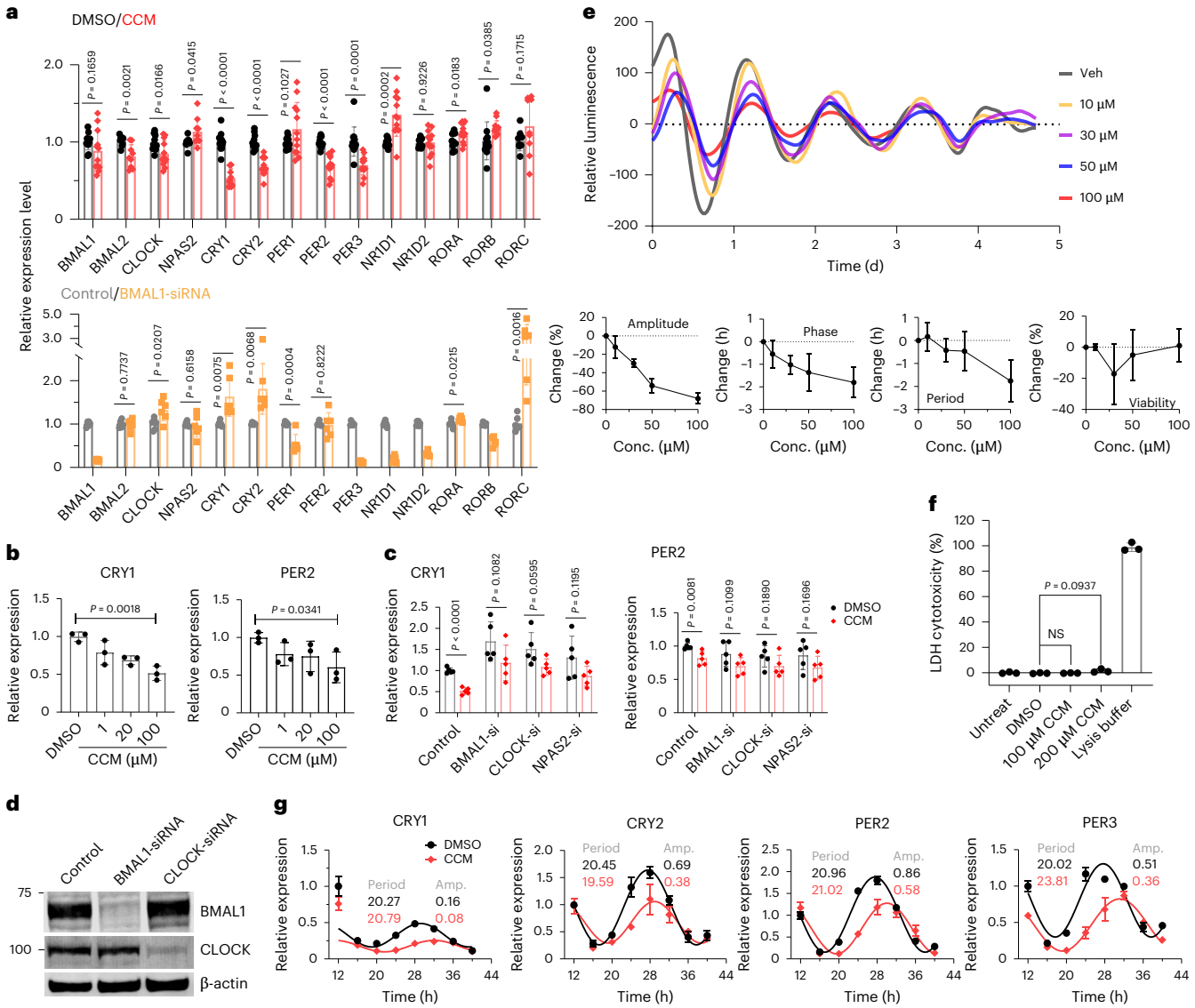

Fig. 3 | CCM modulation of BMAL1–CLOCK target gene expressions. a, Effect of CCM (100 μM) on target genes compared to BMAL1 knockdown. The RNA levels of BMAL1 target genes were quantified by RT–qPCR in unsynchronized U2OS cells. Six and 12 biological replicates were used for knockdown and CCM treatment, respectively. **b**, Dose-dependent effects of CCM on BMAL1 target genes in unsynchronized U2OS cells ($n = 3$, biological replicates). **c**, The effects of CCM (100 μM) are impaired when BMAL1, CLOCK or NPAS2 is knocked down in unsynchronized U2OS cells ($n = 5$, biological replicates). **d**, Validation of BMAL1 and CLOCK siRNAs by confirming reduction in their protein levels in U2OS cells. This experiment was performed independently two times with similar results. **e**, CCM dose-dependent modulation of real-time circadian rhythm observed in peritoneal macrophages directly isolated from Per2–Luc (PER2::Luc) mice (synchronized, $n = 3$–6). **f**, CCM demonstrates no significant cytotoxicity on U2OS cells ($n = 3$, biological replicates) at concentrations of 100 μM and 200 μM for 48 h. The lysis buffer provided in the CyQUANT LDH Cytotoxicity Assay Kit was used as a positive control. **g**, Monitoring of the circadian rhythm in synchronized U2OS cells ($n = 3$, biological replicates) using RT–qPCR, showing differences between DMSO vehicle (black) and 100 μM CCM treatment (red). All error bars (**a**–**c** and **e**–**g**) denote the mean ± s.d. Statistical tests were performed using unpaired two-tailed *t*-test. Amp., amplitude; Conc., concentration; NS, not significant; Veh, vehicle; RLU, relative luminescence.

The limited effects observed in the knockout (KO) macrophages may stem from incomplete penetrance of the gene deletion or limited off-target actions.

Upon conducting Gene Ontology analysis of the effect of CCM on BMAL1-dependent genes, we observed enrichment in functions associated with inflammation and plasma membrane processes (Fig. 4b). Given the pivotal role of phagocytosis for macrophage immune function, and its established reliance on BMAL1, our focus shifted to a selection of BMAL1 target genes associated with phagocytosis (Fig. 4c). Remarkably, CCM significantly suppressed most genes within this panel, indicating a gain of BMAL1 anti-infection function. These findings underscore the potency of CCM as a modulator of BMAL1–CLOCK activities, particularly impacting inflammatory and phagocytic pathways, and provide insights into the pharmacological implications of targeting BMAL1 within established pathways in macrophages.

We then analyzed the differences in splicing events that arise due to CCM (versus DMSO vehicle) across unstimulated and LPS conditions, transcriptome wide, to see if CCM altered transcriptional dynamics. We observed that CCM caused a dramatic increase in alternative splicing in macrophages (Extended Data Table 2). Exon skipping was identified as the predominant feature. These events were observed in WT, but not KO, cells, indicating that they are driven by BMAL1.

https://doi.org/10.1038/s41589-025-01863-x

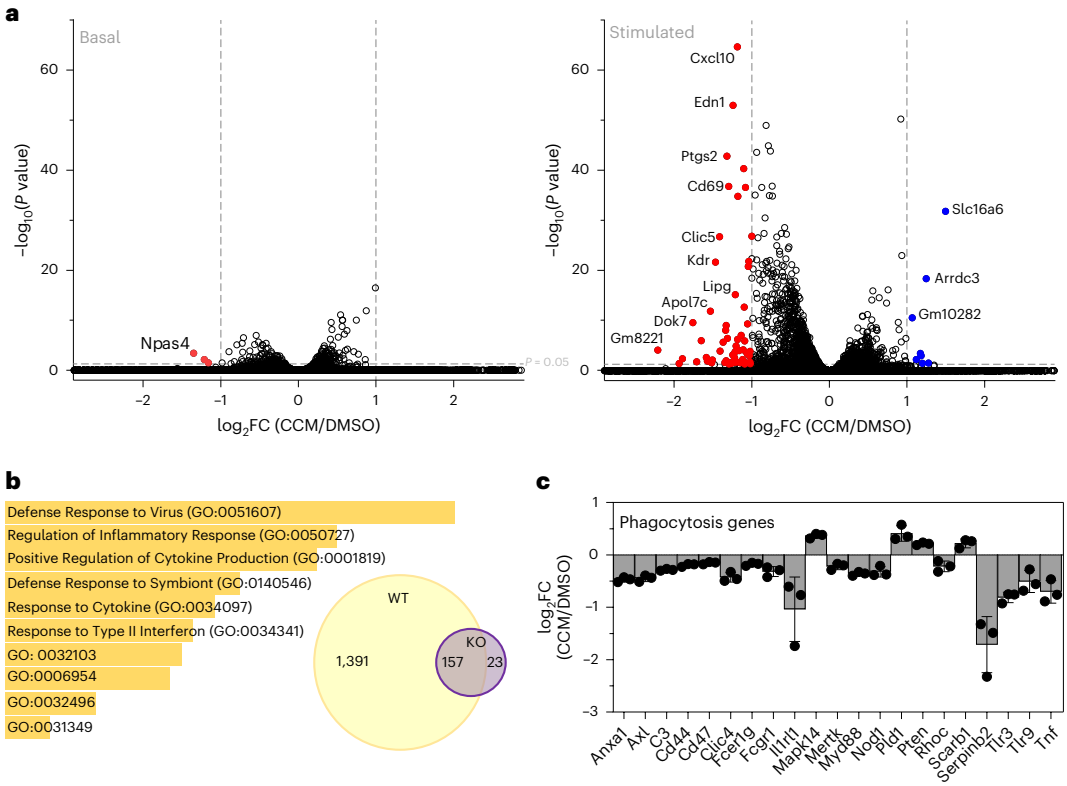

Fig. 4 | Effect of CCM treatment on macrophage gene expression signature. **a**, Volcano plots display differentially expressed genes resulting from CCM treatment in WT BMDMs in both basal and stimulated states (from treatment with LPS). Female mice were used for all conditions ($n = 3$, WT; $n = 6$, KO). Differential expression analysis used DESeq2, and P values were adjusted for multiple comparisons using the Benjamini–Hochberg procedure to control for FDRs. **b**, Gene Ontology (GO) for the 1,391 genes modulated by CCM in WT-stimulated macrophages. The inserted Venn diagram shows the numbers of genes regulated in the WT-stimulated macrophages, intersecting with the genes regulated in the BMAL1-KO-stimulated macrophages. **c**, Genes involved in phagocytosis are predominantly downregulated by CCM in macrophages ($n = 3$, biological replicates). Data are presented as mean values ± s.d. FC, fold change.

CCM's mechanism of action

We began our initial investigations into the mechanisms of action for CCM by drawing from the known effects of other bHLH-PAS protein modulators. The HIF2α antagonist PT2385 uses a mechanism of action by which it allosterically impacts a crucial interaction site in HIF2α for binding to ARNT, leading to reduced heterodimer stability, inhibition of target genes and impaired ventilatory responses to hypoxia[28,35,47]. However, the positions of the PASB domains in BMAL1 and HIF2α within their respective heterodimeric complexes are varied (Fig. 2e). BMAL1's PASB domain is situated within the crystallographically defined BMAL1–CLOCK triple domain heterodimer at the outer perimeter of the six-domain heterodimer[2]. This positioning limits the impact of CCM on overall heterodimerization stability of BMAL1–CLOCK. In contrast, the HIF2α (PASB) domain is centrally located within the HIF2α–ARNT heterodimer, facilitating PT2385-induced structural changes that reduce heterodimer stability[28,35] In addition, our structural observations show that CCM binding does not induce alteration of BMAL1(PASB) HI-loop, responsible for interacting with the CLOCK protein (Extended Data Fig. 3e). This finding implies that the impact of CCM on the stability of the BMAL1–CLOCK heterodimer would be limited, differing from the mechanism of action of PT2385. Co-immunoprecipitation (co-IP) studies validated this expectation, confirming that CCM does not impact BMAL1–CLOCK heterodimerization in cells (Fig. 5a and Supplementary Fig. 5a,b).

We also considered several known mechanisms of action for AhR synthetic agonists and antagonists[48,49]. Small molecules interacting at the PASB domain of AhR can disrupt its binding to cytoplasmic heat shock complexes, leading to the translocation of AhR into the nucleus[33,50]. Unlike AhR, BMAL1 is not known to interact with cytoplasmic chaperone complexes. Nevertheless, we investigated whether CCM might affect the cellular distribution of BMAL1. We isolated cytosolic and nuclear fractions from U2OS cells treated with either DMSO or CCM and conducted western blot analysis. Our results showed no noticeable difference in the distribution of BMAL1 protein between compartments, with BMAL1 being predominantly located in the nuclear fraction (Fig. 5b). Furthermore, analysis of the overall cellular levels of BMAL1 protein after 2 h and 24 h of CCM treatment also revealed no significant changes (Fig. 5c).

Our structural analysis revealed that CCM-induced conformational shifts in BMAL1(PASB) include a repositioning of αF and the amino acid Gln379 (Fig. 5d). Residue Gln379 (equivalent to Gln385 in mouse BMAL1) was identified as a key contact site between BMAL1 and core histones of nucleosomes[51]. The functional significance of this residue was further validated by a mutation at this site, which altered PER2–Luc circadian oscillations, consistent with cryogenic electron microscopy (cryo-EM) studies, indicating its role in BMAL1–CLOCK-dependent chromatin opening[51] for dynamic chromatin alterations necessary for transcriptional regulation[52]. BMAL1 was described previously as a pioneer transcription factor[52].

To gain deeper insights into the mechanism of action, we set out to explore how CCM binding impacts BMAL1 interactions proteome wide. We took an unbiased approach, employing rapid immunoprecipitation mass spectrometry of endogenous proteins (RIME) to identify all interactions of the endogenous BMAL1 in U2OS cells (Fig. 5e). RIME is particularly suited for the study of chromatin and transcription factor complexes in a rapid and robust manner by MS[53]. Nuclei extracted

https://doi.org/10.1038/s41589-025-01863-x

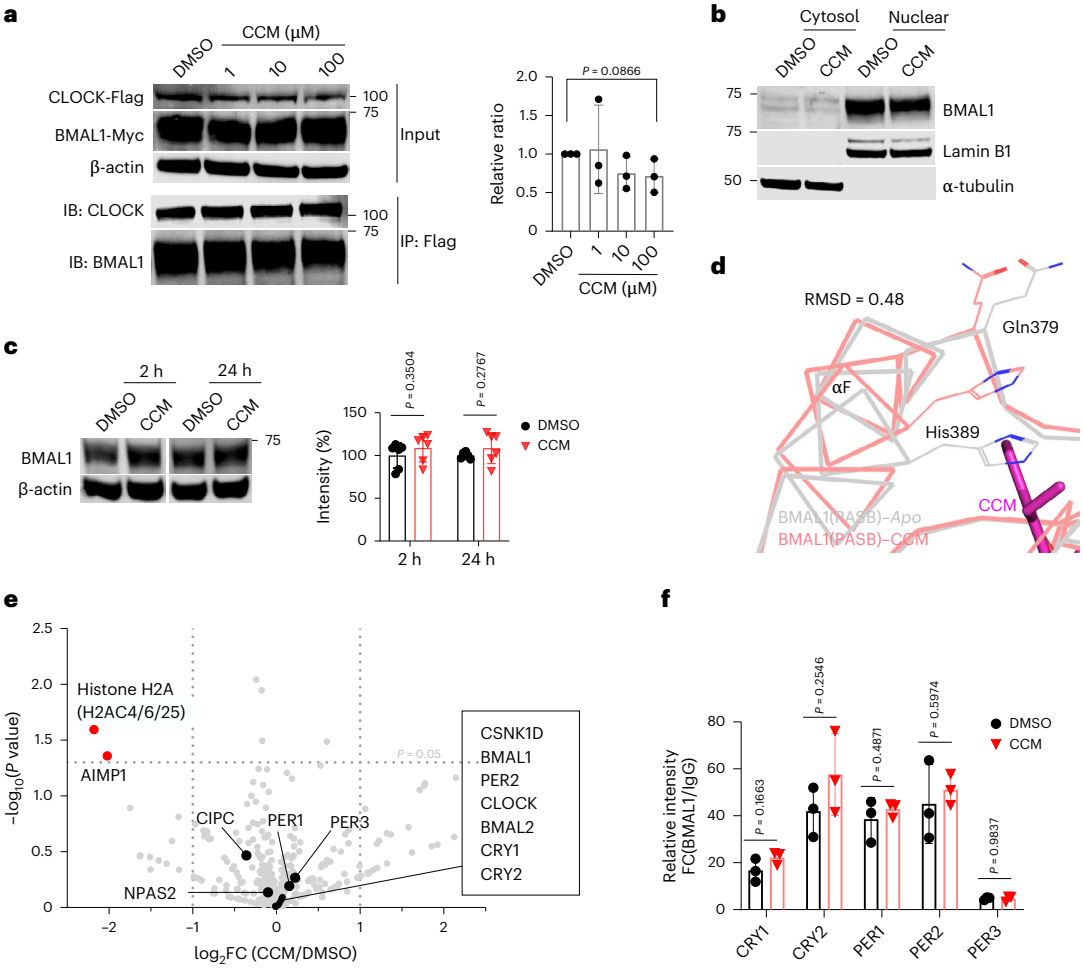

Fig. 5 | Mechanism of action studies. a, Co-IP studies between BMAL1 and CLOCK in U2OS cells ($n = 3$, biological replicates), demonstrating minimal effect of CCM on the stability of their complex. The ratio of BMAL1/CLOCK intensity in each IP sample was calculated and then normalized to DMSO control for each independent experiment. Three independent experiments were integrated for statistical analysis. Error bars denote the mean values ± s.d., and *P* value was generated by unpaired two-tailed *t*-test. **b**, BMAL1 localization in the nucleus of U2OS cells remains unchanged, with no observed alterations in the distribution of cytosolic versus nuclear levels after 3 h of CCM treatment at 100 μM. This experiment was performed independently two times with similar results. **c**, Overall BMAL1 protein levels in U2OS cells ($n = 6$, biological replicates), as detected by western blot, also remain unaltered after CCM treatment at 100 μM (left). BMAL1/β-actin intensity ratio was quantified (right). **d**, The PASB α-helix F and amino acids positioned on this helix, His389 and Gln379, shift positions with CCM binding. **e**, CCM weakens the association of histone H2A with BMAL1. Protein interactions of BMAL1 were analyzed by RIME. U2OS cells ($n = 3$) were treated with 100 μM CCM or 0.1% DMSO for 3 h. **f**, CCM does not change the binding of BMAL1 to the promotor of corresponding genes in U2OS cells ($n = 3$, biological replicates) detected by ChIP–qPCR. Error bars in **a**, **c** and **f** are presented as mean values ± s.d., and statistical tests were performed using unpaired two-tailed *t*-test. FC, fold change; RMSD, root mean square deviation.

from U2OS cells were lysed by sonication, and protein complexes were immunoprecipitated by anti-BMAL1 antibody or rabbit IgG. In total, 54 unique peptides were identified for BMAL1 with a sequence coverage of 71.2%. A total of 366 proteins were quantified in MS, including known BMAL1 binding proteins such as CLOCK, NPAS2, PERs and CRYs, validating the specificity of the RIME study. The interaction between BMAL1 and CLOCK proteins was not affected by CCM treatment, which confirms co-IP data in Fig. 5a.

Other known interactions with BMAL1, such as NAPS2, CRYs and PERs, also remain intact. Few proteins showed significant fold changes between CCM treatment and DMSO control (Fig. 5e). Among these, histone H2A type 1-C or 1-B/E or type 3 (H2AC6/4/25) showed the most significant change (fold change = 0.21, $P = 0.021$). We performed chromatin immunoprecipitation (ChIP) assay studies to examine the binding of BMAL1 to the promotors of CRY1/2 and PER1/2/3. As shown in Fig. 5f and Extended Data Fig. 7, CCM did not markedly alter the binding of BMAL1 protein to these sites.

Discussion

Our studies introduce a straightforward approach to pharmacologically target the master circadian clock transcription factor comprising the central node of the TTFL, by leveraging a resident pocket in the BMAL1 PASB domain. Through complementary studies, including high-resolution structural visualization, we demonstrated that CCM exhibits direct binding to the BMAL1(PASB) pocket. The structural analysis provided a precise understanding of CCM binding mode and induced conformational changes in the protein architecture. These insights should guide future efforts in discovering and optimizing circadian modulators. The development of pharmacological tools to manipulate BMAL1 functions offers opportunities to explore its role in cellular and physiological pathways. Unlike BMAL1 knockdown, CCM treatment preserves BMAL1 protein levels while modulating its transcriptional activity as a pioneer factor. Crucially, our findings reveal that BMAL1 is inherently capable of functional modulation through the direct binding of a compound.

Our assessments of BMAL1 binding specificity consistently demonstrated a very high degree of target selectivity for CCM across various testing platforms, including proteome-wide studies. Structural comparisons of pockets among BMAL1, BMAL2, ARNT and ARNT2 revealed differences at key positions crucial for CCM binding to BMAL1, thus explaining its robust targeting. Further evaluation of CCM's potential targets across the cellular proteome was essential for clarifying the connection between CCM's binding to BMAL1 and the observed cellular effects reported here.

Exploring the impact of CCM on circadian rhythm regulation revealed key insights about the unique pharmacological consequences of harnessing the BMAL1 pocket. Unlike conventional agonists or antagonists previously discovered for the related bHLH-PAS transcription factors AhR and HIF2α, the effects of CCM through the PASB pocket of BMAL1 extend beyond binary classification, influencing circadian parameters in a gene-selective manner. Notably, the effects of CCM on target genes also did not align with observed effects of BMAL1 knockdown in the same cells, suggesting distinct regulatory mechanisms at play. For example, with BMAL1 knockdown, RNA levels of REV-ERBs (NR1D1 and NR1D2) decreased dramatically, whereas RORC increased. In contrast, CCM did not comparably change the levels of REV-ERBs or RORC. Similarly, for CRY1 and CRY2, BMAL1 knockdown increased their expression levels, whereas CCM treatment reduced them. The divergence between the effects of gene knockdown and pharmacological manipulation of BMAL1 can be partly attributed to feedback loops responding differently to the loss of BMAL1 protein level compared to the pharmacological modulation of its transcriptional activities, which occurs without changes in BMAL1 protein level. The compound likely affects BMAL1 chromatin function, as BMAL1 is known to be a pioneer transcription factor[52]. Together with CLOCK, it can engage nucleosomal DNA using critical interactions between the PAS domains and the core histones in the nucleosome. Changes in BMAL1 chromatin function resulting from CCM binding may manifest as alterations in histone binding, elongation dynamics and RNA alternative splicing.

Our findings also show that the binding pocket of the PASB domain exhibits remarkable adaptability, undergoing considerable expansion when binding to CCM. This expansion accompanies an induced shift in the αF helix, which is a crucial site for BMAL1–CLOCK chromatin binding. Rhythmic BMAL1–CLOCK chromatin binding and opening are known to be essential for circadian gene expression[52]. Our investigations into the effects of CCM on BMAL1 nuclear and cytoplasmic distribution, protein levels or heterodimerization with CLOCK ruled out these alternative modes of action. The RIME studies further confirmed that CCM did not alter BMAL1 interactions with CLOCK, CRYs and PERs, which are among its known cellular interaction partners.

Our RIME findings showed that CCM impacted interactions between BMAL1 and histone H2A. This result emerged from an unbiased proteomic experiment designed to identify protein candidates whose interactions with BMAL1 were altered by CCM. This finding aligns with structural observations, which demonstrated that, when CCM binds to the PASB domain of BMAL1, it induces a structural shift in the region of the protein used for chromatin binding. The outcome from the RIME study supports earlier cryo-EM studies and mutagenesis studies of Q379, which revealed that the PAS domain of BMAL1 is involved in chromatin interactions. These findings offer a coherent mechanism by which CCM influences gene expression patterns through its effects on the PASB domain's structure and its subsequent impact on chromatin interactions. The effects of CCM were notably pronounced in reducing expression patterns and circadian amplitudes of genes strictly located inside the core circuitry, namely CRY1/2 and PER2/3.

ChIP data revealed that CCM did not substantially alter the binding of BMAL1 to its PER and CRY DNA elements. However, CCM binding led to a dramatic increase in BMAL1-dependent exon skipping events. Splicing is physically coupled to transcription and influenced by transcript elongation rates[54,55]. Exon skipping serves as an indicator of changes in overall transcriptional dynamics, suggesting that BMAL1 function may have shifted even though its DNA binding remains unchanged. Transcription factors are known to affect elongation dynamics, thereby altering splicing outcomes, such as exon skipping. There are well-established connections between chromatin regulation and RNA alternative splicing, with chromatin structure, nucleosome positioning and histones playing key roles in providing a dynamic scaffold for transcription and splicing[56,57].

Circadian rhythms play a fundamental role in regulating numerous physiological processes, including sleep–wake cycles, hormone secretion, metabolism and immune function. Disruptions of these rhythms, whether due to genetic mutations, shift work, jet lag or lifestyle factors, are linked to numerous human diseases and health conditions. In particular, circadian amplitude has gained attention as important for healthy energy metabolism[58] and also for intact innate immunity[59]. Aging is associated with loss of the circadian variation in macrophage phagocytic function[59]. It is likely that changes in circadian amplitude result in changes in the proportion of downstream gene targets that are captured by the circadian oscillator, resulting in altered physiology. However, the precise role of and importance of circadian amplitude remains undetermined. While our data suggest that anti-inflammatory benefits could be derived from CCM-mediated BMAL1–CLOCK pharmacological modulation, the wider set of associations between circadian disruptions and human diseases underscores the potential benefits of BMAL1–CLOCK-directed modulators.

The mechanism of action of CCM is clearly distinguished from the previously mentioned compound CLK8, which interacts with the bHLH domain of the CLOCK protein and represses the translocation of CLOCK from cytosol to nucleus[22]. Future compounds targeting BMAL1 with improved pharmacokinetics, particularly with enhanced blood–brain barrier penetration in mice, should allow for the probing of connections between pharmacological BMAL1 manipulation and alterations in whole-animal physiological responses and behaviors. Such advancements will deepen understanding of circadian regulation and drive the development of translational clock modulators. Our findings of a modulatory pocket located within the BMAL1 protein architecture also suggest that endogenous cellular ligands could impact and align the central and peripheral functions of BMAL1–CLOCK, potentially influencing circadian parameters and their synchronizations with other signaling pathways. In this context, BMAL1 and its broader bHLH-PAS transcription factor family may be likened to nuclear receptors[60–62], with resident pockets that are configured for sensing and responding to environmental and cellular ligands.

Online content

Any methods, additional references, Nature Portfolio reporting summaries, source data, extended data, supplementary information, acknowledgements, peer review information; details of author contributions and competing interests; and statements of data and code availability are available at https://doi.org/10.1038/s41589-025-01863-x.

References

1. Reppert, S. M. & Weaver, D. R. Coordination of circadian timing in mammals. *Nature* **418**, 935–941 (2002).
2. Huang, N. et al. Crystal structure of the heterodimeric CLOCK:BMAL1 transcriptional activator complex. *Science* **337**, 189–194 (2012).
3. Panda, S., Hogenesch, J. B. & Kay, S. A. Circadian rhythms from flies to human. *Nature* **417**, 329–335 (2002).
4. Takahashi, J. S. Transcriptional architecture of the mammalian circadian clock. *Nat. Rev. Genet.* **18**, 164–179 (2017).
5. Patke, A., Young, M. W. & Axelrod, S. Molecular mechanisms and physiological importance of circadian rhythms. *Nat. Rev. Mol. Cell Biol.* **21**, 67–84 (2020).

6. Bunger, M. K. et al. *Mop3* is an essential component of the master circadian pacemaker in mammals. *Cell* **103**, 1009–1017 (2000).
7. King, D. P. et al. Positional cloning of the mouse circadian clock gene. *Cell* **89**, 641–653 (1997).
8. Gekakis, N. et al. Role of the CLOCK protein in the mammalian circadian mechanism. *Science* **280**, 1564–1569 (1998).
9. Gottesman, R. F. et al. Impact of sleep disorders and disturbed sleep on brain health: a scientific statement from the American Heart Association. *Stroke* **55**, e61–e76 (2024).
10. Akashi, M. & Takumi, T. The orphan nuclear receptor RORα regulates circadian transcription of the mammalian core-clock *Bmal1*. *Nat. Struct. Mol. Biol.* **12**, 441–448 (2005).
11. Guillaumond, F., Dardente, H., Giguere, V. & Cermakian, N. Differential control of Bmal1 circadian transcription by REV-ERB and ROR nuclear receptors. *J. Biol. Rhythms* **20**, 391–403 (2005).
12. Preitner, N. et al. The orphan nuclear receptor REV-ERBα controls circadian transcription within the positive limb of the mammalian circadian oscillator. *Cell* **110**, 251–260 (2002).
13. Lowrey, P. L. & Takahashi, J. S. Genetics of circadian rhythms in mammalian model organisms. *Adv. Genet.* **74**, 175–230 (2011).
14. Cederroth, C. R. et al. Medicine in the fourth dimension. *Cell Metab.* **30**, 238–250 (2019).
15. Crnko, S., Du Pre, B. C., Sluijter, J. P. G. & Van Laake, L. W. Circadian rhythms and the molecular clock in cardiovascular biology and disease. *Nat. Rev. Cardiol.* **16**, 437–447 (2019).
16. Nguyen, C., Murray, G., Anderson, S., Filipowicz, A. & Ingram, K. K. In vivo molecular chronotyping, circadian misalignment, and high rates of depression in young adults. *J. Affect. Disord.* **250**, 425–431 (2019).
17. Difrancesco, S. et al. Sleep, circadian rhythm, and physical activity patterns in depressive and anxiety disorders: a 2-week ambulatory assessment study. *Depress. Anxiety* **36**, 975–986 (2019).
18. Awuah, W. A. et al. Circadian rhythm in systemic autoimmune conditions: potential of chrono-immunology in clinical practice: a narrative review. *Medicine (Baltimore)* **102**, e34614 (2023).
19. Green, C. B., Takahashi, J. S. & Bass, J. The meter of metabolism. *Cell* **134**, 728–742 (2008).
20. Bass, J. & Takahashi, J. S. Circadian integration of metabolism and energetics. *Science* **330**, 1349–1354 (2010).
21. Dong, Z. et al. Targeting glioblastoma stem cells through disruption of the circadian clock. *Cancer Discov.* **9**, 1556–1573 (2019).
22. Doruk, Y. U. et al. A CLOCK-binding small molecule disrupts the interaction between CLOCK and BMAL1 and enhances circadian rhythm amplitude. *J. Biol. Chem.* **295**, 3518–3531 (2020).
23. Hirota, T. et al. Identification of small molecule activators of cryptochrome. *Science* **337**, 1094–1097 (2012).
24. Rasmussen, E. S., Takahashi, J. S. & Green, C. B. Time to target the circadian clock for drug discovery. *Trends Biochem. Sci.* **47**, 745–758 (2022).
25. Chen, Z., Yoo, S. H. & Takahashi, J. S. Development and therapeutic potential of small-molecule modulators of circadian systems. *Annu. Rev. Pharmacol. Toxicol.* **58**, 231–252 (2018).
26. Baggs, J. E. et al. Network features of the mammalian circadian clock. *PLoS Biol.* **7**, e52 (2009).
27. Shi, S. et al. Circadian clock gene *Bmal1* is not essential; functional replacement with its paralog, *Bmal2*. *Curr. Biol.* **20**, 316–321 (2010).
28. Wu, D., Potluri, N., Lu, J., Kim, Y. & Rastinejad, F. Structural integration in hypoxia-inducible factors. *Nature* **524**, 303–308 (2015).
29. Wu, D., Su, X., Potluri, N., Kim, Y. & Rastinejad, F. NPAS1-ARNT and NPAS3-ARNT crystal structures implicate the bHLH-PAS family as multi-ligand binding transcription factors. *eLife* **5**, e18790 (2016).
30. Sun, X. et al. Structures of NPAS4-ARNT and NPAS4-ARNT2 heterodimers reveal new dimerization modalities in the bHLH-PAS transcription factor family. *Proc. Natl Acad. Sci. USA* **119**, e2208804119 (2022).
31. Diao, X. et al. Identification of oleoylethanolamide as an endogenous ligand for HIF-3α. *Nat. Commun.* **13**, 2529 (2022).
32. Wu, D. & Rastinejad, F. Structural characterization of mammalian bHLH-PAS transcription factors. *Curr. Opin. Struct. Biol.* **43**, 1–9 (2017).
33. Esser, C. & Rannug, A. The aryl hydrocarbon receptor in barrier organ physiology, immunology, and toxicology. *Pharmacol. Rev.* **67**, 259–279 (2015).
34. Rannug, A. 6-Formylindolo[3,2-*b*]carbazole, a potent ligand for the aryl hydrocarbon receptor produced both endogenously and by microorganisms, can either promote or restrain inflammatory responses. *Front. Toxicol.* **4**, 775010 (2022).
35. Wu, D. et al. Bidirectional modulation of HIF-2 activity through chemical ligands. *Nat. Chem. Biol.* **15**, 367–376 (2019).
36. Wilkinson, I. V. L. et al. Chemical proteomics and phenotypic profiling identifies the aryl hydrocarbon receptor as a molecular target of the utrophin modulator ezutromid. *Angew. Chem. Int. Ed. Engl.* **59**, 2420–2428 (2020).
37. Zhuang, J., Shang, Q., Rastinejad, F. & Wu, D. Decoding allosteric control in hypoxia-inducible factors. *J. Mol. Biol.* **436**, 168352 (2024).
38. Niesen, F. H., Berglund, H. & Vedadi, M. The use of differential scanning fluorimetry to detect ligand interactions that promote protein stability. *Nat. Protoc.* **2**, 2212–2221 (2007).
39. Martinez, N. J. et al. A widely-applicable high-throughput cellular thermal shift assay (CETSA) using split Nano Luciferase. *Sci. Rep.* **8**, 9472 (2018).
40. Franken, H. et al. Thermal proteome profiling for unbiased identification of direct and indirect drug targets using multiplexed quantitative mass spectrometry. *Nat. Protoc.* **10**, 1567–1593 (2015).
41. Savitski, M. M. et al. Tracking cancer drugs in living cells by thermal profiling of the proteome. *Science* **346**, 1255784 (2014).
42. Scheiermann, C., Gibbs, J., Ince, L. & Loudon, A. Clocking in to immunity. *Nat. Rev. Immunol.* **18**, 423–437 (2018).
43. Keller, M. et al. A circadian clock in macrophages controls inflammatory immune responses. *Proc. Natl Acad. Sci. USA* **106**, 21407–21412 (2009).
44. Partch, C. L., Green, C. B. & Takahashi, J. S. Molecular architecture of the mammalian circadian clock. *Trends Cell Biol.* **24**, 90–99 (2014).
45. Kitchen, G. B. et al. The clock gene *Bmal1* inhibits macrophage motility, phagocytosis, and impairs defense against pneumonia. *Proc. Natl Acad. Sci. USA* **117**, 1543–1551 (2020).
46. Xu, P. et al. NPAS4 regulates the transcriptional response of the suprachiasmatic nucleus to light and circadian behavior. *Neuron* **109**, 3268–3282 (2021).
47. Cheng, X. et al. Marked and rapid effects of pharmacological HIF-2α antagonism on hypoxic ventilatory control. *J. Clin. Invest.* **130**, 2237–2251 (2020).
48. Flegel, J. et al. The highly potent AhR agonist picoberin modulates Hh-dependent osteoblast differentiation. *J. Med. Chem.* **65**, 16268–16289 (2022).
49. Ondrova, K. et al. Monoterpenoid aryl hydrocarbon receptor allosteric antagonists protect against ultraviolet skin damage in female mice. *Nat. Commun.* **14**, 2728 (2023).
50. Rothhammer, V. & Quintana, F. J. The aryl hydrocarbon receptor: an environmental sensor integrating immune responses in health and disease. *Nat. Rev. Immunol.* **19**, 184–197 (2019).
51. Michael, A. K. et al. Cooperation between bHLH transcription factors and histones for DNA access. *Nature* **619**, 385–393 (2023).

52. Menet, J. S., Pescatore, S. & Rosbash, M. CLOCK:BMAL1 is a pioneer-like transcription factor. *Genes Dev.* **28**, 8–13 (2014).
53. Mohammed, H. et al. Rapid immunoprecipitation mass spectrometry of endogenous proteins (RIME) for analysis of chromatin complexes. *Nat. Protoc.* **11**, 316–326 (2016).
54. Close, P. et al. DBIRD complex integrates alternative mRNA splicing with RNA polymerase II transcript elongation. *Nature* **484**, 386–389 (2012).
55. Nogues, G., Kadener, S., Cramer, P., Bentley, D. & Kornblihtt, A. R. Transcriptional activators differ in their abilities to control alternative splicing. *J. Biol. Chem.* **277**, 43110–43114 (2002).
56. Naftelberg, S., Schor, I. E., Ast, G. & Kornblihtt, A. R. Regulation of alternative splicing through coupling with transcription and chromatin structure. *Annu. Rev. Biochem.* **84**, 165–198 (2015).
57. Tilgner, H. et al. Nucleosome positioning as a determinant of exon recognition. *Nat. Struct. Mol. Biol.* **16**, 996–1001 (2009).
58. He, B. et al. The small molecule nobiletin targets the molecular oscillator to enhance circadian rhythms and protect against metabolic syndrome. *Cell Metab.* **23**, 610–621 (2016).
59. Blacher, E. et al. Aging disrupts circadian gene regulation and function in macrophages. *Nat. Immunol.* **23**, 229–236 (2022).
60. Khorasanizadeh, S. & Rastinejad, F. Visualizing the architectures and interactions of nuclear receptors. *Endocrinology* **157**, 4212–4221 (2016).
61. Rastinejad, F. Retinoic acid receptor structures: the journey from single domains to full-length complex. *J. Mol. Endocrinol.* **69**, T25–T36 (2022).
62. Rastinejad, F. The protein architecture and allosteric landscape of HNF4α. *Front. Endocrinol. (Lausanne)* **14**, 1219092 (2023).

Publisher's note Springer Nature remains neutral with regard to jurisdictional claims in published maps and institutional affiliations.

Open Access This article is licensed under a Creative Commons Attribution 4.0 International License, which permits use, sharing, adaptation, distribution and reproduction in any medium or format, as long as you give appropriate credit to the original author(s) and the source, provide a link to the Creative Commons licence, and indicate if changes were made. The images or other third party material in this article are included in the article's Creative Commons licence, unless indicated otherwise in a credit line to the material. If material is not included in the article's Creative Commons licence and your intended use is not permitted by statutory regulation or exceeds the permitted use, you will need to obtain permission directly from the copyright holder. To view a copy of this licence, visit http://creativecommons.org/licenses/by/4.0/.

© The Author(s) 2025

Methods

Cloning, mutagenesis, expression and purification of human BMAL1(PASB)

Human BMAL1 (UniProt O00327) PASB domain (338–449 amino acids) was subcloned into pMKH vector to produce His6-TEV-hBMAL1(PASB) protein. Plasmid was transformed into Rosetta (*DE3*) cells, and a single clone was kept for further protein expression. Cells were grown in LB medium, and protein expression was induced with 0.2 mM IPTG overnight at 18 °C. Cells were harvested by centrifugation and resuspended in buffer containing 20 mM Tris-HCl pH 8.0, 500 mM NaCl, 5% glycerol, 5 mM imidazole and 1× protease inhibitor (Roche, 81410500). Cells were lysed by sonication, and protein was purified through affinity chromatography with nickel resin. The eluted fractions were then loaded on a HiLoad 16/600 Superdex 75 gel filtration column to remove aggregations and imidazole. His-tag was cleaved by overnight TEV cleavage. Tag was separated and protein was isolated by size-exclusion chromatography with a buffer of 20 mM Bis-Tris propane pH 8.0 and 150 mM NaCl, and monomer fractions were collected and concentrated to 4 mg ml^{-1} for further usage. Site-directed mutagenesis was performed with an Agilent QuikChange Kit (200522). The quality control (SDS-PAGE and MS) for BMAL1(PASB) protein is shown in Supplementary Fig. 6.

Crystallization, structure determination and refinement

Crystals were grown in a 96-well crystallization plate (MRC96T-UVP) through sitting-drop vapor diffusion. The reservoir solution consisted of 20% PEG3350 and 0.15 M sodium formate. Protein was dissolved in 20 mM BTP pH 8.0 and 150 mM NaCl at 4 mg ml^{-1}. Protein and reservoir solution was mixed in a 1:1 ratio and incubated at 4 °C for 1 month before harvesting. Compound soaking was performed 24 h before harvesting at a concentration of 1.25 mM. Diffraction datasets were collected at the Diamond Synchrotron Light Source, using beamline I03 operating at a wavelength of 0.9763 Å, with the detector Eiger2 XE 16M and the crystal temperature of 100° K. The diffraction images were indexed, merged and scaled in xia2 DIALS[63]. The initial phase was determined by molecular replacement with a model prepared from Protein Data Bank (PDB) ID 4F3L in Phaser[64]. The entire model of hBMAL1(PASB) was built manually in Coot[65]. Further structure refinements were done in CCP4 (ref. 66) and phenix.refine[67]. The final structures have 98.08% (BMAL1(PASB)-*Apo*) and 97.06% (BMAL1(PASB)-CCM) of residues in the favoured regions of the Ramachandran plot, with 0% outliers in both structures. Structure figures were prepared in PyMoL. Pocket sizes in the protein were examined for ligands and measured with PyVOL[68,69]. The crystal diffraction and refinement statistics are summarized in Extended Data Table 1.

Protein thermal shift assay

Protein thermal shift assays were carried out in a 384-well plate with QuantStudio 7 Flex. Compounds were dispensed by Echo 555 liquid handler, and protein solution was added with multidrop. The protein solutions were prepared by diluting stock to 0.1 mg ml^{-1} in the buffer containing 20 mM Bis-Tris propane pH 8.0, 150 mM NaCl and 8× SYPRO Orange dye (Invitrogen, S6651). Plates were centrifuged at 1,000*g* for 30 s and incubated at room temperature for more than 10 min before measuring. Melting curves were generated by heating the plate from 25 °C to 95 °C with a speed of 0.1 °C s^{-1}. Data were analyzed in Protein Thermal Shift Software version 1.4. Screening data were analyzed in DataWarrior version 6.1.0 (ref. 70). The terms dTm B and dTm D refer to shift of protein melting temperature (delta Tm), calculated by the Boltzmann fitting method and the derivative fitting method, respectively.

Cell culture and viability test

Cells were grown in DMEM media (Gibco, 31966-021) supplied with 10% FBS (Gibco, A3160502) and 50 U ml^{-1} penicillin–streptomycin (P/S) (Gibco, 15070063). All cells were incubated in 5% CO_2 at 37 °C. Medium was refreshed every 2–3 d, and transfection was done at a cell confluence of 60–80%. Transient transfections of cell lines were performed using Lipofectamine 3000 (Invitrogen, L3000-015) according to the manufacturer's instructions. Lipofectamine RNAiMAX (Invitrogen, 13778-075) was used for siRNA knockdown experiments. siRNA oligos targeting BMAL1 (sc-38165), CLOCK (sc-35074) and NPAS2 (sc-38169) were purchased from Santa Cruz Biotechnology. Cell viability was detected with a CyQUANT LDH Cytotoxicity Assay Kit (Invitrogen, C20300). Cells were incubated in DMEM media with indicated amounts of CCM for 48 h before carrying out the viability test. Absorbances at 490 nm and 680 nm were measured in a microplate reader, and data were processed according to the manufacturer's instructions.

CETSA

HEK293T or U2OS cells were cultured in DMEM media, and plasmid was transfected when cells grew to 60–80% confluence. Cells were harvested 2 d after transfection. Cells were washed twice with ice-cold PBS and harvested by scraping on ice and suspended in buffer containing 20 mM Bis-Tris propane pH 8.0, 150 mM NaCl and 1× protease inhibitor cocktail (Roche, 61431800). Cells were sonicated, and supernatant of cell lysate was collected after centrifugation. Compounds were transferred into a 384-well plate through an Echo 555 liquid handler, and 5 µl of cell lysates was added to each well. Plates were centrifuged at 1,000*g* for 10 s and incubated at room temperature for 30 min. Plates were then heated in a PCR thermal cycler (Bio-Rad, C1000 Touch) for 3 min at a 36–60 °C gradient. Denatured protein was removed by centrifugation at 4 °C for 15 min at 4,300*g*. Soluble HiBiT-tag protein was detected using a Nano-Glo HiBiT Lytic Detection System (Promega, N3040) according to the manufacturer's protocol. Isothermal dose–response (ITDR) measurements were done at 48 °C with indicated compound concentration.

ITC

ITC was performed in a Nano ITC (TA Instruments). Compound was dissolved directly in buffer (20 mM BTP pH 8.0 and 150 mM NaCl) and adjusted to a final concentration of 320 µM. Protein was prepared in the same buffer and diluted to 40 µM. Both protein and compound were degassed before loading onto the Nano ITC. The rotation speed was set to 180 r.p.m., and the system was kept at 20 °C. Compound was titrated into protein with an interval of 240 s. Binding data after the subtraction of the buffer titration were analyzed, and thermodynamic parameters were obtained by fitting to a one-site binding model.

SPR

SPR was carried out in a Biacore S200 (GE Healthcare) with sensor chip SA (Cytiva, BR100531). Human BMAL1 residues 338–449 were subcloned into pET-28a vector with an N-terminal His-tag and a C-terminal avi-tag. Plasmid was then transformed into BL21 (*DE3*) competent cells that overexpressed BirA. Then, 200 nM biotin was added along with IPTG during protein expression. Final protein was purified by affinity chromatography and size-exclusion chromatography. SA chip channel was first washed with 1 M NaCl and 50 mM NaOH, and protein was then immobilized directly on the SA chip through capture with pre-immobilized streptavidin. The immobilization level was set to 4,500 response units (RU). Assay cycles were set at 20 °C using a running buffer of 50 mM BTP pH 8.0, 150 mM NaCl and 1% DMSO. A 0–2% DMSO range was used for solvent correction. The analyte was injected at 30 µl min^{-1} for 60 s with a dissociation time of 120 s. Data were fit with a one-site binding model.

Compound synthesis

The hit01 compound in powder form was purchased from Enamine (Z425795906). Compounds A190, A304 and CCM are not commercially available. We designed these compounds using Maestro (Schrodinger Suites 2021-03), and they were synthesized by Cortex Organics Ltd. (https://www.cortexorganics.com/). The starting material for

their syntheses was purchased from BLD Pharmatech (BD110688 and BD281593). Quality control data for A190, A304 and CCM, including MS and NMR spectra, are in Supplementary Figs. 1–3. The steps for their syntheses are shown in Supplementary Fig. 4.

The standard peak listings of CCM. 1H NMR (500 MHz, $CDCl_3$) δ 7.62 (d, *J* = 2.1 Hz, 1H), 6.95 (dt, *J* = 7.9, 0.8 Hz, 1H), 6.80 (d, *J* = 2.1 Hz, 1H), 6.78 (d, *J* = 8.0 Hz, 1H), 5.00 (dqd, *J* = 47.8, 5.0, 3.7 Hz, 1H), 4.43 (ddd, *J* = 20.0, 4.9, 1.9 Hz, 2H), 4.13 – 3.89 (m, 2H), 2.81 (qd, *J* = 7.5, 0.7 Hz, 2H), 1.94 (t, *J* = 6.5 Hz, 1H), 1.29 (t, *J* = 7.6 Hz, 3H); 13C NMR (126 MHz, $CDCl_3$) δ 144.76, 144.42, 142.41, 130.82, 128.57, 121.66, 108.85, 105.65, 91.80 (d, *J* = 173.0 Hz), 68.38 (d, *J* = 25.4 Hz), 62.51 (d, *J* = 22.2 Hz), 25.86, 15.16; 19F NMR (58 MHz, $CDCl_3$) δ −109.28 (s, 1F); LC–MS (*m*/*z*): $[M + H]^+$ calculated for $C_{13}H_{15}FO_3$, 239.1078; found, 238.978.

The standard peak listings of A304. 1H NMR (500 MHz, $CDCl_3$) δ 7.61 (d, *J* = 2.2 Hz, 1H), 6.94 (d, *J* = 8.0 Hz, 1H), 6.79 (d, *J* = 2.2 Hz, 1H), 6.76 (d, *J* = 8.1 Hz, 1H), 4.34 (t, *J* = 6.0 Hz, 2H), 3.93 (q, *J* = 5.7 Hz, 2H), 2.81 (q, *J* = 7.6 Hz, 2H), 2.13 (p, *J* = 5.9 Hz, 2H), 1.89 (t, *J* = 5.5 Hz, 1H), 1.29 (t, *J* = 7.6 Hz, 3H); 13C NMR (126 MHz, $CDCl_3$) δ 144.67, 144.45, 142.96, 130.04, 128.29, 121.61, 107.99, 105.62, 67.37, 60.84, 32.23, 25.86, 15.22; LC–MS (*m*/*z*): $[M + H]^+$ calculated for $C_{13}H_{16}O_3$, 221.1172; found, 221.485.

The standard peak listings of A190. 1H NMR (500 MHz, $CDCl_3$) δ 7.62 (d, *J* = 2.1 Hz, 1H), 7.20 (dd, *J* = 7.8, 1.1 Hz, 1H), 7.14 (t, *J* = 7.8 Hz, 1H), 6.83 (dd, *J* = 7.9, 1.1 Hz, 1H), 6.76 (d, *J* = 2.1 Hz, 1H), 4.36 (t, *J* = 6.0 Hz, 2H), 3.94 (q, *J* = 5.4 Hz, 2H), 2.15 (p, *J* = 5.9 Hz, 2H), 1.95 – 1.87 (m, 1H); 13C NMR (126 MHz, $CDCl_3$) δ 145.08, 144.81, 144.61, 129.40, 123.58, 113.93, 107.82, 107.04, 67.12, 60.68, 32.19; LC–MS (*m*/*z*): $[M + H]^+$ calculated for $C_{11}H_{12}O_3$, 193.0859; found, 193.071.

Western blot and cell subfraction studies

Whole-cell lysate was directly extracted from cells with RIPA buffer or obtained by sonication. For RIPA buffer extraction, cells were harvested and suspended in RIPA buffer for 30 min with rotation and then centrifuged at 17,000*g* for 30 min to collect the supernatant (whole-cell lysate). For sonication, cell pellets were suspended in intended buffer and sonicated in an ice bath for 2 min. A final centrifuge step at 17,000*g* for 30 min was conducted to collect lysate.

To extract subcellular fraction, cells were washed twice in ice-cold PBS and then harvested by scraping. Cell pellets were centrifuged at 1,000*g* for 5 min to remove all liquid. Then, cell pellets were resuspended in hypotonic buffer (20 mM HEPES pH 7.5, 1.5 mM $MgCl_2$, 10 mM KCl, 1 mM EDTA and 0.05% NP40) and incubated on ice for 15 min. The mixtures were centrifuged at 1,000*g* for 10 min, and supernatant was collected (cytosol fraction). The pellets were washed once with hypotonic buffer. All liquid was removed, and the rest was kept for further analysis (nucleus fraction).

Samples were separated in SDS-PAGE with 8% Tris-glycine gels and then transferred to PVDF membranes through the semi-dry transfer method. Membranes were first blocked in 5% BSA and then incubated overnight at 4 °C with the following primary antibodies: BMAL1 (Santa Cruz Biotechnology, sc-365645x, 1:1,000 dilution), CLOCK (Cell Signaling Technology, 5157S, 1:1,000 dilution), α-tubulin (Abcam, ab4074, 1:5,000 dilution), Lamin B1 (Santa Cruz Biotechnology, sc-374015, 1:200 dilution), β-actin (Abcam, ab184092, 1:10,000 dilution), Myc-tag (Cell Signaling Technology, 2278S, 1:1,000 dilution) and Flag-tag (Sigma-Aldrich, F4042, 1:1,000 dilution). Membranes were washed three times in PBST buffer and incubated with LI-COR secondary antibody (anti-mouse, 926-68070, 1:15,000 dilution; anti-rabbit, 926-32211, 1:15,000 dilution) for 1 h at room temperature. Membranes were washed another three times before detecting in a LI-COR Odyssey gel imager. Membranes were stripped with fluorescent western blot stripping buffer (Thermo Fisher Scientific, 62300) for reprobing.

Co-IP

Full-length human BMAL1 or CLOCK was cloned into pCMV vector with a C-terminal Myc or Flag tag. Plasmids were transfected into U2OS cells for transient expression. After 2 d, U2OS cells in 150-mm dishes were then treated with 0.1% DMSO or 1–100 μM CCM for approximately 2.5 h. Cells were then washed twice in ice-cold PBS and harvested by scraping. Then, 1.0 ml of buffer (20 mM HEPES pH 7.5, 100 mM NaCl, 1 mM EDTA, 3% glycerol, 0.1% Tween 20, 0.05% Triton X-100, 1 mM DTT and 1× cocktail protease inhibitor) was added to suspend cell pellets. Additional DMSO/CCM was added into the buffer to maintain in-cell interactions. Lysate was obtained through sonication and centrifugation. Magnetic Flag beads (Millipore, M8823) were washed three times with PBS and then blocked for 1 h in 0.5% BSA (PBS). Beads were then washed twice with IP buffer, followed by transferring of 20 μl of Flag beads into 1.0 ml of cell lysate and incubated for 2.5 h in a cold room with end-to-end rotation. Flag beads were washed twice with IP buffer, and all liquid in the tube was removed. Beads were suspended in 20 μl of 1.5× SDS-PAGE loading buffer and heated at 95 °C for 5 min. Samples were then analyzed by western blot.

RT–qPCR

Next, 2 ml of U2OS cells was seeded into six-well plates at a density of 3×10^5 cells per milliliter. When cells grew to approximately 80% confluency on the next day, cells were synchronized with 100 nM dexamethasone for 2 h. Then, dexamethasone was removed and replaced with fresh media containing 0.1% DMSO or 100 μM CCM. Cells were incubated for another 12 h and then harvested every 4 h. For unsynchronized U2OS, fresh DMEM media containing 0.1% DMSO or 100 μM CCM were added and incubated for 1 d before harvesting. Total RNA was extracted using an RNeasy Plus Mini Kit (Qiagen, 74134). Reverse transcription was performed with a High-Capacity RNA-to-cDNA Kit (Applied Biosystems, 4387406). Then, 2 μg of total RNA was used in reverse transcription. Quantitative PCR reactions were performed in a QuantStudio 7 Flex system using Fast SYBR Green reagent (Applied Biosystems, 4385612). A 10-μl reaction volume was used in a 384-well plate with at least three replicates for each reaction. Primers used here were modified based on a previous study[71] and are listed in Supplementary Table 1. In all reactions, 300 nM forward and reverse primers were used, and β2 microglobulin (B2M) was used as an endogenous control. Relative RNA level was calculated by $2^{-\Delta\Delta Ct}$. Data were analyzed in GraphPad Prism 9, and circadian parameters in time-course rhythmic gene expression were determined by nonlinear regression fitting with sine wave. Wavelength was constrained to be longer than 16 h, and initial values were selected based on individual data. The goodness-of-fit (R^2) values for each condition are as follows: 0.9101 (CRY1-DMSO), 0.9142 (CRY1-CCM), 0.9655 (CRY2-DMSO), 0.8088 (CRY2-CCM), 0.9786 (PER2-DMSO), 0.9236 (PER2-CCM), 0.8728 (PER3-DMSO) and 0.9173 (PER3-CCM). The PER1-DMSO, PER1-CCM, NR1D1-DMSO, NR1D2-CCM, CLOCK-DMSO and CLOCK-CCM data have an R^2 value lower than 0.8.

RIME

RIME was performed based on the protocol from Carroll et al.[53]. In summary, four 150-mm dishes of U2OS cells were cross-linked in 1% formaldehyde for each condition. Nuclear fractions were extracted according to the protocol. For each condition, 50 μl of Dynabeads Protein A (Invitrogen, 10001D) was used. Then, 4 μg of BMAL1 antibody (Abcam, ab93806) or rabbit IgG (Millipore, 12-370) was incubated with the beads at room temperature for 2 h to generate antibody-bound beads. Beads were then washed four times with 0.5% BSA to remove any unbound antibody. Lysate samples and antibody-bound beads were mixed and rotated at 4 °C overnight. Beads were washed five times with RIPA buffer and then twice with 100 mM AMBIC solution before submitting for trypsin digestion.

Peptide mixtures were obtained directly from on-bead digestion. Protein samples on beads were denatured in 8 M urea and reduced in

10 mM TCEP. Cysteines were alkylated with 50 mM 2-chloroacetamide. Protein samples were first digested using LysC (New England Biolabs (NEB), P8109S) for 2 h and then trypsin (NEB, P8101S) for overnight at 37 °C. Digestion reaction was stopped by adding formic acid to 5%. Peptide mixtures were desalted in a C18 column with 0.1% trifluoroacetic acid (TFA) as buffer A and 50% acetonitrile/0.1% TFA as buffer B. Peptides were dried in a vacuum concentrator and stored in −20 °C before injection. Samples were processed in a Bruker TIMS instrument. Raw data were analyzed in MaxQuant[72]. Proteins were identified by search against human proteomes and common contaminants. Carbamidomethylation of cystine was set as a fixed modification. False discovery rates (FDRs) were set to 1% in peptide and protein identification. Proteins were then qualified by using a standard label-free qualification strategy with at least two peptides identified in each protein. The following modifications were included in protein quantification: oxidation of methionine, acetylation of protein N-terminus, acetylation of lysine and phosphorylations of serine and threonine. The intensity of one protein was normalized to the total abundance of all proteins in each sample. The mean values of normalized intensity of the CCM-treated condition divided by that of the DMSO condition gives the fold change.

ChIP

One 150 -mm dish of UO2S cells around 90% confluence was used for each biological replicate in ChIP studies. Cells were incubated in fresh media with 0.1% DMSO or 100 CCM for 3 h in unsynchronized condition or 24 h in synchronized U2OS cells. Cells were crosslinked for 15 min with 1% formaldehyde and then quenched with 125 mM glycine for another 5 min. Cells were then washed twice with ice-cold PBS and harvested by scraping. The chromatin complex was obtained following the RIME protocol. For each condition, 20 µl of Dynabeads Protein A (Invitrogen, 10001D) and 4 µg of BMAL1 antibody (Abcam, ab93806) or rabbit IgG (Millipore, 12-370) was used. To obtain ChIP DNA, 50 µl of 10% (w/v) Chelex 100 slurry (Bio-Rad, 1421253) was added to the final IP beads and boiled for 15 min. Then, 0.5 µl of RNase A (Invitrogen, 12091021) was added to each sample and incubated at 37 °C for 1 h on a thermal mixer (1,200 r.p.m.). Next, 1 µl of proteinase K (Invitrogen, 25530049) was added to the mixture and incubated at 65 °C for 2 h with 1,200-r.p.m. shaking. Samples were boiled for another 10 min and then centrifuged at 17,000*g* for 10 min at 4 °C. Then, 30 µl of supernatant was transferred to a new tube, and 50 µl of MilliQ water was then added to the remaining beads, vortexed and centrifuged at 17,000*g* for 10 min to provide 50 µl of additional supernatant for each sample. The ChIP DNA was further purified with DNA Clean & Concentrator (Zymo Research, D4004) for better qPCR signal. Final ChIP DNA was eluted in 20 µl of elution buffer. One microliter of ChIP DNA was used for a 10-µl qPCR reaction (SYBR Green master kit, 4385612). Three technical repeats were run in parallel for each sample to generate an n number of 1. Both DMSO and CCM conditions had three biological replicates ($n = 3$). The primers for ChIP–qPCR were designed in the National Center for Biotechnology Information (NCBI) with the promotor sequences of correspondent genes, and these are listed in Supplementary Table 2.

Monitoring real-time circadian rhythms

Peritoneal macrophages were isolated from both male and female Per2–Luc mice (expressing luciferase under control of the Period 2 promoter) at age 12–19 weeks. Peritoneal exudate cells (PECs) were isolated via peritoneal lavage with ice-cold PBS. Cells were plated for 90 min and washed to remove non-adherent cells. Macrophages were then immediately treated with CCM at various concentrations or vehicle (0.1% DMSO in recording medium). Circadian oscillations were tracked in a plate reader measuring luminescence hourly across 96 h. In every experiment, three independent wells were measured from each condition. The parameters were then calculated for each well individually and averaged to give an $n = 1$ measurement of period, phase and amplitude. This experiment was then repeated on macrophages from different individual mice to increase the n number. Representative traces in Fig. 3e were chosen from two different biological replicates to cover the full range of concentrations analyzed. Data were first processed in MultiCycle and then smoothed in Prism (second-order smoothing, 10 neighbors). The ATP viability assay (CellTiter-Glo; Promega, G7570) was carried out on peritoneal macrophages after the 5 d of luminometry recording.

The rhythmicity of raw luminometry data was tested in BioDare2 (https://biodare2.ed.ac.uk/)[73]. No linear detrending was used. The test method selected was BD2 eJTK (the BioDare2 implementation of Empirical JTK_CYCLE with asymmetry search from Hutchison et al.[74]). The analysis presets (the set of pattern curves against which the comparison test is run) selected were eJTK Classic. Samples were included in amplitude/period/phase analysis where they were found to be rhythmic (Benjamini–Hochberg correction $P < 0.05$).

For period analysis: raw data were analyzed using default settings in BioDare2 software with the fast Fourier transform-nonlinear least squares (FFT-NLLS) algorithm[75]. Options 'Phases by Fit', 'zero' and 'circadian' were enabled during the process.

For phases: values were reported using a phase by fit method: one cosine function having period matching the estimated data period is fitted to the data. The fitting procedure finds phase and amplitude parameters of the cosine that follow the data the most closely and reports those values as phase and amplitude. Phase was reported relative to zero (as data are periodic and phase has been estimated, it is possible to back-calculate the data to zero). Phase was reported in circadian units (the circadian unit is 1/24 of the free running period, and it allows comparison of peaking times independently of the period).

Protein sequence alignment

Sequences for alignment were extracted from UniProt with the following accession numbers: ARNT_P27540, ARNT2_Q9HBZ2, BMAL1_O00327 and BMAL2_Q8WYA1. Alignment was performed in Clustal X 2.1 (ref. 76) software or Needle[77]. The alignment graph was generated in ESPript 3.0 web service[78].

Thermal proteome profiling

U2OS cells overexpressing HiBiT-hBMAL1(PASB) were suspended in buffer containing 20 mM BTP pH 8.0, 150 mM NaCl and 1× cocktail protease inhibitor, and lysate was obtained after sonication and centrifugation. Cell lysate was diluted to 3 mg ml^{-1} and incubated with DMSO or 50 µM or 200 µM CCM for 1 h at room temperature. After that, a temperature gradient was applied from 37 °C to 60.9 °C for 3 min, followed by centrifugation for 30 min at the highest speed of a pre-cooled centrifuge. For each condition (DMSO or CCM treatment), supernatants across all temperatures were carefully aspirated from the tube and pooled.

Pooled samples were digested with trypsin using S-Trap Mini columns (ProtiFi) following the manufacturer's instructions. Buffers were made using MS-grade water. In brief, SDS was added to samples containing 200 µg of protein in 100 ul to a final concentration of 5% before reduction and alkylation with 20 mM DTT and 40 mM IAA for each 30 min at room temperature. After acidification to a final concentration of 1.2% with phosphoric acid and precipitation with 7 sample volumes of binding buffer (100 mM TEAB, 90% methanol), samples were loaded step-wise on S-Trap Mini columns, washed three times with 400 µl of binding buffer and digested using 4 µg of sequencing-grade modified trypsin (Promega, V5111) in 40 µl of digestion buffer (50 mM TEAB) at 37 °C for 20 h. Peptides were eluted from column with each 40 µl of elution buffer 1 (50 mM TEAB), elution buffer 2 (0.2% formic acid) and elution buffer 3 (50% acetonitrile, 0.2% formic acid) and then dried down in a vacuum centrifuge (Genevac miVAC) overnight.

Peptides were labeled with TMT10plex mass tags (Thermo Fisher Scientific) following the manufacturer's instructions. Dried peptides

were resuspended in 102 µl of 100 mM TEAB. TMT label reagents were equilibrated at room temperature before dissolving in 42 µl of acetonitrile. The TMT10-131 label reagent was not used. Then, 100 µl of samples was mixed with 41 µl of each respective TMT label reagent on a shaker for 1 h at room temperature. The labeling was stopped by adding 8 µl of 5% hydroxylamine for 10 min at room temperature. Samples were combined and cleaned up by standard procedures using Sep-Pak Plus C18 cartridges (Waters) and then dried in a vacuum centrifuge.

Peptides were fractionated using a Dionex UltiMate 3000 system (Thermo Fisher Scientific) on a C18 column (XBridge BEH C18, 2.5 µm, 3 × 150 mm column XP, Waters) with a flow rate of 0.2 ml min^{-1}. Buffer A (100% water (pH 10)) and buffer B (90% acetonitrile (pH 10)) were prepared with MS-grade water, and pH was adjusted with 17% NH_4OH. Peptides were separated using a 100-minute gradient (0–12 min: 0.2% buffer B, 12–72 min: 2–45% buffer B, 72–80 min: 45–95% buffer B, 80–90 min at 95% buffer B, 90–92 min: 95-2% buffer B, 92–100 min at 2% buffer B). A total of 50 fractions were collected with vial switching every 2 min, which were concatenated across the gradient to yield 10 samples. Samples were dried in a vacuum centrifuge.

MS analysis was performed on an Orbitrap Fusion Lumos Tribrid mass spectrometer (Thermo Fisher Scientific) coupled to a Dionex UltiMate 3000 RSLCnano system (Thermo Fisher Scientific) via a Nanospray Flex Ion Source (Thermo Fisher Scientific) interface. Peptides were loaded onto a trap column (PepMap 100 C18, 5 µm, 5 × 0.3 mm; Thermo Fisher Scientific) at a flow rate of 10 µl min^{-1} using 0.1% TFA as loading buffer. After loading, the trap column was switched in-line with a C18 analytical column (2.0 µm particle size, 75 µm ID × 500 mm; Thermo Fisher Scientific). The column temperature was maintained at 50 °C using a PRSO-V2 column oven (Sonation). Mobile phase A consisted of 0.4% formic acid in water, and mobile phase B consisted of 0.4% formic acid in a mixture of 90% acetonitrile and 10% water. Separation was achieved using a four-step gradient over 91 min at a flow rate of 230 nl min^{-1} (increase of initial gradient from 6% to 9% solvent B within 1 min, 9% to 30% solvent B within 81 min, 30% to 65% solvent B within 8 min, 65% to 100% solvent B within 1 min and 100% solvent B for 6 min before equilibrating to 6% solvent B for 18 min before the next injection). In the liquid junction setup, electrospray ionization was enabled by applying a voltage of 1.8 kV directly to the liquid being sprayed, and a non-coated silica emitter was used. The mass spectrometer was operated in data-dependent acquisition (DDA) mode. For MS2 acquisition, we collected a 375–1,650-m/z survey scan in the Orbitrap at 120,000 resolution (FTMS1); the AGC target was set to 'standard'; and a maximum injection time (IT) of 50 ms was applied. Intensity threshold was set to 2.5×10^4; charge states 2–6 were included; and dynamic exclusion after one scan was set to 90 s. Precursor isolation was performed with quadrupole, and isolation window size was set to 0.5 m/z. The RF lens was set to 30%. MS2 was measured in the Orbitrap with a resolution of 50,000. The high-energy collision-induced dissociation (HCD) fragmentation technique was used at a fixed collision energy of 38%. The normalized AGC target was set to 200% with a maximum IT of 110 ms. Xcalibur version 4.3.73.11 and Tune 3.4.3072.18 were used to operate the instrument.

Raw MS data were converted to mzML files using the ProteoWizard msConvert tool and then searched against the human reference proteome (UP000005640; reversed protein sequences as decoys and common contaminants added, downloaded on 8 August 2023 from UniProt) using MSFragger version 3.8 (ref. 79), yuIonQuant version 1.9.8 (ref. 80) and Philosopher version 5.0.0 (ref. 81) within FragPipe version 20.0. The built-in 'TMT10' workflow was loaded with a fragment mass tolerance of 20 ppm, peptide length from 7 to 50, peptide mass from 200 Da to 5,000 Da and 'stricttrypsin' for in silico digestion with up to two missed cleavages. Oxidation of methionine and acetylation of protein N-termini were set as variable modifications. Carbamidomethylation of cysteine and TMT tag modification on N-termini were included as fixed modifications. All other parameters were kept as standard.

Protein intensities were further analyzed using R version 4.3.1 (https://www.R-project.org/). Proteins with missing values across all replicates and conditions and fewer than two unique peptides were removed. Abundance normalization was performed on the remaining proteins. The intensity of a protein was normalized on the total abundance of all proteins for each respective sample (labeled with a separate TMT tag). This resulted in the same total protein abundance in each sample. Next, to obtain the soluble abundance ratio per protein, the median intensity of compound-treated samples was divided by the median intensity of vehicle-treated samples and $\log_2$ transformed. The $-\log_{10}$(P value) was derived from a two-tailed Student's t-test. Volcano plots were visualized using ggplot2.

Mouse-derived macrophages

Per2–Luc mice were originally obtained from Joseph Takahashi's laboratory (University of Texas Southwestern Medical Center) and, together with *LysM-*$^{BmalI-/-}$ mice, were maintained in the University of Oxford Biomedical Services. All protocols were approved by the University of Oxford Animal Welfare and Ethical Review Body and carried out according to the Animals (Scientific Procedures) Act 1986. Food and water were provided ad libitum, and housing was under 12-h light/dark cycles. The Cre-positive mice were age matched and sex matched with flox/flox littermate controls. BMDMs were cultured from females ages 13–17 weeks, and PECs were harvested from both male and female mice. All mice were group housed in standard housing under controlled room temperature (21–23 °C) and 50% humidity. All experimental animals were genotyped. Isolation of BMDMs was performed as follows. Tibias and femurs were dissected; bone marrow was flushed using DMEM; and the resulting single-cell suspension was plated out to non-tissue culture treated dishes. Macrophages harvested from mice at the same time are naturally synchronized.

Resulting cells were cultured in complete DMEM, P/S, 20% FBS and MCSF for 7 d. Cells were then treated with one of four conditions for 6 h before lysis for RNA extraction: DMSO (vehicle control), 100 nM LPS/DMSO, 100 µM CCM/DMSO and 100 nM LPS/100 µM CCM.

RNA-seq studies

Cells were lysed in TRIzol reagent, and RNA was extracted using chloroform followed by RNA Clean & Concentrator (Zymo Research, R1013). RNA-seq was performed by Novogene. Messenger RNA was purified from total RNA using poly(T) oligo-attached magnetic beads. After fragmentation, the first-strand cDNA was synthesized using random hexamer primers, followed by second-strand cDNA synthesis. The library was checked with Qubit and real-time PCR for quantification and Bioanalyzer for size distribution detection. Paired-end reads were generated.

Raw data (raw reads) of fastq format were first processed using fastp software. In this step, clean data (clean reads) were obtained by removing reads containing adapter, reads containing poly(N) and low-quality reads from raw data. At the same time, Q20, Q30 and GC content for the clean data was calculated. All the downstream analyses were based on the clean data with high quality. Reference genome and gene model annotation files were downloaded from the genome website directly. Index of the reference genome was built using HISAT2 version 2.0.5, and paired-end clean 2 reads were aligned to the reference genome using HISAT2 version 2.0.5. featureCounts version 1.5.0-p3 was used to count the read numbers mapped to each gene. Then, fragments per kilobase of transcript per million mapped reads (FPKM) of each gene was calculated based on the length of the gene and reads count mapped to this gene.

Differential expression analysis was performed using the DESeq2 R package (1.20.0). The resulting P values were adjusted using the Benjamini–Hochberg approach for controlling the FDR. Genes with an adjusted $P \leq 0.05$ found by DESeq2 were assigned as differentially expressed.

Statistics and reproducibility

For RNA-seq and macrophage luminometry, sample size was determined by a power calculation based on variance from previous experiments. No statistical method was used to predetermine sample size in other experiments. Sample size was started at $n = 3$ for a minimal statistical analysis and expanded in RT–qPCR based on previous experiments. Cells and mice were randomly allocated into experimental groups. Investigators were not blinded to allocation during experiments and outcome assessment. We followed the standard criteria in data processing for proteomics and next-generation sequencing data. Proteomics data with missing values across all conditions and fewer than two peptides were removed. In RNA-seq studies, raw data were cleaned by removing reads containing adapter, reads containing poly(N) and low-quality reads from raw data. In RT–qPCR, data with extremely low reads for endogenous control (β2 microglobulin) were excluded. In Per2–Luc, extreme outliers (for example, vehicle has much lower amplitude than drug) were excluded. All experiments were repeated at least once with similar results.

Reporting summary

Further information on research design is available in the Nature Portfolio Reporting Summary linked to this article.

Data availability

The structure factors and coordinates generated in this study were deposited to the RCSB Protein Data Bank (https://www.rcsb.org) with the following accession codes: 8RW6 for apo BMAL1 (PASB) and 8RW8 for BMAL1(PASB) in complex with CCM. Source data of RNA-seq were submitted to the Gene Expression Omnibus (https://www.ncbi.nlm.nih.gov/geo/) with accession number GSE255357. The thermal proteome profiling data were deposited to the ProteomeXchange Consortium via the PRIDE[82] partner repository with the dataset identifier PXD049298. Source data are provided with this paper.

References

63. Winter, G. et al. DIALS: implementation and evaluation of a new integration package. *Acta Crystallogr. D Struct. Biol.* **74**, 85–97 (2018).
64. McCoy, A. J. et al. Phaser crystallographic software. *J. Appl. Crystallogr.* **40**, 658–674 (2007).
65. Emsley, P., Lohkamp, B., Scott, W. G. & Cowtan, K. Features and development of Coot. *Acta Crystallogr. D Biol. Crystallogr.* **66**, 486–501 (2010).
66. Agirre, J. et al. The CCP4 suite: integrative software for macromolecular crystallography. *Acta Crystallogr. D Struct. Biol.* **79**, 449–461 (2023).
67. Liebschner, D. et al. Macromolecular structure determination using X-rays, neutrons and electrons: recent developments in Phenix. *Acta Crystallogr. D Struct. Biol.* **75**, 861–877 (2019).
68. Wright, C. S., Mi, L. Z., Lee, S. & Rastinejad, F. Crystal structure analysis of phosphatidylcholine–GM2-activator product complexes: evidence for hydrolase activity. *Biochemistry* **44**, 13510–13521 (2005).
69. Smith, R. H. B., Dar, A. C. & Schlessinger, A. PyVOL: a PyMOL plugin for visualization, comparison, and volume calculation of drug-binding sites. Preprint at *bioRxiv* https://doi.org/10.1101/816702 (2019).
70. Sander, T., Freyss, J., von Korff, M. & Rufener, C. DataWarrior: an open-source program for chemistry aware data visualization and analysis. *J. Chem. Inf. Model.* **55**, 460–473 (2015).
71. van der Watt, P. J., Roden, L. C., Davis, K. T., Parker, M. I. & Leaner, V. D. Circadian oscillations persist in cervical and esophageal cancer cells displaying decreased expression of tumor-suppressing circadian clock genes. *Mol. Cancer Res.* **18**, 1340–1353 (2020).
72. Tyanova, S., Temu, T. & Cox, J. The MaxQuant computational platform for mass spectrometry-based shotgun proteomics. *Nat. Protoc.* **11**, 2301–2319 (2016).
73. Tzioutziou, N. A. et al. Experimental design for time-series RNA-seq analysis of gene expression and alternative splicing. *Methods Mol. Biol.* **2398**, 173–188 (2022).
74. Hutchison, A. L. et al. Improved statistical methods enable greater sensitivity in rhythm detection for genome-wide data. *PLoS Comput. Biol.* **11**, e1004094 (2015).
75. Plautz, J. D. et al. Quantitative analysis of *Drosophila* period gene transcription in living animals. *J. Biol. Rhythms* **12**, 204–217 (1997).
76. Chenna, R. et al. Multiple sequence alignment with the Clustal series of programs. *Nucleic Acids Res.* **31**, 3497–3500 (2003).
77. Madeira, F. et al. Search and sequence analysis tools services from EMBL-EBI in 2022. *Nucleic Acids Res.* **50**, W276–W279 (2022).
78. Robert, X. & Gouet, P. Deciphering key features in protein structures with the new ENDscript server. *Nucleic Acids Res.* **42**, W320–W324 (2014).
79. Kong, A. T., Leprevost, F. V., Avtonomov, D. M., Mellacheruvu, D. & Nesvizhskii, A. I. MSFragger: ultrafast and comprehensive peptide identification in mass spectrometry-based proteomics. *Nat. Methods* **14**, 513–520 (2017).
80. Yu, F., Haynes, S. E. & Nesvizhskii, A. I. IonQuant enables accurate and sensitive label-free quantification with FDR-controlled match-between-runs. *Mol. Cell. Proteomics* **20**, 100077 (2021).
81. da Veiga Leprevost, F. et al. Philosopher: a versatile toolkit for shotgun proteomics data analysis. *Nat. Methods* **17**, 869–870 (2020).
82. Perez-Riverol, Y. et al. The PRIDE database resources in 2022: a hub for mass spectrometry-based proteomics evidences. *Nucleic Acids Res.* **50**, D543–D552 (2022).

Acknowledgements

The authors thank the staff at Diamond Light Source for access to beamline i03 for crystal diffraction. We thank H. Borrmann for primers in RT–qPCR and T. Hannich and A. Tinnacher from the Proteomics and Metabolomics Facility at CeMM for LC–MS/MS sample measurements. We are grateful to A. Ball and S. Cheruku for advice about compound analysis and to D. Mole and P. Ratcliffe for critical reading and insightful suggestions during manuscript preparations. This research was supported by Wellcome Trust Senior Investigator Award 210664/Z/18/Z (F.R.) and National Institute for Health and Care Research (NIHR) Oxford Health Biomedical Research Centre NIHR203316 (D.R.). The views expressed are those of the author(s) and not necessarily those of the NIHR or the Department of Health and Social Care. Additional support was provided from MRC MR/W019000/1 and MR/V034049/1 (D.R.) and Innovative Medicines Initiative 2 Joint Undertaking (JU) under grant agreement number 875510 (K.V.M.H.). The JU receives support from the European Union's Horizon 2020 Research and Innovation Program, the European Federation of Pharmaceutical Industries and Associations, the Ontario Institute for Cancer Research, the Royal Institution for the Advancement of Learning at McGill University, the KTH Royal Institute of Technology (Kungliga Tekniska Hoegskolan) and Diamond Light Source.

Author contributions

H.P. purified the proteins, conducted the screen, developed the CCM molecule, determined crystal structures and performed the biochemical studies and cell-based experiments involving U2OS and HEK293 cells. H.P., L.G.B. and K.V.M.H. carried out thermal profiling. L.B., M.B., M.V. and D.R. conducted the macrophage real-time circadian and RNA-seq studies. H.P. and S.K. conducted structural interpretations to evaluate mechanisms of action. H.P., S.K. and F.R. drafted the manuscript, and all authors participated in editing it.

Bibliography

Adler, B., & Adler, H. (2021). Type i interferon signaling and macrophages: A double-edged sword? *Cellular & Molecular Immunology*, *19*(9), 967–968. https://doi.org/10.1038/s41423-020-00609-0

Alexander, R. K., Liou, Y.-H., Knudsen, N. H., Starost, K. A., Xu, C., Hyde, A. L., Liu, S., Jacobi, D., Liao, N.-S., & Lee, C.-H. (2020). Bmal1 integrates mitochondrial metabolism and macrophage activation. *eLife*, *9*, e54090. https://doi.org/10.7554/eLife.54090

Alibhai, F. J., Reitz, C. J., Peppler, W. T., Basu, P., Sheppard, P., Choleris, E., Bakovic, M., & Martino, T. A. (2018). Female Clock19/19 mice are protected from the development of age-dependent cardiomyopathy. *Cardiovascular Research*, *114*(2), 259–271. https://doi.org/10.1093/cvr/cvx185

An, Y., Yuan, B., Xie, P., Gu, Y., Liu, Z., Wang, T., Li, Z., Xu, Y., & Liu, Y. (2022). Decoupling PER phosphorylation, stability and rhythmic expression from circadian clock function by abolishing PER-CK1 interaction. *Nature Communications*, *13*(1), 3991. https://doi.org/10.1038/s41467-022-31715-4

Anderson, S. T., Meng, H., Brooks, T. G., Tang, S. Y., Lordan, R., Sengupta, A., Nayak, S., Mřela, A., Sarantopoulou, D., Lahens, N. F., Weljie, A., Grant, G. R., Bushman, F. D., & FitzGerald, G. A. (2023). Sexual dimorphism in the response to chronic circadian misalignment on a high-fat diet. *Science Translational Medicine*, *15*(696), eabo2022. https://doi.org/10.1126/scitranslmed.abo2022

Aryal, R. P., Kwak, P. B., Tamayo, A. G., Gebert, M., Chiu, P.-L., Walz, T., & Weitz, C. J. (2017). Macromolecular assemblies of the mammalian circadian clock. *Molecular Cell*, *67*(5), 770–782.e6. https://doi.org/10.1016/j.molcel.2017.07.017

Asai, K., Hiki, N., Mimura, Y., Ogawa, T., Unou, K., & Kaminishi, M. (2001). GENDER DIFFERENCES IN CYTOKINE SECRETION BY HUMAN PERIPHERAL BLOOD MONONUCLEAR CELLS: ROLE OF ESTROGEN IN MODULATING LPS-INDUCED CYTOKINE SECRETION IN AN EX VIVO SEPTIC MODEL: *Shock*, *16*(5), 340–343. https://doi.org/10.1097/00024382-200116050-00003

Astafev, A. A., Mezhnina, V., Poe, A., Jiang, P., & Kondratov, R. V. (2024). Sexual dimorphism of circadian liver transcriptome. *iScience*, *27*(4), 109483. https://doi.org/10.1016/j.isci.2024.109483

Badia-i-Mompel, P., Vélez Santiago, J., Braunger, J., Geiss, C., Dimitrov, D., Müller-Dott, S., Taus, P., Dugourd, A., Holland, C. H., Ramirez Flores, R. O., & Saez-Rodriguez, J. (2022). decoupleR: Ensemble of computational methods to infer biological activities from omics data (M. L. Kuijjer, Ed.). *Bioinformatics Advances*, *2*(1), vbac016. https://doi.org/10.1093/bioadv/vbac016

Bain, C. C., Gibson, D. A., Steers, N. J., Boufea, K., Louwe, P. A., Doherty, C., González-Huici, V., Gentek, R., Magalhaes-Pinto, M., Shaw, T., Bajénoff, M., Bénézech, C., Walmsley, S. R., Dockrell, D. H., Saunders, P. T. K., Batada, N. N., & Jenkins, S. J. (2020). Rate of replenishment and microenvironment contribute to the sexually dimorphic phenotype and function of peritoneal macrophages. *Science Immunology*, *5*(48), eabc4466. https://doi.org/10.1126/sciimmunol.abc4466

Bannister, A. J., & Kouzarides, T. (2011). Regulation of chromatin by histone modifications. *Cell Research*, *21*(3), 381–395. https://doi.org/10.1038/cr.2011.22

Bellet, M. M., Deriu, E., Liu, J. Z., Grimaldi, B., Blaschitz, C., Zeller, M., Edwards, R. A., Sahar, S., Dandekar, S., Baldi, P., George, M. D., Raffatellu, M., & Sassone-Corsi, P. (2013). Circadian clock regulates the host response to *Salmonella*. *Proceedings of the*

National Academy of Sciences, *110*(24), 9897–9902. https://doi.org/10.1073/pnas.1120636110

Bell-Pedersen, D., Cassone, V. M., Earnest, D. J., Golden, S. S., Hardin, P. E., Thomas, T. L., & Zoran, M. J. (2005). Circadian rhythms from multiple oscillators: Lessons from diverse organisms. *Nature Reviews Genetics*, *6*(7), 544–556. https://doi.org/10.1038/nrg1633

Benna, C., Rajendran, S., Spiro, G., Menin, C., Dall'Olmo, L., Rossi, C. R., & Mocellin, S. (2021). Gender-specific associations between polymorphisms of the circadian gene RORA and cutaneous melanoma susceptibility. *Journal of Translational Medicine*, *19*(1), 57. https://doi.org/10.1186/s12967-021-02725-5

Beytebiere, J. R., Greenwell, B. J., Sahasrabudhe, A., & Menet, J. S. (2019a). Clock-controlled rhythmic transcription: Is the clock enough and how does it work? *Transcription*, *10*(4), 212–221. https://doi.org/10.1080/21541264.2019.1673636

Beytebiere, J. R., Trott, A. J., Greenwell, B. J., Osborne, C. A., Vitet, H., Spence, J., Yoo, S.-H., Chen, Z., Takahashi, J. S., Ghaffari, N., & Menet, J. S. (2019b). Tissue-specific BMAL1 cistromes reveal that rhythmic transcription is associated with rhythmic enhancer–enhancer interactions. *Genes & Development*, *33*(5), 294–309. https://doi.org/10.1101/gad.322198.118

Bhasin, J. M., Chakrabarti, E., Peng, D.-Q., Kulkarni, A., Chen, X., & Smith, J. D. (2008). Sex specific gene regulation and expression QTLs in mouse macrophages from a strain intercross (J. Borevitz, Ed.). *PLoS ONE*, *3*(1), e1435. https://doi.org/10.1371/journal.pone.0001435

Blacher, E., Tsai, C., Litichevskiy, L., Shipony, Z., Iweka, C. A., Schneider, K. M., Chuluun, B., Heller, H. C., Menon, V., Thaiss, C. A., & Andreasson, K. I. (2022). Aging disrupts cir-

cadian gene regulation and function in macrophages. *Nature Immunology*, *23*(2), 229–236. https://doi.org/10.1038/s41590-021-01083-0

Bolger, A. M., Lohse, M., & Usadel, B. (2014). Trimmomatic: A flexible trimmer for illumina sequence data. *Bioinformatics (Oxford, England)*, *30*(15), 2114–2120. https://doi.org/10.1093/bioinformatics/btu170

Briggs, P., Hunter, A. L., Yang, S.-h., Sharrocks, A. D., & Iqbal, M. (2021). PEGS: An efficient tool for gene set enrichment within defined sets of genomic intervals. *F1000Research*, *10*, 570. https://doi.org/10.12688/f1000research.53926.2

Brunet, A., Forsberg, F., Fan, Q., Sæther, T., & Collas, P. (2019). Nuclear lamin b1 interactions with chromatin during the circadian cycle are uncoupled from periodic gene expression. *Frontiers in Genetics*, *10*, 917. https://doi.org/10.3389/fgene.2019.00917

Bugge, A., Feng, D., Everett, L. J., Briggs, E. R., Mullican, S. E., Wang, F., Jager, J., & Lazar, M. A. (2012). Rev-erb and rev-erb coordinately protect the circadian clock and normal metabolic function. *Genes & Development*, *26*(7), 657–667. https://doi.org/10.1101/gad.186858.112

Bunger, M. K., Wilsbacher, L. D., Moran, S. M., Clendenin, C., Radcliffe, L. A., Hogenesch, J. B., Simon, M., Takahashi, J. S., & Bradfield, C. A. (2000). Mop3 is an essential component of the master circadian pacemaker in mammals. *Cell*, *103*(7), 1009–1017. https://doi.org/10.1016/S0092-8674(00)00205-1

Burioka, N., Fukuoka, Y., Koyanagi, S., Miyata, M., Takata, M., Chikumi, H., Takane, H., Watanabe, M., Endo, M., Sako, T., Suyama, H., Ohdo, S., & Shimizu, E. (2010). Asthma: Chronopharmacotherapy and the molecular clock. *Advanced Drug Delivery Reviews*, *62*(9), 946–955. https://doi.org/10.1016/j.addr.2010.03.012

Cai, D., Wang, J., Gao, B., Li, J., Wu, F., Zou, J. X., Xu, J., Jiang, Y., Zou, H., Huang, Z., Borowsky, A. D., Bold, R. J., Lara, P. N., Li, J. J., Chen, X., Lam, K. S., To, K.-F., Kung, H.-J., Fiehn, O., … Chen, H.-W. (2019). ROR is a targetable master regulator of cholesterol biosynthesis in a cancer subtype. *Nature Communications*, *10*(1), 4621. https://doi.org/10.1038/s41467-019-12529-3

Cao, X., Yang, Y., Selby, C. P., Liu, Z., & Sancar, A. (2021). Molecular mechanism of the repressive phase of the mammalian circadian clock. *Proceedings of the National Academy of Sciences*, *118*(2), e2021174118. https://doi.org/10.1073/pnas.2021174118

Chalfant, J. M., Howatt, D. A., Johnson, V. B., Tannock, L. R., Daugherty, A., & Pendergast, J. S. (2023). Chronic environmental circadian disruption increases atherosclerosis and dyslipidemia in female, but not male, ApolipoproteinE-deficient mice. *Frontiers in Physiology*, *14*, 1167858. https://doi.org/10.3389/fphys.2023.1167858

Chalfant, J. M., Howatt, D. A., Tannock, L. R., Daugherty, A., & Pendergast, J. S. (2020). Circadian disruption with constant light exposure exacerbates atherosclerosis in male ApolipoproteinE-deficient mice. *Scientific Reports*, *10*(1), 9920. https://doi.org/10.1038/s41598-020-66834-9

Chen, S., Fuller, K. K., Dunlap, J. C., & Loros, J. J. (2020). A pro- and anti-inflammatory axis modulates the macrophage circadian clock. *Frontiers in Immunology*, *11*, 867. https://doi.org/10.3389/fimmu.2020.00867

Chen, S., Saeed, A. F., Liu, Q., Jiang, Q., Xu, H., Xiao, G. G., Rao, L., & Duo, Y. (2023). Macrophages in immunoregulation and therapeutics. *Signal Transduction and Targeted Therapy*, *8*(1), 207. https://doi.org/10.1038/s41392-023-01452-1

Chen, Y., Chen, L., Lun, A. T. L., Baldoni, P. L., & Smyth, G. K. (2025). edgeR v4: Powerful differential analysis of sequencing data with expanded functionality and improved

support for small counts and larger datasets. *Nucleic Acids Research*, *53*(2), gkaf018. https://doi.org/10.1093/nar/gkaf018

Chistiakov, D. A., Bobryshev, Y. V., & Orekhov, A. N. (2016). Macrophage-mediated cholesterol handling in atherosclerosis. *Journal of Cellular and Molecular Medicine*, *20*(1), 17–28. https://doi.org/10.1111/jcmm.12689

Cho, H., Zhao, X., Hatori, M., Yu, R. T., Barish, G. D., Lam, M. T., Chong, L.-W., DiTacchio, L., Atkins, A. R., Glass, C. K., Liddle, C., Auwerx, J., Downes, M., Panda, S., & Evans, R. M. (2012). Regulation of circadian behaviour and metabolism by REV-ERB- and REV-ERB-. *Nature*, *485*(7396), 123–127. https://doi.org/10.1038/nature11048

Chun, S. K., Chung, S., Kim, H.-D., Lee, J. H., Jang, J., Kim, J., Kim, D., Son, G. H., Oh, Y. J., Suh, Y.-G., Lee, C. S., & Kim, K. (2015). A synthetic cryptochrome inhibitor induces anti-proliferative effects and increases chemosensitivity in human breast cancer cells. *Biochemical and Biophysical Research Communications*, *467*(2), 441–446. https://doi.org/10.1016/j.bbrc.2015.09.103

Clausen, B., Burkhardt, C., Reith, W., Renkawitz, R., & Förster, I. (1999). Conditional gene targeting in macrophages and granulocytes using LysMcre mice. *Transgenic Research*, *8*(4), 265–277. https://doi.org/10.1023/A:1008942828960

Cohen, B., Choi, Y. J., Hyman, S., Furuya, E. Y., Neidell, M., & Larson, E. (2013). Gender differences in risk of bloodstream and surgical site infections. *Journal of General Internal Medicine*, *28*(10), 1318–1325. https://doi.org/10.1007/s11606-013-2421-5

Collins, E. J., Cervantes-Silva, M. P., Timmons, G. A., O'Siorain, J. R., Curtis, A. M., & Hurley, J. M. (2021). Post-transcriptional circadian regulation in macrophages organizes temporally distinct immunometabolic states. [MAG ID: 3119784685]. *Genome Research*, *31*(2), 171–185. https://doi.org/10.1101/gr.263814.120

Cook, D. N., Kang, H. S., & Jetten, A. M. (2015). Retinoic acid-related orphan receptors (RORs): Regulatory functions in immunity, development, circadian rhythm, and metabolism. *Nuclear Receptor Research*, *2*. https://doi.org/10.11131/2015/101185

Crosby, P., & Partch, C. L. (2020). New insights into non-transcriptional regulation of mammalian core clock proteins. *Journal of Cell Science*, *133*(18), jcs241174. https://doi.org/10.1242/jcs.241174

Crouch, S., Kozlowski, R., Slater, K., & Fletcher, J. (1993). The use of ATP bioluminescence as a measure of cell proliferation and cytotoxicity. *Journal of Immunological Methods*, *160*(1), 81–88. https://doi.org/10.1016/0022-1759(93)90011-U

Cunningham, P. S., Meijer, P., Nazgiewicz, A., Anderson, S. G., Borthwick, L. A., Bagnall, J., Kitchen, G. B., Lodyga, M., Begley, N., Venkateswaran, R. V., Shah, R., Mercer, P. F., Durrington, H. J., Henderson, N. C., Piper-Hanley, K., Fisher, A. J., Chambers, R. C., Bechtold, D. A., Gibbs, J. E., … Blaikley, J. F. (2020). The circadian clock protein REVERB inhibits pulmonary fibrosis development. *Proceedings of the National Academy of Sciences*, *117*(2), 1139–1147. https://doi.org/10.1073/pnas.1912109117

Curtis, A. M., Fagundes, C. T., Yang, G., Palsson-McDermott, E. M., Wochal, P., McGettrick, A. F., Foley, N. H., Early, J. O., Chen, L., Zhang, H., Xue, C., Geiger, S. S., Hokamp, K., Reilly, M. P., Coogan, A. N., Vigorito, E., FitzGerald, G. A., & O'Neill, L. A. J. (2015). Circadian control of innate immunity in macrophages by miR-155 targeting *Bmal1*. *Proceedings of the National Academy of Sciences*, *112*(23), 7231–7236. https://doi.org/10.1073/pnas.1501327112

Danecek, P., Bonfield, J. K., Liddle, J., Marshall, J., Ohan, V., Pollard, M. O., Whitwham, A., Keane, T., McCarthy, S. A., Davies, R. M., & Li, H. (2021). Twelve years of SAMtools

and BCFtools. *GigaScience*, *10*(2), giab008. https://doi.org/10.1093/gigascience/giab008

Daniel, B., Belk, J. A., Meier, S. L., Chen, A. Y., Sandor, K., Czimmerer, Z., Varga, Z., Bene, K., Buquicchio, F. A., Qi, Y., Kitano, H., Wheeler, J. R., Foster, D. S., Januszyk, M., Longaker, M. T., Chang, H. Y., & Satpathy, A. T. (2023). Macrophage inflammatory and regenerative response periodicity is programmed by cell cycle and chromatin state. *Molecular Cell*, *83*(1), 121–138.e7. https://doi.org/10.1016/j.molcel.2022.11.017

Darnell, J. E., Kerr, L. M., & Stark, G. R. (1994). Jak-STAT pathways and transcriptional activation in response to IFNs and other extracellular signaling proteins. *Science*, *264*(5164), 1415–1421. https://doi.org/10.1126/science.8197455

Davies, J. Q., & Gordon, S. (2004, October 15). Isolation and culture of murine macrophages. In *Basic cell culture protocols* (pp. 091–104, Vol. 290). Humana Press. https://doi.org/10.1385/1-59259-838-2:091

De Giorgi, M., Jarrett, K. E., Burton, J. C., Doerfler, A. M., Hurley, A., Li, A., Hsu, R. H., Furgurson, M., Patel, K. R., Han, J., Borchers, C. H., & Lagor, W. R. (2020). Depletion of essential isoprenoids and ER stress induction following acute liver-specific deletion of HMG-CoA reductase. *Journal of Lipid Research*, *61*(12), 1675–1686. https://doi.org/10.1194/jlr.RA120001006

Dierickx, P., Emmett, M. J., Jiang, C., Uehara, K., Liu, M., Adlanmerini, M., & Lazar, M. A. (2019). SR9009 has REV-ERB–independent effects on cell proliferation and metabolism. *Proceedings of the National Academy of Sciences*, *116*(25), 12147–12152. https://doi.org/10.1073/pnas.1904226116

Doi, M., Hirayama, J., & Sassone-Corsi, P. (2006). Circadian regulator CLOCK is a histone acetyltransferase. *Cell*, *125*(3), 497–508. https://doi.org/10.1016/j.cell.2006.03.033

Druzd, D., Matveeva, O., Ince, L., Harrison, U., He, W., Schmal, C., Herzel, H., Tsang, A. H., Kawakami, N., Leliavski, A., Uhl, O., Yao, L., Sander, L. E., Chen, C.-S., Kraus, K., De Juan, A., Hergenhan, S. M., Ehlers, M., Koletzko, B., … Scheiermann, C. (2017). Lymphocyte circadian clocks control lymph node trafficking and adaptive immune responses. *Immunity*, *46*(1), 120–132. https://doi.org/10.1016/j.immuni.2016.12.011

Du, N.-H., Arpat, A. B., De Matos, M., & Gatfield, D. (2014). MicroRNAs shape circadian hepatic gene expression on a transcriptome-wide scale. *eLife*, *3*, e02510. https://doi.org/10.7554/eLife.02510

Duez, H., Van Der Veen, J. N., Duhem, C., Pourcet, B., Touvier, T., Fontaine, C., Derudas, B., Baugé, E., Havinga, R., Bloks, V. W., Wolters, H., Van Der Sluijs, F. H., Vennström, B., Kuipers, F., & Staels, B. (2008). Regulation of bile acid synthesis by the nuclear receptor rev-erb. *Gastroenterology*, *135*(2), 689–698.e5. https://doi.org/10.1053/j.gastro.2008.05.035

Durrington, H. J., Farrow, S. N., Loudon, A. S., & Ray, D. W. (2014). The circadian clock and asthma. *Thorax*, *69*(1), 90–92. https://doi.org/10.1136/thoraxjnl-2013-203482

Early, J. O., Menon, D., Wyse, C. A., Cervantes-Silva, M. P., Zaslona, Z., Carroll, R. G., Palsson-McDermott, E. M., Angiari, S., Ryan, D. G., Corcoran, S. E., Timmons, G., Geiger, S. S., Fitzpatrick, D. J., O'Connell, D., Xavier, R. J., Hokamp, K., O'Neill, L. A. J., & Curtis, A. M. (2018). Circadian clock protein BMAL1 regulates IL-1 in macrophages via NRF2. *Proceedings of the National Academy of Sciences*, *115*(36). https://doi.org/10.1073/pnas.1800431115

Ewels, P., Magnusson, M., Lundin, S., & Käller, M. (2016). MultiQC: Summarize analysis results for multiple tools and samples in a single report. *Bioinformatics*, *32*(19), 3047–3048. https://doi.org/10.1093/bioinformatics/btw354

FastQC. (2015, June). https://qubeshub.org/resources/fastqc

Fernandes, G., Halberg, F., Yunis, E. J., & Good, R. A. (1976). Circadian rhythmic plaque-forming cell response of spleens from mice immunized with SRBC. *The Journal of Immunology*, *117*(3), 962–966. https://doi.org/10.4049/jimmunol.117.3.962

Fishbein, A. B., Knutson, K. L., & Zee, P. C. (2021). Circadian disruption and human health. *Journal of Clinical Investigation*, *131*(19), e148286. https://doi.org/10.1172/JCI148286

Fontaine, C., Rigamonti, E., Pourcet, B., Duez, H., Duhem, C., Fruchart, J.-C., Chinetti-Gbaguidi, G., & Staels, B. (2008). The nuclear receptor rev-erb is a liver x receptor (LXR) target gene driving a negative feedback loop on select LXR-induced pathways in human macrophages. *Molecular Endocrinology*, *22*(8), 1797–1811. https://doi.org/10.1210/me.2007-0439

Forrest, K. M., Towers, M. E., Paul, O., Cho, H., Padmini, M. V., Naik, A., Lim, H. K., Issah, Y., Tang, S. Y., Deshmukh, H. S., Abt, M. C., Hudock, K. M., Eisenlohr, L. C., Grant, G. R., Brooks, T. G., & Sengupta, S. (2025). Role of IL-10 signaling in the circadian control of host response to influenza infection. *Mucosal Immunology*, S1933021925001278. https://doi.org/10.1016/j.mucimm.2025.11.010

Forsyth, K. S., Jiwrajka, N., Lovell, C. D., Toothacre, N. E., & Anguera, M. C. (2024). The conneXion between sex and immune responses. *Nature Reviews Immunology*, *24*(7), 487–502. https://doi.org/10.1038/s41577-024-00996-9

Freudenberger, T., Röck, K., Dai, G., Dorn, S., Mayer, P., Heim, H.-K., & Fischer, J. W. (2011). Estradiol inhibits hyaluronic acid synthase 1 expression in human vascular smooth muscle cells. *Basic Research in Cardiology*, *106*(6), 1099–1109. https://doi.org/10.1007/s00395-011-0217-5

Galouzis, C. C., & Furlong, E. E. (2022). Regulating specificity in enhancer–promoter communication. *Current Opinion in Cell Biology*, *75*, 102065. https://doi.org/10.1016/j.ceb.2022.01.010

Gal-Oz, S. T., Maier, B., Yoshida, H., Seddu, K., Elbaz, N., Czysz, C., Zuk, O., Stranger, B. E., Ner-Gaon, H., & Shay, T. (2019). ImmGen report: Sexual dimorphism in the immune system transcriptome. *Nature Communications*, *10*(1), 4295. https://doi.org/10.1038/s41467-019-12348-6

Garcia-Alonso, L., Holland, C. H., Ibrahim, M. M., Turei, D., & Saez-Rodriguez, J. (2019). Benchmark and integration of resources for the estimation of human transcription factor activities. *Genome Research*, *29*(8), 1363–1375. https://doi.org/10.1101/gr.240663.118

Geiger, S. S., Geiger, S. S., Anne M. Curtis, Curtis, A. M., Curtis, A., Luke A. J. O'Neill, O'Neill, L. A. J., Richard M. Siegel, & Siegel, R. M. (2019). Daily variation in macrophage phagocytosis is clock-independent and dispensable for cytokine production. [MAG ID: 2918122213 S2ID: a59c23f02cbb255c4c320332d083e4afb43829b0]. *Immunology*, *157*(2), 122–136. https://doi.org/10.1111/imm.13053

Gessani, S., & Belardelli, F. (1998). IFN- expression in macrophages and its possible biological significance. *Cytokine & Growth Factor Reviews*, *9*(2), 117–123. https://doi.org/10.1016/S1359-6101(98)00007-0

Gibbs, J. E., Blaikley, J., Beesley, S., Matthews, L., Simpson, K. D., Boyce, S. H., Farrow, S. N., Else, K. J., Singh, D., Ray, D. W., & Loudon, A. S. I. (2012). The nuclear receptor REV-ERB mediates circadian regulation of innate immunity through selective regulation of inflammatory cytokines. *Proceedings of the National Academy of Sciences*, *109*(2), 582–587. https://doi.org/10.1073/pnas.1106750109

Gontarz, P., Fu, S., Xing, X., Liu, S., Miao, B., Bazylianska, V., Sharma, A., Madden, P., Cates, K., Yoo, A., Moszczynska, A., Wang, T., & Zhang, B. (2020). Comparison of differential accessibility analysis strategies for ATAC-seq data. *Scientific Reports*, *10*(1), 10150. https://doi.org/10.1038/s41598-020-66998-4

Gough, D. J., Messina, N. L., Clarke, C. J., Johnstone, R. W., & Levy, D. E. (2012). Constitutive type i interferon modulates homeostatic balance through tonic signaling. *Immunity*, *36*(2), 166–174. https://doi.org/10.1016/j.immuni.2012.01.011

Greenberg, E. N., Marshall, M. E., Jin, S., Venkatesh, S., Dragan, M., Tsoi, L. C., Gudjonsson, J. E., Nie, Q., Takahashi, J. S., & Andersen, B. (2020). Circadian control of interferon-sensitive gene expression in murine skin. *Proceedings of the National Academy of Sciences*, *117*(11), 5761–5771. https://doi.org/10.1073/pnas.1915773117

Grimaldi, B., Bellet, M. M., Katada, S., Astarita, G., Hirayama, J., Amin, R. H., Granneman, J. G., Piomelli, D., Leff, T., & Sassone-Corsi, P. (2010). PER2 controls lipid metabolism by direct regulation of PPAR. *Cell Metabolism*, *12*(5), 509–520. https://doi.org/10.1016/j.cmet.2010.10.005

Guan, X., Polesso, F., Wang, C., Sehrawat, A., Hawkins, R. M., Murray, S. E., Thomas, G. V., Caruso, B., Thompson, R. F., Wood, M. A., Hipfinger, C., Hammond, S. A., Graff, J. N., Xia, Z., & Moran, A. E. (2022). Androgen receptor activity in t cells limits checkpoint blockade efficacy. *Nature*, *606*(7915), 791–796. https://doi.org/10.1038/s41586-022-04522-6

Halberg, F., Johnson, E. A., Brown, B. W., & Bittner, J. J. (1960). Susceptibility rhythm to e. coli endotoxin and bioassay. *Experimental Biology and Medicine*, *103*(1), 142–144. https://doi.org/10.3181/00379727-103-25439

Hand, L. E., Hopwood, T. W., Dickson, S. H., Walker, A. L., Loudon, A. S. I., Ray, D. W., Bechtold, D. A., & Gibbs, J. E. (2016). The circadian clock regulates inflammatory arthritis. *The FASEB Journal*, *30*(11), 3759–3770. https://doi.org/10.1096/fj.201600353R

Hashimoto, T., Tsuboi, K., Abe, T., Yoshikawa, T., Noguchi, K., Furukawa, T., Tateishi, K., Terashima, Y., Sibanuma, N., Azuma, N., Yamane, T., Matsui, K., & Hashiramoto, A. (2025). Nocturnal baricitinib administration leads to rapid drug responses in rheumatoid arthritis: A multicenter non-randomized controlled study. *Arthritis Research & Therapy*, *27*(1), 91. https://doi.org/10.1186/s13075-025-03555-2

Hayashi, M., Shimba, S., & Tezuka, M. (2007). Characterization of the molecular clock in mouse peritoneal macrophages. *Biological and Pharmaceutical Bulletin*, *30*(4), 621–626. https://doi.org/10.1248/bpb.30.621

He, W., Holtkamp, S., Hergenhan, S. M., Kraus, K., De Juan, A., Weber, J., Bradfield, P., Grenier, J. M. P., Pelletier, J., Druzd, D., Chen, C.-S., Ince, L. M., Bierschenk, S., Pick, R., Sperandio, M., Aurrand-Lions, M., & Scheiermann, C. (2018). Circadian expression of migratory factors establishes lineage-specific signatures that guide the homing of leukocyte subsets to tissues. *Immunity*, *49*(6), 1175–1190.e7. https://doi.org/10.1016/j.immuni.2018.10.007

Heinz, S., Benner, C., Spann, N., Bertolino, E., Lin, Y. C., Laslo, P., Cheng, J. X., Murre, C., Singh, H., & Glass, C. K. (2010). Simple combinations of lineage-determining transcription factors prime cis-regulatory elements required for macrophage and b cell identities. *Molecular Cell*, *38*(4), 576–589. https://doi.org/10.1016/j.molcel.2010.05.004

Hentges, L. D., Sergeant, M. J., Cole, C. B., Downes, D. J., Hughes, J. R., & Taylor, S. (2022). LanceOtron: A deep learning peak caller for genome sequencing experiments (V. Boeva,

Ed.). *Bioinformatics*, *38*(18), 4255–4263. https://doi.org/10.1093/bioinformatics/btac525

Herrada, A. A., Olate-Briones, A., Lazo-Amador, R., Liu, C., Hernández-Rojas, B., Riadi, G., & Escobedo, N. (2022). Lymph leakage promotes immunosuppression by enhancing anti-inflammatory macrophage polarization. *Frontiers in Immunology*, *13*, 841641. https://doi.org/10.3389/fimmu.2022.841641

Himes, B. E., Jiang, X., Wagner, P., Hu, R., Wang, Q., Klanderman, B., Whitaker, R. M., Duan, Q., Lasky-Su, J., Nikolos, C., Jester, W., Johnson, M., Panettieri, R. A., Tantisira, K. G., Weiss, S. T., & Lu, Q. (2014). RNA-seq transcriptome profiling identifies CRISPLD2 as a glucocorticoid responsive gene that modulates cytokine function in airway smooth muscle cells (J. P. Tuckermann, Ed.). *PLoS ONE*, *9*(6), e99625. https://doi.org/10.1371/journal.pone.0099625

Hirano, A., Nakagawa, T., Yoshitane, H., Oyama, M., Kozuka-Hata, H., Lanjakornsiripan, D., & Fukada, Y. (2016). USP7 and TDP-43: Pleiotropic regulation of cryptochrome protein stability paces the oscillation of the mammalian circadian clock (H. Oster, Ed.). *PLOS ONE*, *11*(4), e0154263. https://doi.org/10.1371/journal.pone.0154263

Hirota, T., Lee, J. W., St. John, P. C., Sawa, M., Iwaisako, K., Noguchi, T., Pongsawakul, P. Y., Sonntag, T., Welsh, D. K., Brenner, D. A., Doyle, F. J., Schultz, P. G., & Kay, S. A. (2012). Identification of small molecule activators of cryptochrome. *Science*, *337*(6098), 1094–1097. https://doi.org/10.1126/science.1223710

Hunter, A. L., Hunter, A. L., Pelekanou, C. E., Charlotte E Pelekanou, Adamson, A., Downton, P., Barron, N. J., Nichola J. Barron, Cornfield, T., Poolman, T., Humphreys, N. E., Cunningham, P. S., Hodson, L., Loudon, A. S. I., Iqbal, M., Bechtold, D. A., & Ray, D. W. (2020). Nuclear receptor REVERB is a state-dependent regulator of liver energy

metabolism. [MAG ID: 3090234017 S2ID: d3a5ef70136435fda2bbd7efc5c61978c9c62df1]. *Proceedings of the National Academy of Sciences of the United States of America*, *117*(41), 25869–25879. https://doi.org/10.1073/pnas.2005330117

Hurley, J. M., Jankowski, M. S., De Los Santos, H., Crowell, A. M., Fordyce, S. B., Zucker, J. D., Kumar, N., Purvine, S. O., Robinson, E. W., Shukla, A., Zink, E., Cannon, W. R., Baker, S. E., Loros, J. J., & Dunlap, J. C. (2018). Circadian proteomic analysis uncovers mechanisms of post-transcriptional regulation in metabolic pathways. *Cell Systems*, *7*(6), 613–626.e5. https://doi.org/10.1016/j.cels.2018.10.014

Husse, J., Leliavski, A., Tsang, A. H., Oster, H., & Eichele, G. (2014). The light-dark cycle controls peripheral rhythmicity in mice with a genetically ablated suprachiasmatic nucleus clock. *The FASEB Journal*, *28*(11), 4950–4960. https://doi.org/10.1096/fj.14-256594

Hussell, T., & Bell, T. J. (2014). Alveolar macrophages: Plasticity in a tissue-specific context. *Nature Reviews Immunology*, *14*(2), 81–93. https://doi.org/10.1038/nri3600

Ikeda, R., Tsuchiya, Y., Koike, N., Umemura, Y., Inokawa, H., Ono, R., Inoue, M., Sasawaki, Y., Grieten, T., Okubo, N., Ikoma, K., Fujiwara, H., Kubo, T., & Yagita, K. (2019). REV-ERB and REV-ERB function as key factors regulating mammalian circadian output. *Scientific Reports*, *9*(1), 10171. https://doi.org/10.1038/s41598-019-46656-0

Jang, J., Chung, S., Choi, Y., Lim, H. Y., Son, Y., Chun, S. K., Son, G. H., Kim, K., Suh, Y.-G., & Jung, J.-W. (2018). The cryptochrome inhibitor KS15 enhances e-box-mediated transcription by disrupting the feedback action of a circadian transcription-repressor complex. *Life Sciences*, *200*, 49–55. https://doi.org/10.1016/j.lfs.2018.03.022

Janich, P., Arpat, A. B., Castelo-Szekely, V., Lopes, M., & Gatfield, D. (2015). Ribosome profiling reveals the rhythmic liver translatome and circadian clock regulation by upstream

open reading frames. *Genome Research*, *25*(12), 1848–1859. https://doi.org/10.1101/gr.195404.115

Johnston, J. G., Speed, J. S., Becker, B. K., Kasztan, M., Soliman, R. H., Rhoads, M. K., Tao, B., Jin, C., Geurts, A. M., Hyndman, K. A., Pollock, J. S., & Pollock, D. M. (2020). Diurnal control of blood pressure is uncoupled from sodium excretion. *Hypertension*, *75*(6), 1624–1634. https://doi.org/10.1161/HYPERTENSIONAHA.119.13908

Kagan, J. C., Su, T., Horng, T., Chow, A., Akira, S., & Medzhitov, R. (2008). TRAM couples endocytosis of toll-like receptor 4 to the induction of interferon-. *Nature Immunology*, *9*(4), 361–368. https://doi.org/10.1038/ni1569

Keselman, A., Keselman, A., Xi Fang, Fang, X., Preston B. White, White, P. B., Wills-Karp, M., Nicola Heller, Heller, N. M., & Nicola Mary Heller. (2017). Estrogen signaling contributes to sex differences in macrophage polarization during asthma. [MAG ID: 2740628813 S2ID: fb08082d92f7c511e94ed7955ad677ae47e761c2]. *Journal of Immunology*, *199*(5), 1573–1583. https://doi.org/10.4049/jimmunol.1601975

Kim, D. W., Byun, J. M., Lee, J.-O., Kim, J. K., & Koh, Y. (2023). Chemotherapy delivery time affects treatment outcomes of female patients with diffuse large b cell lymphoma. *JCI Insight*, *8*(2), e164767. https://doi.org/10.1172/jci.insight.164767

Kim, Y. H., Marhon, S. A., Zhang, Y., Steger, D. J., Won, K.-J., & Lazar, M. A. (2018). Rev-erb dynamically modulates chromatin looping to control circadian gene transcription. *Science*, *359*(6381), 1274–1277. https://doi.org/10.1126/science.aao6891

Kitchen, G. B., Cunningham, P. S., Poolman, T. M., Iqbal, M., Maidstone, R., Baxter, M., Bagnall, J., Begley, N., Saer, B., Hussell, T., Matthews, L. C., Dockrell, D. H., Durrington, H. J., Gibbs, J. E., Blaikley, J. F., Loudon, A. S., & Ray, D. W. (2020). The clock gene *Bmal1* inhibits macrophage motility, phagocytosis, and impairs defense against pneu-

monia. *Proceedings of the National Academy of Sciences*, *117*(3), 1543–1551. https://doi.org/10.1073/pnas.1915932117

Klein, S. L., & Flanagan, K. L. (2016). Sex differences in immune responses [MAG ID: 2518536270 S2ID: a693ec1c22fb740f2bc4ad820dbf035cf3ed28db]. *Nature Reviews Immunology*, *16*(10), 626–638. https://doi.org/10.1038/nri.2016.90

Koike, N., Yoo, S.-H., Huang, H.-C., Kumar, V., Lee, C., Kim, T.-K., & Takahashi, J. S. (2012). Transcriptional architecture and chromatin landscape of the core circadian clock in mammals. *Science*, *338*(6105), 349–354. https://doi.org/10.1126/science.1226339

Kojetin, D. J., & Burris, T. P. (2014). REV-ERB and ROR nuclear receptors as drug targets. *Nature Reviews Drug Discovery*, *13*(3), 197–216. https://doi.org/10.1038/nrd4100

Kojima, S., Sher-Chen, E. L., & Green, C. B. (2012). Circadian control of mRNA polyadenylation dynamics regulates rhythmic protein expression. *Genes & Development*, *26*(24), 2724–2736. https://doi.org/10.1101/gad.208306.112

Koronowski, K. B., Kinouchi, K., Welz, P.-S., Smith, J. G., Zinna, V. M., Shi, J., Samad, M., Chen, S., Magnan, C. N., Kinchen, J. M., Li, W., Baldi, P., Benitah, S. A., & Sassone-Corsi, P. (2019). Defining the independence of the liver circadian clock. *Cell*, *177*(6), 1448–1462.e14. https://doi.org/10.1016/j.cell.2019.04.025

Koronowski, K. B., & Sassone-Corsi, P. (2021). Communicating clocks shape circadian homeostasis. *Science*, *371*(6530), eabd0951. https://doi.org/10.1126/science.abd0951

Kusnadi, A., Park, S. H., Yuan, R., Pannellini, T., Giannopoulou, E., Oliver, D., Lu, T., Park-Min, K.-H., & Ivashkiv, L. B. (2019). The cytokine TNF promotes transcription factor SREBP activity and binding to inflammatory genes to activate macrophages and limit tissue repair. *Immunity*, *51*(2), 241–257.e9. https://doi.org/10.1016/j.immuni.2019.06.005

Lam, M. T. Y., Cho, H., Lesch, H. P., Gosselin, D., Heinz, S., Tanaka-Oishi, Y., Benner, C., Kaikkonen, M. U., Kim, A. S., Kosaka, M., Lee, C. Y., Watt, A., Grossman, T. R., Rosenfeld, M. G., Evans, R. M., & Glass, C. K. (2013). Rev-erbs repress macrophage gene expression by inhibiting enhancer-directed transcription. *Nature*, *498*(7455), 511–515. https://doi.org/10.1038/nature12209

Lamia, K. A., Storch, K.-F., & Weitz, C. J. (2008). Physiological significance of a peripheral tissue circadian clock. *Proceedings of the National Academy of Sciences*, *105*(39), 15172–15177. https://doi.org/10.1073/pnas.0806717105

Lang, V., Ferencik, S., Ananthasubramaniam, B., Kramer, A., & Maier, B. (2021). Susceptibility rhythm to bacterial endotoxin in myeloid clock-knockout mice. *eLife*, *10*, e62469. https://doi.org/10.7554/eLife.62469

Langmead, B., & Salzberg, S. L. (2012). Fast gapped-read alignment with bowtie 2. *Nature Methods*, *9*(4), 357–359. https://doi.org/10.1038/nmeth.1923

Laothamatas, I., Rasmussen, E. S., Green, C. B., & Takahashi, J. S. (2023). Metabolic and chemical architecture of the mammalian circadian clock. *Cell Chemical Biology*, *30*(9), 1033–1052. https://doi.org/10.1016/j.chembiol.2023.08.014

Lauterbach, M. A., Hanke, J. E., Serefidou, M., Mangan, M. S., Kolbe, C.-C., Hess, T., Rothe, M., Kaiser, R., Hoss, F., Gehlen, J., Engels, G., Kreutzenbeck, M., Schmidt, S. V., Christ, A., Imhof, A., Hiller, K., & Latz, E. (2019). Toll-like receptor signaling rewires macrophage metabolism and promotes histone acetylation via ATP-citrate lyase. *Immunity*, *51*(6), 997–1011.e7. https://doi.org/10.1016/j.immuni.2019.11.009

Lawrence, M., Huber, W., Pagès, H., Aboyoun, P., Carlson, M., Gentleman, R., Morgan, M. T., & Carey, V. J. (2013). Software for computing and annotating genomic ranges (A. Prlic,

Ed.). *PLoS Computational Biology*, *9*(8), e1003118. https://doi.org/10.1371/journal.pcbi.1003118

Lazarov, T., Juarez-Carreño, S., Cox, N., & Geissmann, F. (2023). Physiology and diseases of tissue-resident macrophages. *Nature*, *618*(7966), 698–707. https://doi.org/10.1038/s41586-023-06002-x

Le Martelot, G., Canella, D., Symul, L., Migliavacca, E., Gilardi, F., Liechti, R., Martin, O., Harshman, K., Delorenzi, M., Desvergne, B., Herr, W., Deplancke, B., Schibler, U., Rougemont, J., Guex, N., Hernandez, N., Naef, F., & the CycliX consortium. (2012). Genome-wide RNA polymerase II profiles and RNA accumulation reveal kinetics of transcription and associated epigenetic changes during diurnal cycles (A. Kramer, Ed.). *PLoS Biology*, *10*(11), e1001442. https://doi.org/10.1371/journal.pbio.1001442

Lévi, F., Focan, C., Karaboué, A., De La Valette, V., Focan-Henrard, D., Baron, B., Kreutz, F., & Giacchetti, S. (2007). Implications of circadian clocks for the rhythmic delivery of cancer therapeutics. *Advanced Drug Delivery Reviews*, *59*(9), 1015–1035. https://doi.org/10.1016/j.addr.2006.11.001

Li, W., Jin, K., Luo, J., Xu, W., Wu, Y., Zhou, J., Wang, Y., Xu, R., Jiao, L., Wang, T., & Yang, G. (2022). NF-b and its crosstalk with endoplasmic reticulum stress in atherosclerosis. *Frontiers in Cardiovascular Medicine*, *9*, 988266. https://doi.org/10.3389/fcvm.2022.988266

Li, X., Li, X., Huang, P., Zhang, F., Du, J. K., Kong, Y., Shao, Z., Wu, X., Fan, W., Tao, H., Zhou, C., Shao, Y., Jin, Y., Ye, M., Chen, Y., Deng, J., Shao, J., Yue, J., Cheng, X., & Chinn, Y. E. (2024). Acetylation of TIR domains in the TLR4-mal-MyD88 complex regulates immune responses in sepsis. *The EMBO Journal*, *43*(21), 4954–4983. https://doi.org/10.1038/s44318-024-00237-8

Liu, B. C., Sarhan, J., Panda, A., Muendlein, H. I., Ilyukha, V., Coers, J., Yamamoto, M., Isberg, R. R., & Poltorak, A. (2018). Constitutive interferon maintains GBP expression required for release of bacterial components upstream of pyroptosis and anti-DNA responses. *Cell Reports*, *24*(1), 155–168.e5. https://doi.org/10.1016/j.celrep.2018.06.012

Lok, R., Qian, J., & Chellappa, S. L. (2024). Sex differences in sleep, circadian rhythms, and metabolism: Implications for precision medicine. *Sleep Medicine Reviews*, *75*, 101926. https://doi.org/10.1016/j.smrv.2024.101926

Love, M. I., Huber, W., & Anders, S. (2014). Moderated estimation of fold change and dispersion for RNA-seq data with DESeq2. *Genome Biology*, *15*(12), 550. https://doi.org/10.1186/s13059-014-0550-8

Luo, R., Yao, Y., Chen, Z., & Sun, X. (2025). An examination of the LPS-TLR4 immune response through the analysis of molecular structures and protein–protein interactions. *Cell Communication and Signaling*, *23*(1), 142. https://doi.org/10.1186/s12964-025-02149-4

Maidstone, R. J., Ray, D. W., Liu, J., Bowden, J., Rutter, M. K., & Durrington, H. J. (2025). Increased risk of asthma in female night shift workers. *ERJ Open Research*, *11*(6), 00137–2025. https://doi.org/10.1183/23120541.00137-2025

Major-Styles, C. T., Munns, J., Zeng, A., Vanden Oever, M., O'Neill, J. S., & Edgar, R. S. (2025). Chronic CRYPTOCHROME deficiency enhances cell-intrinsic antiviral defences. *Philosophical Transactions of the Royal Society B: Biological Sciences*, *380*(1918), 20230344. https://doi.org/10.1098/rstb.2023.0344

Marriott, I., Bost, K. L., & Huet-Hudson, Y. M. (2006). Sexual dimorphism in expression of receptors for bacterial lipopolysaccharides in murine macrophages: A possible mechanism

for gender-based differences in endotoxic shock susceptibility. *Journal of Reproductive Immunology*, *71*(1), 12–27. https://doi.org/10.1016/j.jri.2006.01.004

Menet, J. S., Pescatore, S., & Rosbash, M. (2014). CLOCK:BMAL1 is a pioneer-like transcription factor. *Genes & Development*, *28*(1), 8–13. https://doi.org/10.1101/gad.228536.113

Menet, J. S., Rodriguez, J., Abruzzi, K. C., & Rosbash, M. (2012). Nascent-seq reveals novel features of mouse circadian transcriptional regulation. *eLife*, *1*, e00011. https://doi.org/10.7554/eLife.00011

Mermet, J., Yeung, J., & Naef, F. (2021). Oscillating and stable genome topologies underlie hepatic physiological rhythms during the circadian cycle (D. Noordermeer, Ed.). *PLOS Genetics*, *17*(2), e1009350. https://doi.org/10.1371/journal.pgen.1009350

Michael, A. K., Stoos, L., Crosby, P., Eggers, N., Nie, X. Y., Makasheva, K., Minnich, M., Healy, K. L., Weiss, J., Kempf, G., Cavadini, S., Kater, L., Seebacher, J., Vecchia, L., Chakraborty, D., Isbel, L., Grand, R. S., Andersch, F., Fribourgh, J. L., … Thomä, N. H. (2023). Cooperation between bHLH transcription factors and histones for DNA access. *Nature*, *619*(7969), 385–393. https://doi.org/10.1038/s41586-023-06282-3

Miyamoto, T., Honda, Y., Izawa, K., Kanazawa, N., Kadowaki, S., Ohnishi, H., Fujimoto, M., Kambe, N., Kase, N., Shiba, T., Nakagishi, Y., Akizuki, S., Murakami, K., Bamba, M., Nishida, Y., Inui, A., Fujisawa, T., Nishida, D., Iwata, N., … Yasumi, T. (2022). Assessment of type i interferon signatures in undifferentiated inflammatory diseases: A japanese multicenter experience. *Frontiers in Immunology*, *13*, 905960. https://doi.org/10.3389/fimmu.2022.905960

Mo, D., Palmer, C. S., & Kimmey, J. M. (2025). By dawn or dusk—how circadian timing rewrites bacterial infection outcomes. *FEBS Letters*, 1873–3468.70212. https://doi.org/10.1002/1873-3468.70212

Moharrami, N. N., Bjørkøy Tande, E., Ryan, L., Espevik, T., & Boyartchuk, V. (2018). ROR controls inflammatory state of human macrophages (A. Poltorak, Ed.). *PLOS ONE*, *13*(11), e0207374. https://doi.org/10.1371/journal.pone.0207374

Montaigne, D., Marechal, X., Modine, T., Coisne, A., Mouton, S., Fayad, G., Ninni, S., Klein, C., Ortmans, S., Seunes, C., Potelle, C., Berthier, A., Gheeraert, C., Piveteau, C., Deprez, R., Eeckhoute, J., Duez, H., Lacroix, D., Deprez, B., … Staels, B. (2018). Daytime variation of perioperative myocardial injury in cardiac surgery and its prevention by rev-erb antagonism: A single-centre propensity-matched cohort study and a randomised study. *The Lancet*, *391*(10115), 59–69. https://doi.org/10.1016/S0140-6736(17)32132-3

Müller-Dott, S., Tsirvouli, E., Vazquez, M., Ramirez Flores, R. O., Badia-i-Mompel, P., Fallegger, R., Türei, D., Lægreid, A., & Saez-Rodriguez, J. (2023). Expanding the coverage of regulons from high-confidence prior knowledge for accurate estimation of transcription factor activities. *Nucleic Acids Research*, *51*(20), 10934–10949. https://doi.org/10.1093/nar/gkad841

Mure, L. S., Le, H. D., Benegiamo, G., Chang, M. W., Rios, L., Jillani, N., Ngotho, M., Kariuki, T., Dkhissi-Benyahya, O., Cooper, H. M., & Panda, S. (2018). Diurnal transcriptome atlas of a primate across major neural and peripheral tissues. *Science*, *359*(6381), eaao0318. https://doi.org/10.1126/science.aao0318

Narasimamurthy, R., Hatori, M., Nayak, S. K., Liu, F., Panda, S., & Verma, I. M. (2012). Circadian clock protein cryptochrome regulates the expression of proinflammatory cytokines. *Proceedings of the National Academy of Sciences*, *109*(31), 12662–12667. https://doi.org/10.1073/pnas.1209965109

Nguyen, K. D., Nguyen, K. D., Nguyen, K. D., Sarah J. Fentress, Sarah J. Fentress, Fentress, S. J., Yifu Qiu, Qiu, Y., Karen Yun, Yun, K., Jeffery S. Cox, Cox, J. S., Ajay Chawla,

& Chawla, A. (2013). Circadian gene bmal1 regulates diurnal oscillations of ly6c(hi) inflammatory monocytes. [MAG ID: 2094914236 S2ID: 861a62451d0c510f5149dc2a9c32de941ca73

Science, *341*(6153), 1483–1488. https://doi.org/10.1126/science.1240636

Nguyen, T.-M., Shafi, A., Nguyen, T., & Draghici, S. (2019). Identifying significantly impacted pathways: A comprehensive review and assessment. *Genome Biology*, *20*(1), 203. https://doi.org/10.1186/s13059-019-1790-4

O'Connor, M.-F., Motivala, S. J., Valladares, E. M., Olmstead, R., & Irwin, M. R. (2007). Sex differences in monocyte expression of IL-6: Role of autonomic mechanisms. *American Journal of Physiology-Regulatory, Integrative and Comparative Physiology*, *293*(1), R145–R151. https://doi.org/10.1152/ajpregu.00752.2006

Oishi, Y., Hayashi, S., Isagawa, T., Oshima, M., Iwama, A., Shimba, S., Okamura, H., & Manabe, I. (2017). Bmal1 regulates inflammatory responses in macrophages by modulating enhancer RNA transcription. [MAG ID: 2737221802 S2ID: e0dabeaebf553d1bb65de3ec9a161e229

Scientific Reports, *7*(1), 7086–7086. https://doi.org/10.1038/s41598-017-07100-3

Oliva-Ramírez, J., Jacqueline Oliva-Ramírez, Oliva-Ramírez, J., María Maximina Bertha Moreno-Altamirano, Moreno-Altamirano, M. M. B., Benjamín Pineda, Pineda-Olvera, B., Patricia Isidra Cauich-Sánchez, Cauich-Sánchez, P. I., Francisco Javier Sánchez-García, & Sánchez-García, F. J. (2014). Crosstalk between circadian rhythmicity, mitochondrial dynamics and macrophage bactericidal activity [MAG ID: 1967061101 S2ID: 37fcc04f2f00891d928753c4229b619a4a89e1b2]. *Immunology*, *143*(3), 490–497. https://doi.org/10.1111/imm.12329

O'Siorain, J. R., Cox, S. L., Payet, C., Nally, F. K., He, Y., Drewinksi, T. T., Kennedy, O. D., Dowling, J. K., Mellett, M., Early, J. O., & Curtis, A. M. (2024). Time-of-day control of mitochondria regulates NLRP3

inflammasome activation in macrophages. *The FASEB Journal*, *38*(24), e70235. https://doi.org/10.1096/fj.202400508RR

Pan, X., O'Hare, J., Mowdawalla, C., Mota, S., Wang, N., & Hussain, M. M. (2025). Bmal1 is involved in the regulation of macrophage cholesterol homeostasis. *JCI Insight*, *10*(21), e194304. https://doi.org/10.1172/jci.insight.194304

Pariollaud, M., Gibbs, J. E., Hopwood, T., Brown, S., Begley, N., Vonslow, R., Poolman, T., Guo, B., Baoqiang Guo, Saer, B., Jones, D. H., Tellam, J. P., Bresciani, S., Tomkinson, N. C. O., Wojno-Picon, J., Cooper, A. W. J., Daniels, D. A., Trump, R. P., Grant, D., … Ray, D. W. (2018). Circadian clock component REV-ERB controls homeostatic regulation of pulmonary inflammation [MAG ID: 2793930217 S2ID: c633cdd028b11bd26edb082dfa0268 *Journal of Clinical Investigation*, *128*(6), 2281–2296. https://doi.org/10.1172/jci93910

Partch, C. L., Green, C. B., & Takahashi, J. S. (2014). Molecular architecture of the mammalian circadian clock. *Trends in Cell Biology*, *24*(2), 90–99. https://doi.org/10.1016/j.tcb.2013.07.002

Paschos, G. K., Lordan, R., & FitzGerald, G. A. (2025). Intersection of sex and circadian biology. *Current Opinion in Physiology*, *45*, 100834. https://doi.org/10.1016/j.cophys.2025.100834

Portela, A., & Esteller, M. (2010). Epigenetic modifications and human disease. *Nature Biotechnology*, *28*(10), 1057–1068. https://doi.org/10.1038/nbt.1685

Preußner, M., Wilhelmi, I., Schultz, A.-S., Finkernagel, F., Michel, M., Möröy, T., & Heyd, F. (2014). Rhythmic u2af26 alternative splicing controls PERIOD1 stability and the circadian clock in mice. *Molecular Cell*, *54*(4), 651–662. https://doi.org/10.1016/j.molcel.2014.04.015

Pu, H., Bailey, L. C., Bauer, L. G., Voronkov, M., Baxter, M., Huber, K. V. M., Khorasanizadeh, S., Ray, D., & Rastinejad, F. (2025). Pharmacological targeting of BMAL1 modulates circadian and immune pathways. *Nature Chemical Biology*, *21*(5), 736–745. https://doi.org/10.1038/s41589-025-01863-x

Qin, Q., Fan, J., Zheng, R., Wan, C., Mei, S., Wu, Q., Sun, H., Brown, M., Zhang, J., Meyer, C. A., & Liu, X. S. (2020). Lisa: Inferring transcriptional regulators through integrative modeling of public chromatin accessibility and ChIP-seq data. *Genome Biology*, *21*(1), 32. https://doi.org/10.1186/s13059-020-1934-6

Ramírez, F., Ryan, D. P., Grüning, B., Bhardwaj, V., Kilpert, F., Richter, A. S., Heyne, S., Dündar, F., & Manke, T. (2016). deepTools2: A next generation web server for deep-sequencing data analysis. *Nucleic Acids Research*, *44*, W160–W165. https://doi.org/10.1093/nar/gkw257

Rasmussen, E. S., Takahashi, J. S., & Green, C. B. (2022). Time to target the circadian clock for drug discovery. *Trends in Biochemical Sciences*, *47*(9), 745–758. https://doi.org/10.1016/j.tibs.2022.04.009

Rauluseviciute, I., Riudavets-Puig, R., Blanc-Mathieu, R., Castro-Mondragon, J. A., Ferenc, K., Kumar, V., Lemma, R. B., Lucas, J., Chèneby, J., Baranasic, D., Khan, A., Fornes, O., Gundersen, S., Johansen, M., Hovig, E., Lenhard, B., Sandelin, A., Wasserman, W. W., Parcy, F., & Mathelier, A. (2024). JASPAR 2024: 20th anniversary of the open-access database of transcription factor binding profiles. *Nucleic Acids Research*, *52*, D174–D182. https://doi.org/10.1093/nar/gkad1059

Raza, S., Barnett, M. W., Barnett-Itzhaki, Z., Amit, I., Hume, D. A., & Freeman, T. C. (2014). Analysis of the transcriptional networks underpinning the activation of murine macrophages

by inflammatory mediators. *Journal of Leukocyte Biology*, *96*(2), 167–183. https://doi.org/10.1189/jlb.6HI0313-169R

Reijnders, T. D. Y., Saris, A., Schultz, M. J., & Van Der Poll, T. (2020). Immunomodulation by macrolides: Therapeutic potential for critical care. *The Lancet Respiratory Medicine*, *8*(6), 619–630. https://doi.org/10.1016/S2213-2600(20)30080-1

Rensing, L., Meyer-Grahle, U., & Ruoff, P. (2001). BIOLOGICAL TIMING AND THE CLOCK METAPHOR: OSCILLATORY AND HOURGLASS MECHANISMS. *Chronobiology International*, *18*(3), 329–369. https://doi.org/10.1081/CBI-100103961

Rijo-Ferreira, F., & Takahashi, J. S. (2019). Genomics of circadian rhythms in health and disease. *Genome Medicine*, *11*(1), 82. https://doi.org/10.1186/s13073-019-0704-0

Ripperger, J. A., & Schibler, U. (2006). Rhythmic CLOCK-BMAL1 binding to multiple e-box motifs drives circadian dbp transcription and chromatin transitions. *Nature Genetics*, *38*(3), 369–374. https://doi.org/10.1038/ng1738

Riva, S. G., Georgiades, E., Gur, E. R., Baxter, M., & Hughes, J. R. (2023). CATCH-UP: A high-throughput upstream-pipeline for bulk ATAC-seq and ChIP-seq data. *Journal of Visualized Experiments*, (199), 65633. https://doi.org/10.3791/65633

Rosas, M., Davies, L. C., Giles, P. J., Liao, C.-T., Kharfan, B., Stone, T. C., O'Donnell, V. B., Fraser, D. J., Jones, S. A., & Taylor, P. R. (2014). The transcription factor gata6 links tissue macrophage phenotype and proliferative renewal. *Science*, *344*(6184), 645–648. https://doi.org/10.1126/science.1251414

Scheer, F. A. J. L., Hilton, M. F., Evoniuk, H. L., Shiels, S. A., Malhotra, A., Sugarbaker, R., Ayers, R. T., Israel, E., Massaro, A. F., & Shea, S. A. (2021). The endogenous circadian system worsens asthma at night independent of sleep and other daily behavioral

or environmental cycles. *Proceedings of the National Academy of Sciences*, *118*(37), e2018486118. https://doi.org/10.1073/pnas.2018486118

Scheiermann, C., Kunisaki, Y., Lucas, D., Chow, A., Jang, J.-E., Zhang, D., Hashimoto, D., Merad, M., & Frenette, P. S. (2012). Adrenergic nerves govern circadian leukocyte recruitment to tissues. *Immunity*, *37*(2), 290–301. https://doi.org/10.1016/j.immuni.2012.05.021

Scheuermann, T. H., Li, Q., Ma, H.-W., Key, J., Zhang, L., Chen, R., Garcia, J. A., Naidoo, J., Longgood, J., Frantz, D. E., Tambar, U. K., Gardner, K. H., & Bruick, R. K. (2013). Allosteric inhibition of hypoxia inducible factor-2 with small molecules. *Nature Chemical Biology*, *9*(4), 271–276. https://doi.org/10.1038/nchembio.1185

Schilperoort, M., Van Den Berg, R., Bosmans, L. A., Van Os, B. W., Dollé, M. E. T., Smits, N. A. M., Guichelaar, T., Van Baarle, D., Koemans, L., Berbée, J. F. P., Deboer, T., Meijer, J. H., De Vries, M. R., Vreeken, D., Van Gils, J. M., Willems Van Dijk, K., Van Kerkhof, L. W. M., Lutgens, E., Biermasz, N. R., … Kooijman, S. (2020). Disruption of circadian rhythm by alternating light-dark cycles aggravates atherosclerosis development in APOE*3-leiden.CETP mice. *Journal of Pineal Research*, *68*(1), e12614. https://doi.org/10.1111/jpi.12614

Schmutz, I., Ripperger, J. A., Baeriswyl-Aebischer, S., & Albrecht, U. (2010). The mammalian clock component PERIOD2 coordinates circadian output by interaction with nuclear receptors. *Genes & Development*, *24*(4), 345–357. https://doi.org/10.1101/gad.564110

Schultz, T. E., Mathmann, C. D., Domínguez Cadena, L. C., Muusse, T. W., Kim, H., Wells, J. W., Ulett, G. C., Hamerman, J. A., Brooks, A. J., Kobe, B., Sweet, M. J., Stacey, K. J., & Blumenthal, A. (2025). TLR4 endocytosis and endosomal TLR4 signaling are

distinct and independent outcomes of TLR4 activation. *EMBO Reports*, *26*(10), 2740–2766. https://doi.org/10.1038/s44319-025-00444-2

Scotland, R. S., Stables, M. J., Madalli, S., Watson, P., & Gilroy, D. W. (2011). Sex differences in resident immune cell phenotype underlie more efficient acute inflammatory responses in female mice. *Blood*, *118*(22), 5918–5927. https://doi.org/10.1182/blood-2011-03-340281

Scott, C. L., & Guilliams, M. (2018). The role of kupffer cells in hepatic iron and lipid metabolism. *Journal of Hepatology*, *69*(5), 1197–1199. https://doi.org/10.1016/j.jhep.2018.02.013

Sengupta, S., Tang, S. Y., Devine, J. C., Anderson, S. T., Nayak, S., Zhang, S. L., Valenzuela, A., Fisher, D. G., Grant, G. R., López, C. B., & FitzGerald, G. A. (2019). Circadian control of lung inflammation in influenza infection. *Nature Communications*, *10*(1), 4107. https://doi.org/10.1038/s41467-019-11400-9

Sharif, O., Brunner, J. S., Vogel, A., & Schabbauer, G. (2019). Macrophage rewiring by nutrient associated PI3k dependent pathways. *Frontiers in Immunology*, *10*, 2002. https://doi.org/10.3389/fimmu.2019.02002

Sharma, S., Gibbons, A., & Saphire, E. O. (2025). Sex differences in tissue-specific immunity and immunology. *Science*, *389*(6760), 599–603. https://doi.org/10.1126/science.adx4381

Shim, D.-W., Eo, J.-C., Kim, S., Hwang, I., Nam, B., Shin, J.-E., Han, S. H., & Yu, J.-W. (2024). Deficiency of circadian clock gene bmal1 exacerbates noncanonical inflammasome-mediated pyroptosis and lethality via rev-erb-c/EBP-SAA1 axis. *Experimental & Molecular Medicine*, *56*(2), 370–382. https://doi.org/10.1038/s12276-024-01162-w

Shinohara, Y., Koyama, Y. M., Ukai-Tadenuma, M., Hirokawa, T., Kikuchi, M., Yamada, R. G., Ukai, H., Fujishima, H., Umehara, T., Tainaka, K., & Ueda, H. R. (2017). Temperature-

sensitive substrate and product binding underlie temperature-compensated phosphorylation in the clock. *Molecular Cell*, *67*(5), 783–798.e20. https://doi.org/10.1016/j.molcel.2017.08.009

Siiskonen, H., Oikari, S., Pasonen-SeppÃ¤nen, S., & Rilla, K. (2015). Hyaluronan synthase 1: A mysterious enzyme with unexpected functions. *Frontiers in Immunology*, *6*. https://doi.org/10.3389/fimmu.2015.00043

Silva, J., & Iwasaki, A. (2024). Sex differences in postacute infection syndromes. *Science Translational Medicine*, *16*(773), eado2102. https://doi.org/10.1126/scitranslmed.ado2102

Silva Lagos, L., Luu, T. V., De Haan, B., Faas, M., & De Vos, P. (2022). TLR2 and TLR4 activity in monocytes and macrophages after exposure to amoxicillin, ciprofloxacin, doxycycline and erythromycin. *Journal of Antimicrobial Chemotherapy*, *77*(11), 2972–2983. https://doi.org/10.1093/jac/dkac254

Silver, A. C., Arjona, A., Walker, W. E., & Fikrig, E. (2012). The circadian clock controls toll-like receptor 9-mediated innate and adaptive immunity. *Immunity*, *36*(2), 251–261. https://doi.org/10.1016/j.immuni.2011.12.017

Sitaula, S., Zhang, J., Ruiz, F., & Burris, T. P. (2017). Rev-erb regulation of cholesterologenesis. *Biochemical Pharmacology*, *131*, 68–77. https://doi.org/10.1016/j.bcp.2017.02.006

Spitschan, M., Santhi, N., Ahluwalia, A., Fischer, D., Hunt, L., Karp, N. A., Lévi, F., Pineda-Torra, I., Vidafar, P., & White, R. (2022). Sex differences and sex bias in human circadian and sleep physiology research. *eLife*, *11*, e65419. https://doi.org/10.7554/eLife.65419

Spitz, F., & Furlong, E. E. M. (2012). Transcription factors: From enhancer binding to developmental control. *Nature Reviews Genetics*, *13*(9), 613–626. https://doi.org/10.1038/nrg3207

Stephens, M. (2016). False discovery rates: A new deal. *Biostatistics*, kxw041. https://doi.org/10.1093/biostatistics/kxw041

Takahashi, J. S. (2017). Transcriptional architecture of the mammalian circadian clock. *Nature Reviews Genetics*, *18*(3), 164–179. https://doi.org/10.1038/nrg.2016.150

Takeda, Y., & Jetten, A. M. (2013). Prospero-related homeobox 1 (prox1) functions as a novel modulator of retinoic acid-related orphan receptors - and -mediated transactivation. *Nucleic Acids Research*, *41*(14), 6992–7008. https://doi.org/10.1093/nar/gkt447

Talamanca, L., Gobet, C., & Naef, F. (2023). Sex-dimorphic and age-dependent organization of 24-hour gene expression rhythms in humans. *Science*, *379*(6631), 478–483. https://doi.org/10.1126/science.add0846

Tavsanli, N., Erözden, A. A., & Çalışkan, M. (2024). Evaluation of small-molecule modulators of the circadian clock: Promising therapeutic approach to cancer. *Molecular Biology Reports*, *51*(1), 848. https://doi.org/10.1007/s11033-024-09813-x

Timmons, G. A., Carroll, R. G., O'Siorain, J. R., Cervantes-Silva, M. P., Fagan, L. E., Cox, S. L., Palsson-McDermott, E., Finlay, D. K., Vincent, E. E., Jones, N., & Curtis, A. M. (2021). The circadian clock protein BMAL1 acts as a metabolic sensor in macrophages to control the production of pro IL-1. *Frontiers in Immunology*, *12*, 700431. https://doi.org/10.3389/fimmu.2021.700431

Tong, A.-J., Liu, X., Thomas, B. J., Lissner, M. M., Baker, M. R., Senagolage, M. D., Allred, A. L., Barish, G. D., & Smale, S. T. (2016). A stringent systems approach uncovers gene-specific mechanisms regulating inflammation. *Cell*, *165*(1), 165–179. https://doi.org/10.1016/j.cell.2016.01.020

Tong, C. Y., Li, C., Jacq, A., Nie, X. Y., Guy, C. R., Suh, J. H., Wong, R. K., Merlin, C., Menet, J. S., & Jiang, Y. (2025, April 8). Single-cell multiomic analysis of circadian rhythmicity in mouse liver. https://doi.org/10.1101/2025.04.03.647044

Torcia, M. G., Nencioni, L., Clemente, A. M., Civitelli, L., Celestino, I., Limongi, D., Fadigati, G., Perissi, E., Cozzolino, F., Garaci, E., & Palamara, A. T. (2012). Sex differences in the response to viral infections: TLR8 and TLR9 ligand stimulation induce higher IL10 production in males (A. Pekosz, Ed.). *PLoS ONE*, *7*(6), e39853. https://doi.org/10.1371/journal.pone.0039853

Tretina, K., Park, E.-S., Maminska, A., & MacMicking, J. D. (2019). Interferon-induced guanylate-binding proteins: Guardians of host defense in health and disease. *Journal of Experimental Medicine*, *216*(3), 482–500. https://doi.org/10.1084/jem.20182031

Trott, A. J., & Menet, J. S. (2018). Regulation of circadian clock transcriptional output by CLOCK:BMAL1 (A. Kramer, Ed.). *PLOS Genetics*, *14*(1), e1007156. https://doi.org/10.1371/journal.pgen.1007156

Trump, R. P., Bresciani, S., Cooper, A. W. J., Tellam, J. P., Wojno, J., Blaikley, J., Orband-Miller, L. A., Kashatus, J. A., Boudjelal, M., Dawson, H. C., Loudon, A., Ray, D., Grant, D., Farrow, S. N., Willson, T. M., & Tomkinson, N. C. O. (2013). Optimized chemical probes for REV-ERB. *Journal of Medicinal Chemistry*, *56*(11), 4729–4737. https://doi.org/10.1021/jm400458q

Ueno, M., Fujita, Y., Tanaka, T., Nakamura, Y., Kikuta, J., Ishii, M., & Yamashita, T. (2013). Layer v cortical neurons require microglial support for survival during postnatal development. *Nature Neuroscience*, *16*(5), 543–551. https://doi.org/10.1038/nn.3358

Vasimuddin, M., Misra, S., Li, H., & Aluru, S. (2019). Efficient architecture-aware acceleration of BWA-MEM for multicore systems. *2019 IEEE International Parallel and Distributed Processing Symposium (IPDPS)*, 314–324. https://doi.org/10.1109/IPDPS.2019.00041

Vermillion, M. S., Ursin, R. L., Kuok, D. I. T., Vom Steeg, L. G., Wohlgemuth, N., Hall, O. J., Fink, A. L., Sasse, E., Nelson, A., Ndeh, R., McGrath-Morrow, S., Mitzner, W., Chan, M. C. W., Pekosz, A., & Klein, S. L. (2018). Production of amphiregulin and recovery from influenza is greater in males than females. *Biology of Sex Differences*, *9*(1), 24. https://doi.org/10.1186/s13293-018-0184-8

Vom Steeg, L. G., Flores-Garcia, Y., Zavala, F., & Klein, S. L. (2019). Irradiated sporozoite vaccination induces sex-specific immune responses and protection against malaria in mice. *Vaccine*, *37*(32), 4468–4476. https://doi.org/10.1016/j.vaccine.2019.06.075

Walton, J. C., Bumgarner, J. R., & Nelson, R. J. (2022). Sex differences in circadian rhythms. *Cold Spring Harbor Perspectives in Biology*, *14*(7), a039107. https://doi.org/10.1101/cshperspect.a039107

Wang, C., Lutes, L. K., Barnoud, C., & Scheiermann, C. (2022). The circadian immune system. *Science Immunology*, *7*(72), eabm2465. https://doi.org/10.1126/sciimmunol.abm2465

Wang, G.-Z., Hickey, S. L., Shi, L., Huang, H.-C., Nakashe, P., Koike, N., Tu, B. P., Takahashi, J. S., & Konopka, G. (2015). Cycling transcriptional networks optimize energy utilization on a genome scale. *Cell Reports*, *13*(9), 1868–1880. https://doi.org/10.1016/j.celrep.2015.10.043

Wang, S., Lin, Y., Yuan, X., Li, F., Guo, L., & Wu, B. (2018). REV-ERB integrates colon clock with experimental colitis through regulation of NF-b/NLRP3 axis. *Nature Communications*, *9*(1), 4246. https://doi.org/10.1038/s41467-018-06568-5

Wang, T., Wang, Z., Yang, P., Xia, L., Zhou, M., Wang, S., Du, J., & Zhang, J. (2016). PER1 prevents excessive innate immune response during endotoxin-induced liver injury through regulation of macrophage recruitment in mice. *Cell Death & Disease*, *7*(4), e2176–e2176. https://doi.org/10.1038/cddis.2016.9

Wang, X., Yin, D., Sun, J., Zhang, L., Ye, Y., & Guo, Q. (2025). AR deficiency protects against sepsis-induced acute lung injury by inhibiting macrophage m1 polarization and inflammatory cytokine secretion. *Inflammation*. https://doi.org/10.1007/s10753-025-02321-5

Wang, X., Magkos, F., & Mittendorfer, B. (2011). Sex differences in lipid and lipoprotein metabolism: It's not just about sex hormones. *The Journal of Clinical Endocrinology & Metabolism*, *96*(4), 885–893. https://doi.org/10.1210/jc.2010-2061

Wang, Y., Pati, P., Xu, Y., Chen, F., Stepp, D. W., Huo, Y., Rudic, R. D., & Fulton, D. J. R. (2016). Endotoxin disrupts circadian rhythms in macrophages via reactive oxygen species (N. Cermakian, Ed.). *PLOS ONE*, *11*(5), e0155075. https://doi.org/10.1371/journal.pone.0155075

Weger, B. D., Gobet, C., Yeung, J., Martin, E., Jimenez, S., Betrisey, B., Foata, F., Berger, B., Balvay, A., Foussier, A., Charpagne, A., Boizet-Bonhoure, B., Chou, C. J., Naef, F., & Gachon, F. (2019). The mouse microbiome is required for sex-specific diurnal rhythms of gene expression and metabolism. *Cell Metabolism*, *29*(2), 362–382.e8. https://doi.org/10.1016/j.cmet.2018.09.023

Welz, P.-S., Zinna, V. M., Symeonidi, A., Koronowski, K. B., Kinouchi, K., Smith, J. G., Guillén, I. M., Castellanos, A., Furrow, S., Aragón, F., Crainiciuc, G., Prats, N., Caballero, J. M., Hidalgo, A., Sassone-Corsi, P., & Benitah, S. A. (2019). BMAL1-driven tissue clocks respond independently to light to maintain homeostasis. *Cell*, *177*(6), 1436–1447.e12. https://doi.org/10.1016/j.cell.2019.05.009

Wu, Y., Tang, D., Liu, N., Xiong, W., Huang, H., Li, Y., Ma, Z., Zhao, H., Chen, P., Qi, X., & Zhang, E. E. (2017). Reciprocal regulation between the circadian clock and hypoxia signaling at the genome level in mammals. *Cell Metabolism*, *25*(1), 73–85. https://doi.org/10.1016/j.cmet.2016.09.009

Xu, H., Li, H., Woo, S.-L., Kim, S.-M., Shende, V. R., Neuendorff, N., Guo, X., Guo, T., Qi, T., Pei, Y., Zhao, Y., Hu, X., Zhao, J., Chen, L., Chen, L., Ji, J.-Y., Alaniz, R. C., Earnest, D. J., & Wu, C. (2014). Myeloid cell-specific disruption of period1 and period2 exacerbates diet-induced inflammation and insulin resistance. *Journal of Biological Chemistry*, *289*(23), 16374–16388. https://doi.org/10.1074/jbc.M113.539601

Xu, S., Hu, E., Cai, Y., Xie, Z., Luo, X., Zhan, L., Tang, W., Wang, Q., Liu, B., Wang, R., Xie, W., Wu, T., Xie, L., & Yu, G. (2024). Using clusterProfiler to characterize multiomics data. *Nature Protocols*, *19*(11), 3292–3320. https://doi.org/10.1038/s41596-024-01020-z

Xu, Y., Meng, C., Liu, G., Yang, D., Fu, L., Zhang, M., Zhang, Z., Xia, H., Yao, S., & Zhang, S. (2016). Classically activated macrophages protect against lipopolysaccharide-induced acute lung injury by expressing amphiregulin in mice. *Anesthesiology*, *124*(5), 1086–1099. https://doi.org/10.1097/ALN.0000000000001026

Yaekura, A., Yoshida, K., Morii, K., Oketani, Y., Okumura, I., Kaneshiro, K., Shibanuma, N., Sakai, Y., & Hashiramoto, A. (2020). Chronotherapy targeting cytokine secretion attenuates collagen-induced arthritis in mice. *International Immunopharmacology*, *84*, 106549. https://doi.org/10.1016/j.intimp.2020.106549

Yoo, S.-H., Yamazaki, S., Lowrey, P. L., Shimomura, K., Ko, C. H., Buhr, E. D., Siepka, S. M., Hong, H.-K., Oh, W. J., Yoo, O. J., Menaker, M., & Takahashi, J. S. (2004). PERIOD2::LUCIFERASE real-time reporting of circadian dynamics reveals persistent

circadian oscillations in mouse peripheral tissues. *Proceedings of the National Academy of Sciences*, *101*(15), 5339–5346. https://doi.org/10.1073/pnas.0308709101

Zeng, F., Wang, M., Li, Z., & Zhang, Y. (2025). Overexpression of the circadian gene bmal1 regulates the nrf2/HO-1 oxidative stress pathway to alleviate inflammation and apoptosis in PC12 cells following cerebral ischemia-reperfusion injury. *Medicine*, *104*(24), e42763. https://doi.org/10.1097/MD.0000000000042763

Zhang, D., Jin, C., Obi, I. E., Rhoads, M. K., Soliman, R. H., Sedaka, R. S., Allan, J. M., Tao, B., Speed, J. S., Pollock, J. S., & Pollock, D. M. (2020). Loss of circadian gene *Bmal1* in the collecting duct lowers blood pressure in male, but not female, mice. *American Journal of Physiology-Renal Physiology*, *318*(3), F710–F719. https://doi.org/10.1152/ajprenal.00364.2019

Zhang, R., Lahens, N. F., Ballance, H. I., Hughes, M. E., & Hogenesch, J. B. (2014). A circadian gene expression atlas in mammals: Implications for biology and medicine. *Proceedings of the National Academy of Sciences*, *111*(45), 16219–16224. https://doi.org/10.1073/pnas.1408886111

Zhang, X., Procopio, S. B., Ding, H., Semel, M. G., Schroder, E. A., Viggars, M. R., Seward, T. S., Du, P., Wu, K., Johnson, S. R., Prabhat, A., Schneider, D. J., Stumpf, I. G., Rozmus, E. R., Huo, Z., Delisle, B. P., & Esser, K. A. (2025). The core circadian clock factor, *Bmal1* , transduces sex-specific differences in both rhythmic and nonrhythmic gene expression in the mouse heart. *Function*, *6*(1), zqae053. https://doi.org/10.1093/function/zqae053

Zhang, Y., Fang, B., Emmett, M. J., Damle, M., Sun, Z., Feng, D., Armour, S. M., Remsberg, J. R., Jager, J., Soccio, R. E., Steger, D. J., & Lazar, M. A. (2015). Discrete functions

of nuclear receptor rev-erb couple metabolism to the clock. *Science*, *348*(6242), 1488–1492. https://doi.org/10.1126/science.aab3021

Zhao, H., Sifakis, E. G., Sumida, N., Millán-Ariño, L., Scholz, B. A., Svensson, J. P., Chen, X., Ronnegren, A. L., Mallet de Lima, C. D., Varnoosfaderani, F. S., Shi, C., Loseva, O., Yammine, S., Israelsson, M., Rathje, L.-S., Németi, B., Fredlund, E., Helleday, T., Imreh, M. P., & Göndör, A. (2015). PARP1- and CTCF-mediated interactions between active and repressed chromatin at the lamina promote oscillating transcription. *Molecular Cell*, *59*(6), 984–997. https://doi.org/10.1016/j.molcel.2015.07.019

Zhou, M., Zhang, J., Zhao, J., Liao, M., Wang, S., Xu, D., Zhao, B., Yang, C., Hou, G., Tan, J., Liu, J., Zhang, W., & Yin, L. (2023). Sex difference in cardiac performance in individuals with irregular shift work. *International Journal of Cardiology Cardiovascular Risk and Prevention*, *19*, 200219. https://doi.org/10.1016/j.ijcrp.2023.200219

Zhu, L., Meng, Q., Liang, S., Ma, Y., Li, R., Li, G., & Zeng, H. (2014). The transcription factor GFI1 negatively regulates NLRP3 inflammasome activation in macrophages. *FEBS Letters*, *588*(23), 4513–4519. https://doi.org/10.1016/j.febslet.2014.10.025

Zhuang, X., Tsukuda, S., Wrensch, F., Wing, P. A., Schilling, M., Harris, J. M., Borrmann, H., Morgan, S. B., Cane, J. L., Mailly, L., Thakur, N., Conceicao, C., Sanghani, H., Heydmann, L., Bach, C., Ashton, A., Walsh, S., Tan, T. K., Schimanski, L., … McKeating, J. A. (2021). The circadian clock component BMAL1 regulates SARS-CoV-2 entry and replication in lung epithelial cells. *iScience*, *24*(10), 103144. https://doi.org/10.1016/j.isci.2021.103144

Zieliński, T., Hay, J., & Millar, A. J. (2022). Period estimation and rhythm detection in time-series data using BioDare2, the free, online, community resource [Series Title: Methods in Molecular Biology]. In D. Staiger, S. Davis, & A. M. Davis (Eds.), *Plant circadian*

networks (pp. 15–32, Vol. 2398). Springer US. https://doi.org/10.1007/978-1-0716-1912-4_2